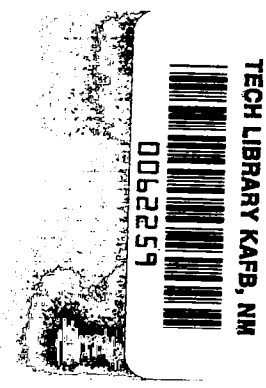

NASA Contractor Report 3486

Study To Perform Preliminary Experiments To Evaluate Particle Generation and Characterization Techniques for Zero-Gravity Cloud Physics Experiments

Ulrich Katz

CONTRACT NAS8-32313
JANUARY 1982

NASA

NASA Contractor Report 3486

Study To Perform Preliminary Experiments To Evaluate Particle Generation and Characterization Techniques for Zero-Gravity Cloud Physics Experiments

Ulrich Katz
Desert Research Institute
Reno, Nevada

Prepared for
George C. Marshall Space Flight Center
under Contract NAS8-32313

NASA
National Aeronautics
and Space Administration

Scientific and Technical
Information Branch

1981

TABLE OF CONTENTS

I. INTRODUCTION

Cloud physics experiments originally planned for the zero-gravity Atmospheric Cloud Physics Laboratory (ACPL) aboard the Space Shuttle stipulated a need for cloud condensation nuclei (CCN) of specified properties. The aim of the present investigation was to scrutinize methods of particle generation and characterization with regard to their applicability to the ACPL program. Subsequent to the initiation of this program in December, 1976, the concept of an ACPL as a flight facility was abandoned by NASA; however, the objective of this study remained unchanged since the results would still be applicable to future low-g flights.

While the absence of gravity unavoidably introduces constraints in some techniques of aerosol generation, at least as many difficulties in the tasks of the present project can be traced to the stringent specifications regarding the output of particle generators. The need to achieve particularly high degrees of aerosol monodispersity, output constancy, reproducibility, etc., previously not common in cloud physics experimentation stems from the fact that the ACPL experiments were specifically intended to be of great sensitivity in order to clearly detect the effects unmasked by the low gravity environment.

At the outset of this study, most of the tasks outlined in the proposal were assigned similar levels of effort; however, as work progressed, it became evident that priorities had to be established, leading to a very inhomogeneous distribution of efforts. There were two reasons for this development. First, pneumatic atomization of solutions, the

particle generation method favored on the basis of literature studies (Anderson, 1977; Liu and Lee, 1975) was found to pose unexpected output stability problems, and, secondly, numerous discussions between cognizant NASA and DRI personnel indicated that on initial flights of the ACPL, especially on the very first one, there would be less elaborate experiments with simpler hardware and fewer accessories than originally planned. Thus it was possible and advisable to concentrate more on the problems of the prime particle generator at the expense of less urgently needed equipment.

These deviations from the original work plan will not be discussed any further in this report since the DRI's course of action was communicated through monthly progress reports to and implicitly approved by NASA.

Since the aerosol characterization is a prerequisite to assessing performance of particle generation equipment, redundancy is avoided by devoting the following section of this report to the evaluation of techniques for characterizing aerosol particles.

The third section contains the discussion of aerosol generation whereby the studies of atomizer and photolytic generators represent the major portion, including subsections on preparation of hydrosols (used with atomizers), and on the evaluation of the flight version of the GE atomizer.

No separate sections were established for the discussion of the joint workshops with the University of Wyoming and of the problem of gaseous contamination of aerosol particles. Pertinent information on these topics is presented in the proper context in various other subsections.

Conclusions and recommendations are summarized in the fourth and final section.

II. AEROSOL CHARACTERIZATION

A. REQUIREMENTS

Ideally, aerosol generators to be used in low-g should perform in such a reproducible fashion that subsequent measurements of particle size spectra would not be necessary; however, as will be seen in Section III, the reliability of particle generators is not good enough to guarantee a flawless performance as shown by terrestrial calibration over a period of a flight duration. Thus, in order to ensure accurate knowledge of the characteristics of the aerosol used in each experiment, it is necessary to obtain in-flight measurements of the particles generated.

Due to the use of high purity substances from which to generate particles, the chemical composition of the resulting aerosols is essentially known (except for difficult to detect surface contamination as discussed later). Therefore, aerosol characterization does not require a chemical investigation, but can be limited to the determination of size distribution and number concentration.

Two types of aerosol assessment have to be considered - real time and "hard copy." While a real time characterization is essential, allowing the investigator to take corrective steps if necessary, a "hard copy" (an actual representative collection of particles) is equally important because it permits detailed scrutiny with instrumentation not available in flight (such as electron microscopes) which, in many cases, provide a nearly-absolute determination of particle size and number.

B. REAL TIME METHODS FOR AEROSOL GENERATION

The most relevant factor in the selection of a suitable method for onboard aerosol characterization is the particle size range. Since the upper size limit of the primary range was specified as 100 nm, optical particle counters/classifiers such as the familiar Royco 225 were ruled out for this task. Although optical counters can, in principle, contribute to the particle assessment if combined with a condensation device that increases the particle size into the optical range, this process involves the condensational behavior of the particles themselves and thus, the procedure cannot be used for an independent characterization of the aerosols in question.

Two well-researched, size-dependent properties of aerosol particles that lend themselves to middle and lower submicron range measurement are electrical mobility and diffusivity. The last decade has brought profound advances in the design and application of particle measuring devices based on electrical mobility assessment. Two such instruments have been used extensively in this investigation and will be discussed below. Based on classical diffusion theory, "diffusion batteries" consisting of considerable lengths of tubing were used initially to determine aerosol size distributions. A modern, compact version originally scheduled to be part of the ACPL, and used a number of times on the present project, was also evaluated.

1. Electrical Mobility Instruments

Recent literature treats most aspects of theory and design of this type of particle analyzer (Knutson and Whitby, 1975a, b; Knutson, 1975; Hoppel, 1978; Liu and Pui, 1974, to name a few).

For the purpose of the present investigation, only a brief description of the underlying principles of operation and a discussion of problems pertaining to the ACPL application will be presented.

The two instruments used in this study are the Electrical Aerosol Analyzer (EAA) by TSI (Model 3030),and the Electrostatic Classifier (EC), also by TSI (Model 3071). In both instruments, the aerosol is first electrically charged (differently for EC and EAA) and subsequently passed through the electric field of a cylindrical high voltage condenser where discrimination takes place according to charge vs. size relationships; the third element in this sizing method is a device that counts the particles of the selected size fractions.

a. Electrostatic Classifier

(1) General Principle

The essential features of this instrument are depicted in Figure 2-1. The central part of the device is the cylindrical analyzer section in which a uniform clean air sheath flow (q_{sh}) is maintained while the aerosol is injected at a much slower rate (q_a) through a peripherally-located annular slot. For a given voltage applied between cylinder wall and axial collector rod, particles of a certain mobility

$$Z_{pn} = neC(Dp)/3\pi\eta D_p$$

(where n number of elementary charges, e; C the Cunningham slip correction; η the viscosity of air; and D_p the particle diameter) reach the axially located opening where a flow equal to the aerosol inlet flow is withdrawn ("monodisperse aerosol outlet"). All particles with higher mobility end up on the central rod while the ones with lower mobility and the neutral particles are trapped in the filter at the exit end of the cylinder.

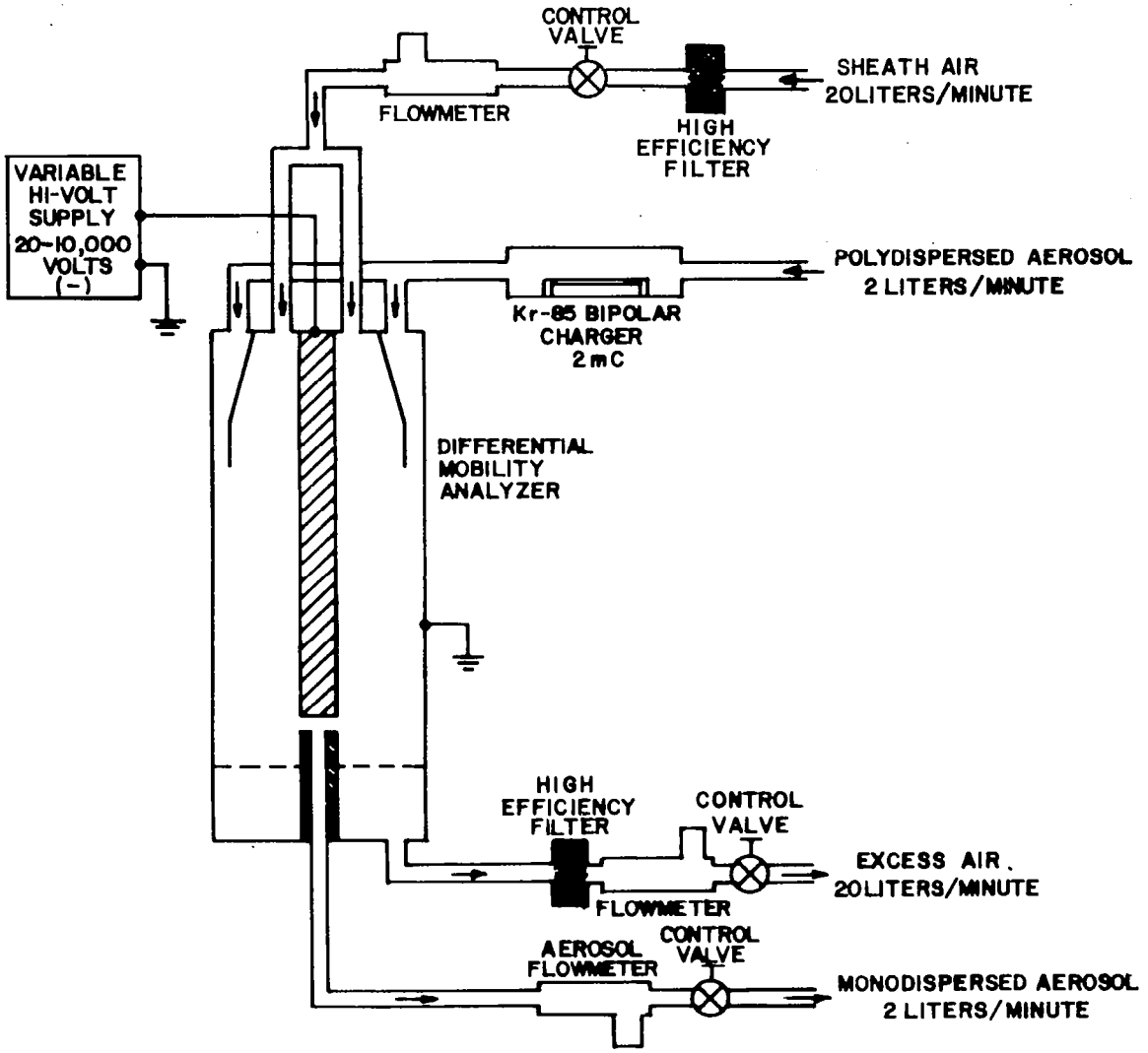

Figure 2-1. Schematic of air flow in TSI, Model 3071, Electrostatic Classifier (EC) [from Instrument Manual].

Figure 2-2 depicts the relationship between electrical particle mobility and the size of singly, doubly, and triply charged particles; it also shows the voltage that needs to be applied to the condenser to obtain singly charged particles of diameter D_p in the outlet under the stated flow conditions and the particular geometry of this device. Knutson and Whitby (1975a) have shown that mobility Z_p, the voltage V, and the sheath flow q_{sh} follows the relationship $Z_p = G\ q_{sh}/V$, where the factor G incorporates dimensions of the condenser.

From the above expression for the mobility and Figure 2-2, it is quite clear that the knowledge of the distribution of charges on the particles is a determining factor for the usefulness of the device. For the primary particle size range under consideration here, the method of charge neutralization provides a convenient means of establishing a relatively well-known charge distribution, the Boltzmann charge equilibrium, achieved by letting the particles interact for a sufficient time with highly concentrated bi-polar ions. The latter have been generated in this study by radioactive Kr^{85} in the TSI charge neutralizer (Model 3077 and/or 3012) through which the aerosol was passed prior to entering the analyzer section of the EC.

Figure 2-3 illustrates what charge distributions can be expected after passage through the charge neutralizer; shown are the fractions of singly, doubly, and triply charged particles (of either sign) as a function of particle size based on values tabulated by Pui and Liu (1979). It is immediately evident that, in the size range of interest, the singly charged particles become increasingly dominant over multiply charged ones with decreasing size. This fact, which translates into pre-

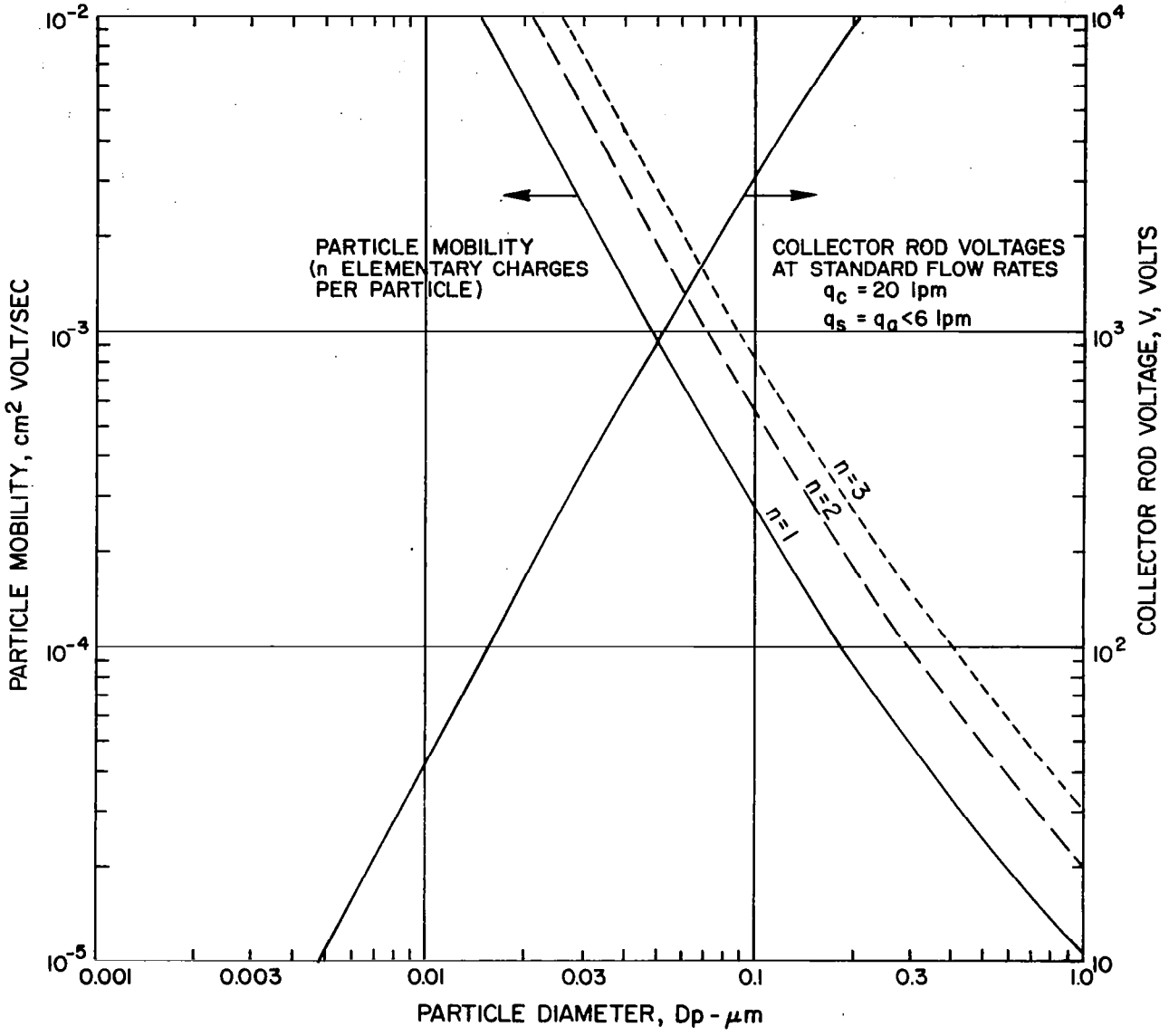

Figure 2-2. Electrical mobility of particles with one, two and three elementary charges as a function of particle diameter. EC collector rod voltage, V, to pass singly charged particles of diameter D_p through the instrument at standard conditions. [After Instrument Manual].

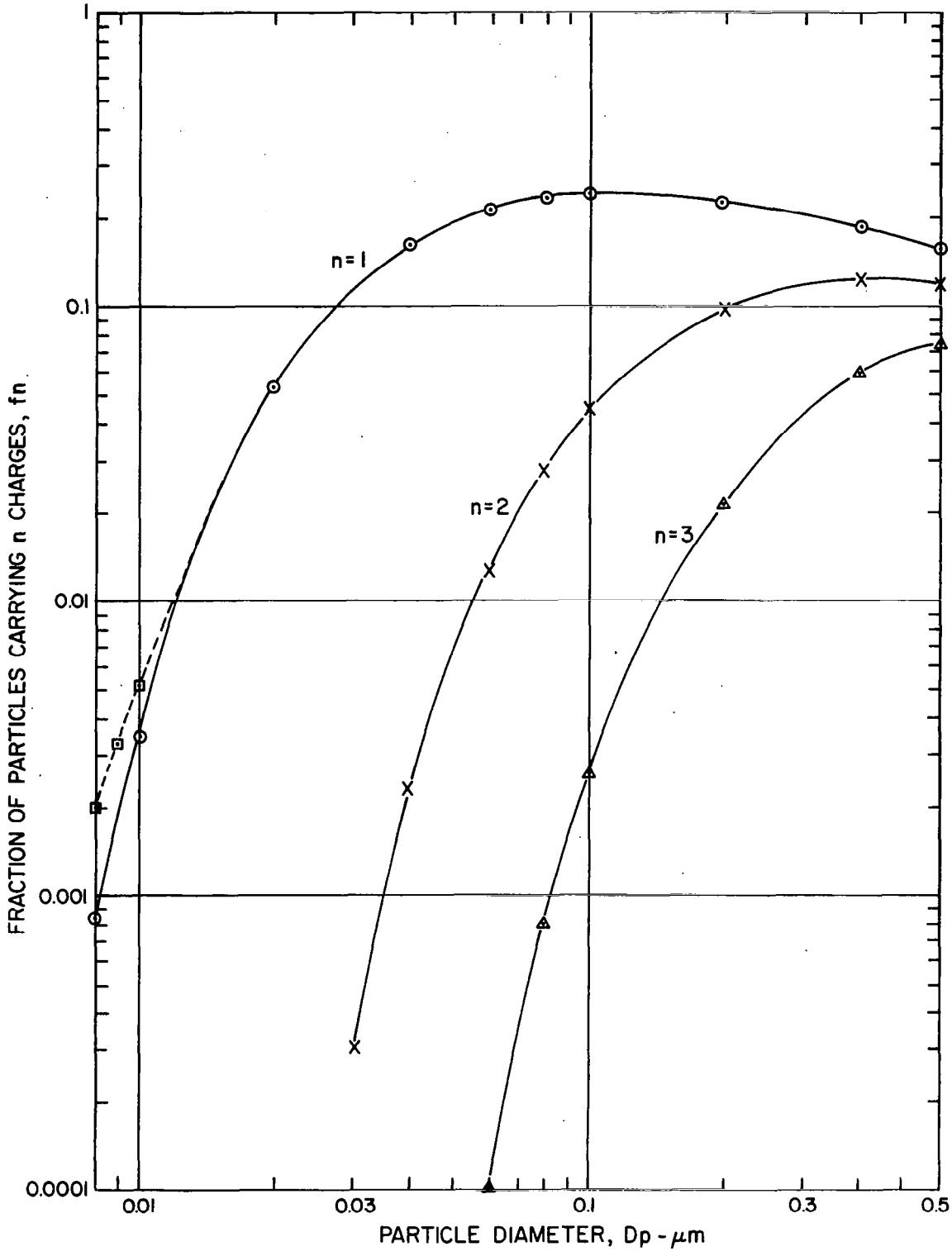

Figure 2-3. Fractions of particles with one, two or three elementary charges (of either sign) as a function of particle diameter (according to Pui and Liu, 1979). Dashed line tentatively according to DRI experiments.

dominant passage of one size of particles for a given set of voltage and flow rates, makes the EC also a primary tool for generating monodisperse aerosols in the 10-100 nm range (more about this aspect in Section III.D.3). Figure 2-3 also indicates that, with decreasing diameter, the fraction of singly charged particles becomes very small which, in effect, reduces the sensitivity for particle number measurement.

The essential function (in size distribution measurement) of counting the particles in the selected size fraction is not incorporated into the EC, but has to be performed by an external instrument connected to the "monodisperse aerosol" outlet of the EC. In this study, the TSI Electrical Aerosol Detector (EAD), Model 3070, was used most of the time. The device uses an electrometer to measure the current produced by the charges of the passing particles - requiring, once more, knowledge of the charge distribution.

In principle, any "total particle counter" could provide the necessary information; even instruments based on size enhancement through condensation are suitable since, at this stage, no size discrimination is needed. However, peculiarities of the various available counters (to be discussed later) made the EAD the preferred instrument.

(2) Specific Problems

(a) Uncertainties in Equilibrium Charge Distribution

While knowledge of the equilibrium charge distribution is considered sufficient for most practical applications, uncertainties exist which become more pronounced with decreasing particle size. In the course of establishing the droplet size distribution of some nebulizers by measuring the size distribution of the dry residue particles, it was

noticed that, when nebulizing salt solutions of different concentrations, a distinct deviation from the expected overlap of size distribution curves occurred for particle sizes below about 15 nm if the values for the singly charged fraction of the solid curve of Fig. 2-3 were applied. Based on these discrepancies, the dashed line in Figure 2-3 was tentatively established by empirical means and used in subsequent work with satisfactory results. However, the real depth and difficulty of the problem can be seen from Fig. 2-4, taken from the Knutson (1975) paper which should be consulted for further details. It appears that the user of the EC will have to look out for future development in this matter in order to achieve the most valid interpretation of EC data.

(b) Establishing Charge Equilibrium

According to manufacturer's specifications, the charge neutralizer (TSI Model 3077) built into the EC should suffice to provide Boltzmann equilibrium for aerosol flow rates up to the maximum recommended for the EC (6 ℓ min^{-1}). With the intent to confirm this information, experiments were performed by passing a nominally monodisperse latex aerosol through the EC with and without an additional charge neutralizer (TSI Model 3012). An example of this comparison is shown in Figure 2-5, where the EC output is plotted in terms of charge counts (by EAD) versus the EC voltage; as expected, the latex aerosol consisted of singlets, doublets and higher multiplets with singly, doubly, etc. charged fractions in each category. These show up as the peaks in Figure 2-5 and can be identified with the aid of Figs. 2-2 and 2-3.

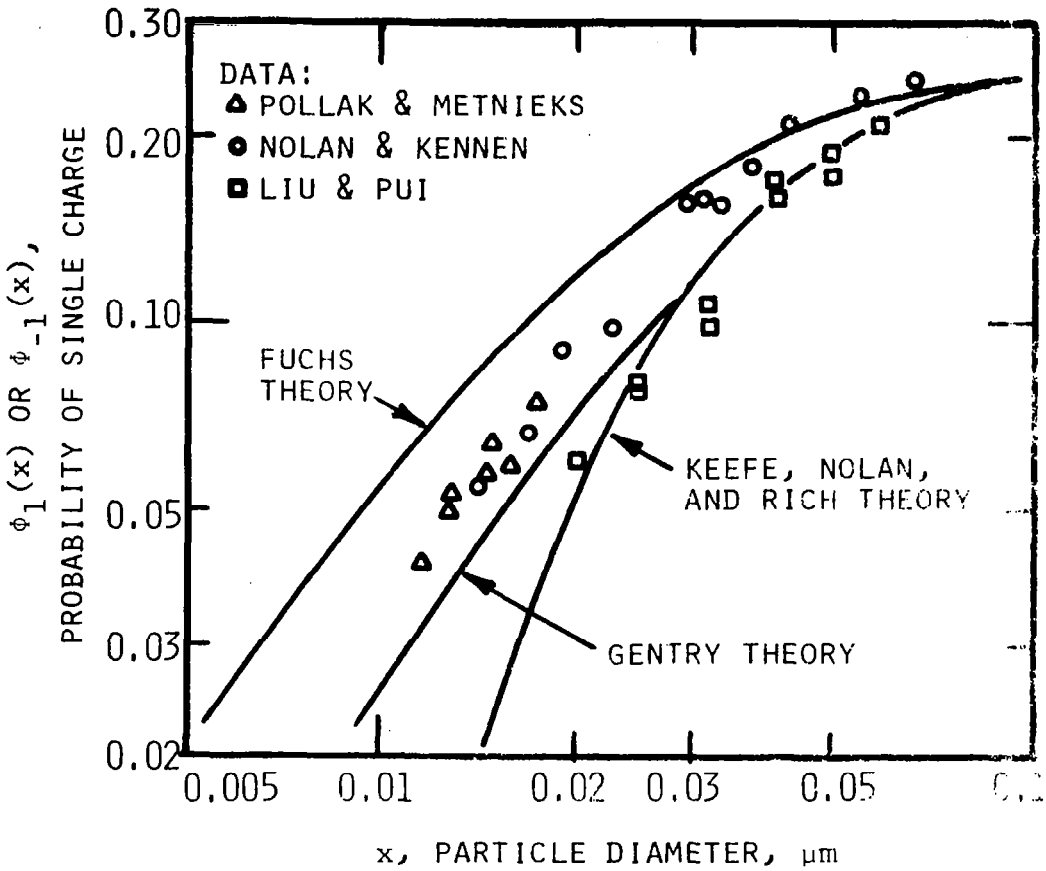

Figure 2-4. Theoretical and experimental values for fraction of singly charged particles at Boltzmann charge equilibrium as a function of diameter according to indicated authors (from Knutson, 1975).

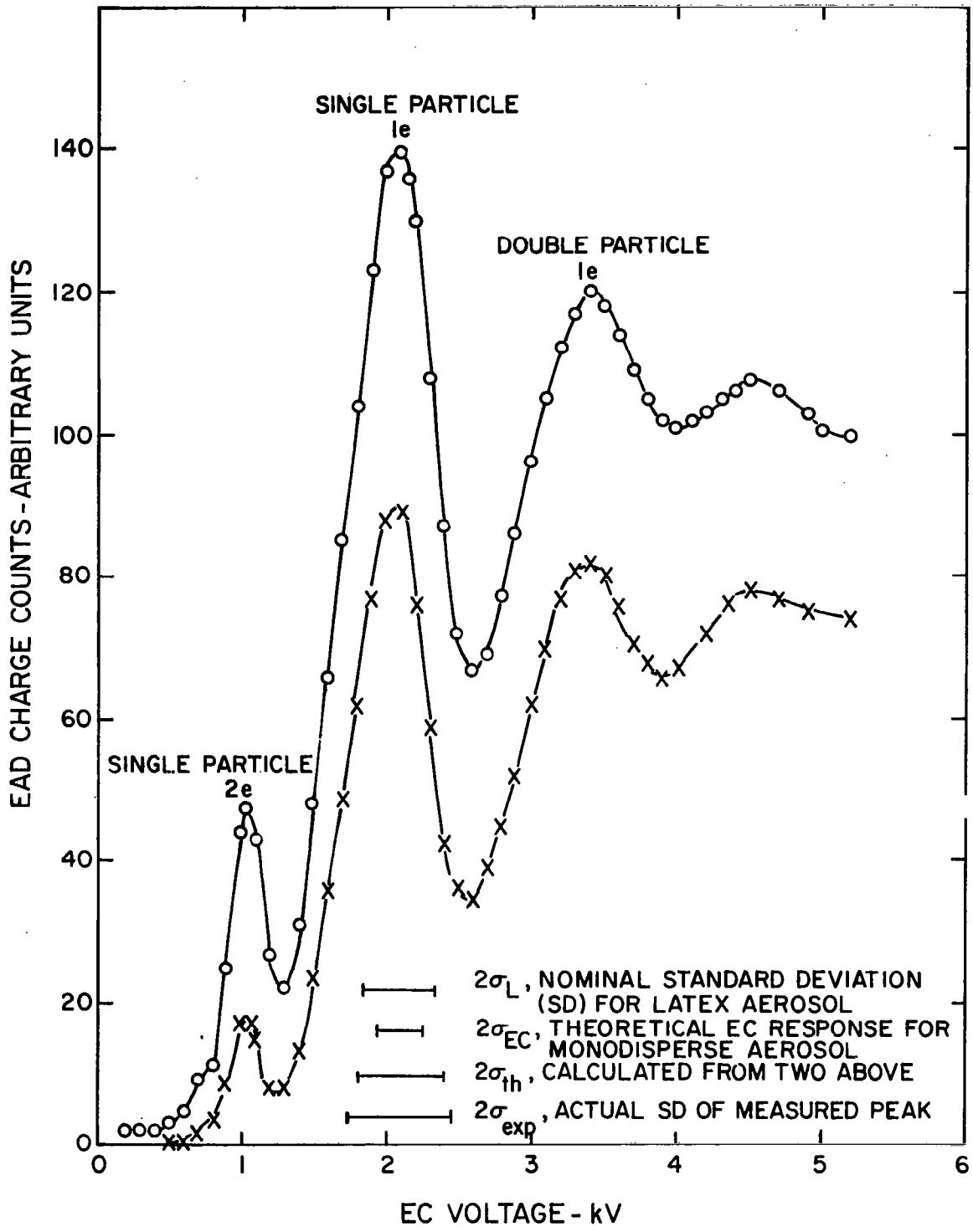

Figure 2-5. EC voltage scan for 91 nm diameter monodisperse latex aerosol, with (X) and without (Θ) additional charge neutralizer.

Of principle interest here are the relative peak heights of the singly and doubly charged singlets. Despite the difficult-to-assess interference of doubly charged multiplets (e.g., doubly charged doublets have approximately the same mobility as the singly charged singlets - thus the two are superimposed on the main peak) the measurements show that the addition of a second charge neutralizer causes the ratio of doubly over singly charged particles to drop by about 50%. Since no further significant change was observed when the additional 2 mCi neutralizer was replaced with a more powerful 10 mCi unit (TSI Model 3054) it is assumed that the added 2 mCi ionizer does provide the equilibrium charge distribution. All subsequent EC work was carried out with an added neutralizer.

(c) Sensitivity and Resolution

It is important to determine whether and how these two essential quantities can meet the requirements given by the ACPL task. Since the principle of operation of the EC is to cut out of the total input spectrum a narrow segment (ΔDp), the particles of which are then counted, it is obvious that the better the size resolution (i.e., the smaller ΔDp) the worse the number sensitivity becomes (though somewhat dependent on the type of particle counter).

- Size Resolution

As shown by Knutson and Whitby (1975a,b) in their rigorous mathematical treatment of the EC, the shape of the narrow ("monodisperse") size distribution extracted by the instrument from a primary aerosol with a flat size distribution is triangular if aerosol input and output

flow rates are equal, and provided the particle number is plotted against a logarithmic EC voltage scale (rather than Dp). Thereby the base width of the triangle represents a suitable measure of the size resolution which can be expressed by D_1/D_2, the particle diameters associated with V_1, V_2, the end points of the triangle base. Since the particle mobility Z_p is approximately proportional to D_p^{-2} (see Fig. 2-2) in our range of interest,

$$\frac{D_1}{D_2} \approx \sqrt{\frac{Z_2}{Z_1}} = \sqrt{\frac{V_1}{V_2}}$$

and, following Knutson and Whitby (1975)

$$\frac{Z_2}{Z_1} = \frac{q_{sh} + q_a}{q_{sh} - q_a} = \left(\frac{V_1}{V_2}\right)$$

Thus, for typical values of q_{sh} = 20 ℓ min and q_a = 2 ℓ min^{-1} or 6 ℓ min^{-1} (maximum recommended for preservation of laminar flow), the voltage ratios V_1/V_2 become 1.22 and 1.86, respectively, which translates for D_1/D_2 to approximately 1.10 and 1.36, respectively. These values are not only important in the context of size resolution but even more so for determining absolute number densities in the input aerosol since one usually plots $\Delta N/\Delta \log D_p$ vs. D_p.

Experimental verification of these theoretical values for the EC's resolution can, in principle, be obtained by passing a perfectly monodisperse aerosol through the device while varying the voltage. The resulting number vs. voltage relationship then provides an exact duplicate of the aforementioned triangular size distribution passed by the EC at the

fixed voltage corresponding to the size of the monodisperse aerosol. While truly monodisperse aerosols in the desired size range are generally unavailable, commerical latex spheres with known standard deviation (SD, σ) were used as documented in Fig. 2-5. The bars at the base of the main peak indicate 2σ as the measure for the width of the size distributions involved: $2\sigma_L$, latex particles; $2\sigma_{EC}$, the SD for theoretical response of the EC to a perfectly monodisperse input (above mentioned triangle); $2\sigma_{exp.}$, represents the experimentally obtained peak; and $2\sigma_{th}$ signifies the theoretically expected EC response to the actual latex distribution, calculated according to $(\log \sigma_{th})^2 = (\log \sigma_L)^2 + (\log \sigma_{EC})^2$.

As a second EC became briefly available late in this program, the soluble salt output of one EC was used as "monodisperse" test aerosol and passed through the second EC. This provided a two-fold improvement for performance verification tests: (1) no interference from multiply-charged multiplets, and (2) a narrower size distribution that has inherently the same shape as the instrument's response to a truly monodisperse aerosol. The theoretically expected particle number count vs EC voltage is illustrated in Fig. 2-6 as the bell-shaped curve,* while the triangle represents the input size distribution centered (in this example) at about 58 nm. Results of an actual measurement are shown in Fig. 2-7 (an excerpt from Fig. 3-70); the dashed triangle, representing the most likely input distribution, was obtained from the

*Note that this should not be confused with the size distribution of the aerosol that emerges from the second EC at a given voltage setting. More on this in Chapter III.

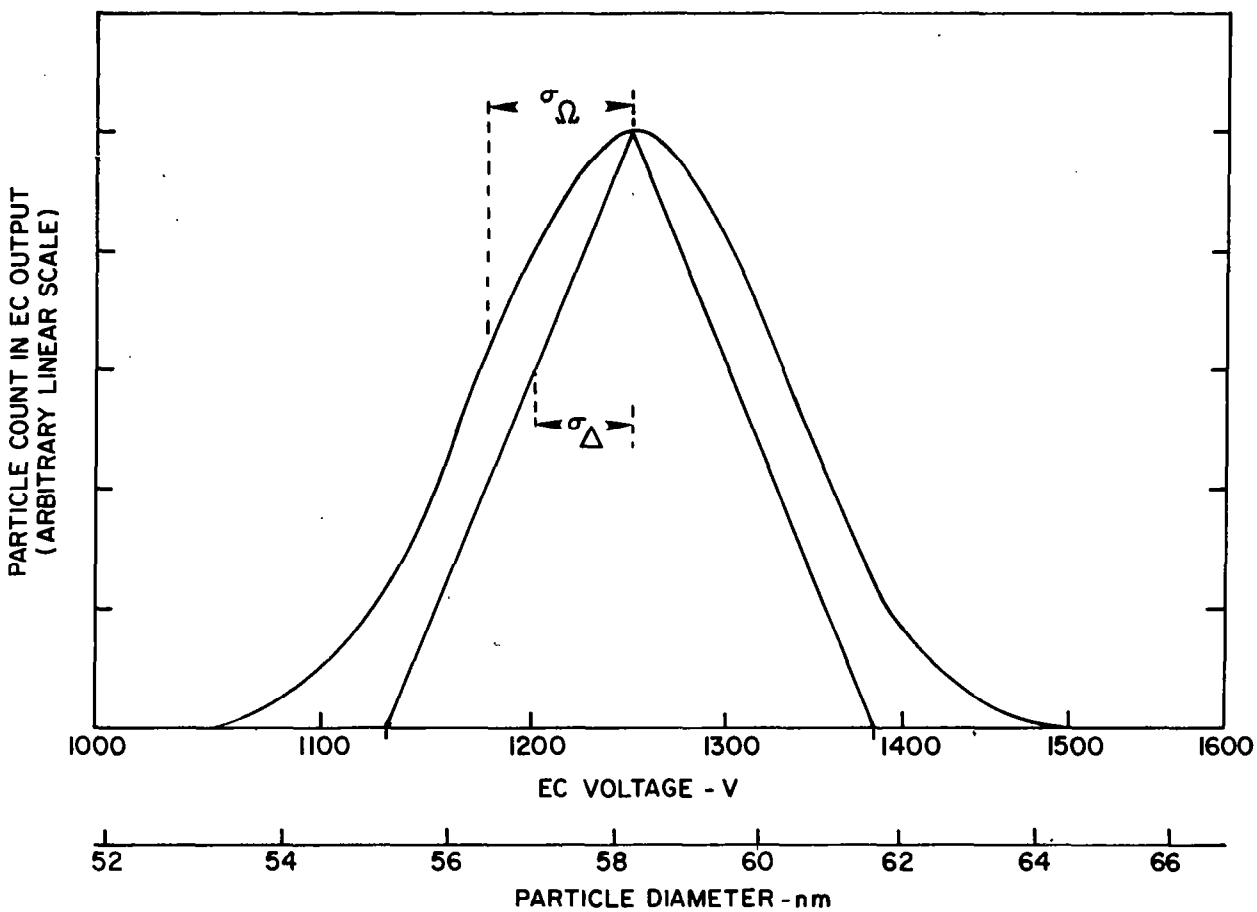

Figure 2-6. Theoretical response of EC (bell-shaped curve) to triangular shaped input size distribution (which represents theoretical output of another EC with an input having a flat size distribution).

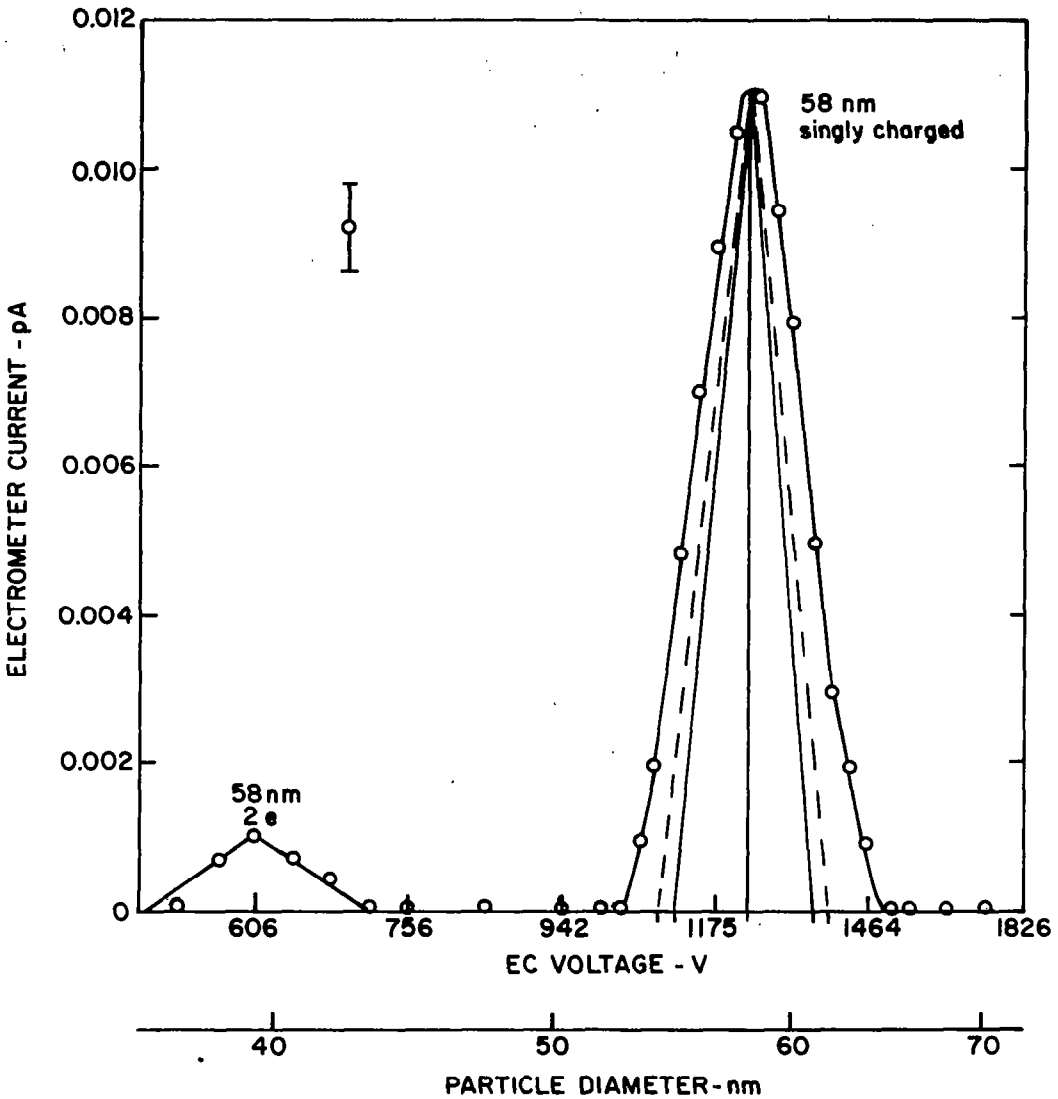

Figure 2-7. Experimental counterpart to Fig. 2-6. The narrower triangle represents the theoretically expected input (based on flow rate ratios) while the wider triangle is the assumed actual input (i.e., output of other EC) based on Fig. 2-6. (Peak to left of figure is caused by doubly charged particles of same size).

measured curve according to the relationships developed for Fig. 2-6, while the solid triangle corresponds to the theoretically expected output size distribution of the first EC based on the flow rate ratio. Data from both Fig. 2-5 and 2-7 are in agreement showing that the actual peak widths obtained with the EC are about 20% larger than predicted. Thus, the experimentally determined geometric standard deviation $\sigma_{g\Delta}$ of the triangular distributions (in terms of particle size), an appropriate measure for the size resolution of the EC, is below 1.03 for a 2 ℓ min^{-1} aerosol flow rate. Translated into terms of supersaturation for the case of soluble CCN (according to the Köhler relationship) we obtain $\sigma_{gss} \approx 1.04$. This value indicates that the EC's size resolution is more than adequate for proper characterization of test aerosols in ACPL applications.

In the above discussion, it was tacitly assumed that the number density of singly charged particles was size independent; however, this is generally not the case because: (1) the singly charged fraction of particles varies with size as shown in Fig. 2-3, and (2) the number size distribution of the input aerosol usually has a distinct peak. Therefore curves of the type shown in Fig. 2-6 may become somewhat distorted; however, it appears that the previous considerations regarding the EC's size resolution remain essentially valid.

- Absolute Size Calibration

For satisfactory aerosol characterization in the context of ACPL experimentation, absolute size information is as important as size resolution. Obviously, the accurate size selection in the EC depends as much on the rigorous control of air density and velocity in the

instrument as it does on the precise voltage control. While the latter did not appear to be a problem, maintenance and measurement of the exact aerodynamic conditions inside the EC required particular care and attention.

The calculated calibration curve furnished by the manufacturer and shown in Fig. 2-2 correlates voltage and particle size for "standard flow rates", 20 ℓ min^{-1} sheath flow and up to 6 ℓ min^{-1} of aerosol flow. These conditions were applied throughout our tests; however, at times it was difficult to maintain all flows as steadily as desired, and $\pm$5% deviations were not unusual. Therefore, the effects of flow on sizing were determined experimentally by inputting fixed size aerosols and performing voltage scans at various flows. Fig. 2-8 illustrates the effect of variations in aerosol flow (using the fixed output of another EC); as discussed previously, the width of the resulting peaks increases predictably with increasing flow, but there is also a noticeable shift towards higher voltages with increasing flow, corresponding to a 1 to 2 nm increase in particle diameter. Considering that (in this example) the flow was more than doubled, no significant size shifts due to small inadvertent aerosol flow changes have to be expected. However, since the number concentration of the passing aerosol fraction is approximately proportional to the aerosol flow, changes in the latter could noticeably distort a measured size distribution.

Figs. 2-9 and 2-10 show how the voltage associated with the peak of a latex aerosol shifts as the sheath and/or excess flows through the EC are varied. The relative changes in apparent particle size and flow rate are about equal and, therefore, the effect of changing sheath flow cannot be ignored.

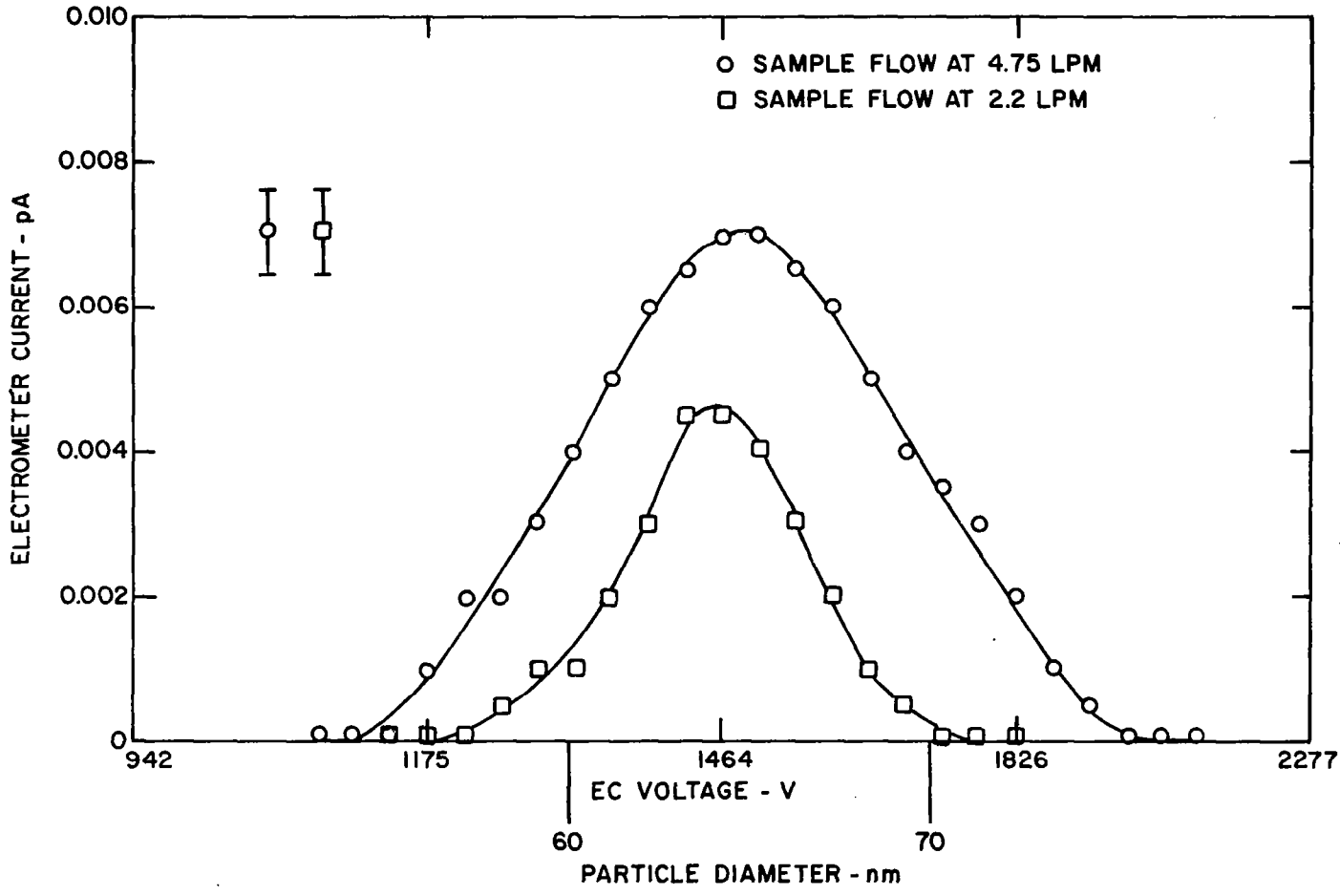

Figure 2-8. Effect of sample flow variation on response of EC to fixed input (triangular size distribution).

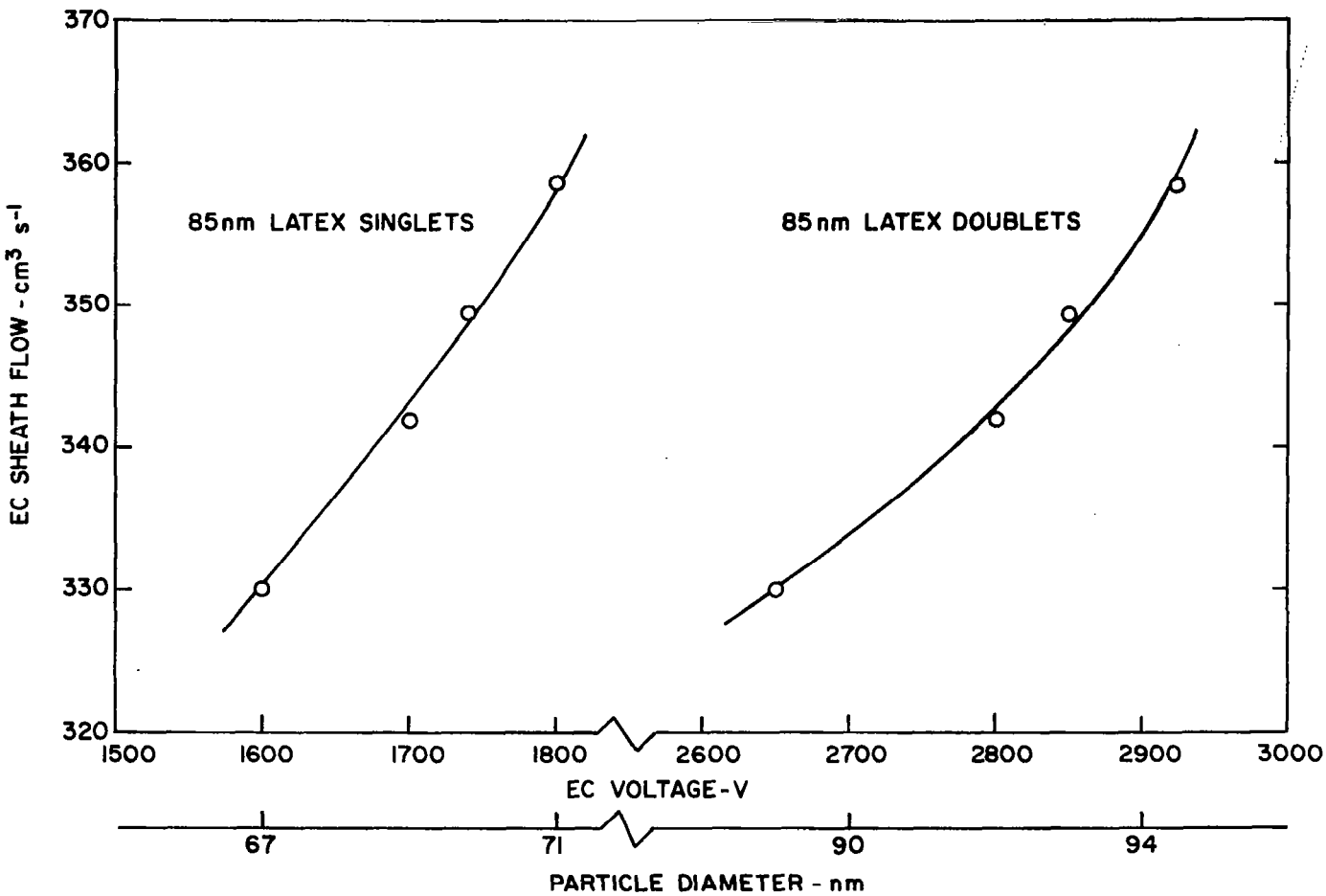

Figure 2-9. Effect of sheath flow on position of response peak from a "monodisperse" latex input (85 nm).

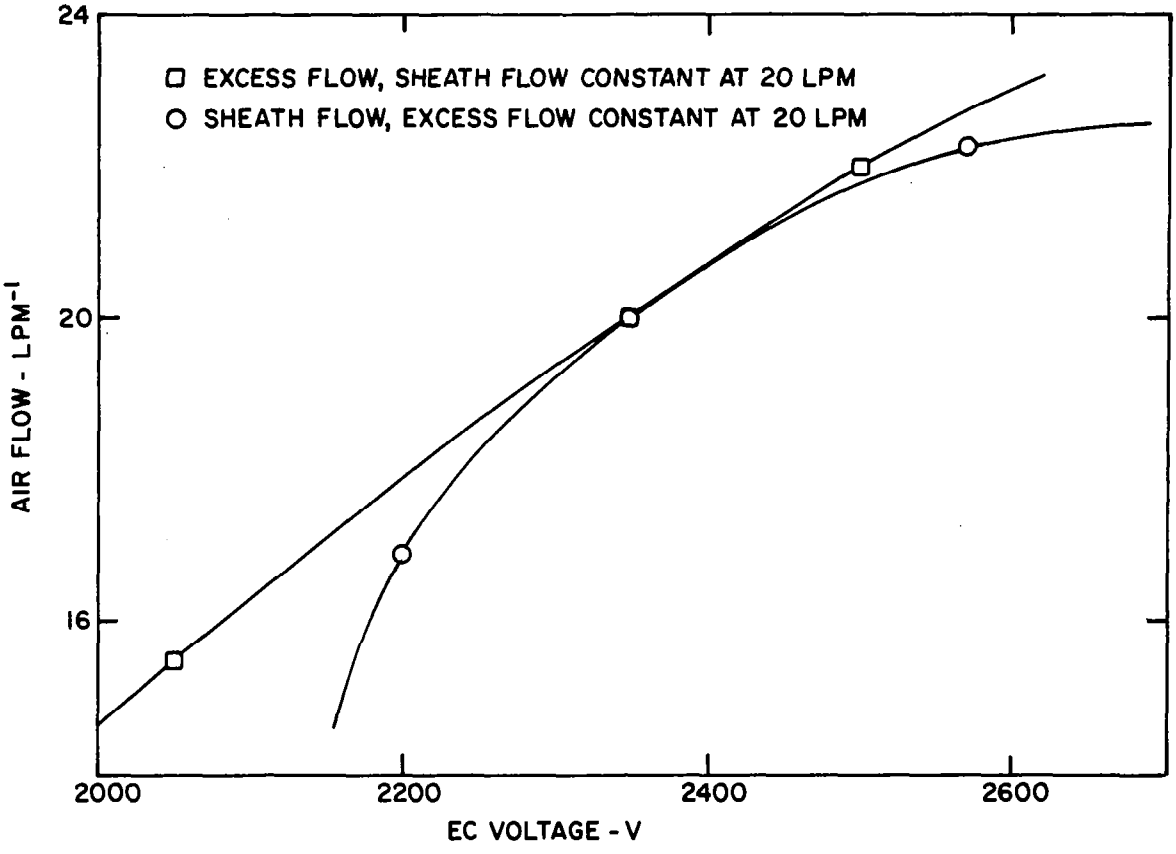

Figure 2-10. Effect of change of sheath or excess flow on output peak position; input: 91 nm latex.

In order to avoid the problems associated with flow inaccuracies and variabilities, the thermal flow meters of the EC were frequently recalibrated and, if necessary, their output recorded over the duration of particularly sensitive experiments. Since the EC's flow meters measure mass flow, it is important to perform calibrations at the pressure regime used during experimentation.

A further reason for monitoring air pressure in the EC is the pressure dependence of the mean free path of the gas molecules which determines the Cunningham slip correction to which the mobility of the particles is directly proportional. While the curves in Fig. 2-2 are based on standard pressure, calculations show that, for DRI's altitude of 1500 m, particles would, for instance, measure 54 nm instead of 50 nm for a voltage of 950 V, or 106 nm instead of 100 nm at 3400 V. This correction did bring most of the latex sphere test results very close to the calibration curve. However, for very accurate experiments, it will be advantageous to take into account whether the EC is run in an overpressure or underpressure mode.

Since even "monodisperse" diagnostic latex aerosols are not always of the stated size, precision work requires true size calibration of the EC with monodisperse aerosols (preferably generated with another EC) which are suitable for transmission electron micrography without susceptibility for size changes in vacuum and electron beam.

- Number Sensitivity

As pointed out earlier, the excellent size resolution of the EC leads to a relatively small number output of the instrument, which is further reduced due to the small fraction of singly charged particles

available for the classification process, diminishing especially rapidly with decreasing size below about 50 nm. The effects of this problem are illustrated in Fig. 2-11 which relates particle size to the minimum aerosol concentration* required in the EC input to provide sufficient particle numbers in the output for counting with either the EAD or the TSI-CNC at 2 or 6 ℓ min^{-1} aerosol flow rates. Low flow rate not only narrows the size interval (thereby reducing the output particle concentration) but, in the case of the EAD, also diminishes the particle (i.e., charge) flow rate, thus compounding the effect of low flow rate. If a TSI-CNC** could be used to monitor the EC output, the sensitivity could be increased considerably; the curves in Fig. 2-11 pertaining to the CNC were calculated on the basis of a required concentration of 10 cm^{-3} although the TSI-CNC per se could be used at one to two orders of magnitude lower concentration, but counting statistics might be unsatisfactory. Below 20 nm particle diameter this instrument's sensitivity drops rapidly, thus the curves were not extended below that limit.

- Multiple Charge Compensation

While uncertainties in the exact value of the fraction f_1 of singly charged particles (see Figs. 2-3 and 2-4) of sizes below about 30 nm may lead to questionable values in that low size range for size distributions obtained with the EC, above the size of 30 nm interference from multiply charged particles has to be taken into account; however,

*Note that the values of the ordinate are normalized to a diameter interval of a decade.

**The TSI-CNC Model 3020 was put on the market too late to be used on this program. For zero-g applications, a substantial modification would be required.

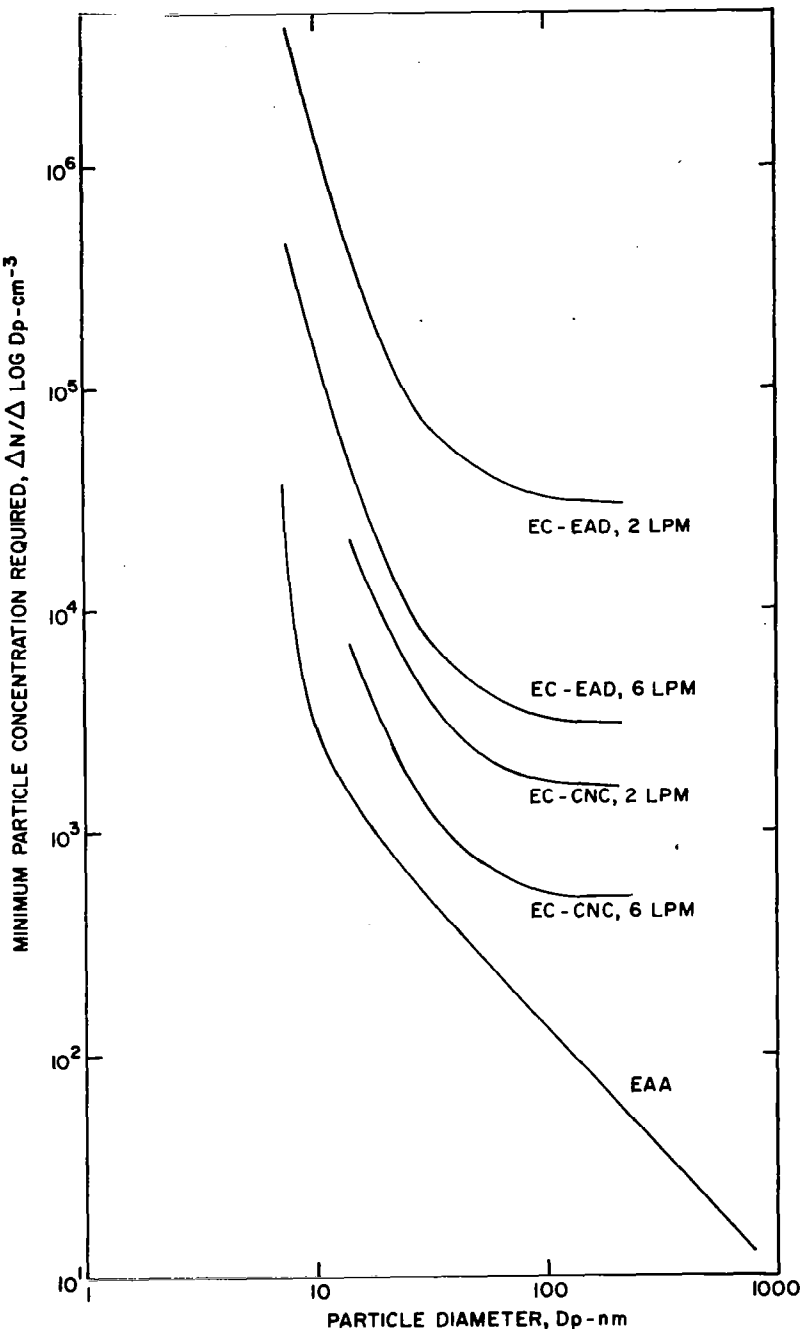

Figure 2-11. Minimum required particle number density ($\Delta N/\Delta \log D_p$) versus diameter for EC at different flow rates and with different particle sensors. Same for EAA at standard operating conditions (quarter-decade channel width).

this is not a problem of physics, but rather one of computational expediency.

As Fig. 2-2 indicates, at a given voltage setting, the EC passes particles possessing the corresponding mobility. This population is comprised of particles with single charges and diameter D_1, with two charges and D_2, with triple charge and D_3, etc. whereby approximately $D_2 \approx \sqrt{2} \cdot D_1$ and $D_3 \approx \sqrt{3} \cdot D_1$. Again, these are narrow triangular size distributions centered at D_1, D_2, D_3 (the doubly charged particles of Figs. 25 and 2-7 are of the same size as the singly charged ones and thus distinguishable from them). If N_i denotes the true particle concentration at D_i, f_{iD_i} the fraction of particles with i charges at D_i, and N_i' represents the measured particle concentration at the voltage corresponding to D_1, then $N_1' = N_1 f_{1\,D_1} + N_2 f_{2\,D_2} + \ldots$*

The question is what to substitute for N_2, N_3 in order to obtain N_1. Depending on the size range and the shape of the size distribution different approaches can be taken. For instance, in the size range of interest to ACPL triply charged particles might be neglected, and one could follow procedures by Liu and Pui (1974) or the improved method of Cooper and Langer (1978). However, since highest accuracy is desired and programmable computing facilities were to have been on hand in the ACPL it is recommended that the more elaborate iterative procedure by Hoppel (1978) be applied. However, regardless of which of the computational schemes one selects, if a significant portion of the investigated size distribution is located beyond the upper size limit of the

*If measurements are made with the EAD which senses charges, not particles, the equation has to be modified accordingly ($N_k \rightarrow iN_i$).

EC, N_1, if near, but below that limit cannot be calculated since N_2', N_3' for D_2, D_3 are not available to approximate N_2, N_3. For the originally intended ACPL application, most size spectra of interest would have existed within the EC's range (which, if necessary, could have been extended upwards to some extent by reducing the flow rates).

b. Electrical Aerosol Analyzer

(1) Principle of Operation

The Electrical Aerosol Analyzer (EAA), another TSI product, Model 3030, uses essentially the same cylindrical high voltage condenser as the EC to size discriminate by electrical mobility; however, it differs from the EC in two important aspects:

- Aerosol particles are exposed to unipolar ions produced in a corona discharge. This leads to a higher charge level and associated increased number sensitivity, especially for the larger particles (100 to 1000 nm); but no charge equilibrium is achieved, and, therefore, the time of exposure to the charging region (and thus the flow rate) has to be controlled very carefully.

- A built-in electrometer measures the number of those particles (i.e., their charges) which are not deposited at the center electrode. Thus, a voltage scan produces a cumulative mobility spectrum from which a differential size spectrum is derived in the evaluation process. These features and associated air flows are shown schematically in Fig. 2-12. It is important to note that a charger sheath flow keeps the aerosol at a distance from the ion source in order to prevent formation of a wide charge distribution for a given particle size.

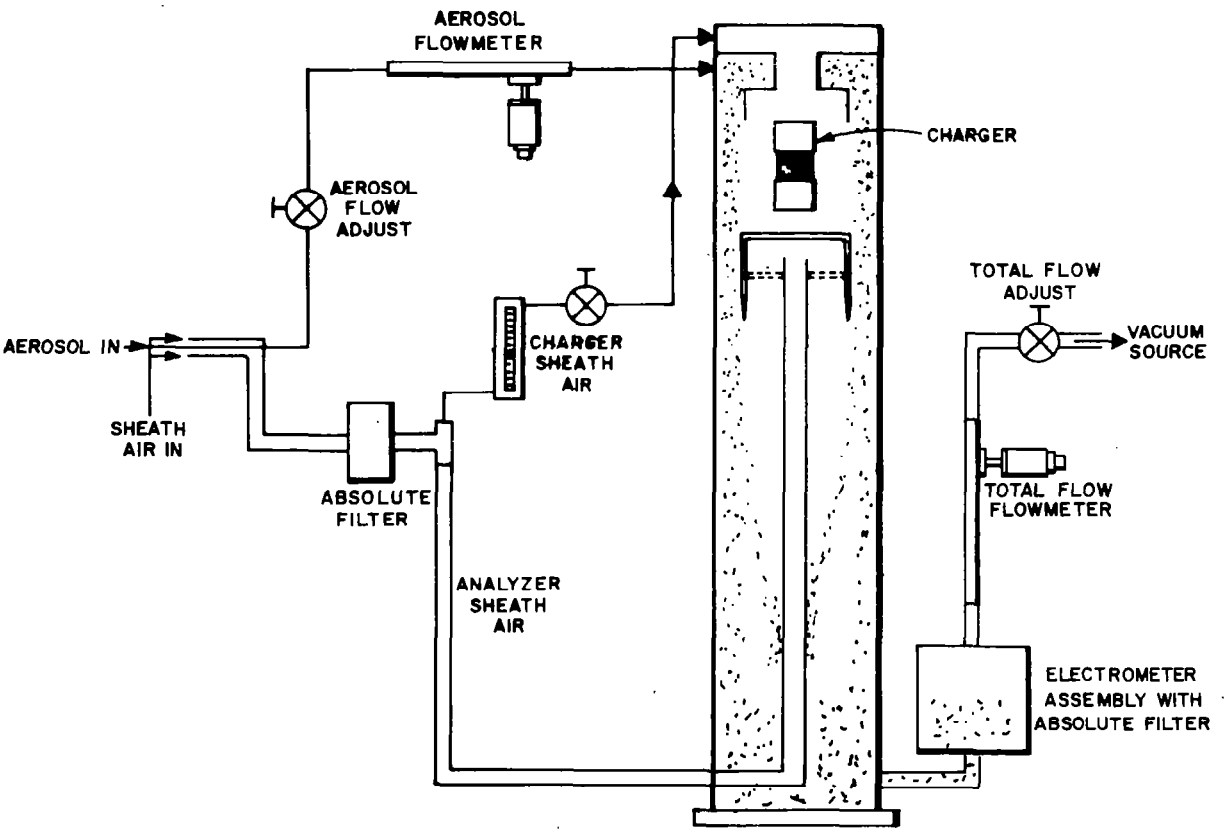

Figure 2-12. Schematic of TSI Model 3030 Electrical Aerosol Analyzer (EAA) [from Instrument Manual].

Detailed descriptions of the apparatus are given by the designers (Liu, et al., 1974; Liu and Pui, 1975).

(2) Special Problems

In the process of evaluating the EAA a number of comparisons with the EC provided the following information. With respect to the minimum particle concentration needed to obtain a signal, Fig. 2-11 shows that the EAA has some advantage over the EC, especially for particle sizes above about 100 nm. However, the values of Fig. 2-11 were obtained with the assumption of four size steps per size decade since the standard version is usually operated in that manner. Would one use, e.g., size intervals of 1/20 decade, as in the case of the EC at 2 ℓ min^{-1} flow, the EAA values of Fig. 2-11 would have to be moved up by a factor of 5, narrowing the EAA's advantage over the EC considerably.

While the higher number sensitivity of the EAA is helpful in many applications where particle concentrations are not very high, it also contributes to the lack in resolution through large size intervals. In order to determine the response of the EAA to a monodisperse aerosol, an experiment was conducted where the EAA sampled an aerosol of 91 nm latex spheres which had been passed through an EC for further narrowing of its size distribution (which also reduced and narrowed the small portion of doubly charged doublets - see III.D.3). Fig. 2-13 illustrates the input into the EAA in the form of a singlet and a doublet peak (triangles) as expected from the various EC experiments, and the actual response from the EAA. It clearly shows that the EAA cannot resolve a detailed structure such as the two peaks, and it also indicates that considerable broadening occurs. The same observation was reported by Vali et al.

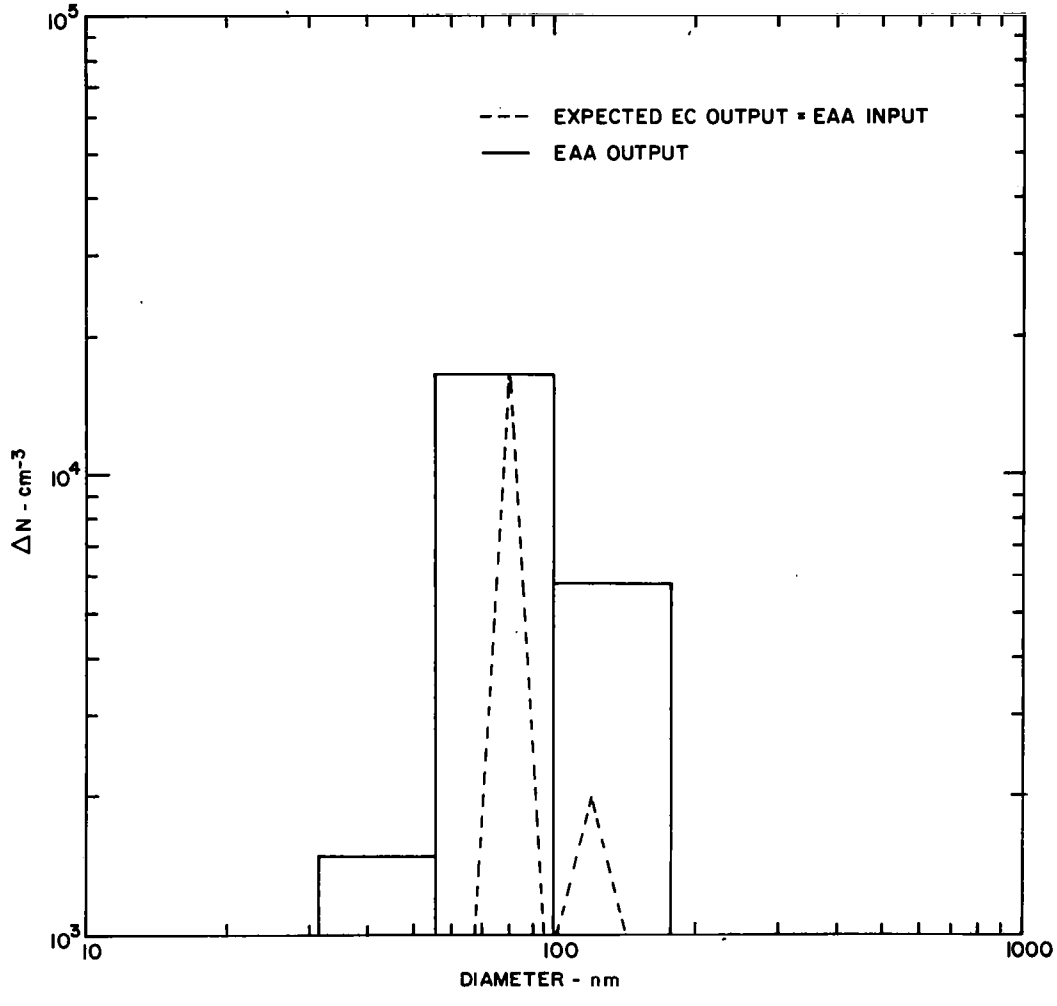

Figure 2-13. Response of EAA (solid line) to input with bimodal size distribution (dashed).

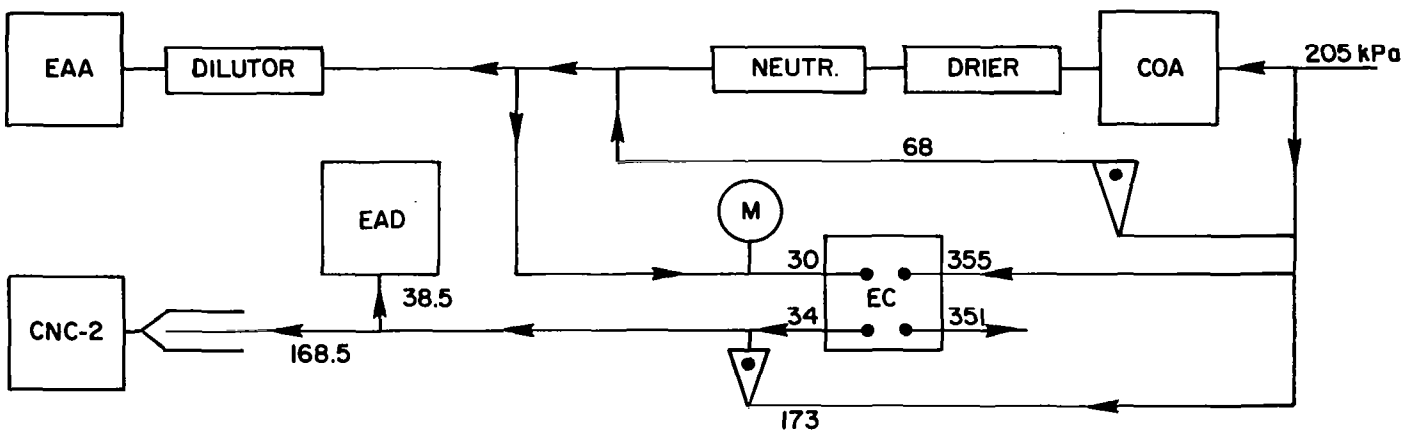

Figure 2-14. Flow diagram for EAA - EC/EAD comparison of polydisperse NaCl aerosol (numbers indicate flow rates in $cm^3 s^{-1}$; 205 kPa refers to input air pressure; M = manometer).

(1978) regarding similar experiments during the DRI - Univ. of Wyoming Workshop in Laramie. This effect probably stems from a rather broad charge distribution generated in the charging section of the EAA. No explicit data on how the charges are distributed for each particle size could be found in the literature, only average charge vs. size for various ion concentrations and residence times. While the EAA's resolution might be satisfactory for most applications involving polydisperse aerosols in the atmosphere or industrial environments, it is not sufficient for high precision work as proposed for ACPL.

Another drawback of the EAA regarding laboratory applications, and especially ACPL, is the high sheath air and sample flow rate which is twice the value needed for the EC.

In further comparative experiments during the joint DRI-Univ. of Wyoming Workshops, the particle concentration aspect of the instrument was examined. Two types of comparisons were made:

- Polydisperse salt aerosols were size-analyzed by the EAA and a EC-EAD, and the measured size distributions compared; the experimental set-up which also included a total particle counter (GE CNC-2) is shown schematically in Fig. 2-14. The dilutor upstream of the EAA was necessary because of the large difference in sensitivity between the EAA and the EC-EAD (see Fig. 210). Although the normalized size distributions coincided very well, the experiment had to be termed inconclusive due to a large discrepancy in absolute number concentration (EAA much lower) which had to be traced, in part, to unsatisfactory performance of the dilutor, but which may also have been related to problems of the EC; namely, to the uncertainty in the fraction of singly-charged particles

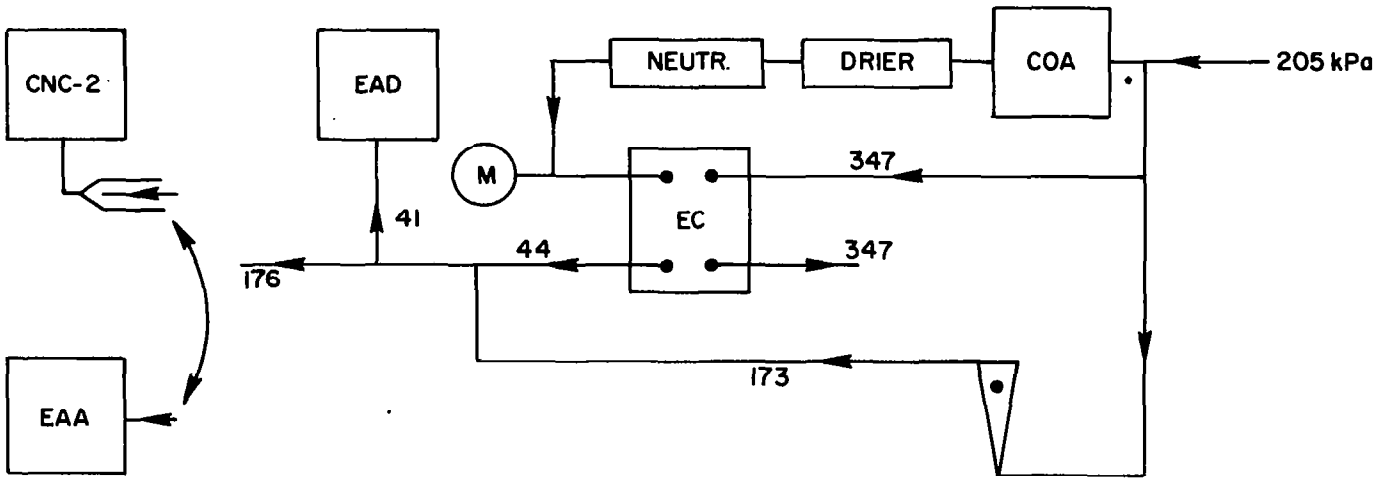

Figure 2-15. Flow diagram for EAA - EC/EAD - CNC-2 comparison with monodisperse NaCl aerosol (numbers indicate flow rate in $cm^3 s^{-1}$; 205 kPa refers to input air pressure; M = manometer).

or the width ΔDp of the passing fraction. It should be noted that CNC-2 and EAD measurements agreed within 5 to 10% with each other.

- The monodisperse output of an EC was measured by the EAD, a GE CNC-2 and the EAA according to the flow diagram of Fig. 2-15 (not sufficient flow could be generated to simultaneously feed the EAA and the CNC-2).

Particle Diameter (nm)	Particle Concentration (cm^{-3})		
	EC	CNC-2	EAA
30	5,300	5,300	7,400
50	17,700	14,700	22,000
70	24,900	22,500	37,000
90	28,300	26,000	49,000
110	25,000	23,500	33,000

This represents a better test for the EAA as it is essentially a comparison with the EAD (not the EC), a more basic measurement. As the above table indicates, the relatively good agreement of EAD and CNC-2 (which was checked periodically with a Pollak counter) suggests that the EAA did overcount by at least 50% over most of its range. Further comparisons are presented by Vali et al. (1978) which essentially led to the same conclusion.

2. Diffusion Battery

Characterization of aerosol size distributions is a special problem since: (1) typical aerosol size spectra span four to five orders of magnitude; (2) the best optical methods cover only the largest two of these decades; and (3) aerosol systems are dynamic in character, constantly evolving in response to events such as Brownian diffusion and coagulation. Since the 1940's when the first reliable aerosol counters

were developed, workers have been aware of the magnitude of this problem, as well as some possible solutions.

One of the earliest approaches to size spectra characterization is still one of the most reliable. Early workers in aerosol science were acquainted with the results of molecular physics and kinetic theory derived in the early part of the century (principally by Einstein); these give the inverse relationships between the size of a particle and its mobility while undergoing Brownian diffusion for particle sizes of order one mean free path or smaller. Therefore, by suitable data inversion techniques, one can infer particle size distributions by looking at the way in which the total aerosol count (measured by an Aitken counter) is decreased when the sample is forced to pass through some kind of duct or tube. Physically what takes place is that, due to the inverse relationship between size and mobility, the smallest particles in the distribution diffuse most quickly to the walls of the duct. While the mechanisms of adhesion of aerosol particles to surfaces are not very well understood, careful experiments have shown that detachment almost never occurs. Therefore, it is a relatively straightforward manner to incorporate the theory of diffusion mobilities and the boundary conditions or geometry of the duct into a partial differential equation, the solution of which allows prediction of the decrease in aerosol caused by diffusion to the boundaries.

It is now possible to obtain commercial "diffusion batteries" which basically provide the duct mentioned above, and aerosol sampling ports. When such a device is used together with a detector of the total count of the aerosol which has survived the diffusion process, the

resulting data can be inverted to give back the original size distribution of the aerosol particles. The DRI program has utilized the TSI 3040 Diffusion Battery, basically the same model intended for use in ACPL, together with a standard Pollak (Aitken particle) counter for aerosol counting. While use of this method is laborious (since up to 20 measurements must be taken to characterize one aerosol sample) other methods are relatively indirect and unproven. In addition, a diffusion battery which utilizes a Pollak counter as detector is probably more reliable than commercial differential mobility analyzers (e.g., the TSI Electrical Aerosol Analyzer) at small aerosol diameters (around 0.01 μm).

The diffusion battery, the DRI CFD chamber, and the University of Wyoming Electrical Aerosol Analyzer (EAA) were compared in a series of experiments during the University of Wyoming/DRI Workshop of September, 1977. Figures 2-16 through 2-20 show the results of five of these experiments, using bagged NaCl, H_2SO_4, and AgI aerosols (a sixth experiment is discussed in the section on the Photolytic Aerosol Generator). At least for the (very soluble) NaCl and H_2SO_4 aerosols, one would expect good agreement between the diffusion battery and CFD chamber; this is reflected in the results. The EAA, as expected, tends to come into agreement with the other two devices as size increases. It is noteworthy that this type of EAA-diffusion battery discrepancy has frequently been observed in sampling of ambient atmospheric aerosols, carried out by this laboratory in various field operations.

In general, the three devices related consistently to one another with the CFD chamber giving the lowest or nearly the lowest count at a

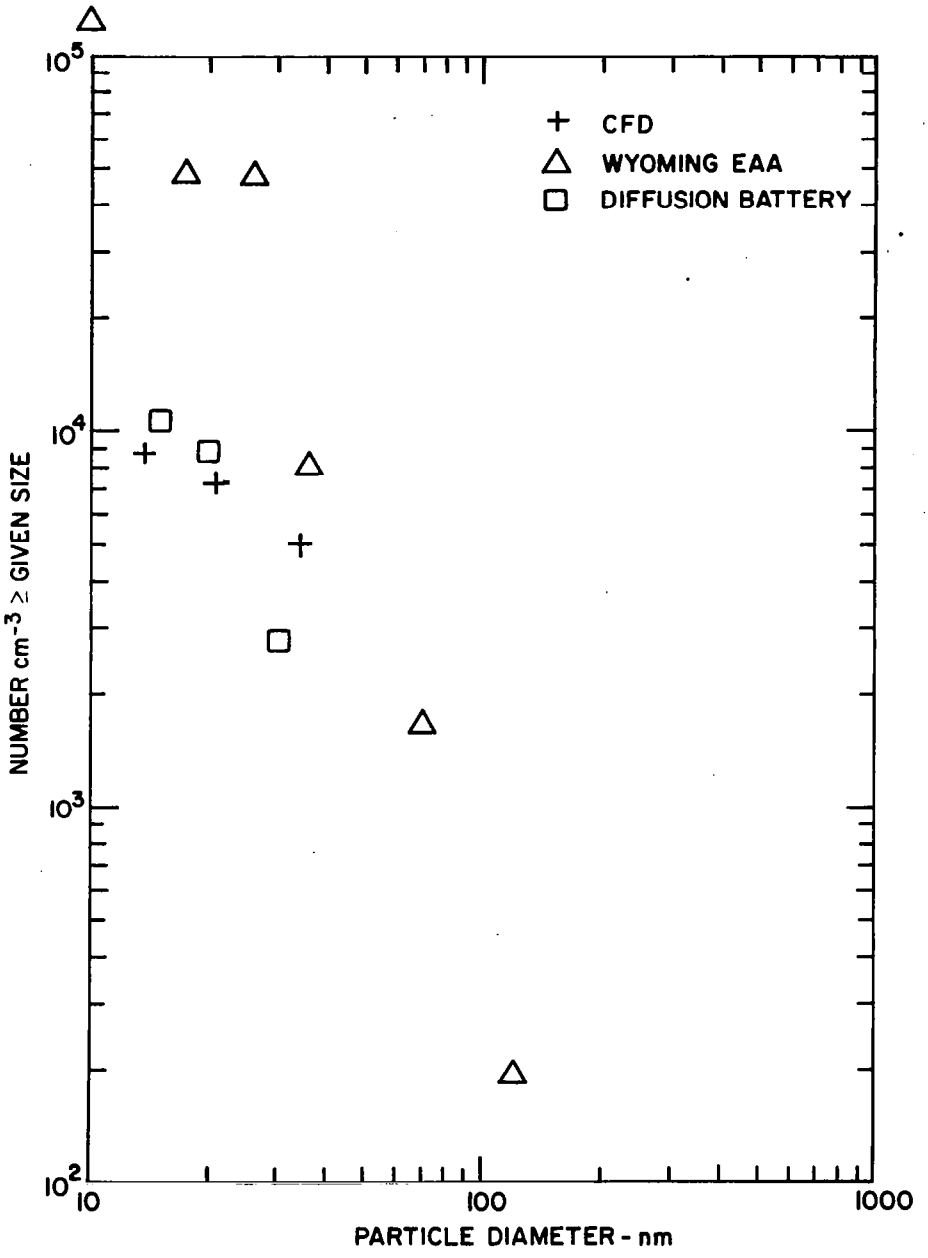

Figure 2-16. Cumulative number size distribution of bagged NaCl aerosol as measured with diffusion battery (DRI), EAA (Wyoming) and CFD chamber (DRI). Univ. Wyoming-DRI Workshop 1977, expt. 2.

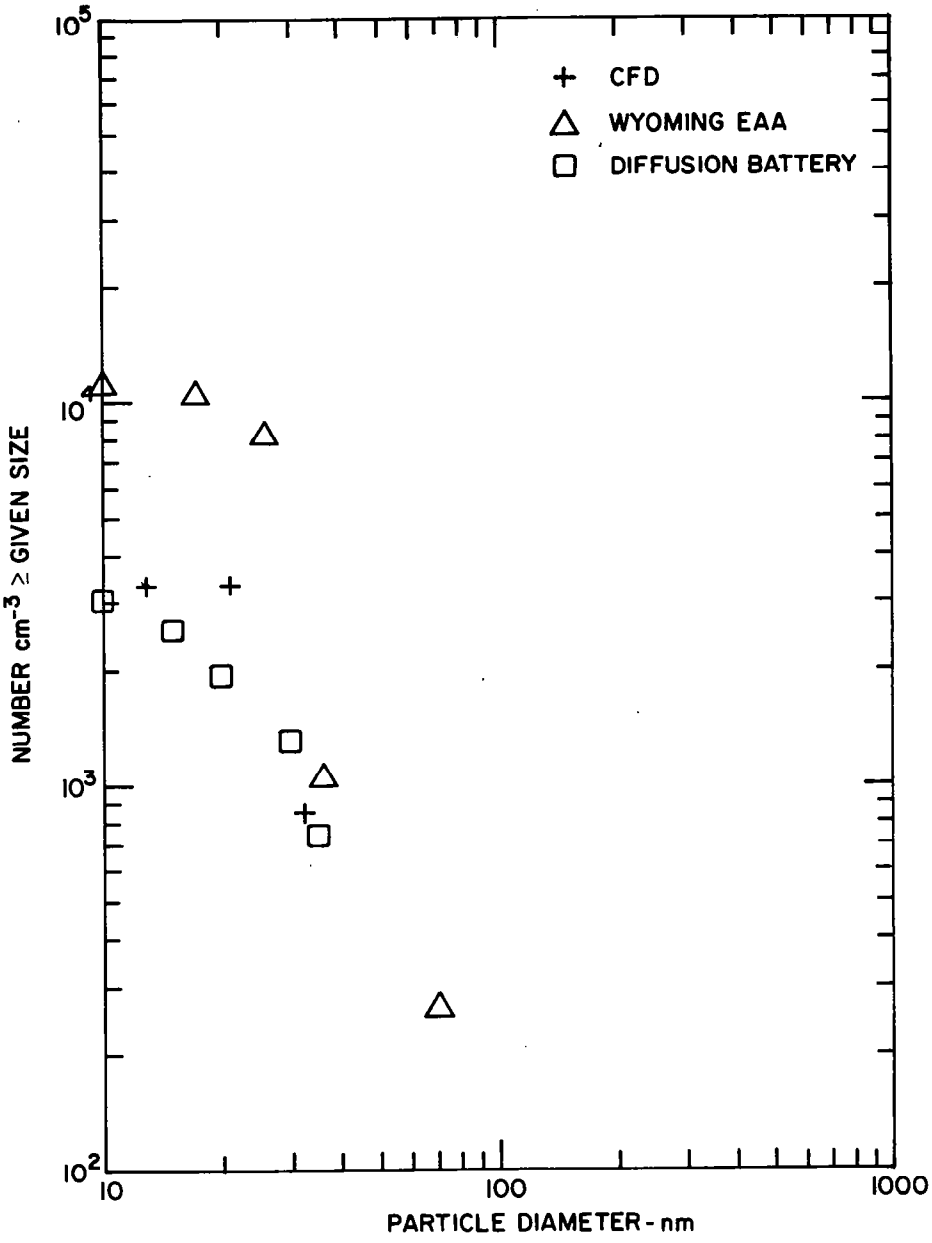

Figure 2-17. Cumulative number size distribution of bagged NaCl aerosol as measured with diffusion battery (DRI), EAA (Woming) and CFD chamber (DRI). Univ. Wyoming-DRI Workshop 1977, expt. 3.

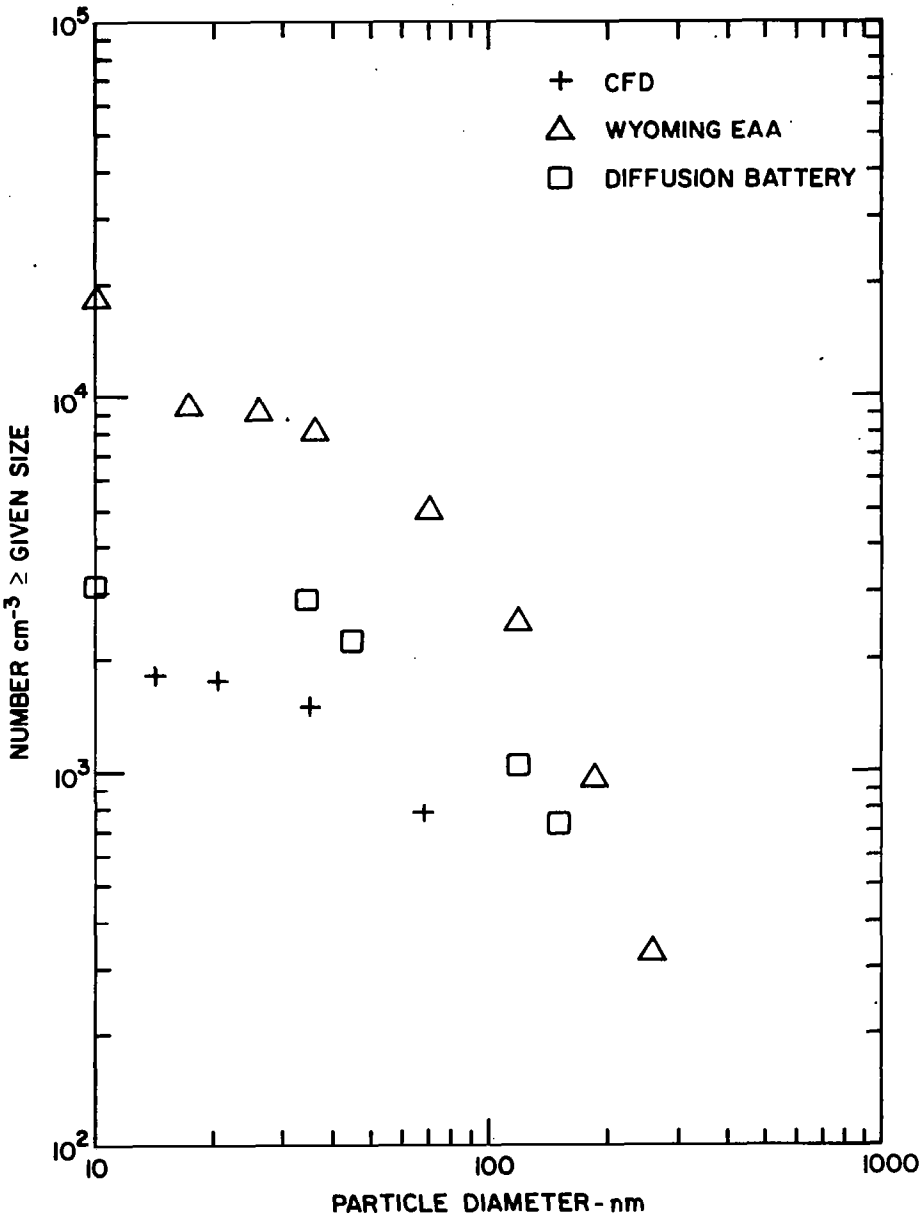

Figure 2-18. Cumulative number size distribution of bagged NaCl aerosol as measured with diffusion battery (DRI), EAA (Wyoming) and CFD chamber (DRI). Univ. Wyoming-DRI Workshop 1977, expt. 5.

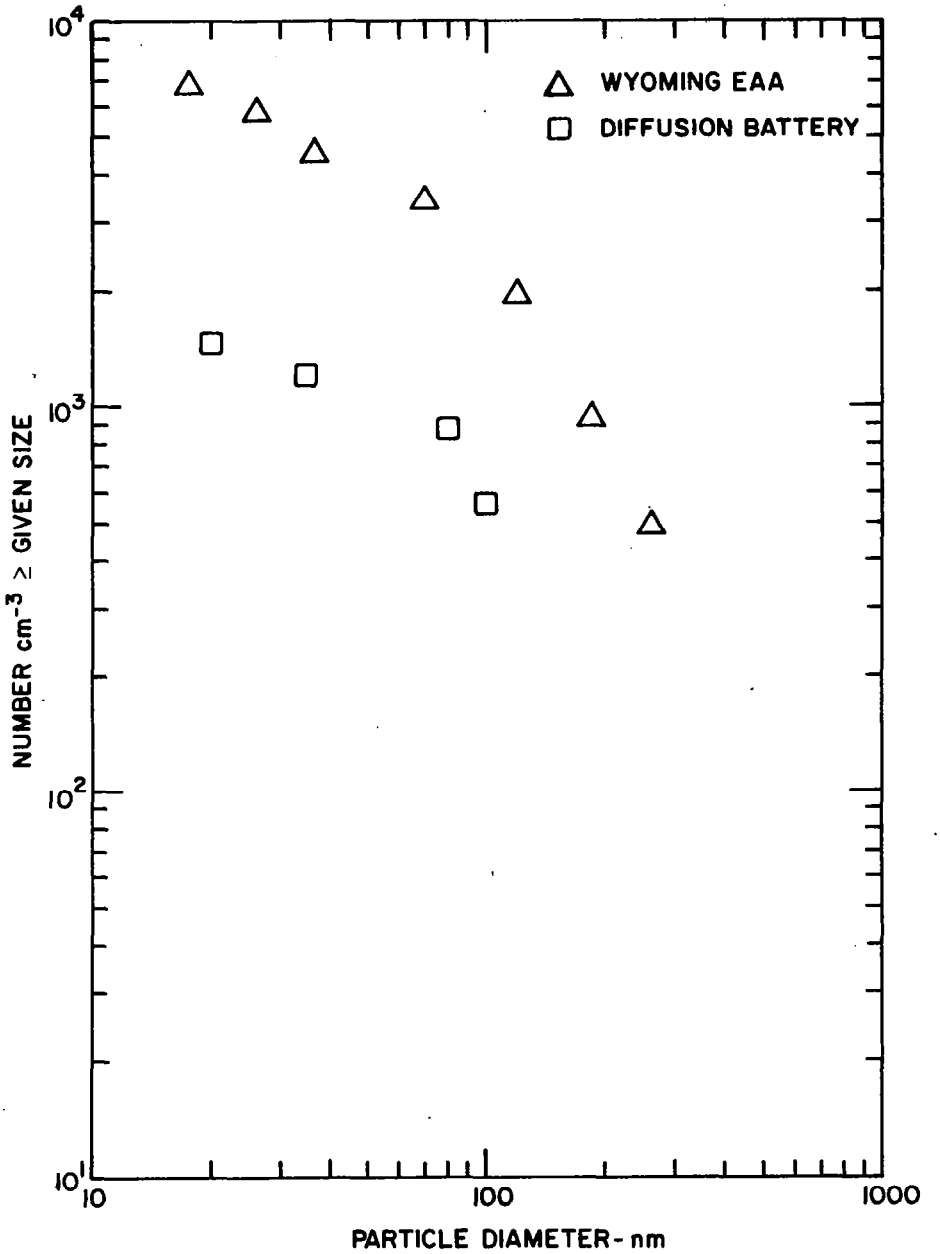

Figure 2-19. Cumulative number size distribution of bagged AgI-NH_4I complex aerosol as measured with diffusion battery (DRI) and EAA (Wyoming). Univ. Wyoming-DRI Workshop 1977, expt. 9.

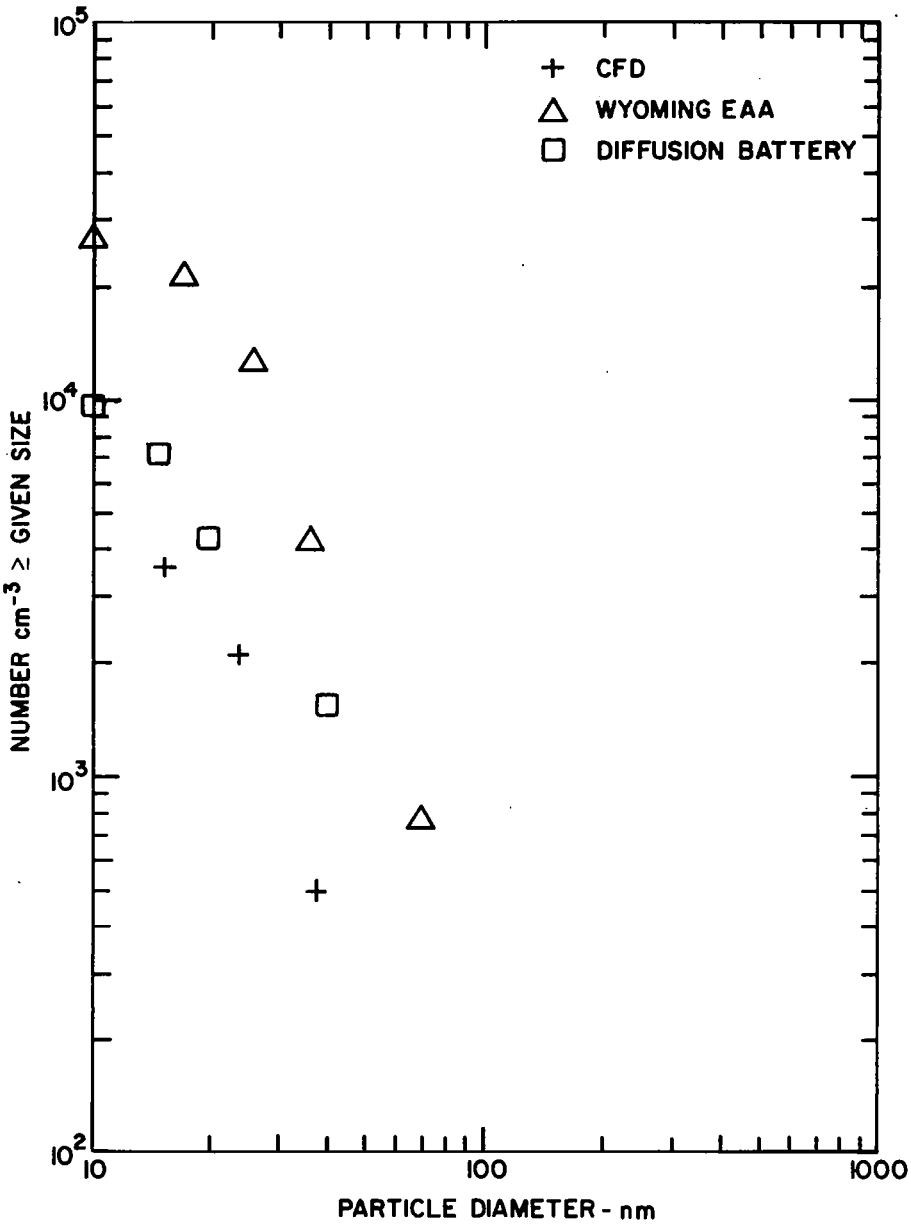

Figure 2-20. Cumulative number size distributions of bagged H_2SO_4 aerosol as measured with diffusion battery (DRI), EAA (Wyoming) and CFD chamber (DRI). Univ. Wyoming-DRI Workshop 1977, expt. 15.

given size, the diffusion battery reading about the same or slightly higher, and the EAA usually reading highest.

The TSI 3040 Diffusion Battery was found to suffer some disadvantages which probably prevent the user from realizing the full accuracy inherent in the diffusion battery method. The 3040 is an array of randomly-oriented screens, the mesh of which measures about 20 μm per side. This geometry is understandably resistant to description by an analytical model; the commercial devices were actually calibrated by experiment using monodisperse aerosols (Sinclair, et al., 1979). One may either use aerosol penetration nomograms, provided with the 3040, or a computer program (Sinclair, et al., 1977) for reduction of the data from the Model 3040, but in either case the technique is a sequential, "graphical stripping" process when one starts with a data point at the largest size and proceeds point-by-point to the smallest size. The actual penetration data are compared to the manufacturer-supplied calibration data at each point; note that a new calibration is required for each flow rate to be used. Each derived data point depends upon the results of the previous (next largest size) data point, so considerable opportunity exists for cumulative error to develop by the time the small-size data are finally extracted.

The reader may refer to Twomey (1975) for a qualitative description of the resolution and accuracy of a diffusion battery consisting of an array of cylindrical holes, a considerably more ideal situation than the Model 3040, and one amenable to analytical modeling. Twomey (op. cit.) has presented an inversion algorithm which is not subject to the cumulative error described above, but which may strictly only be applied

to diffusion battery geometries which may be analytically described. Very recently, Remiarz, et al. (1980) have modified this algorithm in order to apply it to the Model 3040. The result should be a significant improvement in this device - e.g., in its ability to resolve two monodisperse aerosols closely spaced in peak radius.

The basic accuracy specification of the Model 3040 is probably much worse than if the same device is used with Twomey's inversion scheme, or if a more ideal geometry is used with Twomey's method. In a brief computational experiment with data from the Model 3040, it was estimated that simple cumulative errors in the graphical stripping method could be as high as $\pm$25% (of the number concentration assigned to the smallest-size end of the inferred distribution). In the data shown in Figs. 2-16 through 2-20, every effort was made to keep such error to a minimum.

C. "HARD COPY" SAMPLE ACQUISITION

There are several reasons for acquiring actual physical samples of aerosol particles. Hard copy samples, first of all, serve as back-up in case of malfunction of real-time, on-board aerosol characterization equipment. However, as pointed out in Section II.B (Absolute Size Calibration), size verification is of utmost importance in order to assure validity of in-flight experimental results, even if pre- and post-flight terrestrial calibrations are carried out. Furthermore, it may be very advantageous to be able to retrieve additional information from particle deposits not otherwise available, e.g., particle shape which could be important in various respects; also chemical information or indications of particle generator problems could be obtained.

1. Methods of Investigation

The size of particles in question rules out any other method but electron microscopy and related investigative tools such as energy dispersive X-ray emission analysis. Most basic information needed for the ACPL experiments, e.g., size, number and morphology of particles can be obtained from straightforward electron micrographs. The two basic choices are scanning (SEM) or transmission electron microscopy (TEM).

The SEM offers the advantages of a pseudo three-dimensional appearance of the sample with great depth of focus and no particular requirements with regard to sample substrate. On the negative side, there is insufficient resolution for most of the CCN particle size range of interest to ACPL. Depending on the particular instrument, the resolution is on the order of 10 nm or somewhat better; thus for particles about 50 nm and larger, a SEM analysis may be of value. Fig. 2-21 illustrates a case of that type where 75 nm NaCl particles (nominal diameter from the EC) were deposited on a 200 nm pore nuclepore filter. While it seems quite possible to achieve a sizing accuracy (on well-focused micrograph) on individual particles of $\pm$5% an additional problem is caused by the gold coating applied to prevent charge build-up under the electron beam. This coating typically adds 10 to 20 nm to the diameters of the particles but, on this program, it was not possible to determine how reproducible in thickness this coat can be applied from sample to sample - 10% is an estimate based on the limited number of samples taken during the course of this project.

The major advantage of examining CCN by TEM lies in its much better resolution - about an order of magnitude higher than the SEM. On

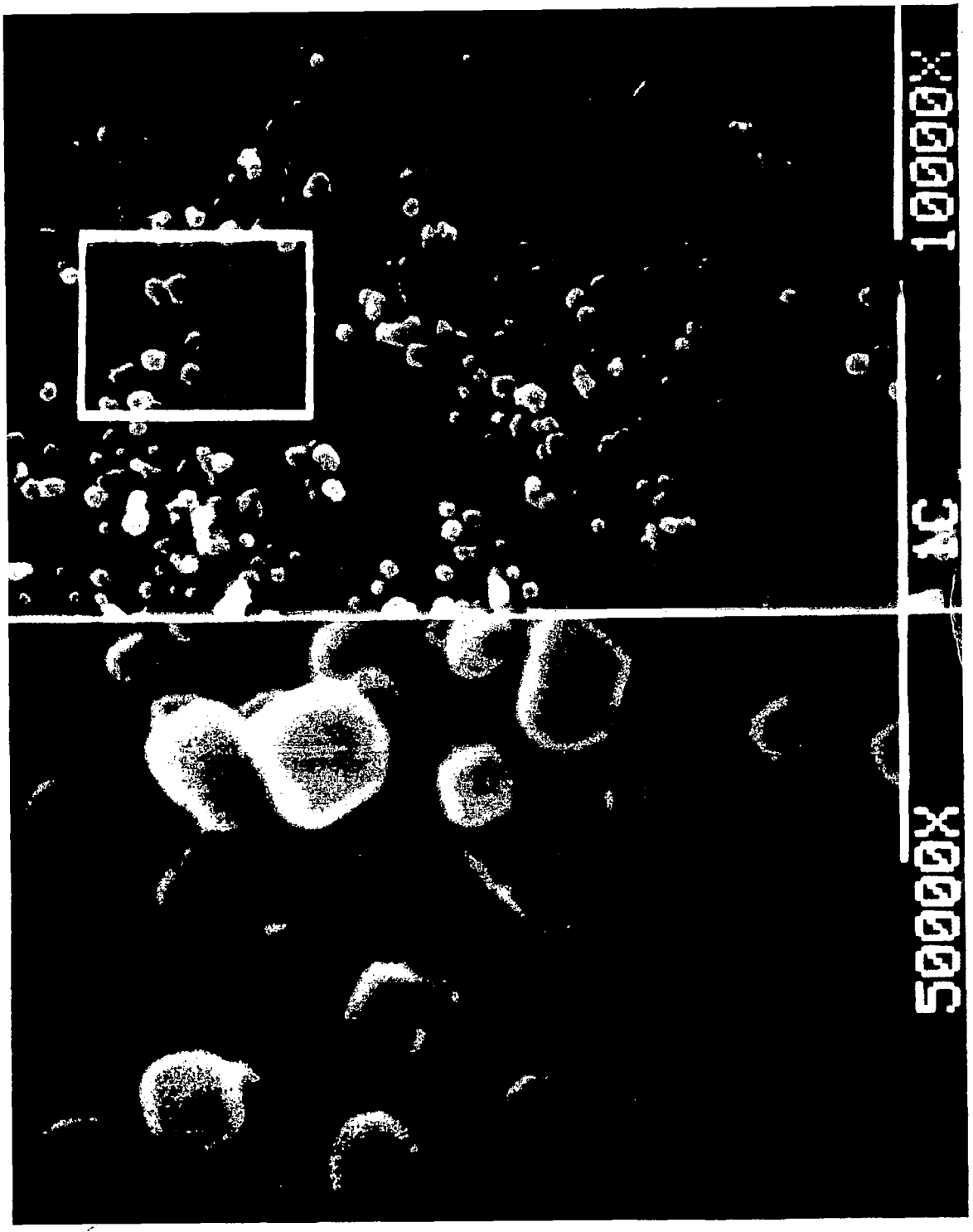

Figure 2-21. Scanning electron micrograph of 75 nm diameter (nominal) NaCl aerosol sample on 200 nm pore nuclepore filter. (Many larger, multiply charged particles are present, while the majority of 75 nm particles are trapped inside pores).

the other hand, the TEM method only produces what amounts to shadowgraphs, and any information on the third dimension has to be obtained by oblique shadowing. A further difficulty stems from the need for a very thin (electron transparent) substrate that is not only mechanically weak, but also is often unable to remove the heat generated by the electron beam fast enough to prevent damage to the sample. Preparation of samples for TEM also requires more delicate handling and often tedious procedures to achieve the most informative shadowing. However, the amount of material deposited in the shadowing process generally does not add significantly to the size of the deposited particles; otherwise, an estimate of the size increase can be obtained through careful examination of the micrographs.

Since the study of particle samples by SEM and TEM has become mostly a routine operation by specialized laboratories, only a low priority was assigned to generating electron micrographs. In those instances during the present investigation where particle samples had to be examined at high magnification, an ISI Miniscan III SEM accessible to the DRI investigators was used.

2. Preparation of Samples

The above discussion on electron microscopy implied that it would be most advantageous to prepare aerosol samples such that they could be investigated with either instrument, SEM and/or TEM. It was therefore necessary to review methods of sample preparation with this objective in mind.

a. Particle Sample Substrates

Sample preparation consists, in principle, of bringing a representative population of particles in sufficient numbers onto a surface

suitable to support the sample during investigative procedures. While such a substrate has the primary function to hold the particles in place, which mainly requires a material not reactive with the sample, it also has to be compatible with the conditions in the SEM or TEM (preferably both). Ideally, a substrate would also serve as the sampling surface which would greatly facilitate sample preparation and reduce the risk of sample alteration by loss or contamination during transfer onto the substrate.

For work with TEM, only thin films of carbon, silicon monoxide or similar materials mounted on standard 3 mm specimen screens can be used, whereas SEM accept most anything as long as the surface can be made conductive. For the limited amount of SEM work performed on this project, Nuclepore filters were used which have a particularly smooth surface, very low background contamination and could also serve as aerosol samplers.

b. Aerosol Precipitation Devices

Methods suitable to remove aerosol particles in the 10 to 100 nm size range from the suspended state onto a collection surface are based on Coulomb, thermophoretic and inertial forces. Instruments using these forces to collect aerosol samples - electrostatic precipitators, thermal precipitators, centrifuges and filters - were taken into consideration for obtaining hard copy aerosol samples on the ACPL.

In addition to the obvious criterion of providing representative samples, the selection of the most suitable sampling device has to be based on several other conditions. Due to the multitude of instruments sampling from a relatively limited aerosol source, it is important that

the sample can be acquired efficiently with little waste. In principle, from a statistical viewpoint, a sample containing as few as 10^4 particles could be acceptable. However, in order to study it by SEM or TEM, there should be at least a minimum particle concentration on the substrate of 1 μm^{-2}; this would concentrate the total sample to an area of only 100 x 100 μm^2 which is of the order of one mesh of a TEM specimen grid. This clearly illustrates that a much larger sample is required to reduce the risk of loosing the sample through substrate breakage or accidental local contamination; also, it would be difficult to concentrate a sample on an area that small (except with jet impactors which are unsuited for our size range).

Thus, it appears that the area represented by a TEM specimen grid (0.3 cm diameter) is the smallest practically acceptable sample. Combined with the postulated minimum particle number density on the substrate, this translates into a sample requirement of 10^7 particles. Assuming that aerosol of the final dilution* is to be sampled (i.e., 100 to 1000 cm^{-3}), at least 10^4 to 10^5 cm^3 (10 to 100 ℓ) aerosol would have to be ingested by the particle collector in a time period not to exceed normal experiment duration ($\sim$1000 sec), unless sampling prior to final dilution can be justified.

*Since it is anticipated that test aerosols in the ACPL are diluted in two stages from the original high concentration off the generator to a final particle concentration in the range of 100 to 1000 cm^{-3} for use in cloud chambers, a choice exists as to where (i.e., at what concentration) hard copy samples should be withdrawn. Obviously, one should aim for sampling on the final dilution rather than to assume a high concentration sample to be representative; nevertheless, the need to obtain samples from high concentration aerosol may arise under certain conditions.

In order to determine whether the above mentioned candidate collectors are compatible with the sampling requirements just developed, it is necessary to briefly examine the collection characteristics of these devices.

(1) Aerosol Centrifuges

In concept, aerosol centrifuges consist of an annular or helical channel through which the aerosol is passed in a slow laminar flow while the whole annulus or helix rotates about its axis at several thousand rpm; thus, by design, particles settle along the whole channel length at positions governed by their size, density and initial position at the inlet. This spectrometric feature is particularly advantageous where evaluation is not performed by EM study of individual particles and where copious amounts of aerosol are available. However, in the present application, it would be very difficult to achieve a particle coverage suitable for SEM or TEM work considering that tens of square centimeters of deposition surface are available. A large number of specimen grids would have to be placed at intervals on the deposition surface, but with risks of missing an important deposit in between grids. Therefore, it was felt that current designs of centrifuges would not be suitable for tasks on ACPL.

(2) Filters

Two types of filters were considered which had been used by other investigators in conjunction with electron microscopy. Nuclepore filters (NF) consist of a polycarbonate foil of 10 μm thickness that contains randomly distributed cylindrical holes of fairly uniform size (with a wide range of hole sizes to choose from: 50 nm to 10 μm). The membrane

filters (MF) on the other hand, are composed of a fiber-like cellulosic matrix about 150 μm thick; they also are available in a range of nominal pore sizes although the pore dimensions are not as well defined as in the NF case. Both filter types have similar flow resistance (depending on pore size), but the main differences between the two types from the user's standpoint are the surface characteristics, the retentivity and the mechanical strength. NF have a very smooth surface most suitable as a substrate for SEM work whereas the network structure of the MF seriously impedes detection and assessment of deposits. A further advantage of NF is their superior mechanical strength (tear resistance) over MF. With regard to particle retention (a most important parameter) however, NF does not perform as well as MF, especially in the particle size range of interest to ACPL (see the detailed study by Spurny, et al., 1969).

Before going into further details, the sampling conditions and requirements as they apply to the filters have to be examined. In order to be able to handle the filter and to transfer the sample onto a TEM specimen grid, a filter area somewhat larger than the grid should be available - typically on the order of 0.5 cm^2. Recalling that we need at least 1 particle/μm^2, the necessary sample volume containing 5×10^7 particles would be 50 to 500 ℓ for aerosol concentrations of 1000 or 100 cm^{-3}, respectively. If one postulates that sample acquisition should not last longer than about 1000 seconds, the required filter face velocities would be 100 or 1000 cm s^{-1}, respectively.

Consulting the diagrams of Spurny, et al. (1969), one finds that these flow requirements can, at best, only be fulfilled marginally by NF

for the case of the higher particle concentration. If the pores are large enough to allow a high flow rate, the particles do not diffuse to the filter surfaces in the short time available, whereas pores small enough for diffusive capture of CCN-size particles would prevent the air flow from reaching the needed rate. For instance, the sample exhibited in Fig. 2-21 was collected by using a 4 cm s^{-1} face velocity which, as our measurements showed, provided total retention in the NF, though only to a small degree on the filter face, but mostly inside the 200 nm pores (the good surface coverage was possible only because of a particle concentration of over $10^5 cm^{-3}$ in the aerosol). Operation of the filter at more than 20 times higher speeds would have caused passage of possibly half the particles.

MF, on the other hand, offer a more efficient way to capture particles as they are more than ten times thicker than NF; also, the air takes a more tortuous path through MF giving the particles a better chance to diffuse to the fiber surfaces even at face velocities that would meet our sampling requirements.

Thus it appears that there are two non-ideal possibilities for employing filters for hard copy aerosol samples:

(1) NF could be used only for sampling undiluted aerosol, and even then part of the sample would most likely deposit inside the holes such that a direct evaluation by SEM would not yield a representative picture. Therefore, the sample would have to be transferred to a different substrate, preferably a TEM grid, by slowly dissolving the NF on top of the new substrate in chloroform vapor according to tried recipes (e.g., Frank, et al., 1970; Chatfield, et al., 1978). This procedure

removes one major reason for using NF, its capability to act as both collector and viewing substrate. A further disadvantage, as Frank, et al. (1970) point out, stems from the fact that particles trapped in the filter's holes (which are much longer than wide) in the three-dimensional arrangement will be projected onto the new substrate in two dimensions, forming spots of very high particle density at the hole locations; this agglomeration may cause difficulties in the evaluation.

(2) By using MF of proper porosity, one could obtain specimens of the dilute aerosol; however, caution has to be applied when interpreting the transferred sample: motion of the particles during dissolution of the 150 μm thick filters may lead to some coagulation depending on the number densities involved. Chatfield, et al. (1978) indicate that when using identical transfer procedures NF did not cause this problem while MF had to be rejected because the sample was too much "rearranged" after the transfer. Although, their case was somewhat different as they studied fibers which did not enter the pores of the NF.

Weighing the two possibilities (partly based on literature, partly on our own experiments), it seems at this point that the MF would be the better sampling medium although, in the course of this project, only NF were used for their convenience in SEM work. A final decision would require a series of additional experiments which could not be performed in the framework of the present program.

(3). Thermal Precipitation

Thermophoresis, the motion of particles in a gas in the direction opposite to a temperature gradient depends on particle size and material, carrier gas and temperature gradient. Theory and utilization of

this effect have been described in the literature (see, e.g., Fuchs, 1964). While there are still numerous discrepancies between theory and observation, for the present discussion it is sufficient to indicate that the thermophoretic velocity, v_T decreases only about 20% with an increase in particle size from 10 to 100 nm. As a guideline, we select as an average value $v_T = 0.2$ cm s^{-1} for a temperature gradient of 1000°C cm^{-1}. Since v_T is proportional to the temperature gradient, it would seem simple to obtain a high velocity by merely increasing the temperature difference between the cold collection plate and the heated area on the opposite side of the sample air stream. However, the limitations are (1) for the cold collection plate that its temperature be high enough to prevent particles from deliquescing and (2) for the hot area that it would not thermally alter the collected particles (e.g., decomposition, evaporation). This immediately suggests a further constraint, the dependence on the substance the particles consist of. Another limitation for the hot area is given by the condition that the cold plate should not be warmed by radiation from the heated parts. Increase of the temperature gradient can also be achieved by narrowing the gap between hot and cold plate; however, practical considerations put the limit in the vicinity of 0.05 cm.

By selecting a hot plate temperature of a moderate 150°C in order not to damage thermally delicate CCN, such as $(NH_4)_2SO_4$, a temperature gradient of about 2000°C cm^{-1} can be established which results in $v_T \sim$ 0.5 cm s^{-1}. Since the sample air flow can only be parallel to the cold collection plate v_T essentially determines the density of the deposit, while the sample flow rate mainly governs the area covered by the

sample, although its magnitude does have some secondary effects on the deposit density. As a result, it is evident that, v_T being one to two orders of magnitude less than the face velocity of the above discussed filters, the thermal precipitator cannot compete in the sampling of diluted aerosol. Thus it could play a role in the ACPL only where particle densities are of the order of $10^5 cm^{-3}$ or more.

One advantage of the thermal precipitator is its potential to produce a deposit of very small dimensions with correspondingly small flow rate. For instance, Binek (1965) designed a thermal precipitator for exposure of just one TEM grid with a flow rate of only 0.1 $cm^3\ s^{-1}$. On the other hand, this does raise questions regarding diffusional losses in sampling lines.

4. Electrostatic Precipitation

Basically, all electrostatic precipitators (EP) operate on the same principle of charging the particles in order to cause them to move in an electric field towards a collection surface. In some designs, the same field is used to charge the particles and precipitate them (e.g., Morrow and Mercer, 1964), while other models have separate charging and precipitating fields. It is essentially the same procedure used in the EAA to size discriminate particles, a fact that already points to a potential problem of the EP: since the sample air flow has to be more or less parallel to the collection surface, i.e., perpendicular to the electric field, particles of different size are precipitated at different locations on the collection surface. In order to achieve a uniform representative aerosol particle sample distribution on a TEM grid, special design efforts had to be applied. An example of such an

advanced sampler was described by Liu, et al. (1967) while the commercial version of the device, TSI model 3100, was used in the course of this project. The essential novel idea of the designers was to pulse the precipitating field such that it is off for three seconds and on for 1.5 seconds; the effect is that the particles (which were being charged prior to entering the precipitating field) fill the whole area of the field in the off period and precipitate everywhere in the field area while the voltage is on. Sample flow velocity ($\sim$10 cm s^{-1}), length of precipitating area (17 cm), voltage (4200 V) and gap between electrodes (0.8 cm) were matched to achieve best results. The designers determined experimentally that the somewhat size dependent collection efficiency (e) ranged from about 0.5 for 10 nm (extrapolated) to 0.8 for 3 μm particles, the losses occurring mainly in the charger and partly due to uncharged particles.

Again, we need to know the density of the particle deposit (N_s) as a function of sampling duration (t) and aerosol density (N_a). Since during the voltage pulse all particles between the electrodes (distance h) are precipitated, the density due to one pulse $N_s' = N_a \cdot h \cdot e$ and $N_s = N_a \cdot h \cdot e \cdot f$, where f denotes the frequency of voltage pulses (0.22 s^{-1}). For N_a = 1000 cm^{-3} (final dilution) and 1000 seconds of sampling $N_s \sim 10^5 cm^{-2}$ or three orders of magnitude short of the required 1 μm^{-2} - a result very similar to what thermal precipitation offers which is quite plausible since the deposition velocity in the EP is also only of the order of 1 cm s^{-1}, a value that could not be changed drastically by a different design. This clearly means that the electrostatic precipitator, as its thermal counterpart, could be used on the ACPL only for

sampling undiluted aerosol.

5. Concluding Remarks on Hard Copy Sampling

In the above review of sampling devices, the question was mainly whether a particular technique could furnish a sample in the allotted time, and it has become quite clear that the membrane filter method has to be given first preference on that account alone - the other devices could only be used to sample aerosols prior to final dilution.

There are, however, other points to be considered, as, e.g., handling, risk of contamination, and weight.

With respect to handling, it is again the filter that ranks highest if in-flight procedures are the decisive factor since it is possible to package each filter in a holder that can be connected very easily to sampling lines. The other sampling methods all require insertion and retrieval of TEM grids into and from the devices for each experiment, an operation requiring great care and concentration. Post-flight handling of the filters, of course, would also involve TEM grids, but a terrestrial laboratory offers many advantages that contribute to reducing the risk of failure.

The probability of contaminating filters enclosed in individual holders is negligible during flight and experimentation. TEM grids, on the other hand, could suffer from contamination while being handled in flight. The one advantage, however, that TEM grids have over filters is the possibility to inspect and preshadow them before flight. In contrast, filters, especially MF, can only be examined for flaws on the surface while the inner structure can only be appraised destructively on a spot-check per batch basis. The transfer of sample from filter to TEM

grid also provides a chance for contamination, though in the terrestrial laboratory it is easier to devise precautionary measures.

With respect to weight limitations, the filter system would have an advantage, though the weight would be proportional to the number of anticipated samples. If carefully engineered, thermal and electrostatic precipitators designed according to Binek's (1965) miniaturized versions could possibly be kept quite light.

The discussion on hard copy sampling so far implied that only solid aerosols were to be used, and our experiments concentrated on this type of aerosols. However, it had always been planned for the ACPL to conduct experiments with H_2SO_4 aerosols, the particles of which remain liquid even at low humidity. Since the size of these sulfuric acid droplets depends on humidity, preservation of samples is considerably more difficult, especially if preparation for electron microscopy is involved. One should contemplate use of encapsulation schemes such as the one applied by Phalen, et al. (1975), on cigarette smoke, and Ho, et al. (1979) on NaCl solution droplets. The question is whether an encapsulating (or fixing) agent can be found that is compatible with H_2SO_4 and meets toxicity standards set for ACPL by NASA. This leads to the question of whether the encapsulation could be carried out after sampling on filters or TEM grids. Due to the preliminary nature of the present investigation, it was not possible to perform any experiments on this topic.

III. AEROSOL GENERATION

In order to cover a broad range of conditions in ACPL tests of cloud condensation models, CCN of a wide variety of properties were deemed necessary. Soluble, insoluble and hydrophobic particles were the main categories as defined by their interaction with water substance. As representatives of the water soluble CCN, NaCl, $(NH_4)_2SO_4$ and H_2SO_4 were specified while, for the two other types, no particular substances had been decided on at the outset of this program.

Aerosol generation techniques and associated problems are very much dependent on and tied to the materials being used to form the particles. The following chapters describe evaluative experimentation with the various generation methods judged suitable or promising for application with the particular types of CCN on the ACPL. The first case is the photolytic system for producing H_2SO_4 aerosol via gas-to-particle reactions. This scheme represents an interesting alternative to aerosolization by pneumatic atomization which is the subject of the second chapter. Subsequent chapters are devoted to the formation of, and experiments with, hydrosols of water insoluble particles (which, again are aerosolized by atomization), and to the application of thermal methods for generating certain insoluble and hydrophobic aerosols. The fifth chapter deals with techniques for shaping size distributions, mainly to achieve a high degree of monodispersity.

A. PHOTOLYTIC AEROSOL GENERATOR (PAG)

When this project was initiated, the PAG was a prime contender for ACPL particle generation due to the conceptual simplicity of photolytic

production of H_2SO_4 and the potential that sulfuric acid aerosols generated in that manner could best simulate anthropogenic aerosol. However, as indicated in the introduction, it became necessary, as the program progressed, to redistribute the levels of effort in favor of the atomizer. Thus, the originally intended extensive study of all pertinent parameters had to be reduced to an investigation of a rather exploratory character yielding mainly qualitative results.

While it never was a goal of this study to contribute to the elucidation of the mechanisms leading to the formation of sulfuric acid aerosol, existing concepts served as a guide in interpreting some of the results obtained in the present investigation.

Considerable work carried out under other sponsorship* (see Lamb, 1978 and 1979) contributed to this study, mainly in the form of a gas and humidity delivery system (which controls the input into the PAG) and experience gained in related experimentation with longer wavelength UV (λ>300 nm). While that gas delivery system will not be described here, the PAG input values will be discussed.

In conformance with this contract, the final PAG model developed in this study (Model D) represents the deliverable item. The first section below describes how this final version evolved from the original model and points to the rationale for the various changes in design. In order to facilitate comparisons, performance data of all versions are presented and discussed in Section III.A.2. A brief description of the SO_2 stripper, Section III.C, has been incorporated in this chapter since this device is mainly thought of as an accessory to the PAG.

*Southern California Edison Company.

1. Design Considerations

In order to arrive at an initial "baseline" design, the following factors were taken into consideration. Simplicity and an obvious aim for compactness and light weight called for restriction to SO_2 as the only ingredient in addition to readily available air (including water vapor).

Previous experience had indicated that copious aerosol production in such a system required the use of short wavelength UV radiation (λ<300 nm). Thus, the availability of small germicidal lamps (G.E. No. G8T5, 1.5 cm diameter and 26.6 cm active length) tentatively determined the approximate dimensions of the initial PAG model. Off-the-shelf lamp and reflector assembly suggested a configuration of four lamps clustered around a cylindrical reaction chamber of about 10 cm in diameter and 30 cm in length (see Figures 3-1 and 3-2). Due to its excellent transmissivity in the short UV (see Figure 3-3), quartz was used as chamber material and conical ends with 1/4 inch connector nipples were affixed to the 10 cm diameter quartz tube.

This one-piece, all-quartz design of the PAG chamber was used for many of the measurements which will be discussed in the next section. The advantage of this version (Model A) was its freedom from leaks and from contamination by other materials. However, its main disadvantage was the impracticability of altering the geometry. For instance, it was suspected that turbulence inside the quartz chamber was the source of output instabilities, and thus, based on auxiliary tests, a flow straightener was to be installed. Since this was not possible in the original one-piece construction, an alternate design had to be sought

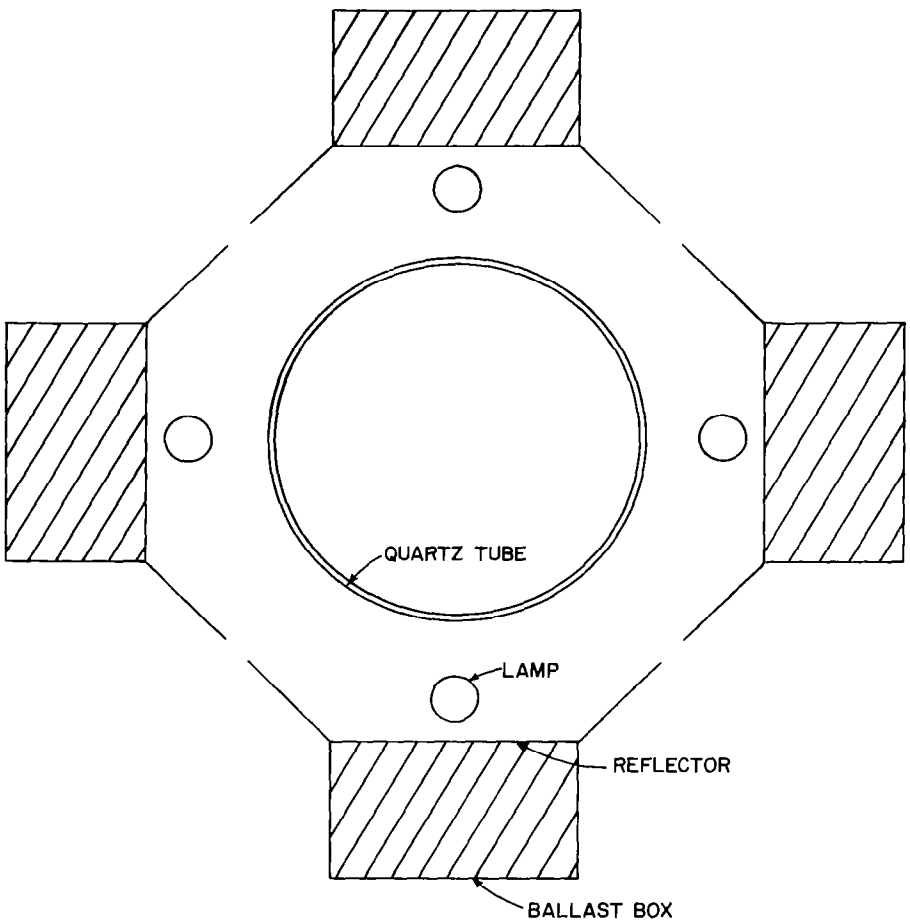

Figure 3-1. Cross-section of photolytic particle generator (Models A,D).

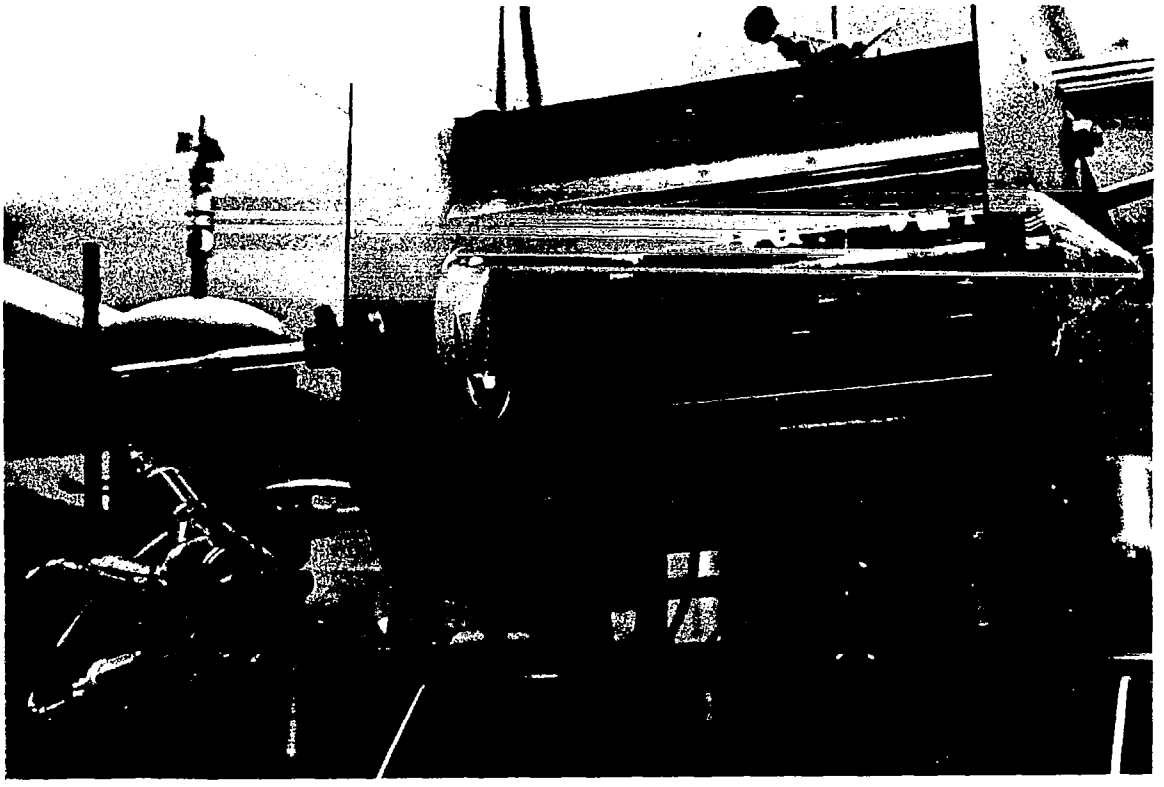

Figure 3-2. Photograph of photolytic aerosol generator (Model A). One of the four lamps was removed to show the horizontal quartz irradiation chamber.

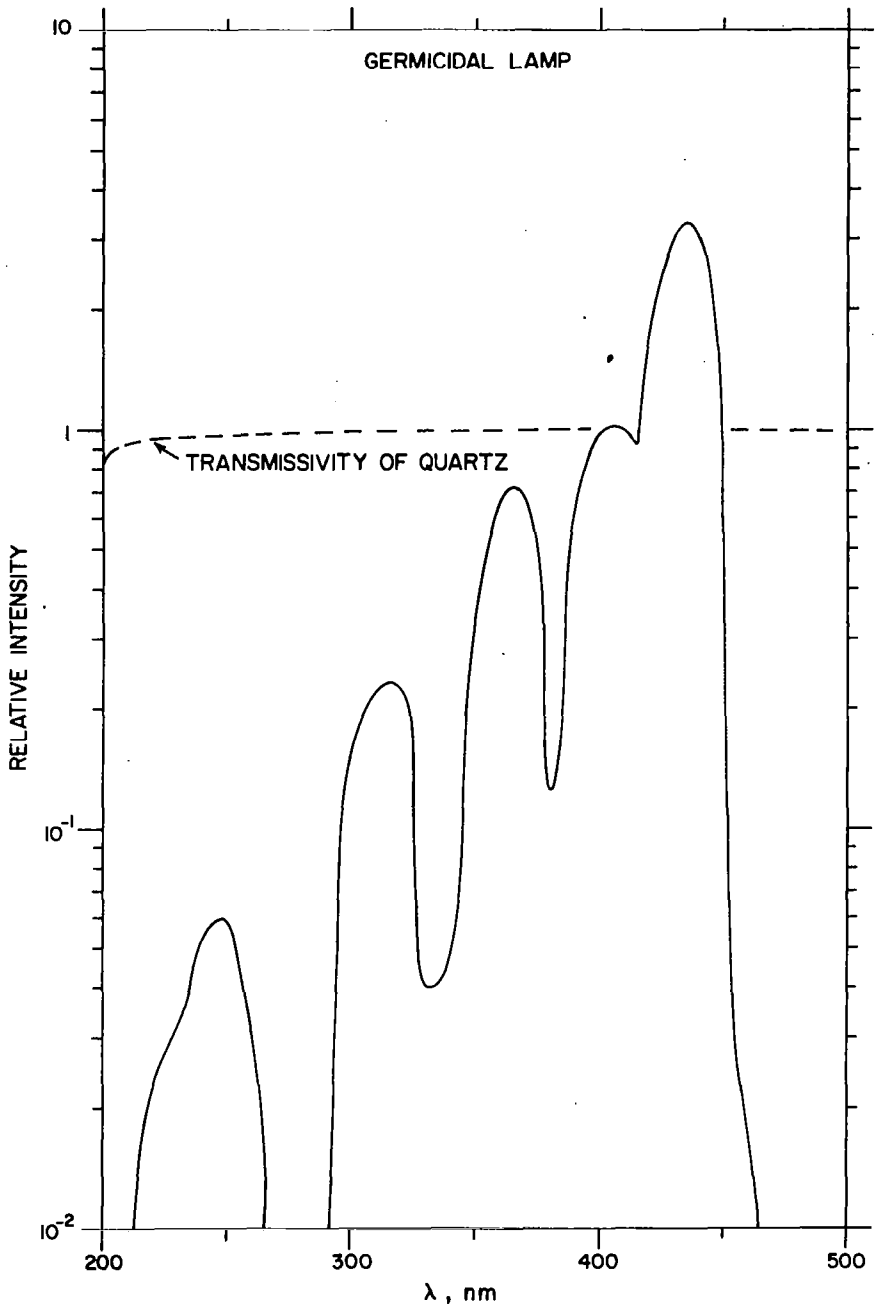

Figure 3-3. Spectrum of light output of GE germicidal lamp.

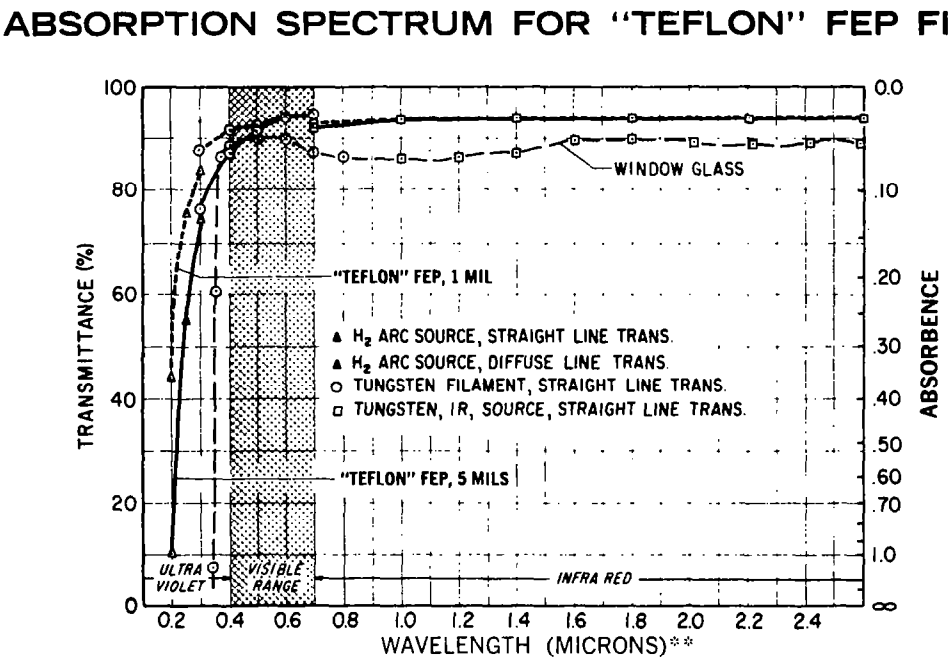

Figure 3-4. Absorption spectrum for Teflon FEP film, suggesting considerable transmissivity between 200 and 300 nm. [From DuPont, Bulletin T-5A].

which would also allow one to change length or diameter of the chamber.

This led to experiments with a modular concept whereby the chamber end caps (which take on the role of adapters between tubing of ∿.6 cm diameter and the 10 cm diameter chamber) consisted of ceramic Büchner funnels while the cylindrical portion was made from 1 mil FEP Teflon foil stretched between and clamped to the rigid ends. This design (Model B) also allowed for convenient installation of a stainless steel felt-metal disc acting as flow straightener at the upstream end of the chamber. The FEP Teflon foil chamber would, in addition, have provided a considerable weight savings in case the need for a larger chamber had arisen.

Prior to deciding on this type of design, the available specifications on the Teflon foil's transmittance were consulted (Figure 3-4) which indicated that, between 200 and 300 nm, a value of 60-80% could be expected. However, actual tests with the prototype revealed that practically no particles were generated under conditions otherwise identical to the ones with Model A.

Thus it was necessary to resume work with quartz as a chamber wall material, though without abandoning the modular concept. In this Model C, the ceramic end caps were joined to a quartz cylinder with silicone RTV sealant. While this PAG version was again able to produce large numbers of particles, initial tests immediately showed that the latter were present in the chamber outflow even when the SO_2 flow was turned off. Since this behavior suggested that SO_2 was being held up in the silicone rubber and later released, it was necessary to design a new version (Model D) in which the three main parts were connected by

reversible mechanical means under avoidance of problematic glue-like material.

Figure 3-5 depicts a partial cross-section of an end cap and its connection with the quartz tube. Basically, the end cap fits over the end of the quartz tube, and an O-ring is squeezed against the cap and the quartz tube by a compression ring that screws onto the cap. This not only provides a gas-tight seal, but also a strong mechanical connection. Due to the fact that the quartz tube is thin-walled, fragile, slightly out of round and has a dimpled surface, it is necessary that the O-ring be of a relatively soft material and of considerable width to properly contact the uneven surfaces without exerting too much pressure on the quartz tube. Thus, the original design calling for Teflon as O-ring material had to be changed to Viton. This, in turn, required the addition of a Teflon ring between the compression ring and the Viton O-ring to reduce friction during tightening of the compression ring.

As Figure 3-5 indicates, the stainless steel end caps are not machined from one piece, but rather three pieces to provide a convenient method of installing and clamping in place the stainless steel filter which serves as a flow straightener; the downstream end cap is identical to the inlet one except that the flow straightneer has been deleted. Connections to the Teflon or stainless steel 1/4" gas lines are made via Swagelok fittings which have on one end a male 1/4" NPT (the latter shown in Figure 3-5) screwed into the end caps.

The UV lights on this last model PAG are arranged as in Model A shown in cross-section in Figure 3-1. A photographic view of Model D in vertical configuration with the inlet at the bottom is provided in Figure 3-6.

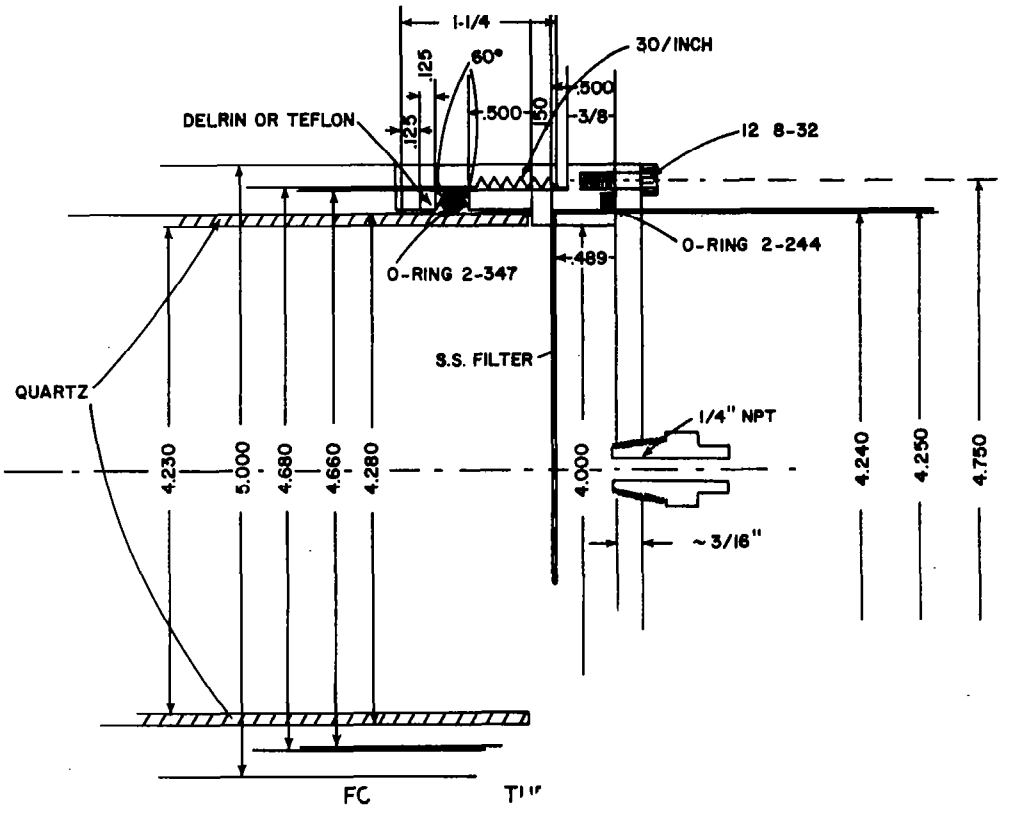

Figure 3-5. Axial cross-section of stainless steel end cap for quartz tube (Model D) [all dimensions in inches].

Obviously, this last model does not offer great flexibility with regard to its geometry - only the chamber length could easily be changed by using different lengths of quartz tube - but, while work on this design was in progress, it became apparent that size limitations for the flight model would be imposed which would not allow dimensions to go beyond the ones in the present model. Thus, no preparations were made for constructing larger end caps to accommodate quartz tubes of, e.g., 20 cm diameter.

2. PAG Performance

a. Output Variables

Three output parameters were used to assess performance of the PAG:

- The total particle number concentration detected at the exit of the generator by an Aitken counter (E-1 or TSI-CNC) was monitored during all experiments. The goal was to obtain typical particle concentrations of the order of $10^5 cm^{-3}$ which would allow shaping of the size distribution by coagulation or passage through an electrostatic classifier while still preserving a concentration sufficient for cloud chamber experimentation.

- Particle size was monitored in some experiments by diffusion battery, electrical aerosol analyzer, or indirectly by continuous flow diffusion (CFD) chamber. As in the case of the other particle generators, the desired size range of the final product was 10 to 100 nm radius.

- The constancy of the particle concentration was of particular concern and was monitored by continuous recording (on stripchart) of the Aitken counter output signal. Using the same procedure as in the

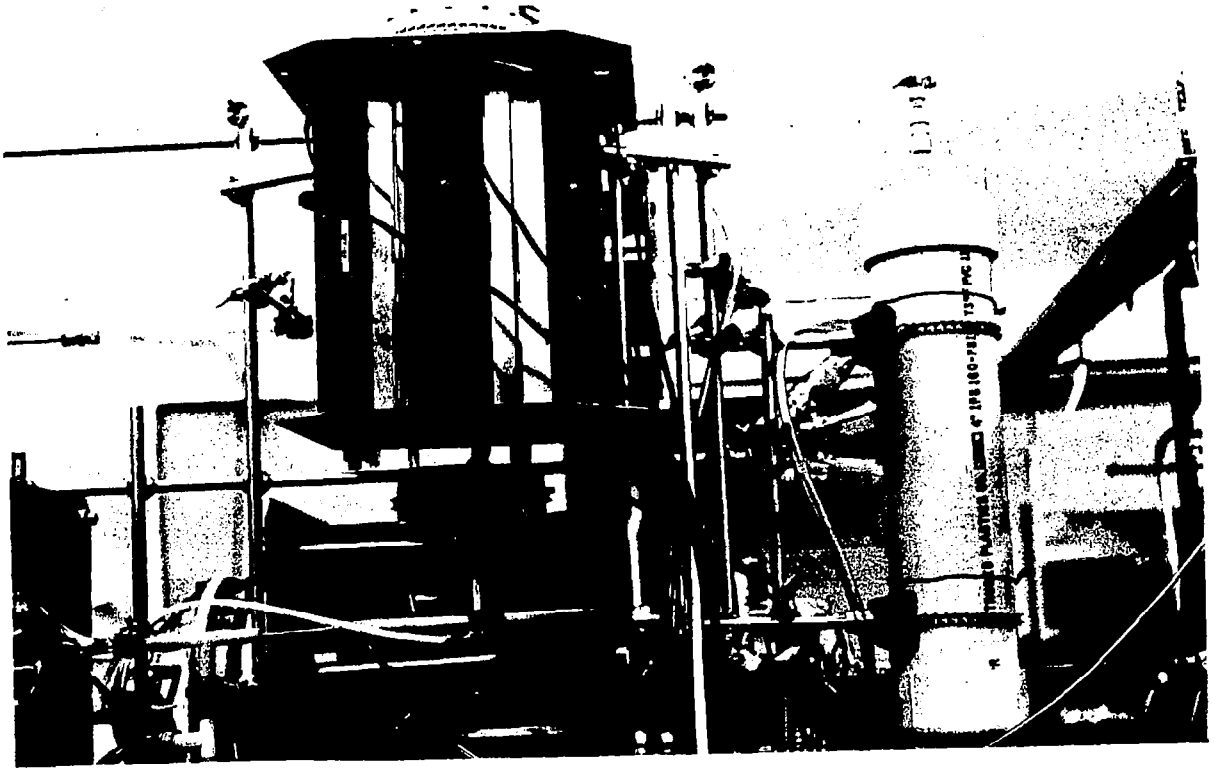

Figure 3-6. Photograph of photolytic aerosol generator (Model D) in vertical position. Cylinder on right side is the SO_2 vapor stripper.

atomizer study, the output fluctuations of the PAG were measured as 200% (Max-Min)/(Max+Min) for a given time interval. Where comparisons between different operational modes were of interest, it was not necessary to calculate standard deviations.

b. Input Parameters

Two types of input variables were taken into consideration. The first kind pertained to the geometry of the generator chamber which, in this case, is described by model designation. Specifically, valid measurements were carried out only with either Model A (one-piece quartz) or Model D (straight quartz tube with stainless steel ends and flow straightener). The other input parameters are a measure of the intensities of the various ingredients entered into the chamber, namely, SO_2 concentration, O_2 concentration, humidity, temperature, flow rate of gas mixture through chamber, and light intensity. Effects of most of these variables on the output were investigated only in one of the two chamber models (either A or D), since Model D was not drastically different from A, but rather a refinement mainly intended to increase output stability.

(1) Light Intensity, Flow Rate

An example of how these two variables affect the output of the generator is shown in Figure 3-7, an excerpt from a stripchart. The light intensity was varied by activating either two or all four lights. The tests were carried out with Model A at the flow rates of 15 and 30 cm^3s^{-1}. For both variables, the results as depicted appear at first glance to be paradoxical - increased output with less light and faster passage through the irradiation zone. However, if one considers the

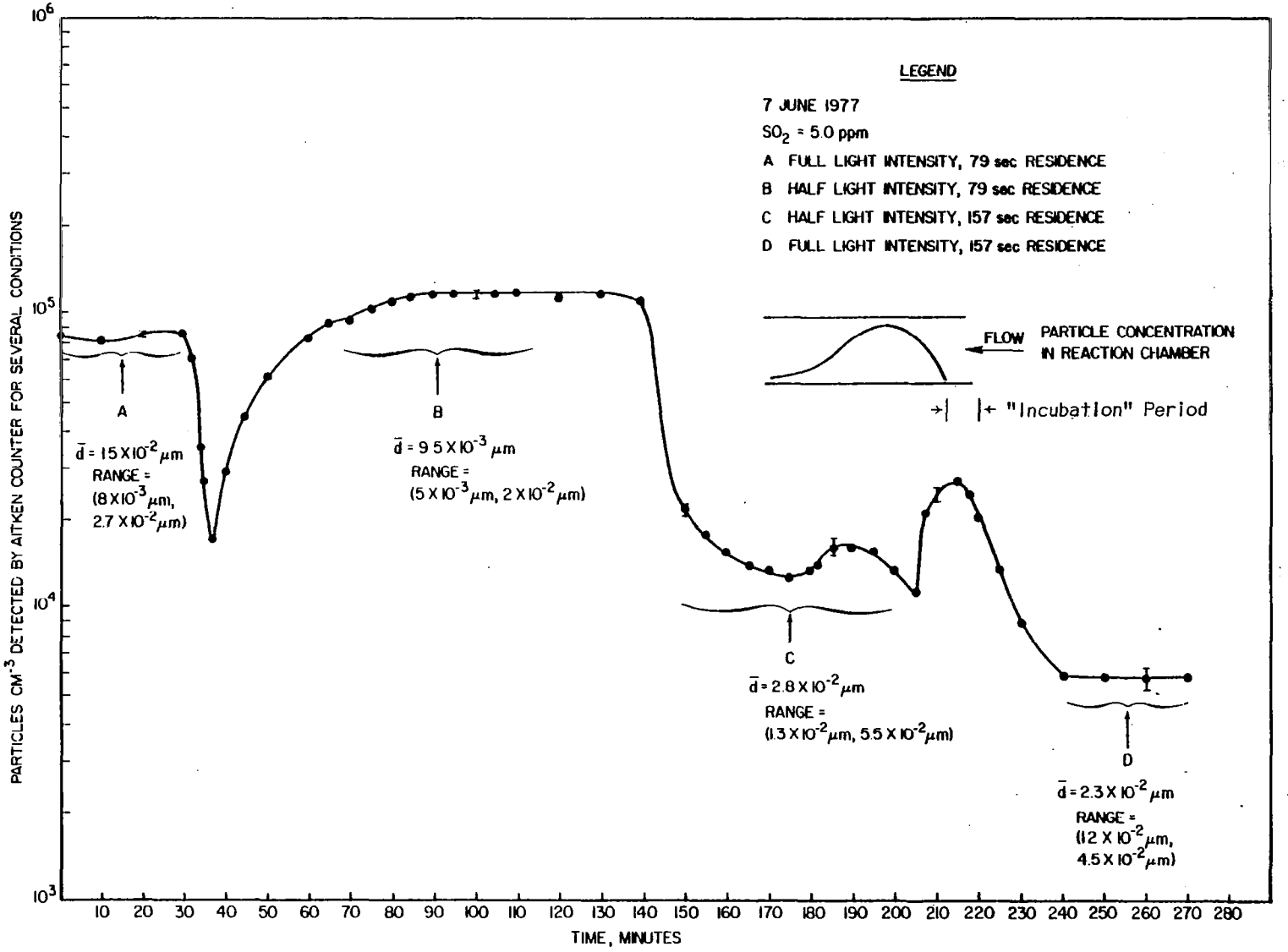

Figure 3-7. Particle output of PAG versus time indicating effect of four different operational regimes. Inset showing likely particle density versus position in reaction chamber (see text for details).

particle concentration versus time (or position in the chamber) as indicated in the figure inset, it appears plausible that slower flow provides more time for coagulation, thus fewer but larger particles; conversely, lesser light means slower particle build-up and later onset of significant coagulation which results in a higher particle number but smaller size at the chamber exit. The latter situation is also confirmed by the data on Figure 3-8 which were obtained by analyzing the generator output in CFD chambers where sizes are determined via supersaturation using the Köhler relationship.

While there is little doubt that the data displayed in Figure 3-7 are at least qualitatively descriptive of the end result of the processes occurring in the PAG, the above mechanistic reasoning has to be regarded as just one hypothesis which could not be further pursued in the framework of this program. In subsequent research under different sponsorship, it became quite clear that systems such as the PAG are much more complex and difficult to interpret than originally assumed.

For further tests, the light and flow conditions selected were: all four lamps on and a flow rate of 2 ℓ min^{-1}. In this context, it is interesting to note in Figure 3-9 the drastic effect of a 1 mil FEP Teflon foil (as used on Model B) positioned between the lights and the quartz tube: no observable particle generation when foil is in place (left side of figure), but immediate onset of aerosol formation as soon as Teflon foil is removed. This clearly demonstrates that lack of transmissivity below 300 nm was the reason for Model B to fail, despite the misleading data of Figure 3-4.

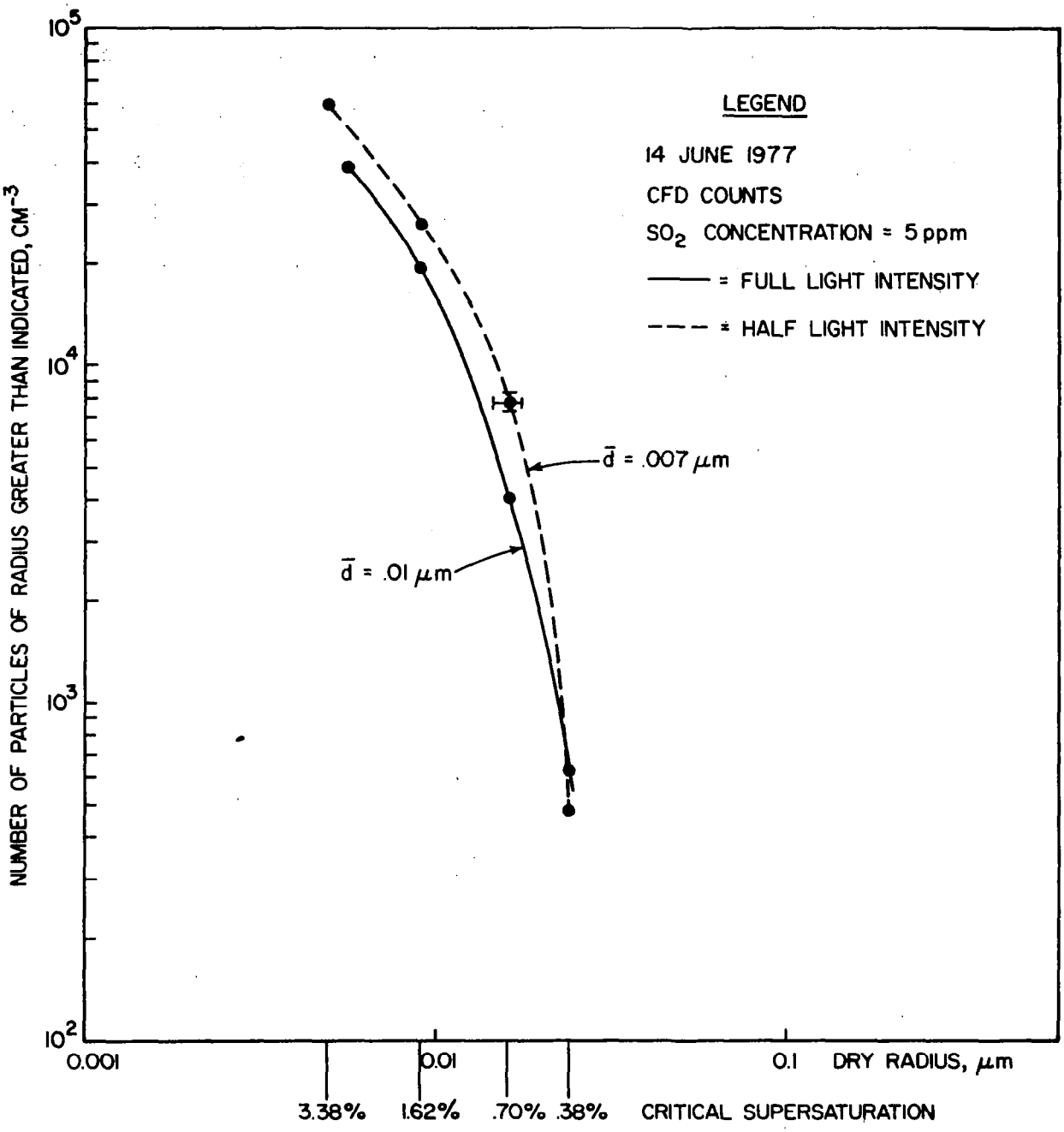

Figure 3-8. Cumulative PAG particle size distributions for two different light intensities as obtained by continuous flow diffusion chamber measurements.

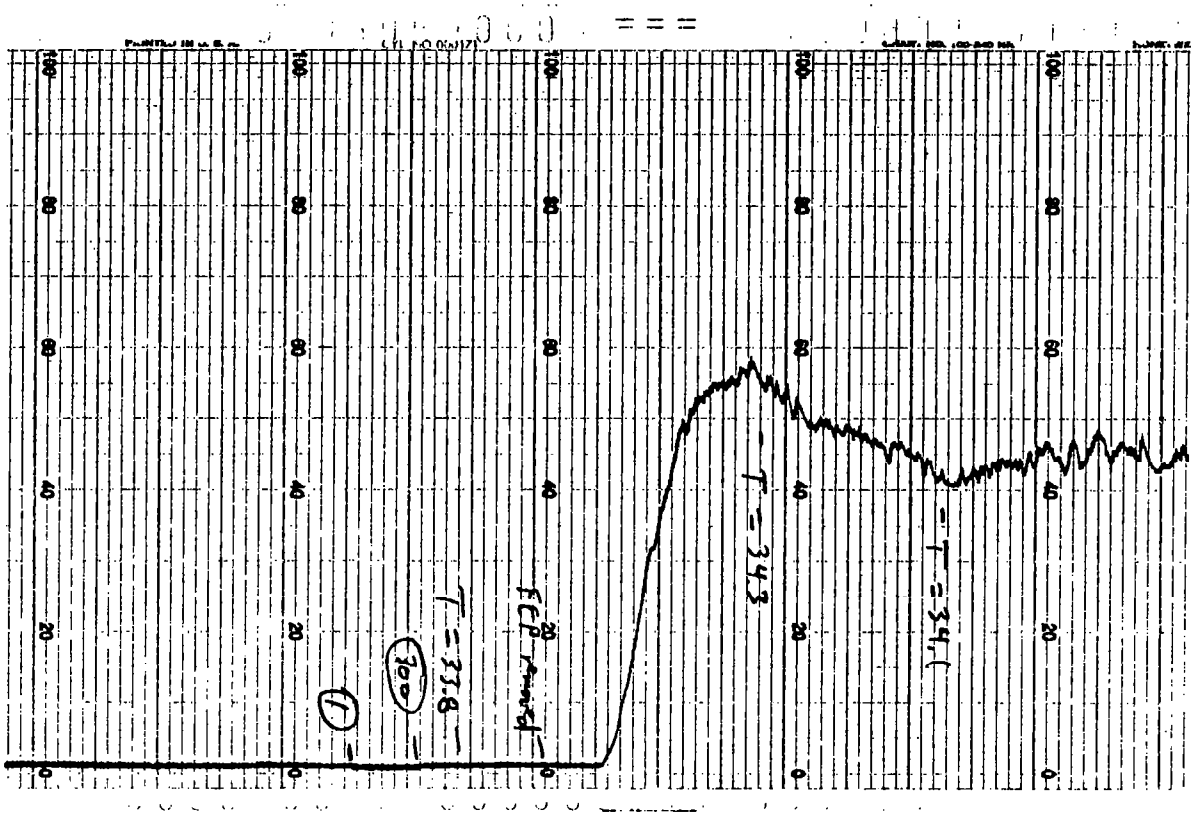

Figure 3-9. Stripchart showing PAG particle output versus time. The drastic effect of 1 mil FEP Teflon foil (the type used in Model B), between lights and quartz tube - no particles generated - is seen on left side. Removal of the Teflon film brings the particle output immediately to over $10^5 cm^{-3}$.

(2) SO_2, Water Vapor and O_2 Concentration

Initially, the experimental set-up did not include humidity control or measurement. Thus, measurements such as the ones of the SO_2 concentration effect on the particle number as shown in Figure 3-10 are difficult to compare with later measurements; however, this figure points to two observations: within the range 1 to 10 ppm SO_2, the resulting particle number appears to be approximately proportional to the SO_2 concentration and, more importantly, the resulting average particle size does not depend strongly on the SO_2 concentration as determined by diffusion battery methods (note the mean diameters indicated on the graph).

After adding a humidifier and a dewpoint temperature controller to the gas-handling equipment, the data of Figures 3-11 and 3-12 were obtained. Figure 3-11 shows the particle number output as a function of humidity (as expressed by the dewpoint temperature, T_D) for three different SO_2 concentrations. While these measurements were carried out with the Model A chamber and O_2 as carrier gas, the data set of Figure 3-12 was generated with the Model D PAG and air as carrier. The plot shows that the SO_2 concentration was varied over a wide range (0.03 to 10 ppm) for three different humidity values.

Both figures indicate the same trend for the effect of SO_2 concentration on particle output: a strong increase in particle concentration with increasing SO_2 concentration at low SO_2 values, but becoming weaker or zero for higher SO_2 concentrations and higher humidities. Similarly, increasing humidity caused sharp increases in particle production - more pronounced at low humidity and low SO_2 concentration.

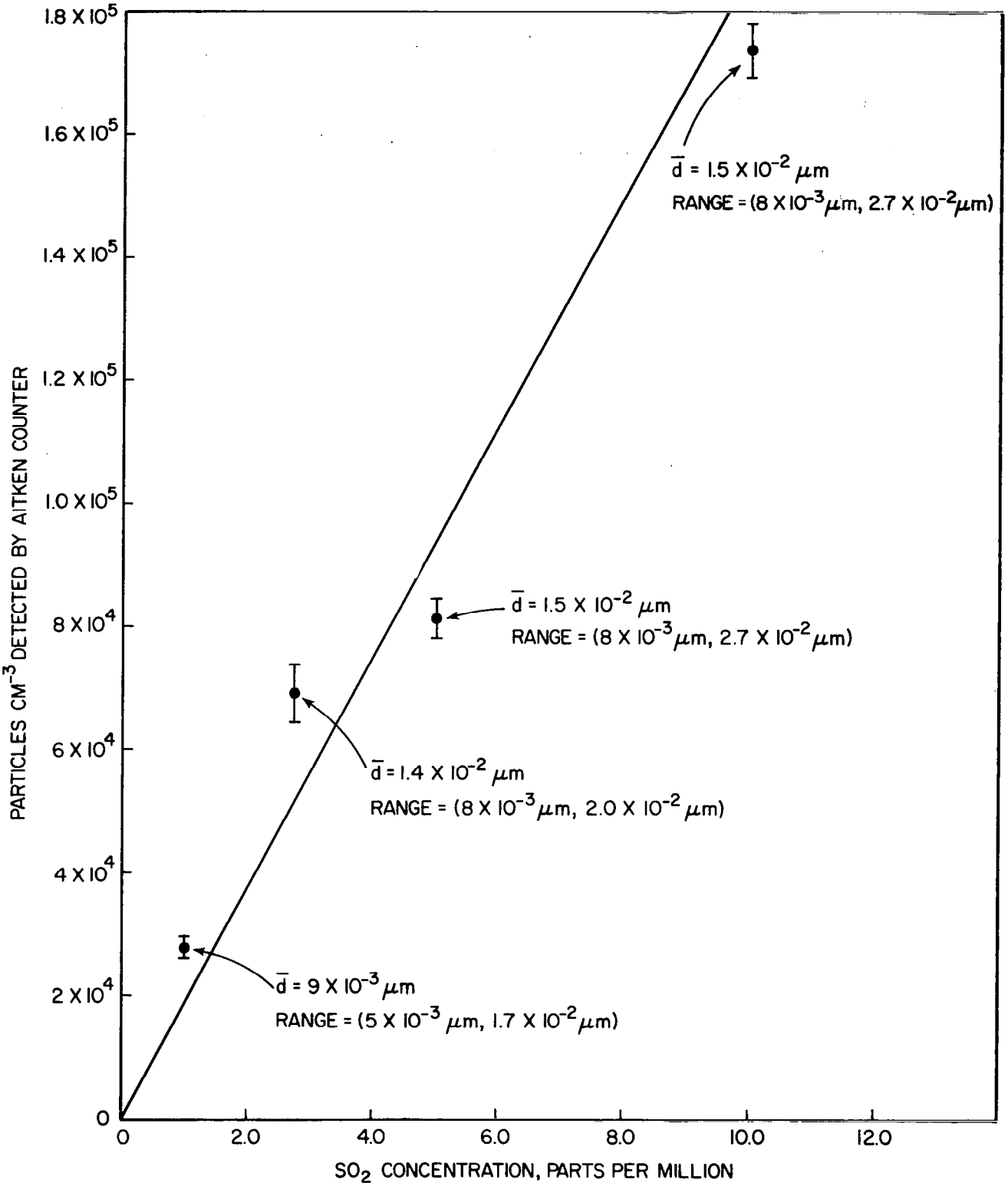

Figure 3-10. PAG (Model A) particle output as a function of SO_2 concentration. Indicated particle size values are based on diffusion battery measurements.

Besides not having completely overlapping ranges in SO_2 and humidity, the two sets of measurements differ mainly in absolute particle concentration for identical pairs of $[SO_2]$ and T_D, whereby the values of Figure 3-12 are more than an order of magnitude lower than those of Figure 3-11. To a considerable extent, this has to be attributed to the difference in carrier gas - higher O_2 concentration leading to increased aerosol formation.

c. Effects of Temperature on PAG Output

While the temperature dependence of the particle output is of general interest, it is of particular importance in the present case because an ACPL version of the PAG would require an enclosure which would need to be cooled to remove the heat generated by the lamps.

For the present experiment, the PAG was fitted with an insulating jacket of glass wool which caused the chamber temperature to increase gradually from the normal ∿35°C to nearly 50°C under the influence of the four UV lamps. The temperature was measured by a thermistor taped to the outside surface of the quartz tube. Using air at a dewpoint of 10°C with 0.03 ppm of SO_2, the particle output dropped to approximately 1/8 of the original value for a 15°C increase in temperature.

While higher temperatures in the reaction chamber may indeed reduce the particle formation rate, it is quite likely that, in part, the heat-related reduction in light output was responsible for the observed effect. The two possible causes were not investigated separately.

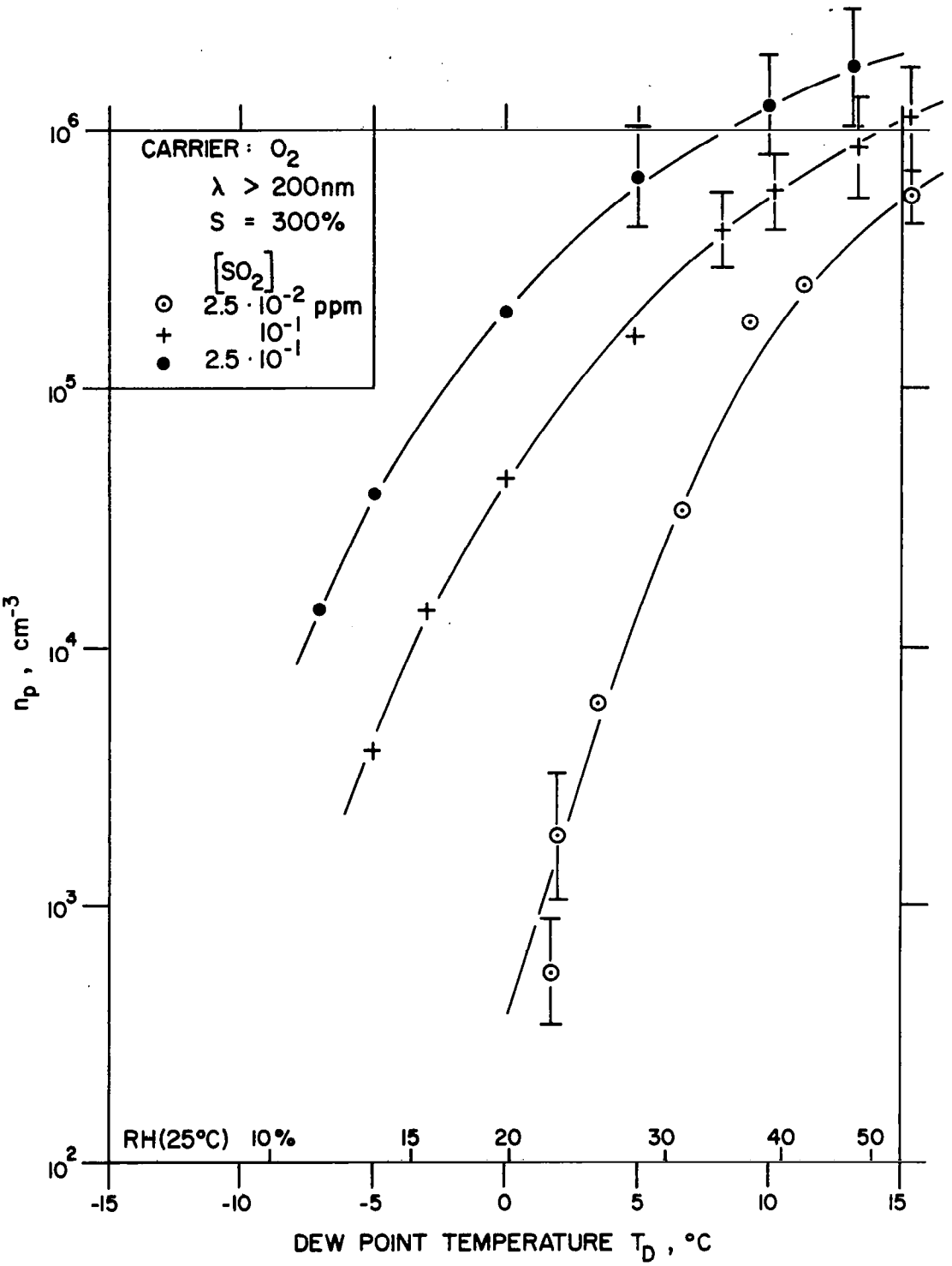

Figure 3-11. Influence of humidity on the PAG output for three different SO_2 concentrations. Data obtained with PAG Model A.

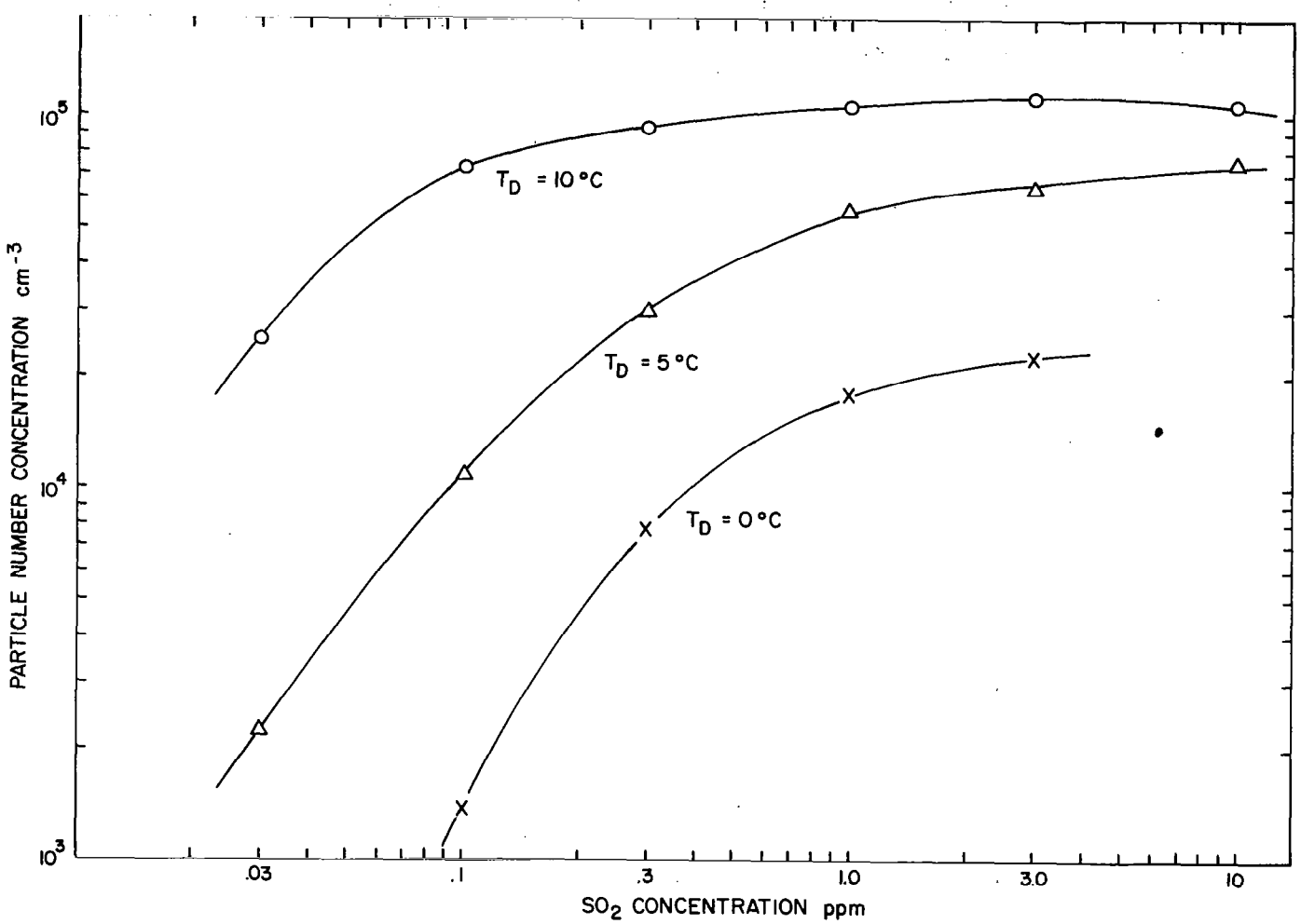

Figure 3-12. PAG (Model D) output as a function of SO_2 concentration for three different humidities (carrier gas: air).

d. Size Distribution of the PAG Particles

It was previously mentioned that the sizes of the particles generated in the PAG were of the order of 10 nm. Size distributions as obtained indirectly by feeding the output to several CFD chambers operating in parallel and set at different supersaturations are depicted in Figure 3-8 where supersaturation values were translated into particle sizes according to the Köhler relationship. It is evident that the majority of particles were smaller than the lower limit of the primary range specified for the ACPL. This was reconfirmed while acquiring the data of Figure 3-12 where one CFD chamber provided some values for 1% supersaturation; on the average, only about 5% of total particles were activated at that supersaturation.

An example of an aged PAG aerosol (generated at the occasion of the first DRI-University of Wyoming Workshop) is shown in Figure 3-13. A storage bag was filled with the PAG output in order to be able to measure the size distributions with three different instruments of which the combined sample flow rate was far greater than the PAG flow rate. It is easy to see (from the differing steepness of the curves) that the spectrum of Figure 3-8 is, as expected, much narrower than the ones of Figure 3-13. The latter diagram also demonstrates the typical quality of agreement between such diverse instruments as the Electrical Aerosol Analyzer, the CFD chambers, and the Diffusion Battery.

e. Output Constancy

Early in this investigation, it became evident that it would be difficult to meet the specifications for constancy of the PAG output. Fifteen to twenty percent fluctuations over a 1000 sec period were not

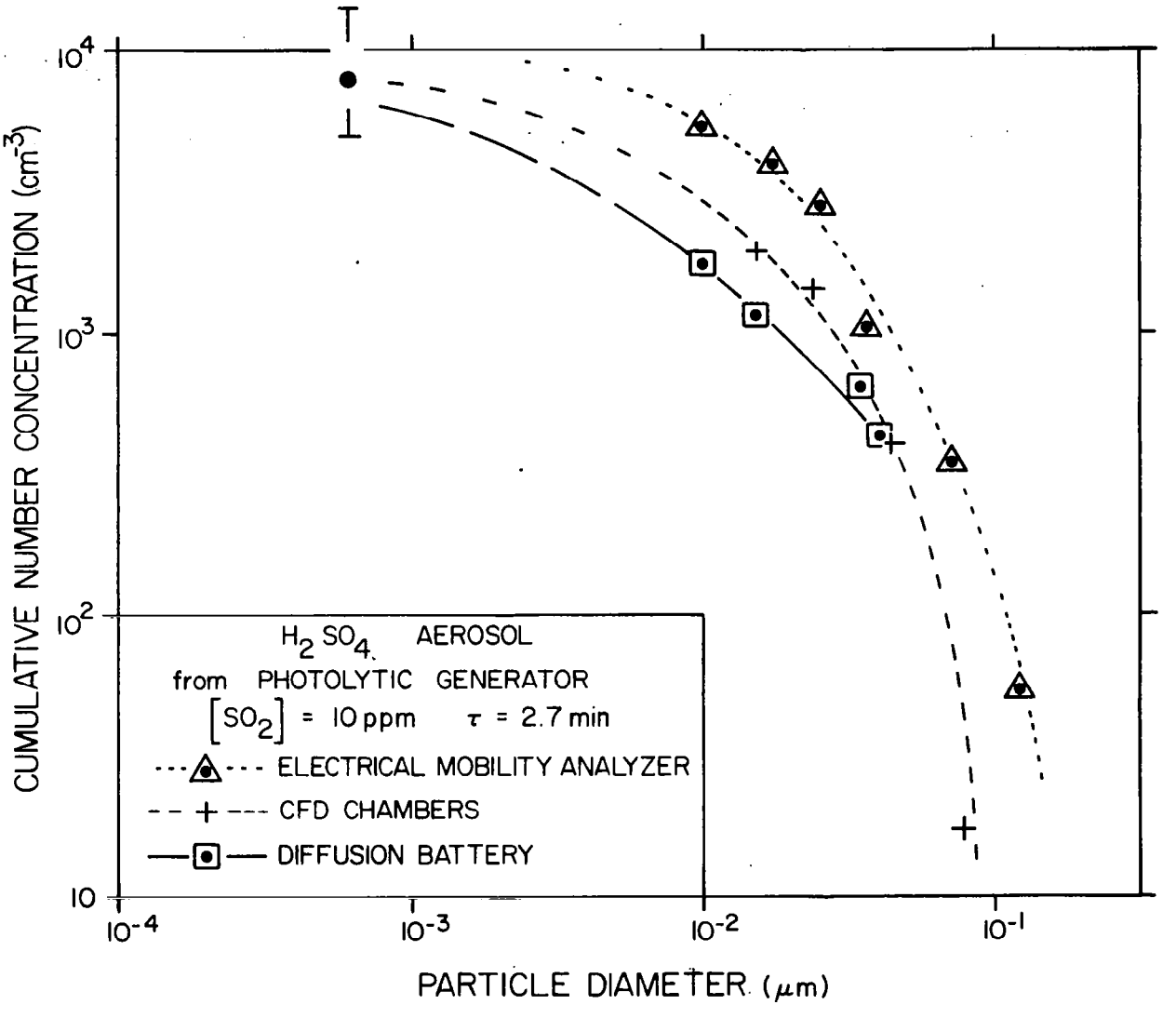

Figure 3-13. Cumulative size distribution of PAG (Model A) particle output stored in Mylar bag (for $\sim 10^3$ sec) as measured by the indicated instruments.

unusual and a 50% drift over one-hour intervals could frequently be observed. A particularly large number of time-consuming tests were devoted to this problem. All parameters previously discussed were scrutinized for their potential influence on output fluctuations.

Prior to installation of the humidity control system in the gas-handling portion of the experimental set-up, it appeared, based on flow tests with smoke, that unsteadiness of the flow was caused at the transition from the thin inlet line to the 10 cm diameter chamber. This prompted the installation of a stainless steel filter as a flow straightener at the inlet side of the irradiation chamber. Figure 3-14 shows the modest improvement that was achieved by this alteration of the flow in the chamber: (a) represents a somewhat better than average output recording of the Model A, while (b) was obtained with Model D under slightly less favorable conditions (less SO_2); the fluctuations were down to ∿8% from ∿15% in (a).

Humidification and strict control of the dewpoint temperature led to considerable improvement of the output quality. Output drift over longer periods was reduced substantially while short-term fluctuations could be counteracted by increasing the humidity. Figure 3-15 demonstrates this effect as well as the influence of SO_2 concentration on output steadiness. The seven-minute excerpts from stripcharts are arranged according to SO_2 concentration (from left to right, 0.1, 1.0, 10 ppm) and dewpoint temperature, T_D (from top to bottom 10, 5 and 0°C). It is unquestionable that increases in each of the two parameters resulted in improved constancy of the output (less than 5% fluctuations) with respect to fluctuations with frequencies higher than about 0.2 min^{-1}.

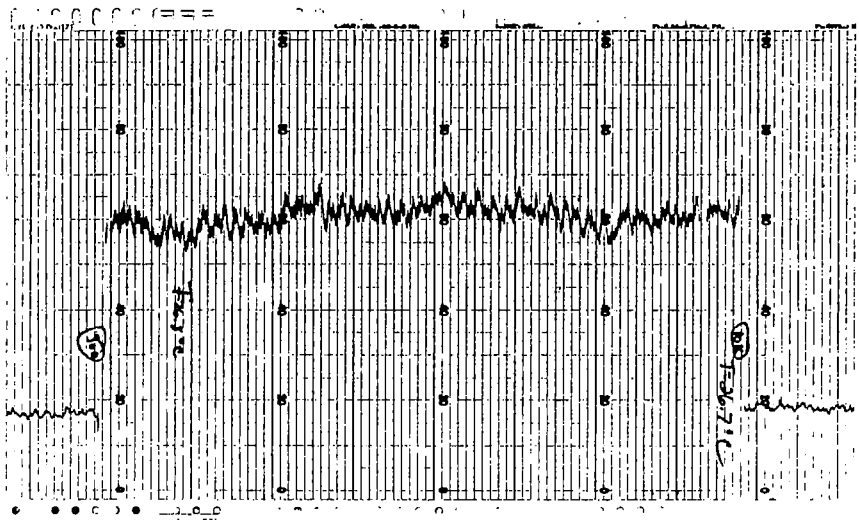

(a)

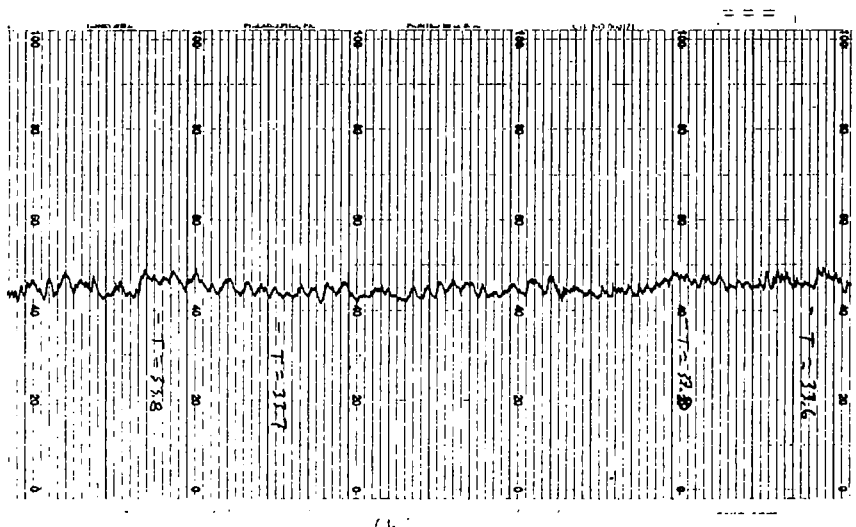

(b)

Figure 3-14. Stripchart samples of PAG output. Comparison of output fluctuation: (a) Model A and (b) Model D, showing improvement by about a factor of 2.

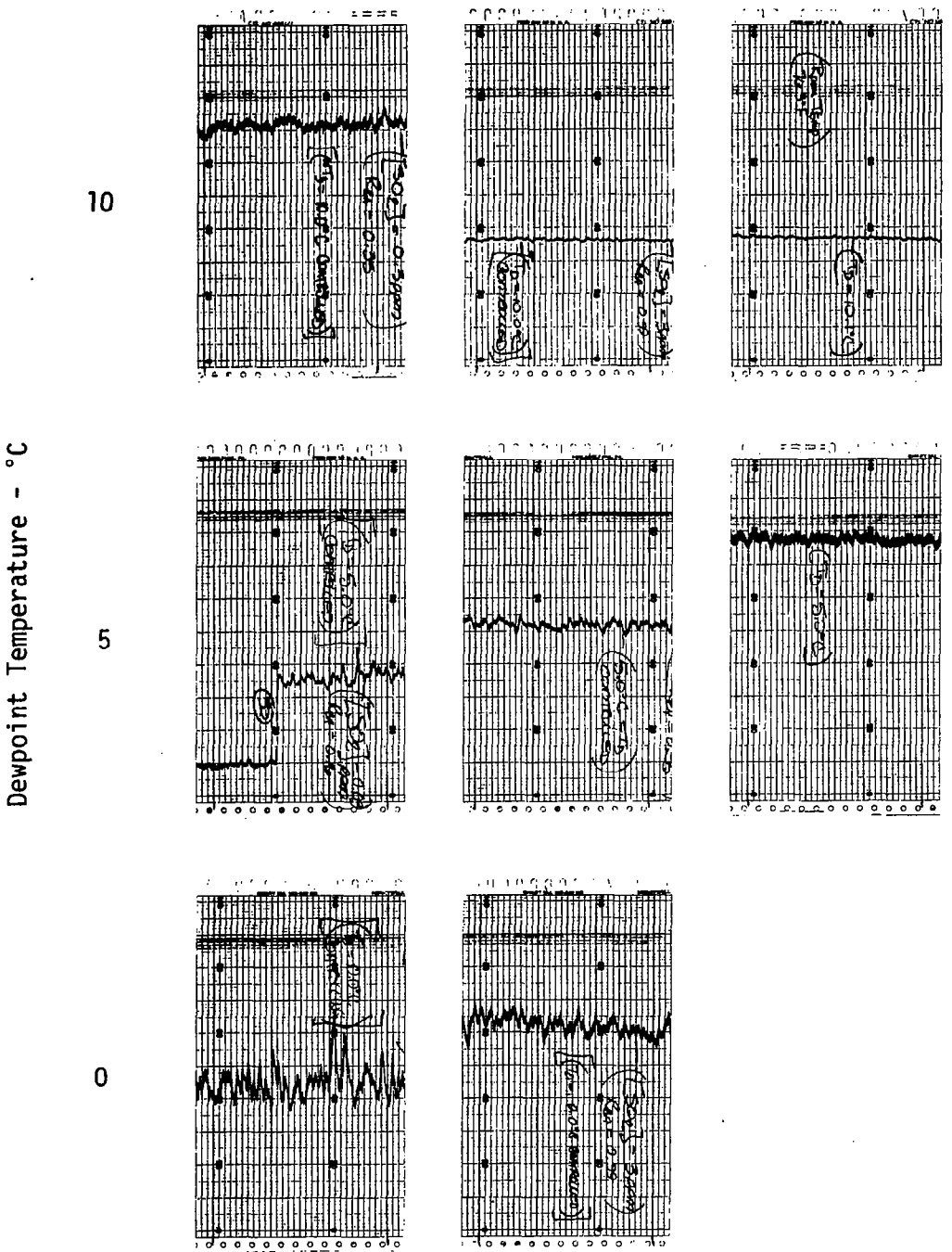

Figure 3-15. Seven-minute stripchart segments demonstrating dependence of PAG output fluctuations on SO_2 concentration (increase from left to right) and humidity (increase from bottom to top).

While long-term (30-60 min) fluctuations and drifts could be reduced considerably by improved control of the pertinent variables, especially humidity, it is still to be expected that output changes on the order of 10% occasionally occur. Output differences before and after periods of shut-down were found to be even larger, but difficult to quantify since there is not a sufficient number of comparable observations due to the multitude of variables involved. For the same reason, it has not yet been possible to determine with certainty what causes the lack of reproducibility.

3. Vapor Stripper

Although not an integral part of the PAG, a device to remove excess SO_2 downstream of the PAG would have been an absolute necessity for ACPL operations and, therefore, it is appropriate to briefly discuss that device (stripper) in this chapter.

The essential design goal for the stripper was high retention of the SO_2 component in the passing gas mixture combined with a small loss of aerosol particles. Since the latter condition could not be met in a conventional activated charcoal bed (which acts much like a particle filter, too), a design was chosen that is very similar to the diffusion dryer (TSI Model 3062) used in conjunction with atomizers (see Section III.3.a). Thereby, unimpeded passage for particles is provided by a tube made from fine wire mesh which is surrounded by the charcoal bed. Since the SO_2 has to diffuse through the wire mesh to be adsorbed to the charcoal, it is plausible that more SO_2 penetrates this device than would pass through a regular, complete bed of charcoal granules.

In approximate analogy to the above-mentioned diffusion dryer, the dimensions of the DRI stripper were selected as follows: wire mesh tube, 50 cm long and 1 cm diameter, axially located inside a 12 cm diameter capped plastic cylinder filled with 6-14 mesh coconut charcoal granules. The device appears in Figure 3-6 to the right of the PAG.

Figure 3-16 depicts the results of preliminary performance tests. The upper diagram shows the flow rate dependence of the percentage of SO_2 that passes through the device. At a flow of 2 ℓ/min^{-1} used in most PAG experiments about 15% SO_2 would penetrate the stripper (in its present configuration). The lower curve relates the particle loss in the stripper to the SO_2 concentration which, in turn, influences the particle size - thus the dependence of the particle loss on SO_2 concentration (due to smaller diffusivity of larger particles). Since the findings in the previous section mandate the use of a high SO_2 concentration ($\geq$1 ppm), the particle loss would be of the order of 2% - a tolerable value.

Considering that no attempt had been made in the design of this first model to optimize the geometry to achieve simultaneously low SO_2 penetration and low particle loss, the present results are quite encouraging. The simplest approach towards reduction of the SO_2 penetration would be to increase the length of the unit, e.g., by doubling the length the penetration could be lowered to less than 2.5% while the particle loss would merely double to 4%.

However, proper optimization of the device would require a more extensive study of the various properties of the stripper; also, e.g., the minimum required diameter of the charcoal cylinder around the wire

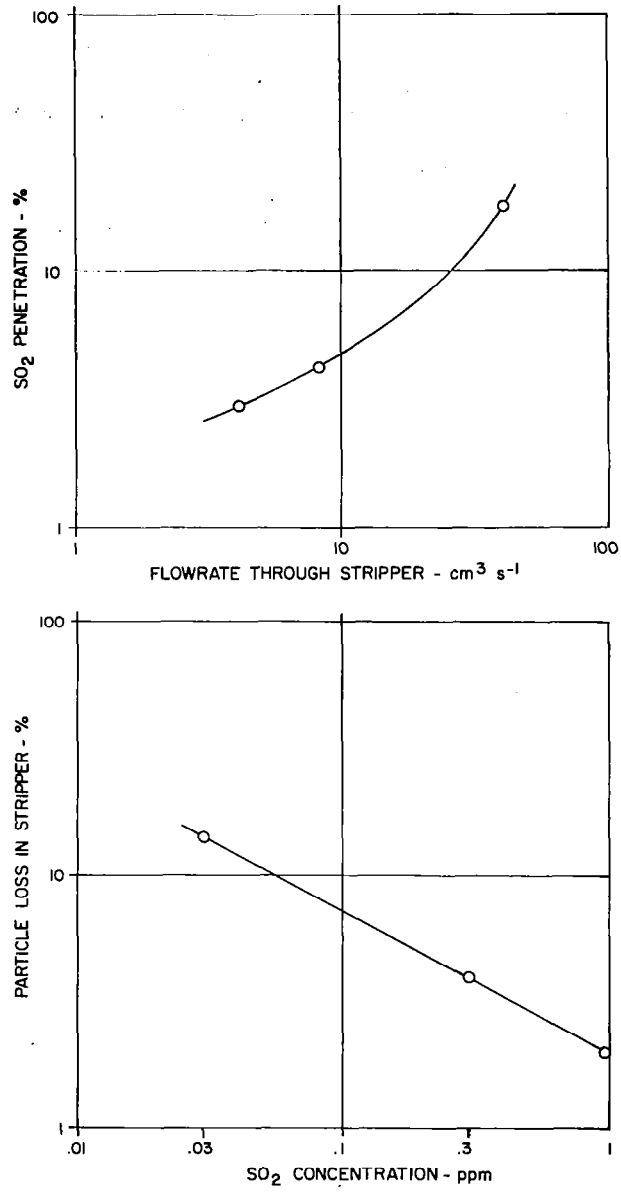

Figure 3-16. Performance of SO_2 stripper: (top) SO_2 penetration versus flow rate, and (bottom) particle loss in stripper versus SO_2 concentration (which dictates particle size).

mesh tube would have to be determined on the basis of SO_2 consumption and flight duration.

In summary, then, it can be stated that the concept of a stripper to drastically reduce the SO_2 content in the effluent of an aerosol generator is feasible. Further development work is required to determine the best compromise between SO_2 retention and particle loss.

B. AEROSOL GENERATION BY ATOMIZATION

1. Selection of Suitable Candidate Atomizers for Evaluation

Atomization (or nebulization) of liquids - breaking up of the bulk substance into a large number of very small droplets - can be achieved in several ways, all of which require energy to generate the large amount of new surface. Regardless of the method applied, the primary aerosol emerging from an atomizer consists of liquid droplets. To obtain an aerosol of solid particles, the solid material either has to be dissolved, the solution atomized and the solvent evaporated, or the solid material can be hydrosolized first, the hydrosol atomized and the liquid evaporated; a third method consists of operating an atomizer above the melting point of the solid material and subsequent solidification of the droplets.

The most frequently used method is pneumatic atomization whereby liquid is injected into and broken up by a jet of air (or other gas). Another technique, ultrasonic atomization, consists of imparting ultrasonic vibrations to the liquid which may be dispersed if certain conditions are met. A third method uses hydraulic pressure of the liquid alone to cause breakup after passage through an appropriately designed nozzle. In addition, there are hybrid systems such as vibrating orifice

droplet generators in which the vibration forces the liquid to break up into segments of equal size, leading to high monodispersity.

From the beginning of this program, the pneumatic atomizer was given preference over the other liquid-dispersing methods for the following reasons.

Due to their basic simplicity and versatility, pneumatic atomizers have for years proven to be extremely useful aerosol generators as documented in the literature (e.g., Liu and Lee, 1975, or review by Raabe, 1975). Furthermore, the present investigators' previous experience has shown that ultrasonic and hydraulic atomizers have serious shortcomings. The performance of ultrasonic atomizers (which have the advantage of not requiring compressed air) seems to be more sensitive to the physical characteristics of the liquid to be dispersed than the pneumatic type - e.g., the ability to atomize salt solutions may rapidly decrease with increasing, but still moderate, salt concentration. Hydraulic atomizers require very high pressures to achieve satisfactory dispersal of liquid with high surface tension (such as water). The vibrating orifice type droplet generators produce droplets too large to be useful for CCN production of the ACPL specified size range. Late in the project period, a hybrid device became available for testing which consists of a pneumatic atomizer, but incorporates a nozzle design that generates acoustic waves which assist in the dispersion (manufacturer's claim).

2. Evaluation of Pneumatic Atomizers as ACPL Aerosol Generators

While the above considerations, supported by the findings of Anderson (1977) led to the conclusion that penumatic atomizers were the

best choice as primary aerosol generators for ACPL, the description by Liu and Lee (1975) on the TSI Model 3076 "Constant Output Atomizer" (COA) suggested that this particular device would indeed fulfill the requirements set forth by NASA except for some necessary low-gravity adaptations. Thus, the atomizer evaluation effort was initially focused entirely on the COA.

a. Laboratory Set-up for Atomizer Evaluation

The evaluation of the COA as well as of other atomizers was to elucidate the following points with regard to their suitability or applicability to ACPL: output number size distribution, required air pressure for the nozzle, liquid flow characteristics and, most important, output constancy and reproducibility.

Most measurements were carried out with the set-up shown schematically in Figure 3-17. The atomizer, shown on top left, is supplied with dried, filtered and pressure-regulated air conveniently prepared with the TSI Model 3074 auxiliary air supply depicted in the sketch of Figure 3-18. The air flow rate through the atomizer is adjusted to the desired value by pressure regulation; thereby, the flow-pressure relationship depends on the atomizer model - to a lesser extent even on the individual device. With regard to liquid supply, some atomizers such as the COA can be operated in two different configurations: (1) In the recirculating mode (not shown on figure) the liquid is aspirated by the venturi effect of the air jet, and the excess liquid (impacted large drops) is returned by gravity to the reservoir (in most atomizers an integral part, in some such as the COA, a separate container); and (2) in the non-recirculating mode, the liquid is pumped - as indicated on

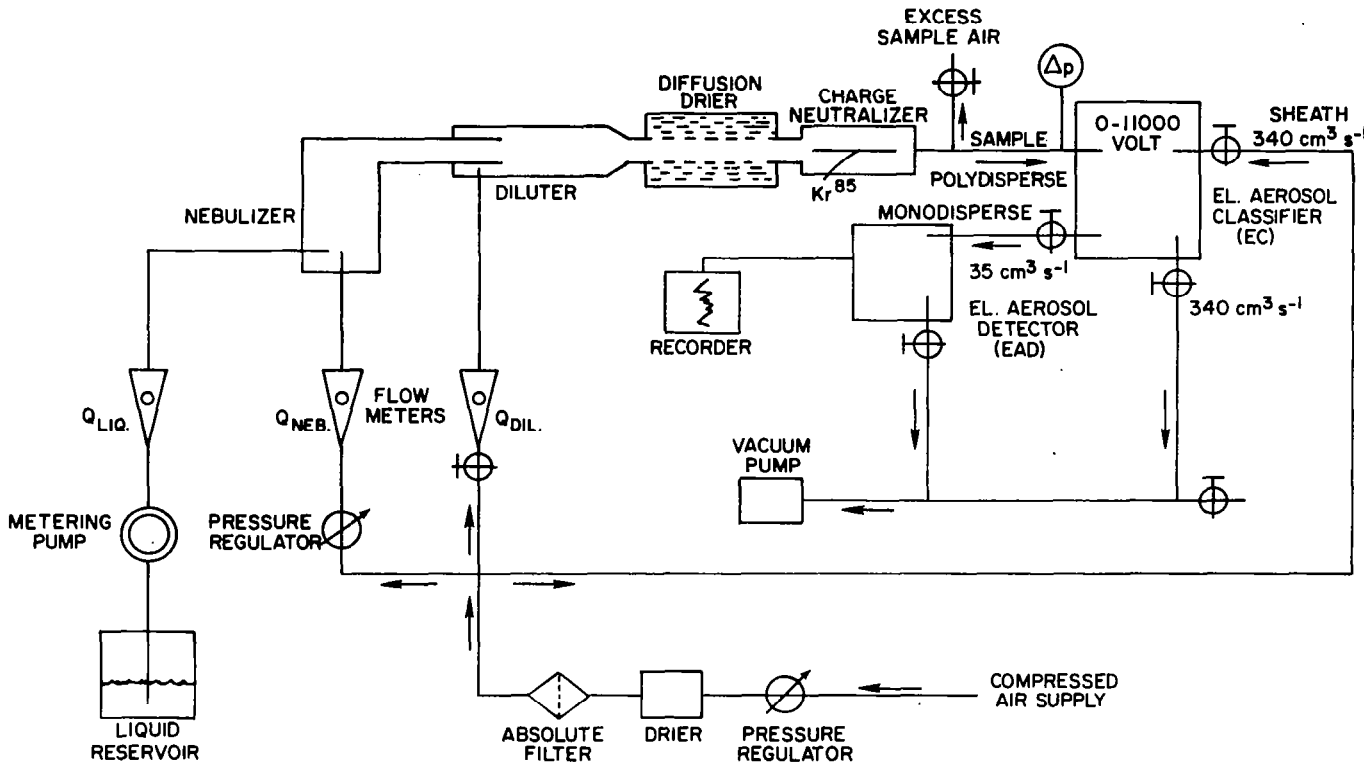

Figure 3-17. Schematic of test set-up for evaluation of atomizers.

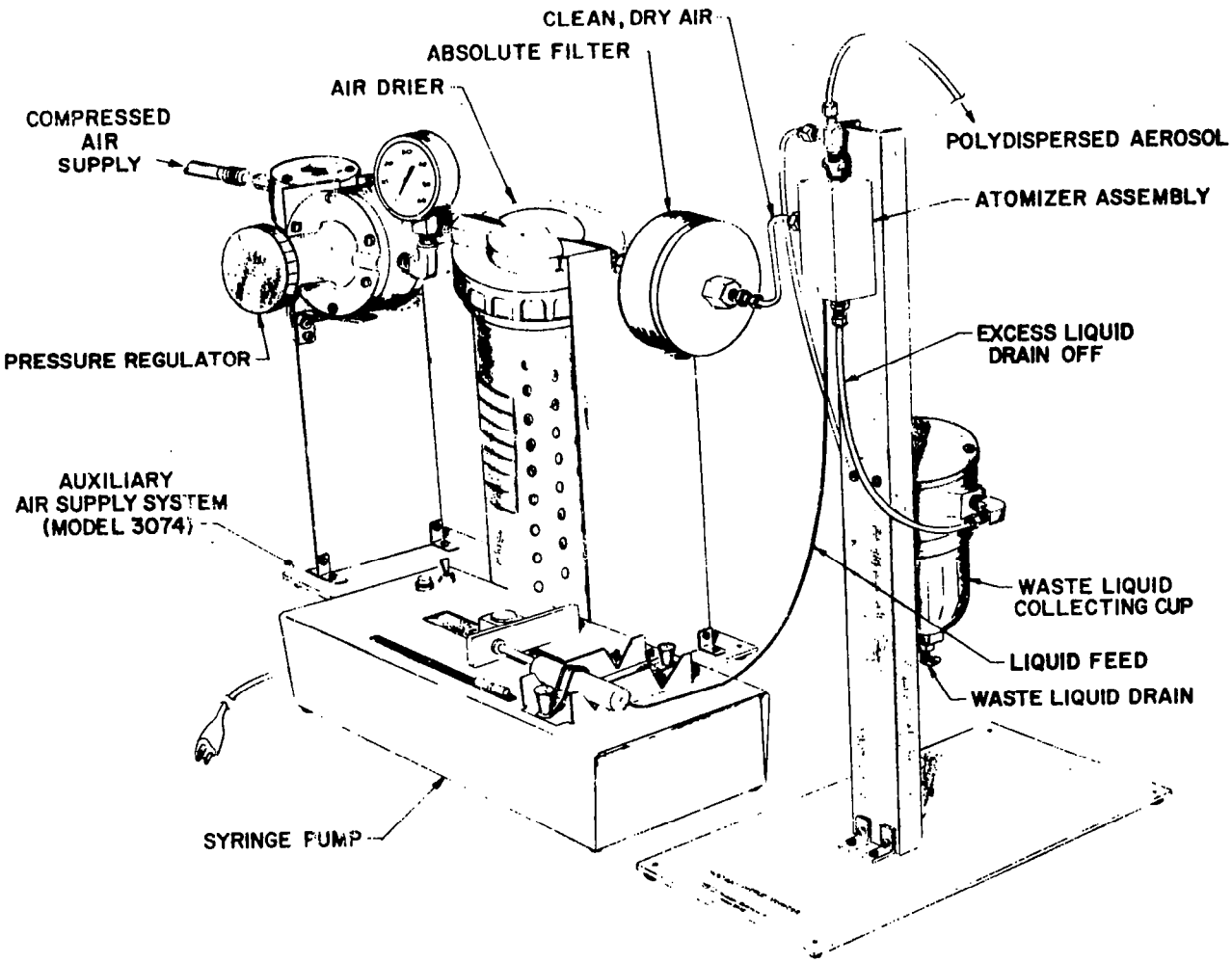

Figure 3-18. Sketch of TSI-Constant Output Atomizer with air supply system and syringe pump (from TSI Manual).

the schematic (Figure 3-17) - at a selectable but steady rate into the jet, and the excess is discarded. (A discussion on the two modes will ensue in the next subsection.)

Two versions of the fluid delivery system are shown in Figure 3-19; during the first year of the program, the syringe pump (Harvard Apparatus*, Model 975), on the left in the photograph was used to pump the liquid directly into the atomizer. Later on, addition of a flowmeter (Matheson No. 610) between pump and atomizer indicated oscillations in the output; this defect and the limit on the experiment time due to the small 50 or 100 ml syringe volume prompted a switch to the FMI** metering pump Model RHOCKC visible in Figure 3-19 above the reservoir bag. This final set-up permitted uninterrupted test runs of many hours.

As the mist emerges from the atomizer, dry dilution air is added to start the process of droplet evaporation which is completed in the subsequent passage through the diffusion dryer (TSI Model 3062) consisting of a wire mesh tube surrounded by a drying agent and a cylindrical, airtight enclosure. The dry aerosol then undergoes charge neutralization prior to entering the EC as discussed in Section II.B.(b). Since the aerosol flow through the EC should be kept low (e.g., 2 ℓ min^{-1}) to achieve high resolution, and since the combined rate of atomizer and dilution flows may be considerably higher, the excess sample air is dumped just before entering the EC. The effluent of the EC and

---

*Harvard Apparatus, Millis, MA

**Fluid Metering, Inc., Oyster Bay, NY.

Figure 3-19. Photograph of fluid delivery system with syringe pump (left), FMI-RHOCKC metering pump (top), and collapsible fluid reservoir.

EAD were aspirated by a vacuum pump which provided most of the pressure drop through those two instruments. This resulted in low overpressure on the downstream side of the atomizer which was advisable when comparing performance at various jet nozzle pressure drops.

Initially, all connections shown in Figure 3-17 were made with Tygon plastic tubing; however, aerosol carrying lines were later replaced with stainless steel tubing to prevent buildup of electric charges which may drastically affect the loss rate of aerosol in transit.

b. Evaluation of the TSI-COA and Comparison with Selected other Atomizers

The TSI-COA shown in a cross-section in Figure 3-20 incorporates essential elements of the typical Collison nebulizer* several modern versions of which have been described by May (1973). Dimensions and mutual positions of air jet nozzle and liquid feed orifice are practically unchanged from the original design. The novel features include an exchangeable air jet nozzle in the form of a platinum disc (TEM aperture), an external fluid reservoir that permits one-time use of the liquid and, most importantly, a 1.2 cm diameter vertical cylindrical cavity into which the jet is directed, perpendicular to the cylinder axis so that the cylinder wall opposite the jet opening serves as a baffle where the large droplets impact and run off. An exterior view of the device is seen in Figures 3-18 and 3-21 where the atomizer is connected to a spent-liquid reservoir. The significance of these features will be discussed as pertinent tests are described below.

*Atomizer and nebulizer are treated here as synonyms.

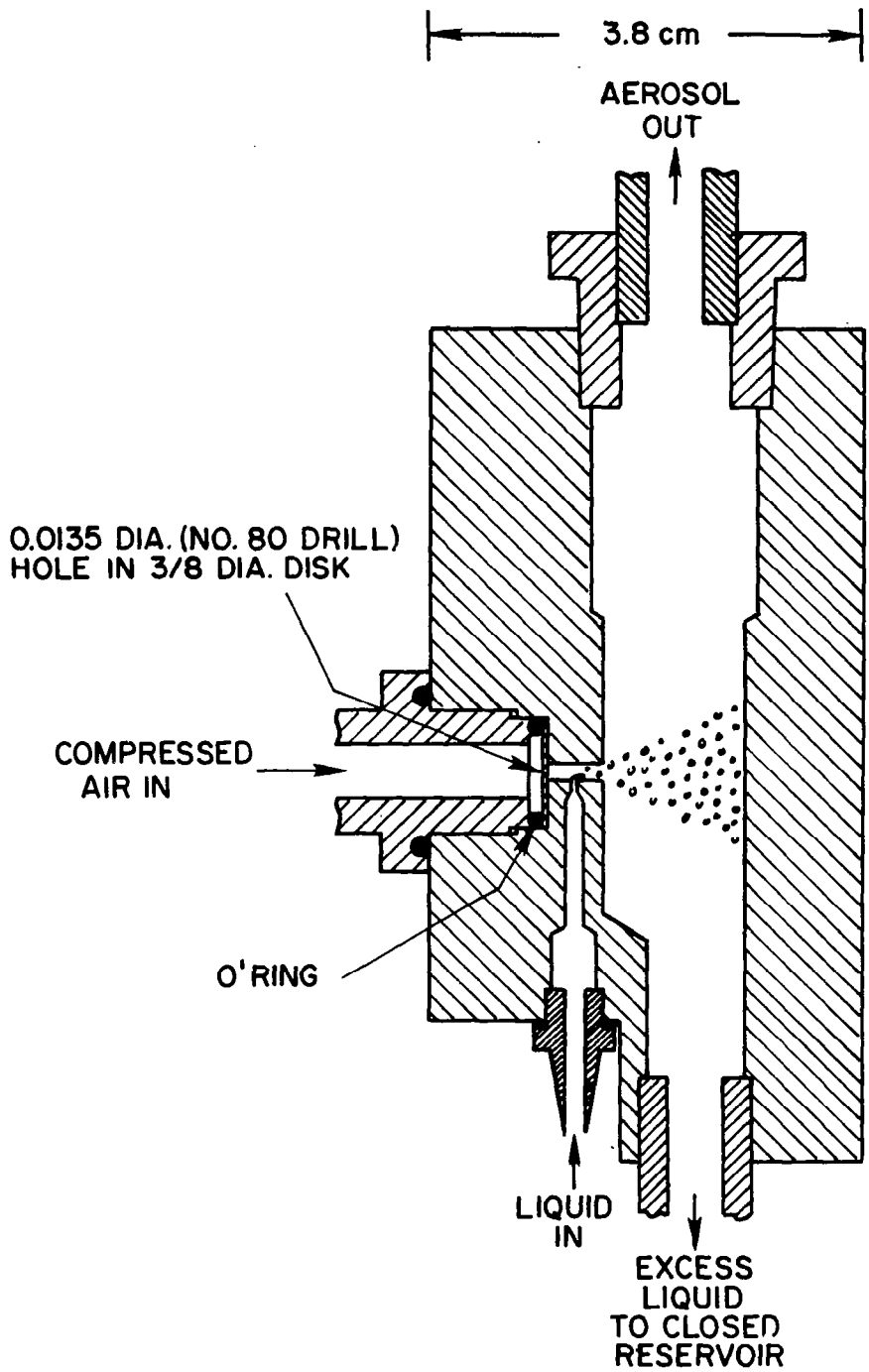

Figure 3-20. Cross-section of TSI-COA (from TSI Manual).

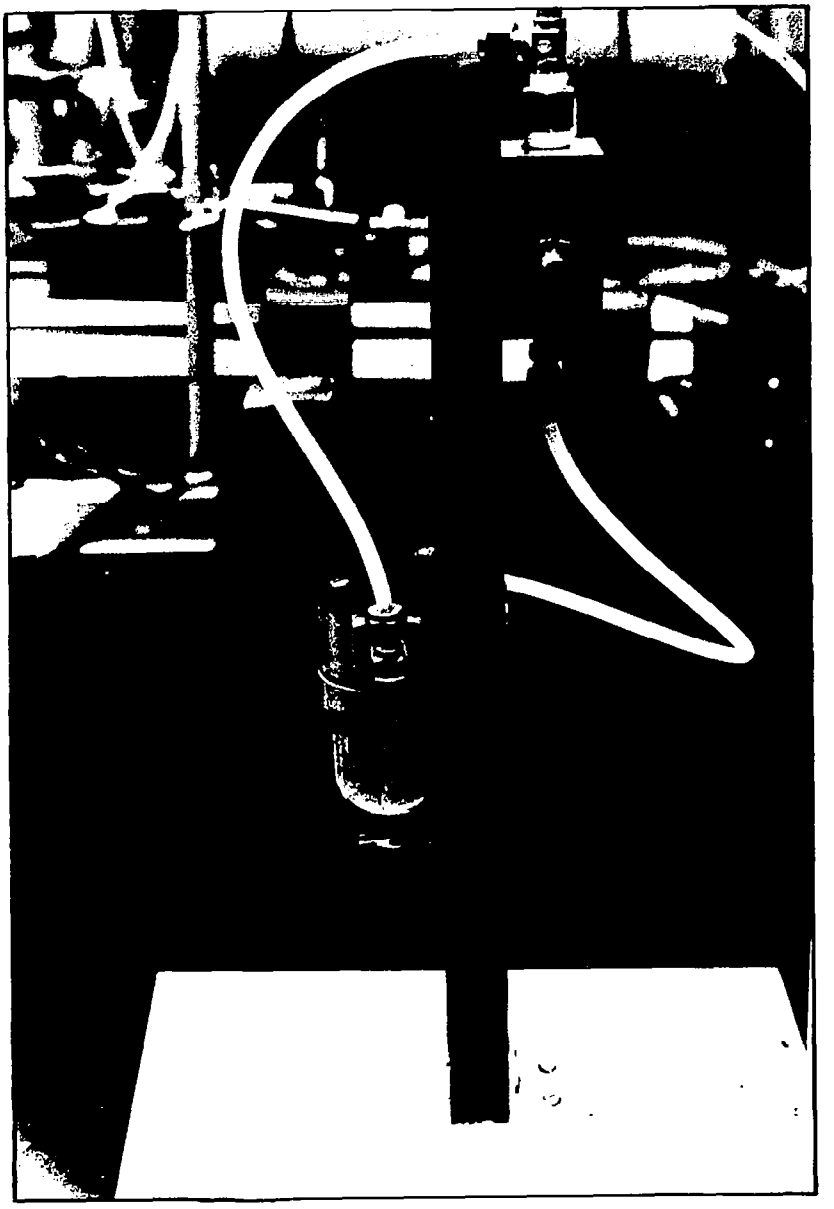

Figure 3-21. Photograph of TSI-COA.

One can obviously determine, without tests, that the recirculating mode of the fluid feed would not be acceptable for zero-gravity since separation of the recirculating liquid from the aerosolized fraction is by gravity, whereas in the nonrecirculating mode the spent, but not aerosolized, liquid can be ingested and retained by wicking material. A further disadvantage of the recirculating mode stems from the fact that the solution concentration gradually increases with time due to evaporation. On the other hand, the nonrecirculating mode demands much larger fluid reservoirs adding to the weight and volume problem.

(1) Number Size Distributions

Most testing of the COA was carried out at an operating pressure of about 30 psi as this is generally considered the optimum range judging from May's (1973) performance tables. The main effect of increased air pressure is increased output number concentration, but not a substantial change in size distribution. The latter can best be manipulated by varying the salt concentration. Figure 3-22 demonstrates the two effects by means of the two size distributions as indicated. The solution strength differs by a factor of 40 and, as expected, the size ratio is indeed in the vicinity of 3.4. As a consequence of the pressures being 30 and 35 psi for the 0.025% and 1% solution, respectively, the number concentration of the distribution on the right is nearly twice the one generated with lower pressure.

Although Figure 3-22 indicates that selection of the appropriate solute concentration will provide CCN populations commensurate with ACPL specifications, it is interesting to compare the COA with the performance of other nebulizers designed to produce submicrometer droplets

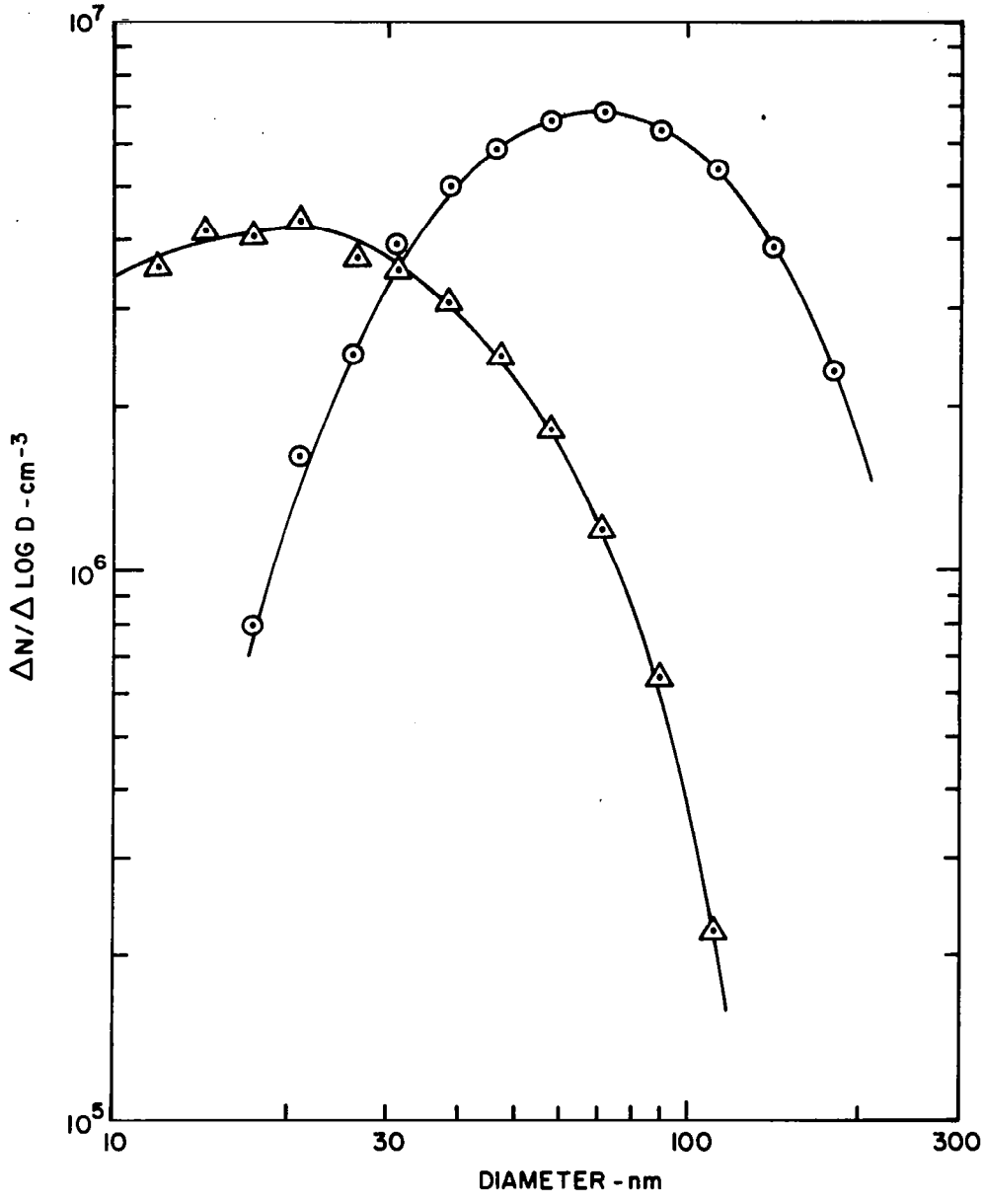

Figure 3-22. NaCl particle size distributions obtained with TSI-COA in recirculating mode at 30 psi with 0.025% solution (▲), and at 35 psi with 1% solution (⊙).

(even though these devices could not be used in the ACPL in their present configuration).

The DeVilbiss Model 644* nebulizer, widely used for inhalation therapy, is shown in Figure 3-23 with its hemispherical top (with outlet) removed to make the nozzle and impaction surface visible. This device was designed for low air pressure (manual compression of rubber bulb) and was operated at 3 psi for measuring the size distribution displayed in Figure 3-24. The modal size of this distribution is the same as the one of the COA (with the same 1% NaCl solution), but it is more polydisperse (σ_g = 2.2) than the COA's (σ_g = 1.9).

One of the latest developments in inhalation nebulizers is the "Nano-Mist"**, depicted in Figure 3-25. This instrument represents the Dautrebande type atomizer where large droplets are eliminated not only by impaction on a baffle, but also when the mist is forced to penetrate a liquid curtain formed by the excess liquid on its return to the reservoir. Another unusual feature of the Nano-Mist is the annular liquid feed orifice concentric with the jet nozzle. Three size distributions obtained with this device at a pressure of 10 psi are plotted in Figure 3-26 for NaCl solutions of 0.034, 2.16 and 33.7 g/l (the low and high values being the practical concentration limits for use in atomizers). Had the same salt concentrations been used as in the case of the COA, Figure 3-22, the two corresponding size distribution curves would fall in between the three present curves; thus, it is evident that the modal sizes of the Nano-Mist distributions are about one-third of those

*The DeVilbiss Company, Somerset, PA.

**by Eastfield Corp., Noroton, CT.

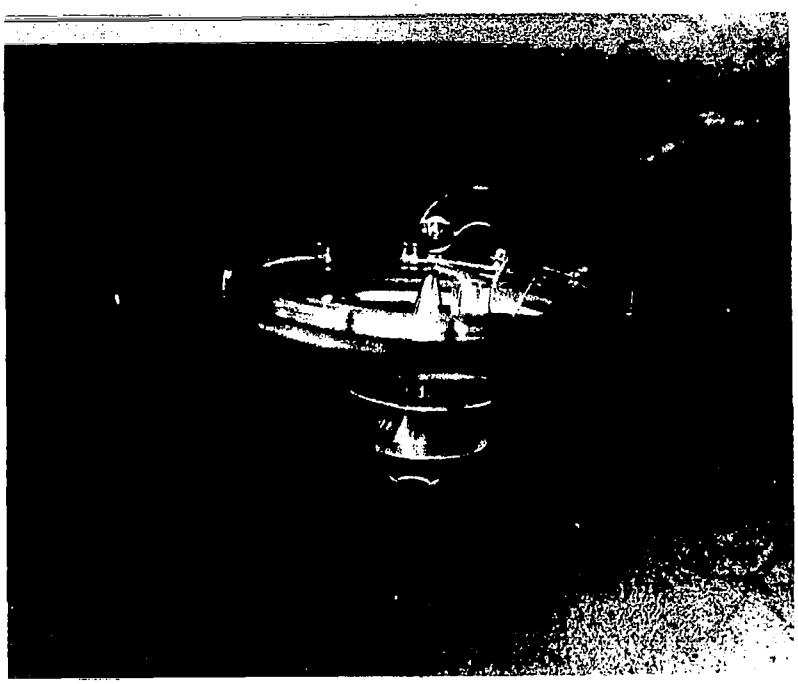

Figure 3-23. Photograph of DeVilbiss No. 644 Nebulizer (top with outlet removed).

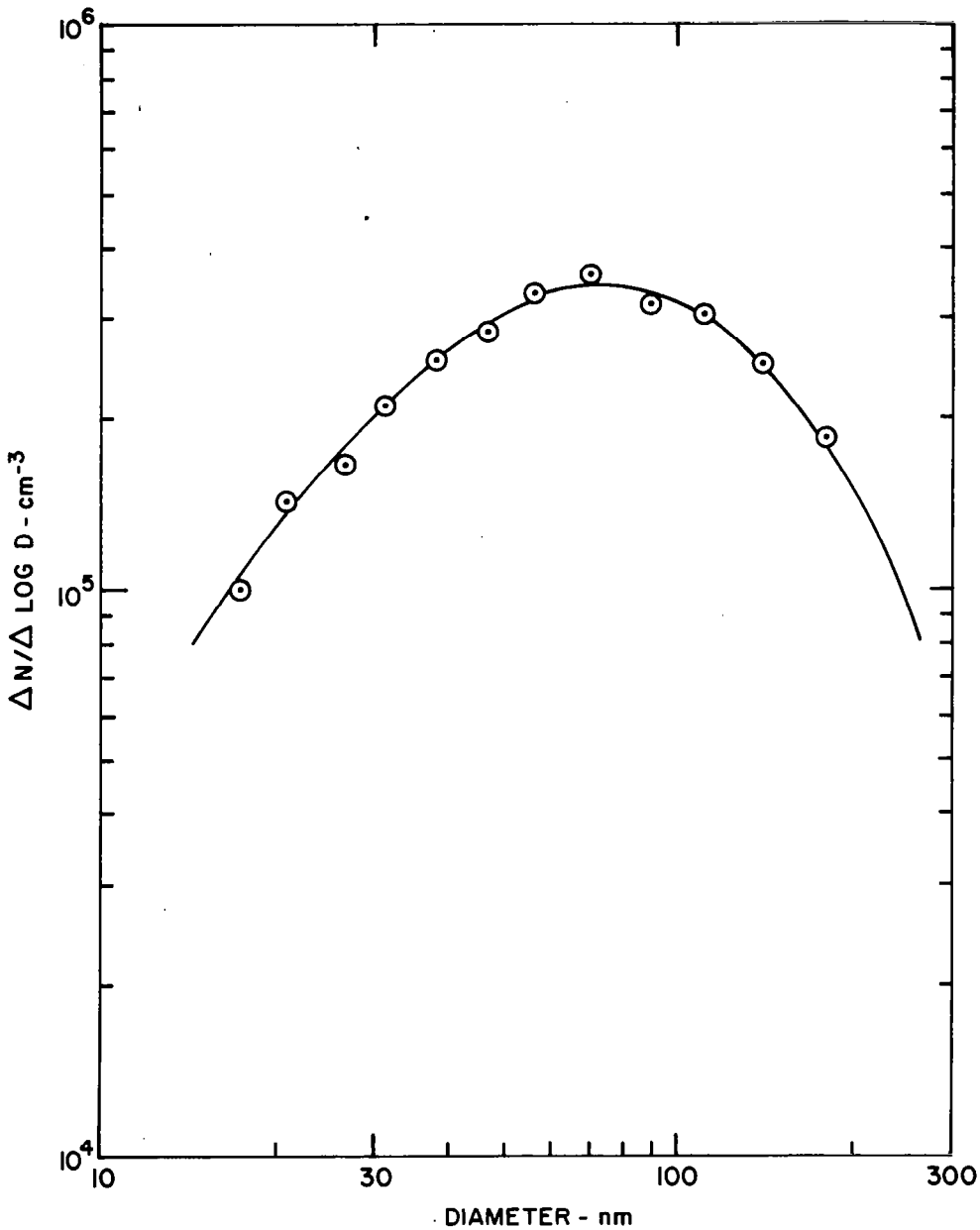

Figure 3-24. NaCl particle size distribution obtained with DeVilbiss No. 644 at 3 psi and 1% solution.

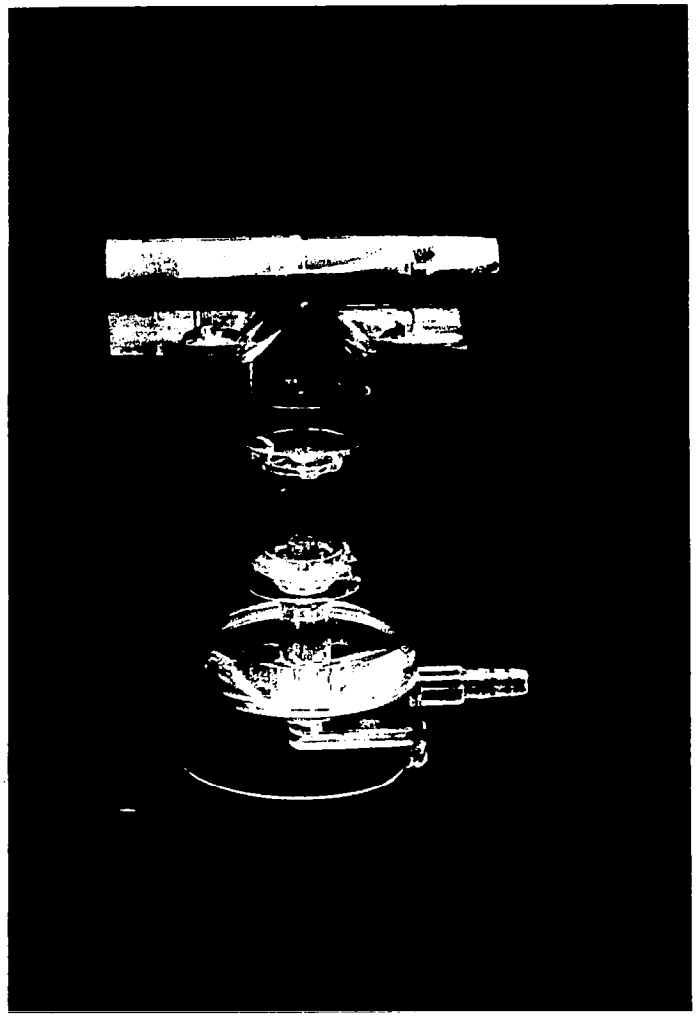

Figure 3-25. Photograph of Nano-Mist nebulizer.

of the TSI-COA. For low concentration solutions, the dispersity of the Nano-Mist output is similar to the COA's, but with increasing solute concentration a "shoulder" on the large particle side of the distribution develops that causes the high concentration curve to be remarkably flat (the existence of this feature was confirmed by several repeat measurements carried out over a period of two years).

A device that became available near the completion of this project is claimed to disperse the liquid by sonic waves generated in the nozzle by the compressed air, as depicted in Figure 3-27. The Sonimist 600-1* was briefly tested with the result displayed in Figure 3-28. The size distribution is very similar to the one of the TSI-COA for the same salt concentration. Considering that the liquid consumption is about twice as high as in the COA, no advantage can be found at all in using the Sonimist in the ACPL.

Although NaCl solutions have generally been used for these performance tests, it had been planned to demonstrate the ability of the atomizer to generate sulfuric acid aerosols as an alternative to the photolytic method. Figure 3-29 shows the size distribution obtained from 1% (by vol.) H_2SO_4 atomized by the TSI-COA at 30 psi in the recirculating mode. As with salt solutions, appropriate further dilution would shift this distribution towards smaller sizes, though in this case, the size is not only governed by the degree of dilution but also by the relative humidity since H_2SO_4 deliquesces even at very low humidity in contrast to salt particles where deliquescence occurs at fairly high values (i.e., 75% for NaCl). No specific measurement was

*by Heat Systems Ultrasonics, Inc., Plainview, NY.

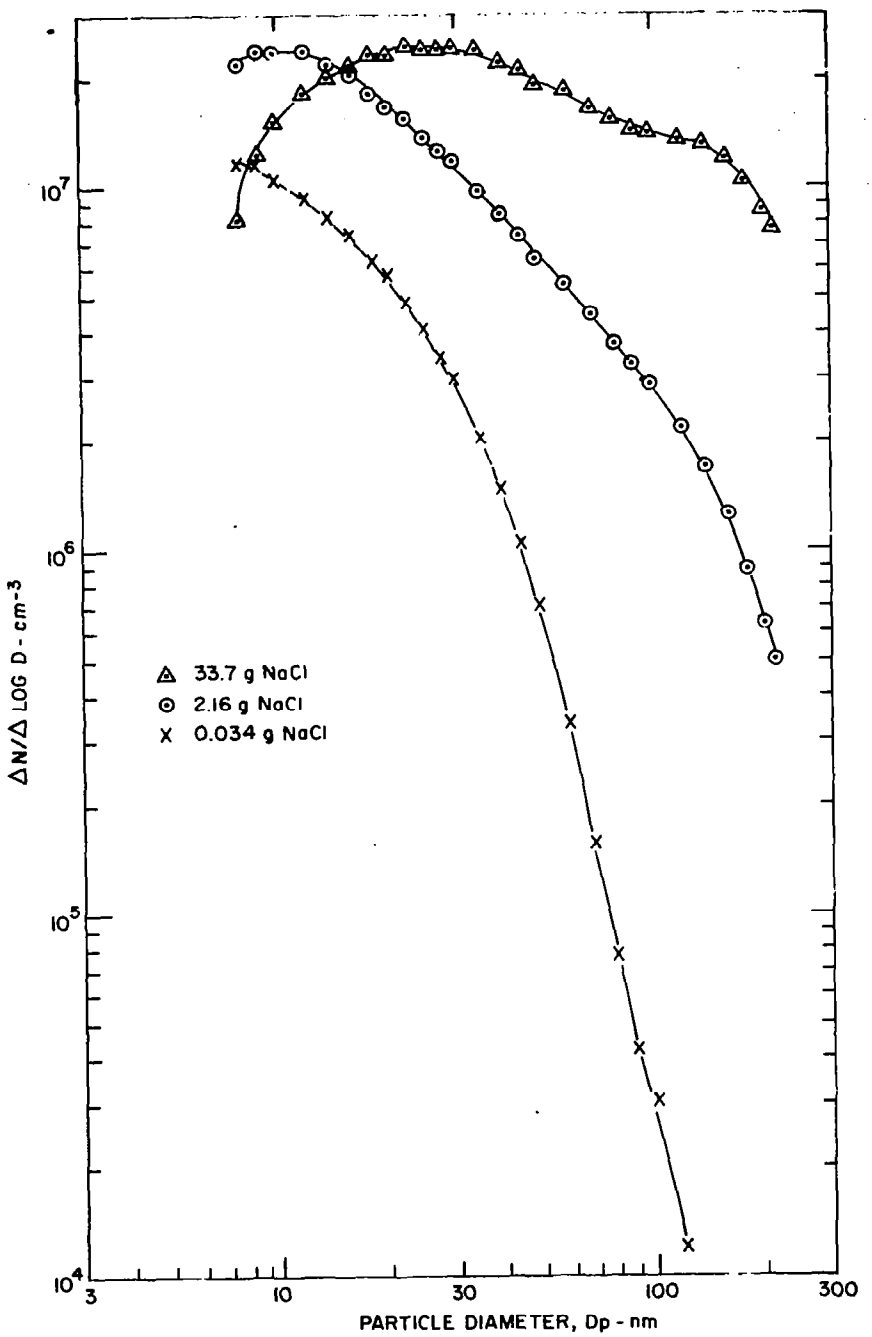

Figure 3-26. NaCl particle size distributions obtained with Nano-Mist nebulizer at 10 psi and with solutions of indicated concentrations.

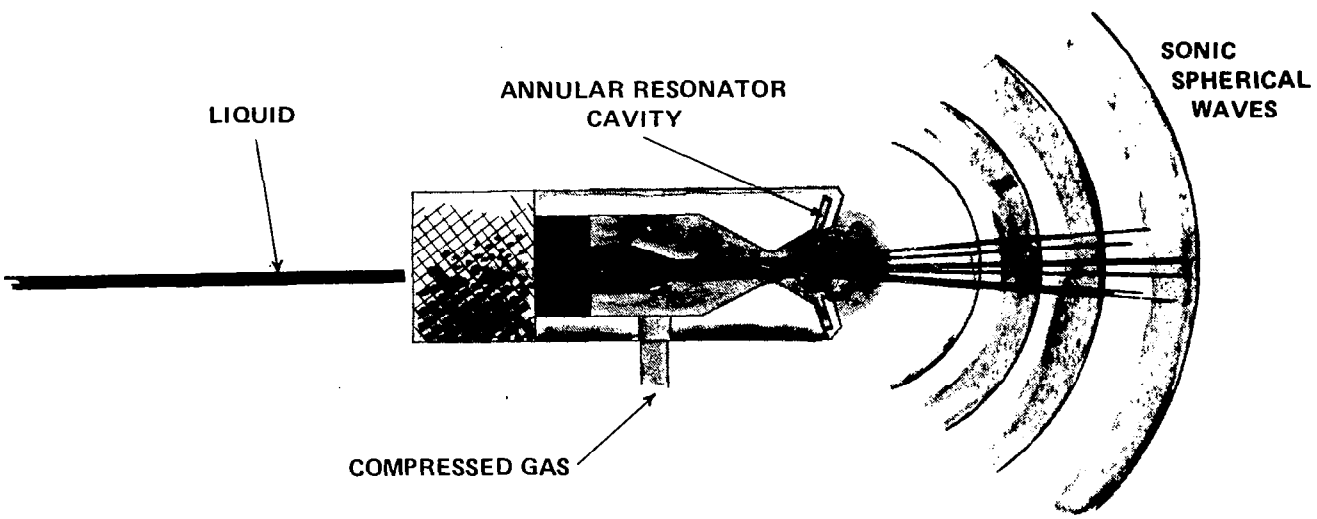

Figure 3-27. Schematic of Sonimist 600-1 Atomizer (from Sonimist specification sheet).

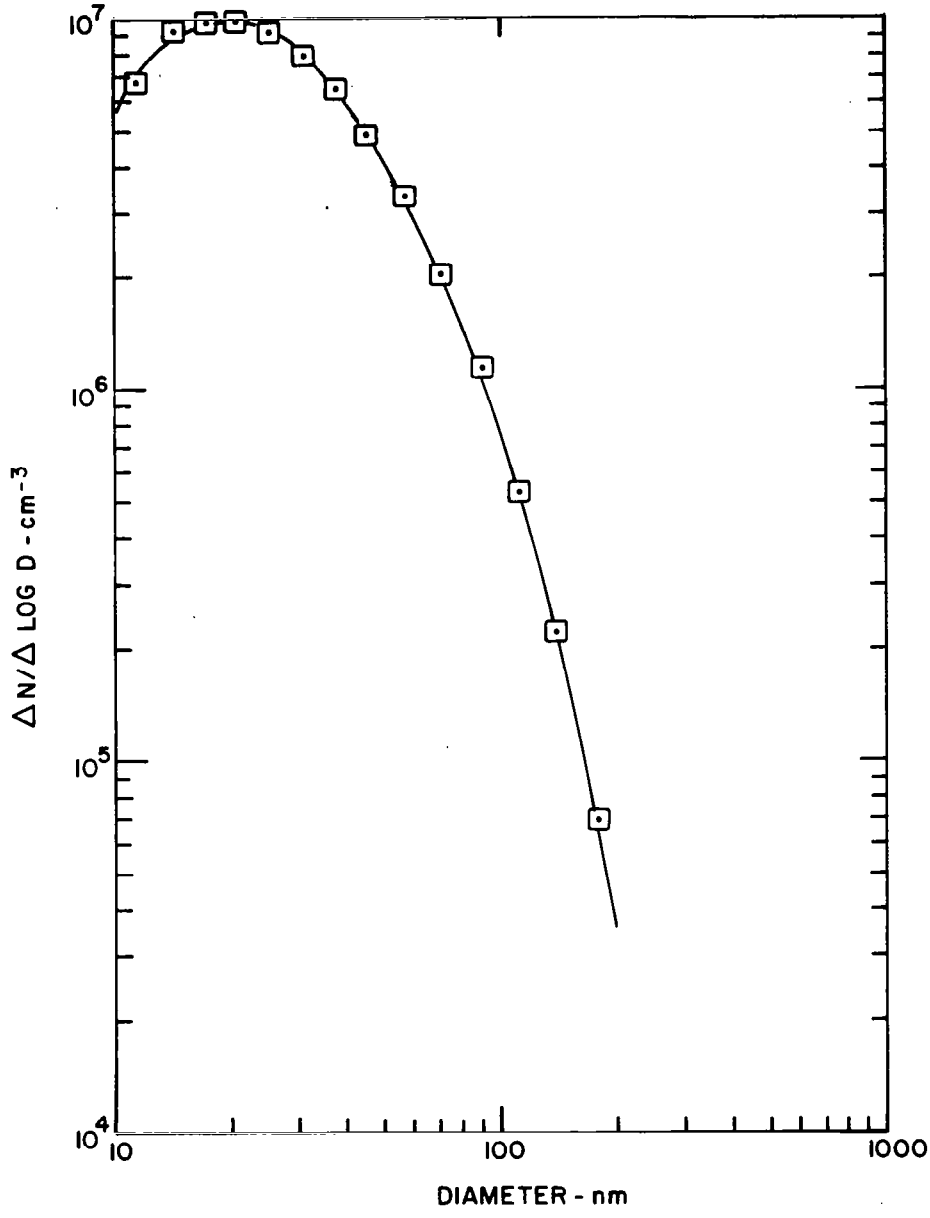

Figure 3-28. NaCl particle size distribution from Sonimist 600-1 atomizer (30 psi air pressure, 2.2 ml min^{-1} flow rate of 0.025% solution).

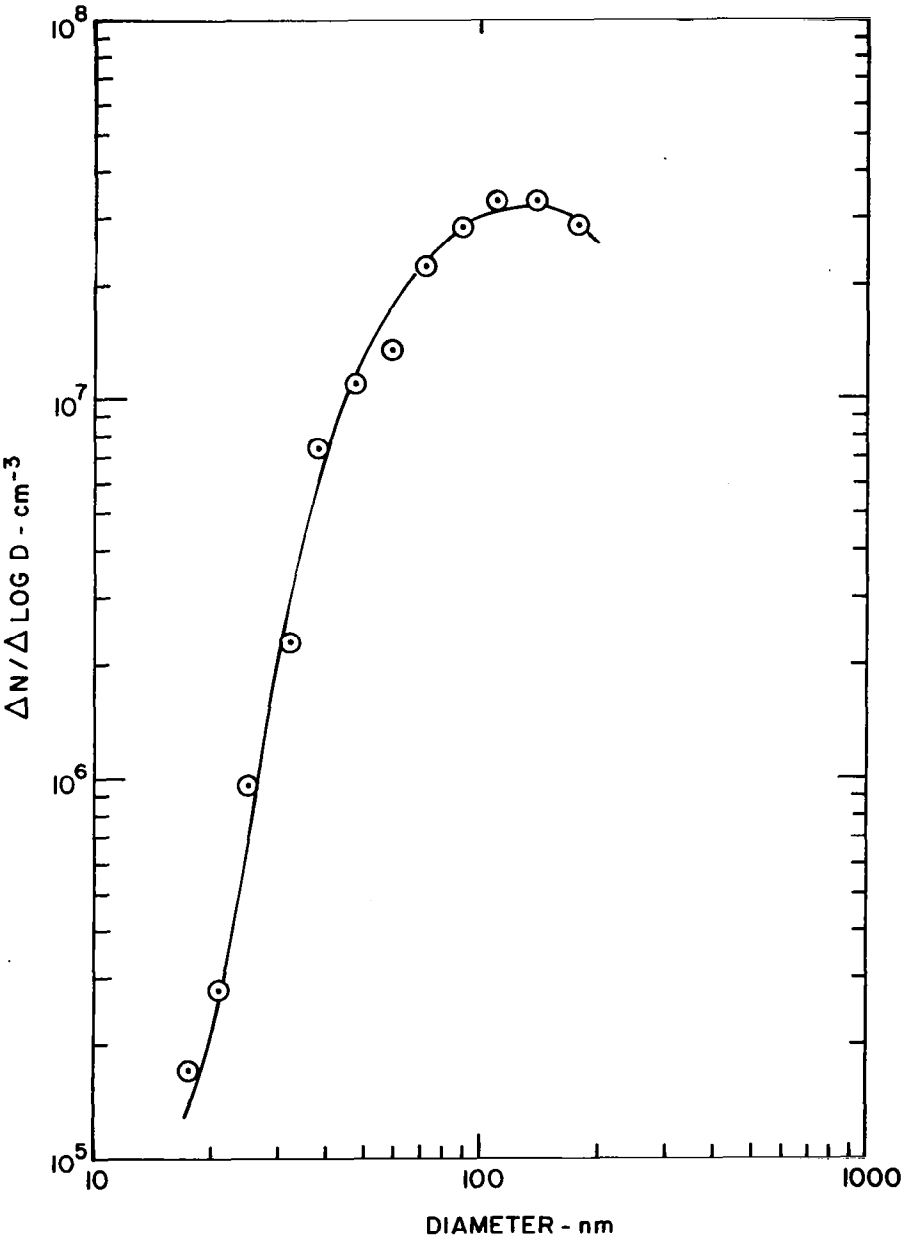

Figure 3-29. Sulfuric acid droplet size distribution obtained with the TSI-COA (1% diluted H_2SO_4, 30 psi air pressure).

taken in the present case as the humidity after the dryer in our test set up was always in the vicinity of 10%.

(2) Atomizer Output vs. Time

In the course of establishing size distributions from the COA with the set up shown in Figure 3-17, it became apparent that the COA's output was not always constant, but was showing large fluctuations (±10% or more), sometimes deteriorating gradually, sometimes abruptly. The strip-chart excerpts in Figure 3-30 illustrate (on top) an example of an unstable output while the recording at the bottom represents the kind of stable output expected from the COA and acceptable for ACPL purposes; both measurements were taken with the EAD and the same EC settings with a 0.01% NaCl solution. As no immediate cause for the atomizer's behavior could be detected, the EC-EAD were suspected of producing an artifact. This hypothesis was quickly rejected when the atomizer excess output (between neutralizer and EC, Figure 3-17) was connected to either the total particle counter (GE-CNC-2) or the EAA with the same result. The latter case is documented in Figure 3-31 where the upper trace represents the EAA reading (Channel 1, total number), and the trace below indicates the EAD measured EC output set for 58 nm particles. In addition to the perfect correlation, this Figure also shows a quasi-periodic behavior observed at times, though usually much less pronounced, as in Fig. 3-32. This output recording appeared to be more typical of higher salt concentrations as opposed to the trace in Figure 3-30 obtained with a 100 times more dilute solution.

Evidence that more and larger particles are produced during conditions of output instability is presented in Figure 3-33; these data were

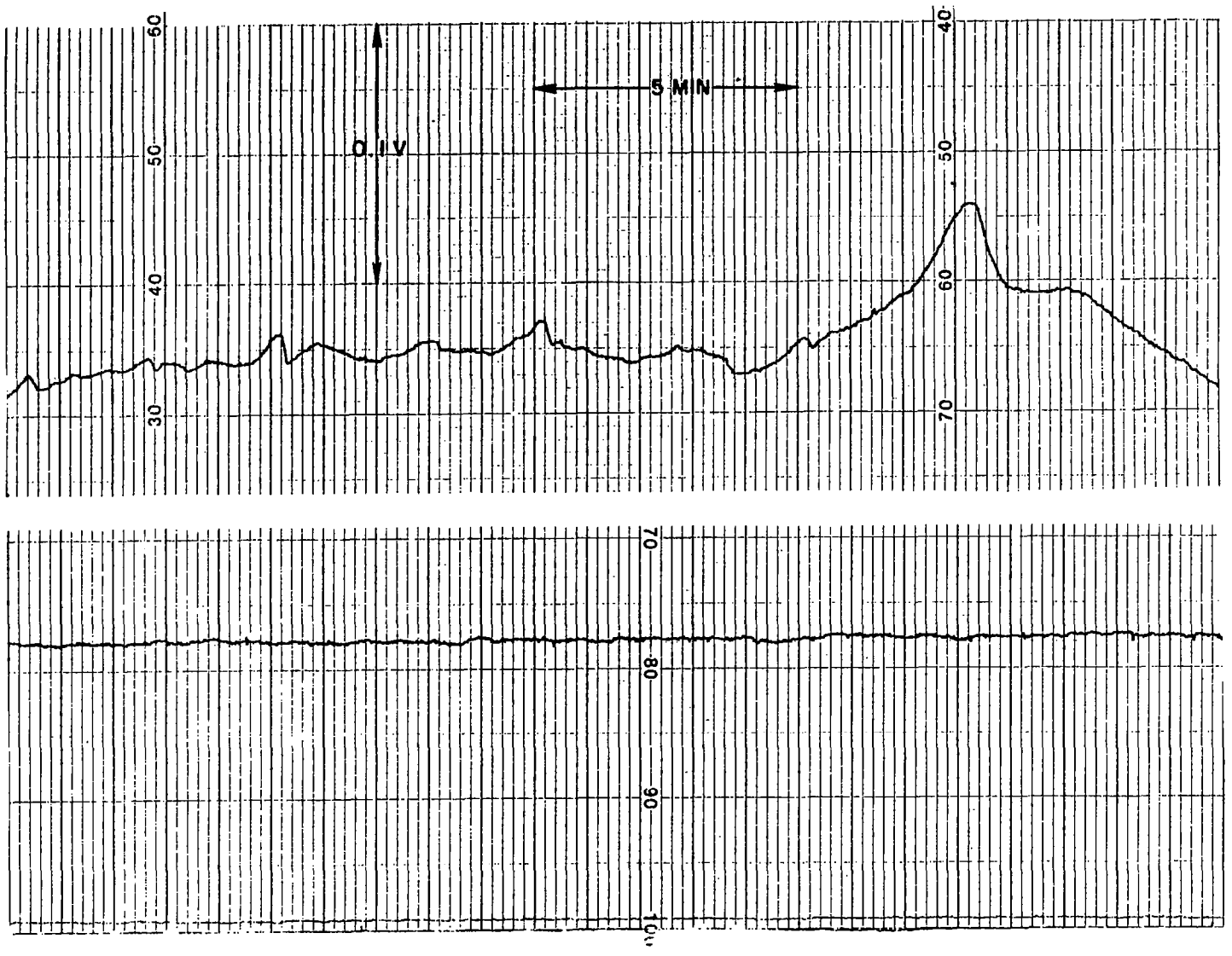

Figure 3-30. Example of stable (bottom) and unstable (top) output of NaCl aerosol from the TSI-COA at 30 psi and with 0.01% solution.

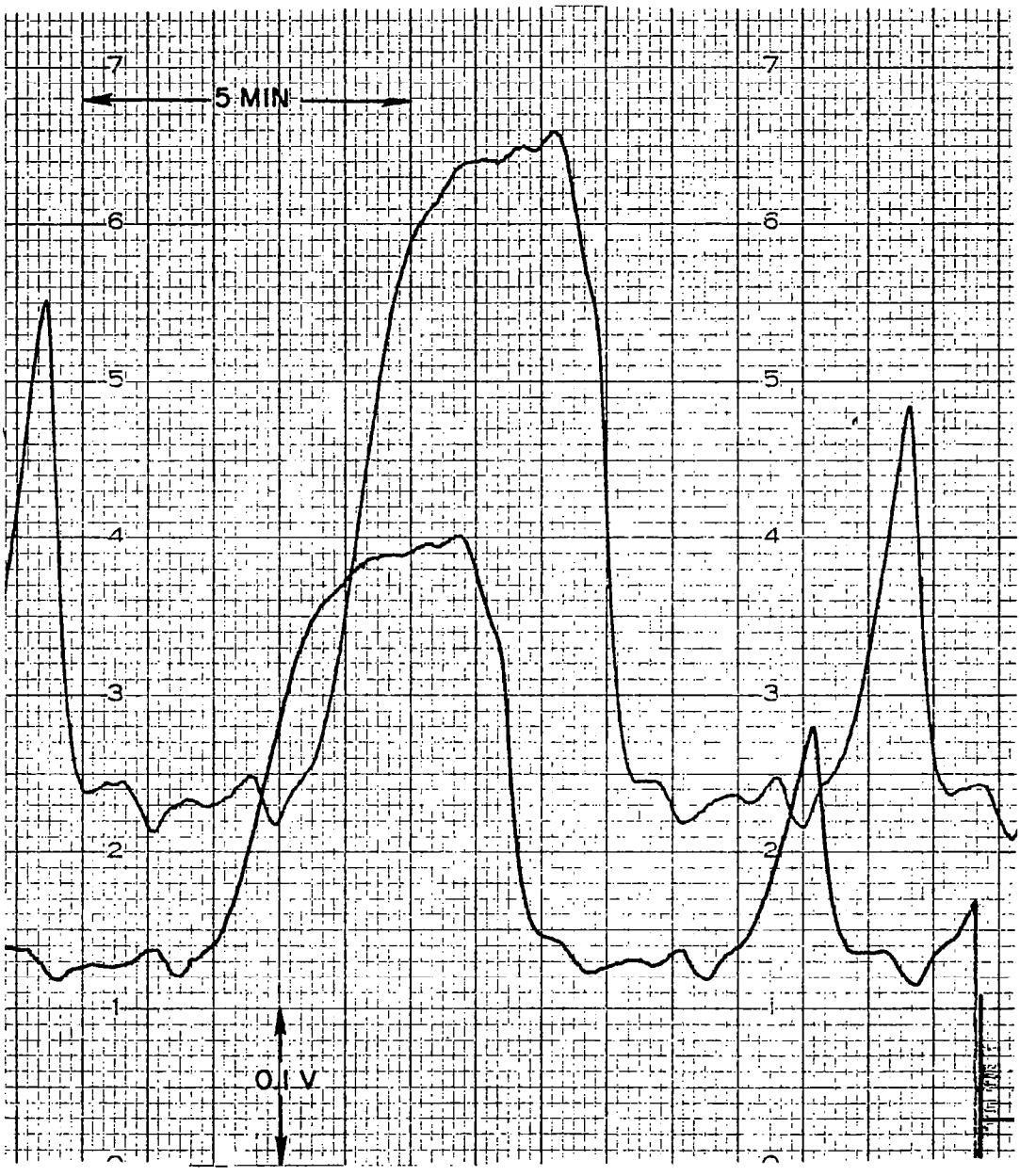

Figure 3-31. Unstable TSI-COA aerosol output measured with EAA, Channel 1 (total particles), upper trace, and with EC-EAD set for 58 nm particles (lower trace).

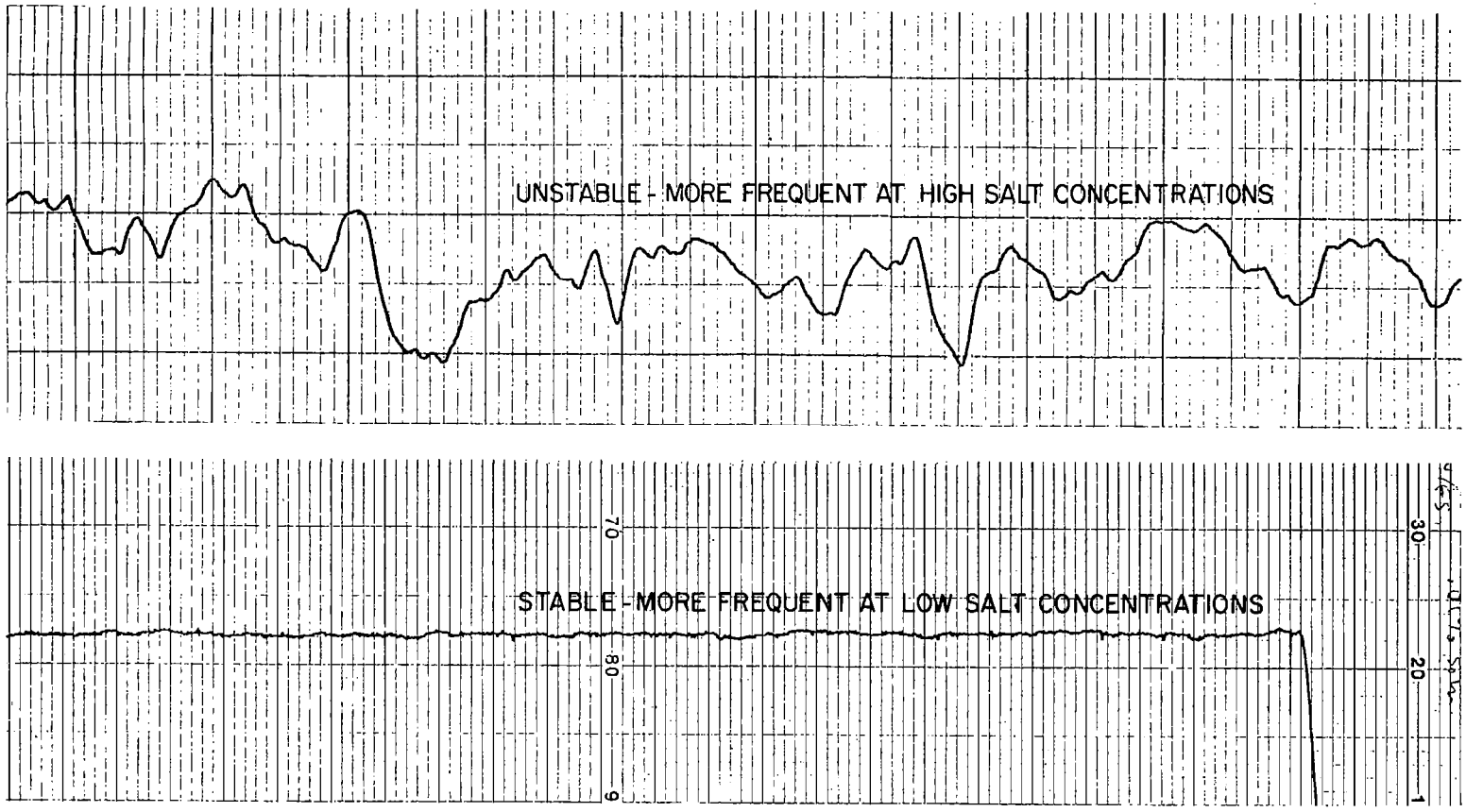

Figure 3-32. EC-EAD recording of unstable output from TSI-COA operated at 30 psi with 1% NaCl solution (top) and stable output from use of 0.01% solution (lower trace).

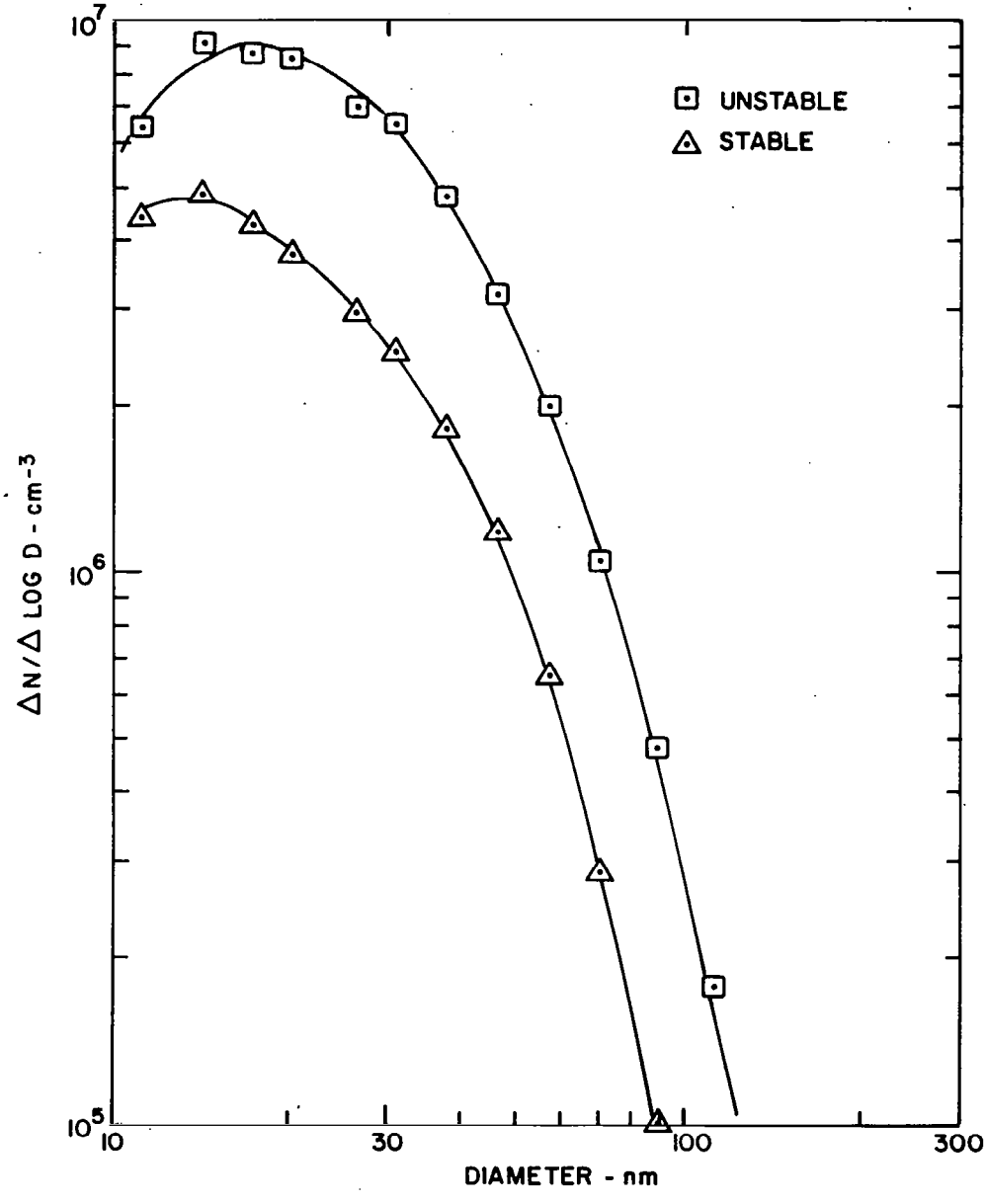

Figure 3-33. NaCl particle size distributions from TSI-COA for stable and unstable running mode (30 psi, 0.01% NaCl solution).

obtained with a dilute (0.01%) NaCl solution which, on the average, was less frequently associated with instability problems than higher salt concentrations.

Remedial measures in the form of a buffer vessel were considered; however, as the results of such a trial show in Figure 3-34, the fluctuations could not be suppressed sufficiently with the 2-liter container used.

In comparison, the DeVilbiss atomizer never gave a steady output as illustrated in Figure 3-35, while the Nano-Mist device displayed a consistently stable performance (see Figure 3-36) except for slow drifts that could tentatively be linked to temperature changes in the atomizer cavity. Tests with the Sonimist 600-1 showed it to be unsatisfactory with respect to output constancy; the stripchart (Figure 3-37) demonstrates the typical behavior involving long-term drifts of the order of 1% min^{-1} (the high frequency oscillations were caused by the liquid pump).

It was concluded that of the various atomizers we evaluated the TSI-COA gave the most constant output as long as it remained in its stable mode. The following section pertains to the search for causes of the unstable behavior.

c. Investigation of Output Instability and Design of Improved Constant Output Atomizer (ICOA)

(1) Information from Existing Atomizers

While atomizer output dependency on various input and design parameters has been discussed by several authors (e.g. May, 1973; Mercer, et al., 1968; Novak and Browner, 1980), output stability with

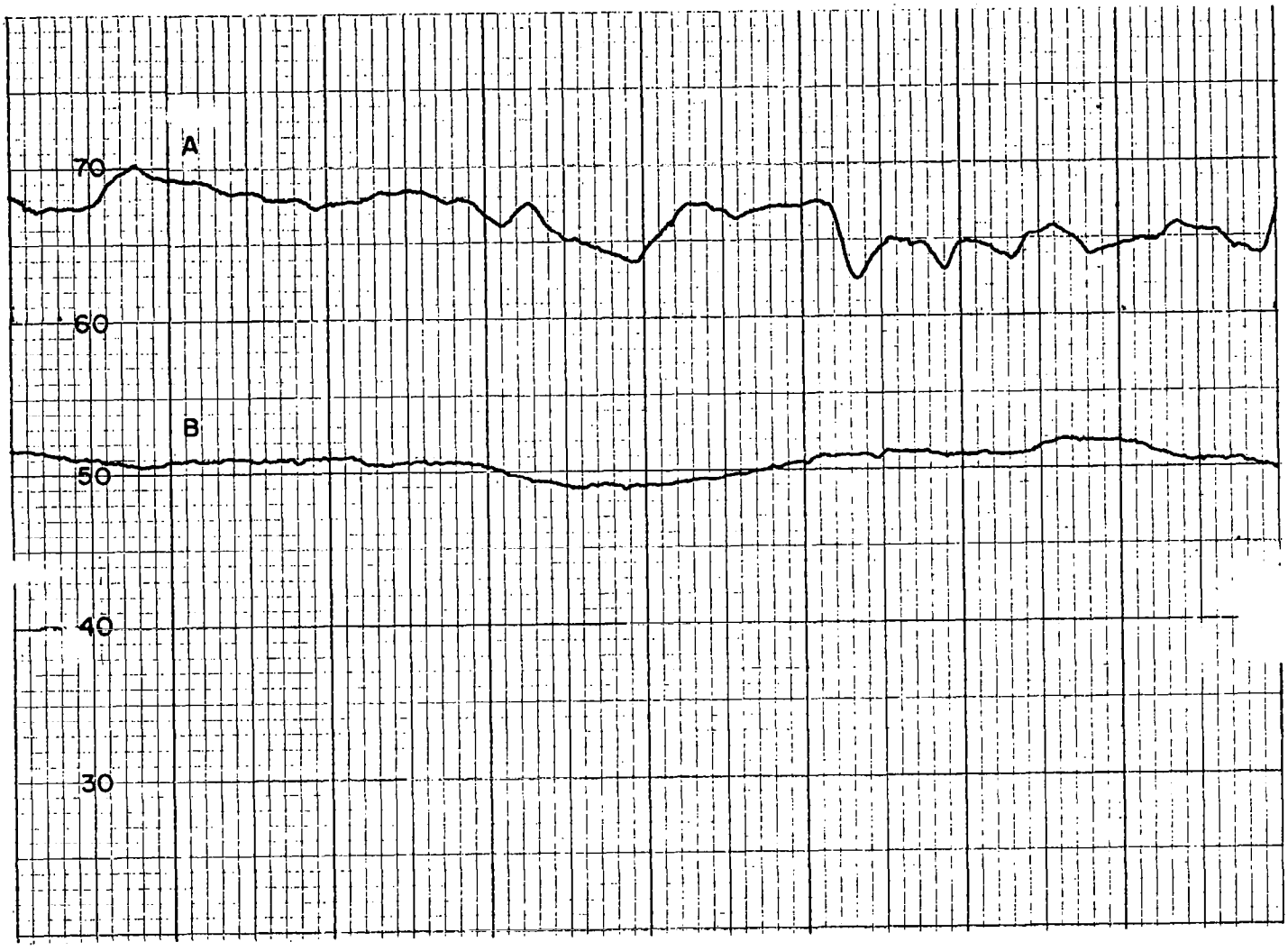

Figure 3-34. Unstable TSI-COA output undampened (A) and dampened by passage through 2 liter buffer vessel (B). Same time scale as in 3-31.

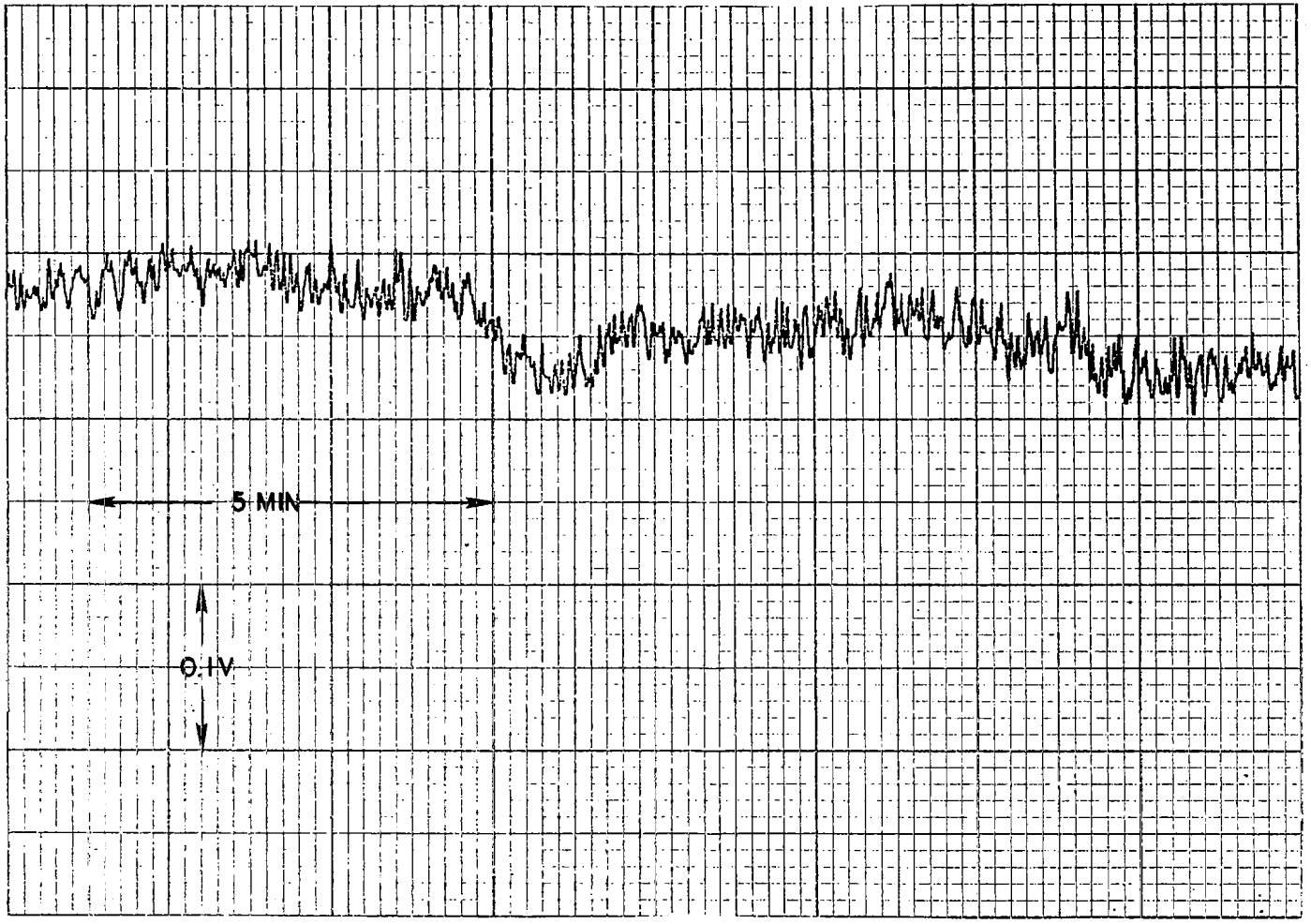
5 MIN
0.1V

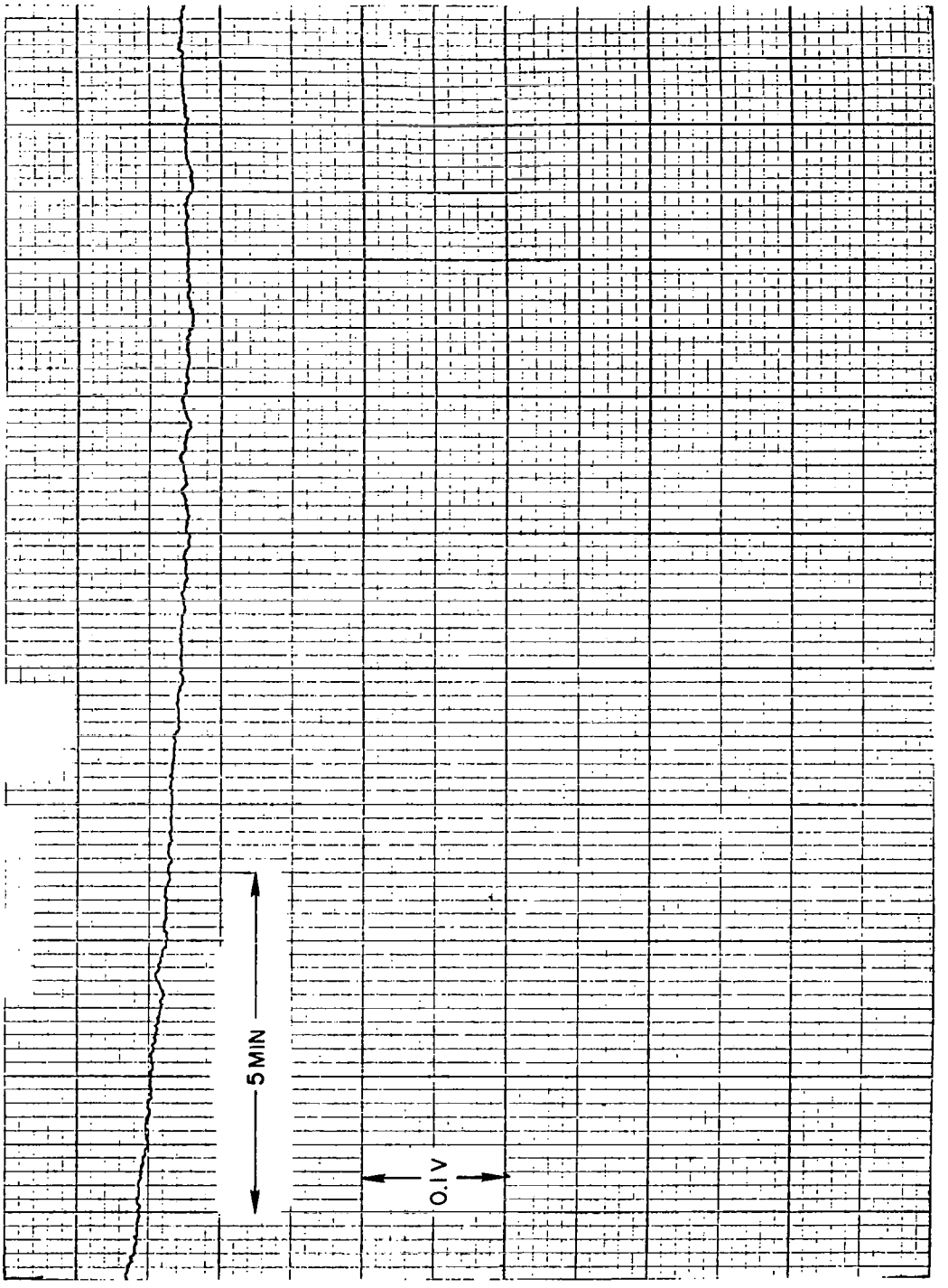

Figure 3-36. Example of generally steady output of Nano-Mist nebulizer.

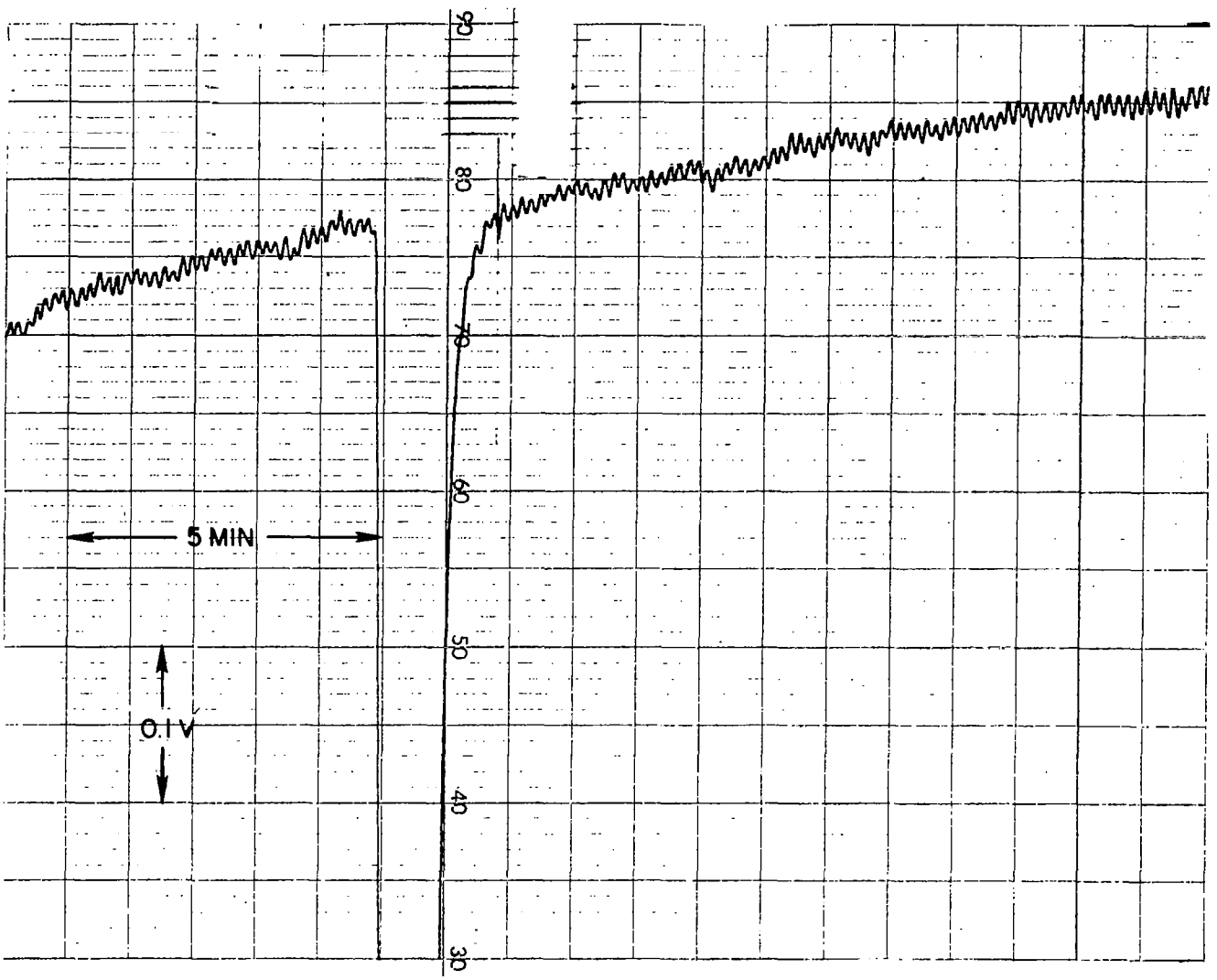

Figure 3-37. Output of Sonimist 600-1 atomizer showing frequently occurring drift (small oscillations caused by fluid pump).

time has been the subject of only few investigations (Liu and Lee, 1975; Collins, 1975). Results of the latter did not provide any assistance in solving the present problem of atomizer output instability.

After concluding that the cause or causes of the atomizer's output fluctuations were occurring inside the atomizer itself an extensive test series was started with the aim to determine which parameter or mechanism was responsible for the detrimental behavior of the COA.

One relatively delicate component of the device is the air nozzle, a platinum disc with a 0.034 cm hole in the center. Removal and cleaning of the nozzle occasionally had a beneficial effect, though never long lasting. For further scrutiny of the small hole, SEM pictures were taken after cleaning and also after 12 hours operation. Output fluctuations became progressively worse with operation. The result, shown in Fig. 3-38, indicated no changes due to erosion or deposits. It was found, however, that the nozzle plate had some lateral play in its mount which caused differences in output after each removal and reinstallation, but could not explain the fluctuations.

It was noticed that drainage of excess liquid out of the COA body often fluctuated in patterns similar to the ones of the output, but it was not possible to quantify the result sufficiently to establish a clear correlation.

Furthermore, at high salt concentration, it was observed that foam was carried by the output airstream 10 to 20 cm beyond the COA's output opening where it would gradually collapse and drain back into the atomizer. However, the impossibility of actually observing the action inside the COA pointed to the need for continuing the study with transparent atomizers.

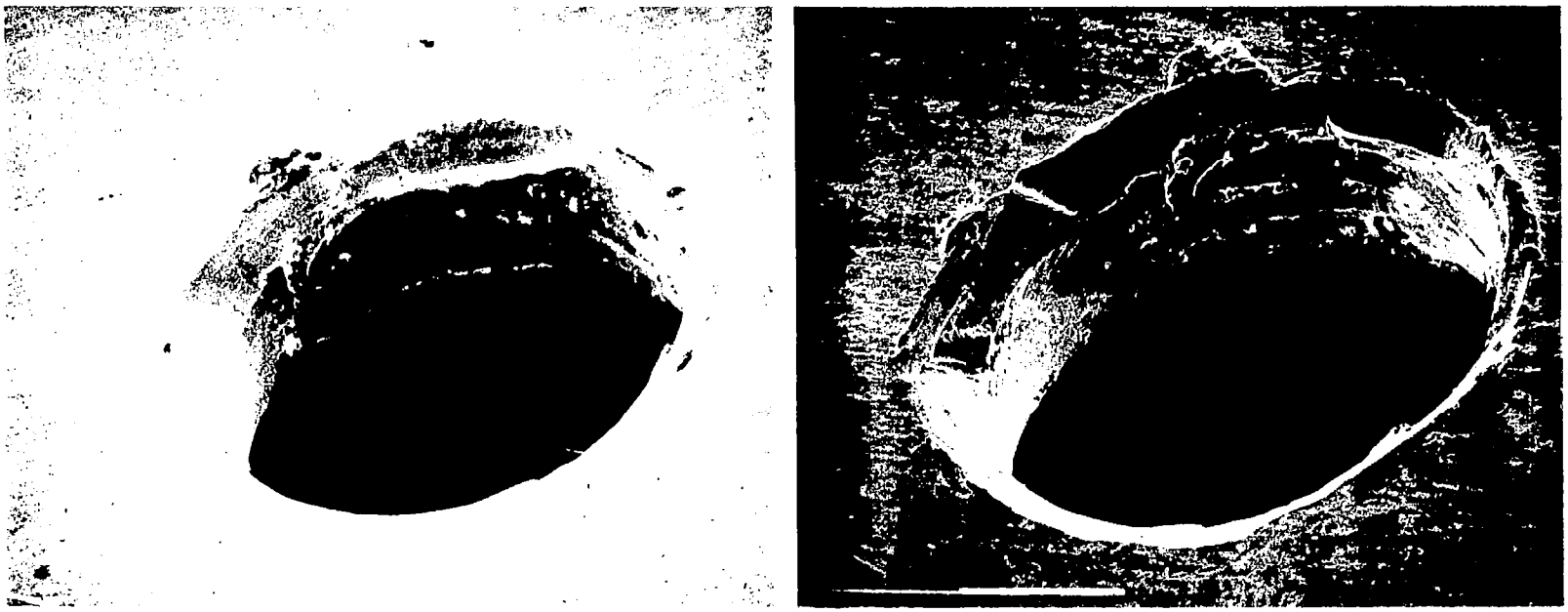

Figure 3-38. Scanning electron micrograph of TSI-COA nozzle plate before use (left) and after 12 hours of operation with increasingly unstable output. (Hole diameter = 0.343 mm).

The previously discussed DeVilbiss and Nano-Mist units which are molded from clear plastic were briefly used with the intent of visually detecting phenomena in the nozzle area that would provide some clue to the irregular behavior. In the DeVilbiss device, the impaction surface (small sphere) is mounted very close to the nozzle which has the effect that the whole atomizer cavity is filled with a turbulently moving mist impacting and accumulating on all surfaces and thus obstructing a clear view of the nozzle area to be scrutinized. However, a few tentative observations suggested that accumulated fluid dripping from the impaction sphere and fluid feed tube into the jet was at least contributing to the output fluctuations. The Nano-Mist nebulizer, by its very design, shrouds the nozzle and primary impaction area behind a curtain of fluid, and thus was not useful for this aspect of the investigation.

(2) Variable Geometry Atomizer (VGA)

In order to improve the conditions for observing the atomization process and to detect the influence of various nozzle configurations on the quality of the aerosol output, a variable geometry atomizer (VGA) was designed and fabricated. This device consisted of a compressed air nozzle* at the end of a metal tube to which liquid feed tubes of different sizes and shapes could be attached in different positions. The basic type with open jet is shown in Figure 3-39 which illustrates how the liquid feed tube can be shifted relative to the air nozzle. Figure 3-40 depicts the nozzle assembly installed in its cylindrical plexiglass housing in which a baffle or impaction plate can be positioned at any

*During most of the investigation sapphire nozzles were used as GE, for some time, considered their application in the final flight version of the ACPL atomizer.

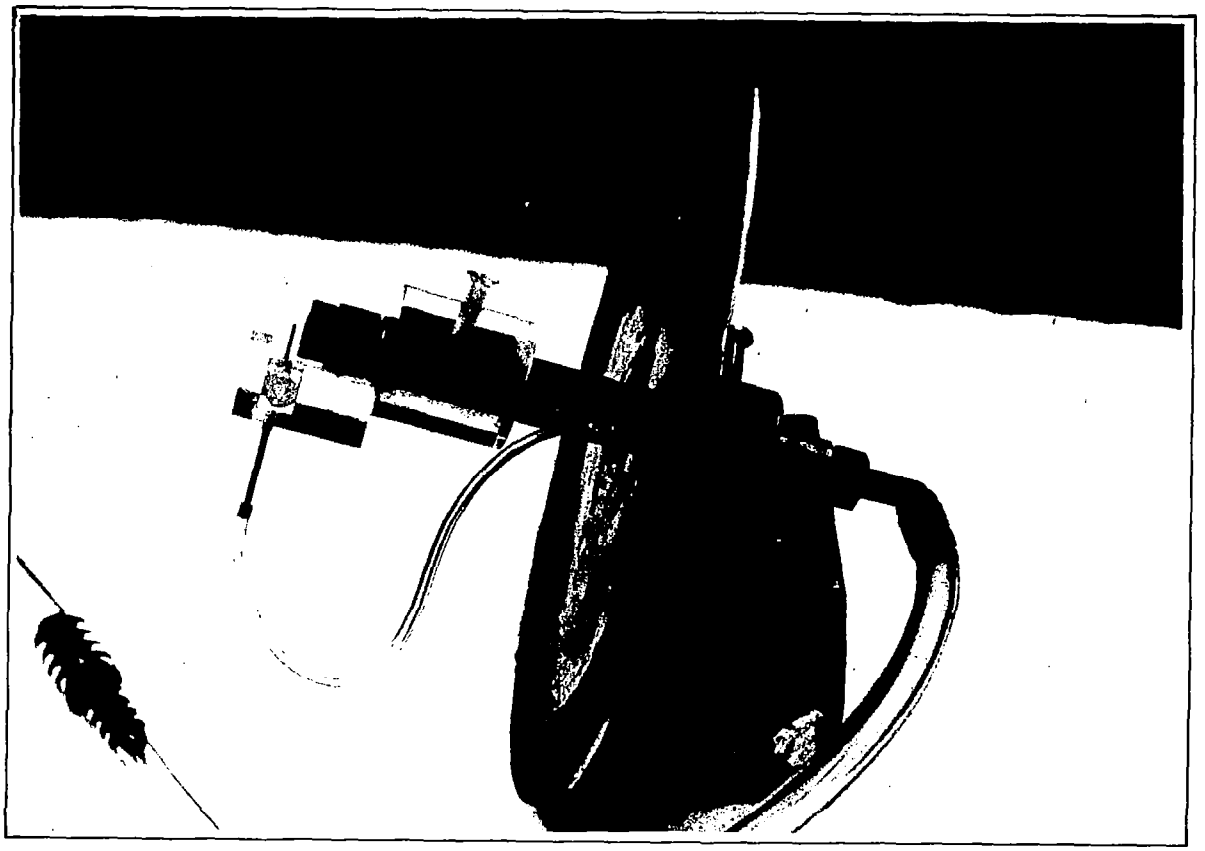

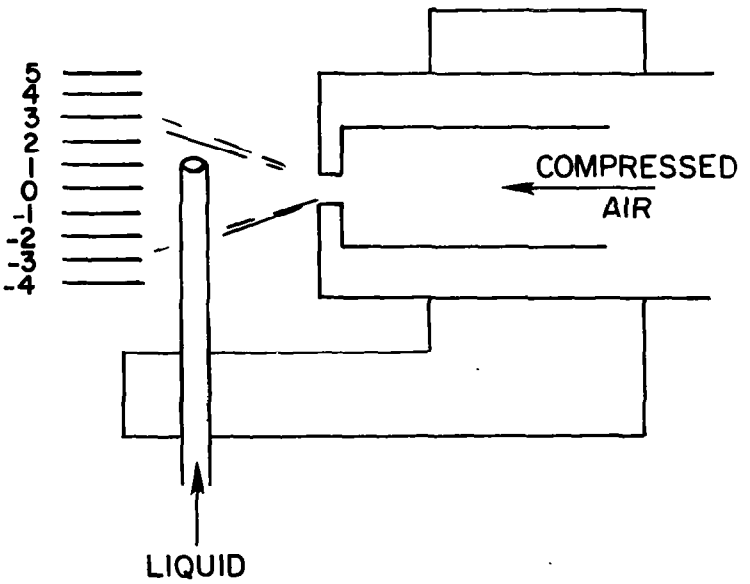

Figure 3-39. Photograph and schematic of Variable Geometry Atomizer. OD of compressed air tube is 1.25 cm. Scale in schematic refers to positions used in Figure 3-46.

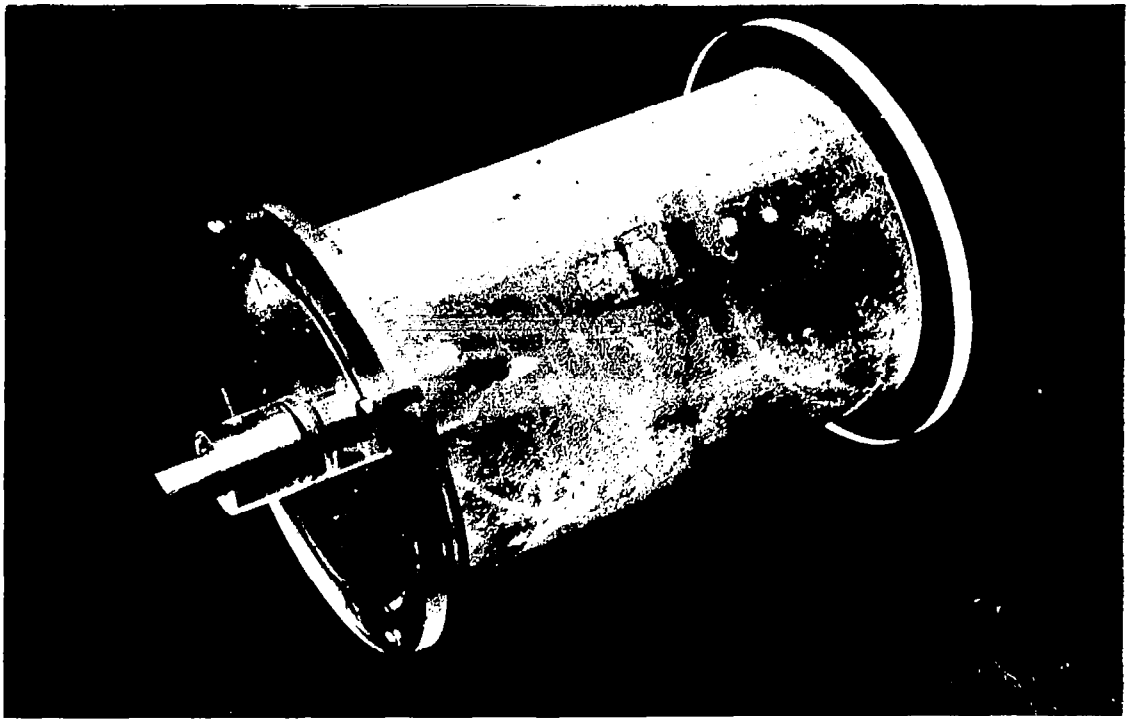

Figure 3-40. Photograph of VGA in one of its transparent housings.

desired distance from the nozzle. A liquid feed arrangement with ducted air jet as in the TSI-COA or the GE-ACPL model is shown in Figure 3-41; as the diagram indicates, the plexiglass part shown in the photograph fits on the same air nozzle used in the open jet configuration. Typical size distributions obtained with the open and the ducted jet version are plotted in Figure 3-42 and 3-43, respectively.

(3) Study of Output Fluctuations

It was suspected that unstable behavior of the air jet was a prime contributor to the output variations, and thus our first concern was to observe the motion of the air jet. For this purpose, the nozzle assembly was mounted such that a wall of the atomizer housing served as impaction surface, on which the area of the jet as delineated by the impinging spray droplets, could be scrutinized. Thus, it was found that the VGA's output varied monotonically with the apparent solid angle of the jet. At times, the jet was not only expanding and contracting, but also noticeably changing direction. Initially, the cause of these effects was thought to be located in the jet nozzle which was examined repeatedly without detecting any irregularities.

Since it was noticed that the position of the liquid feed orifice influenced the output of the VGA, this relationship was explored systematically. Figure 3-44 summarizes the results with respect to the output fluctuations; it is interesting to note that the steadiest output was obtained at a lateral misalignment of 0.5 mm between air jet and liquid feed. Careful observation revealed that one contribution to the output fluctuations originated as liquid accumulations (source to be discussed later) on the liquid feed tube as shown in Figure 3-45 which,

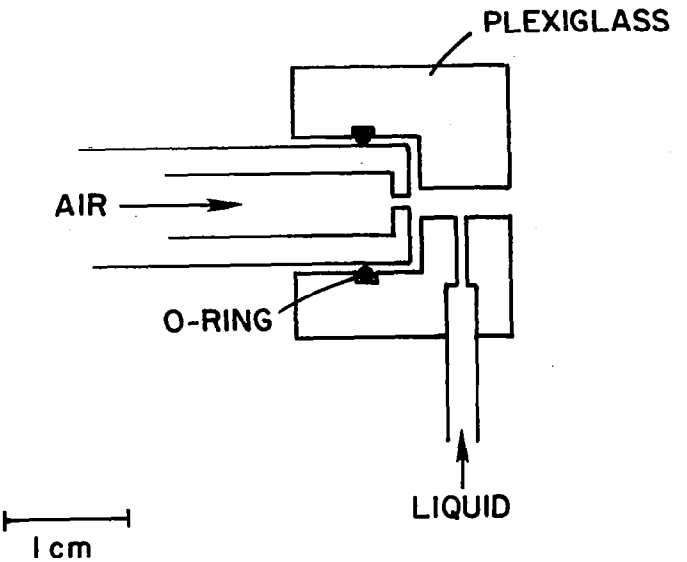

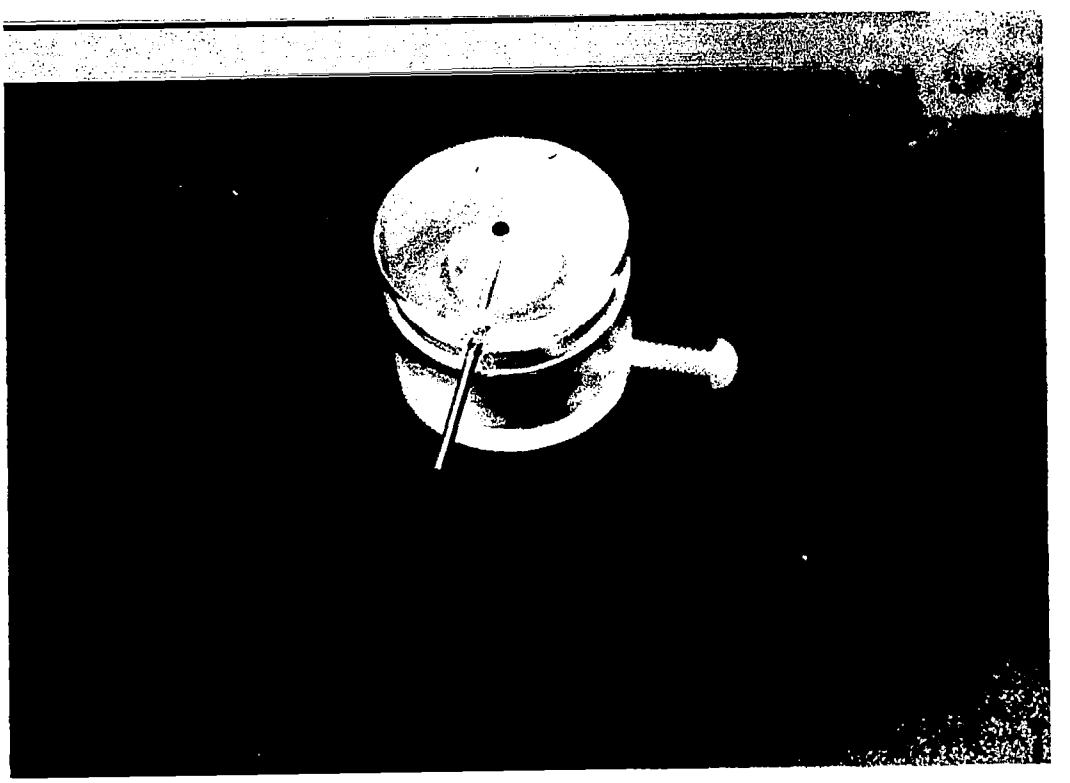

Figure 3-41. Schematic and photograph of ducted jet version of VGA.

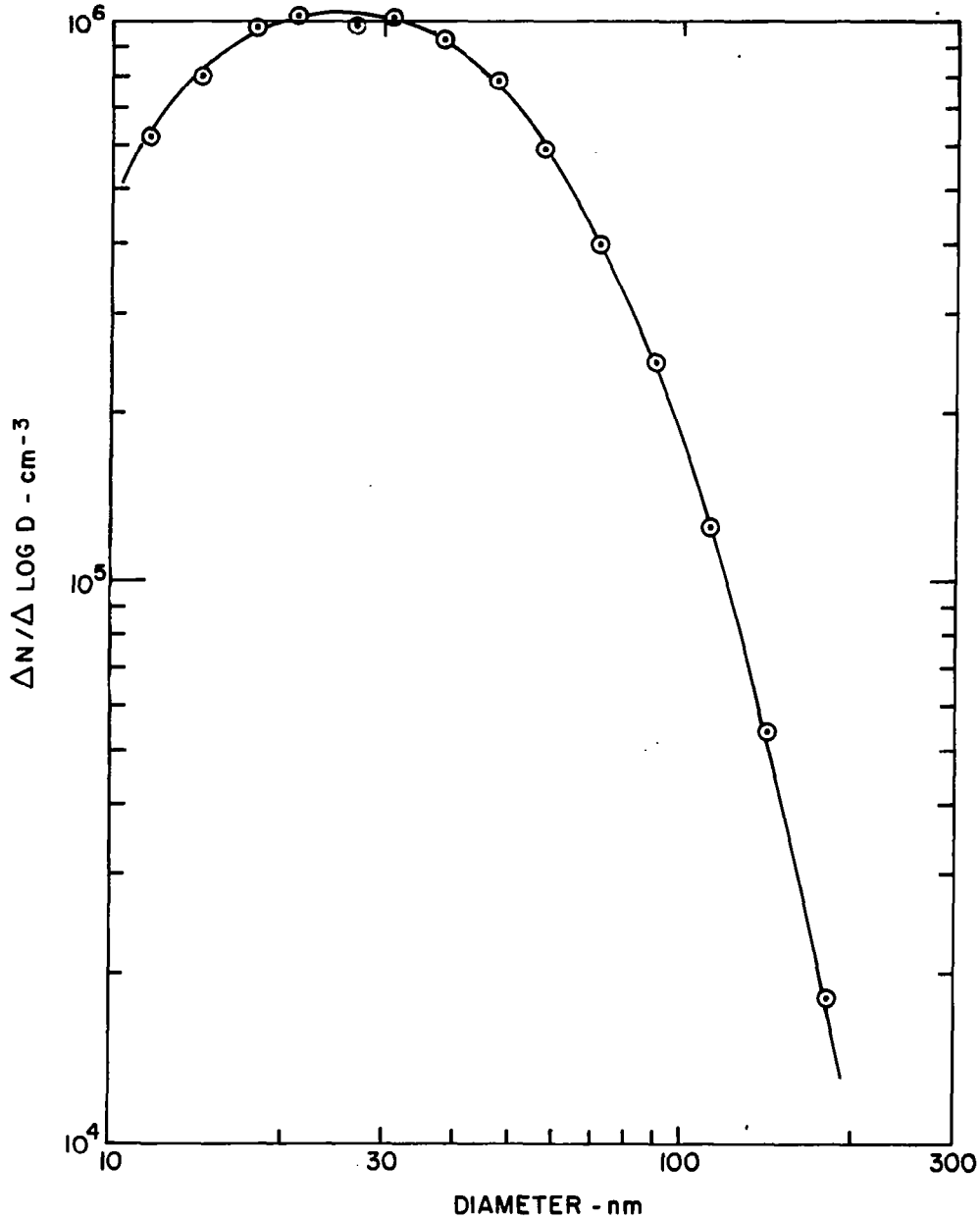

Figure 3-42. NaCl particle size distribution generated by open jet VGA with 0.025% solution and 30 psi.

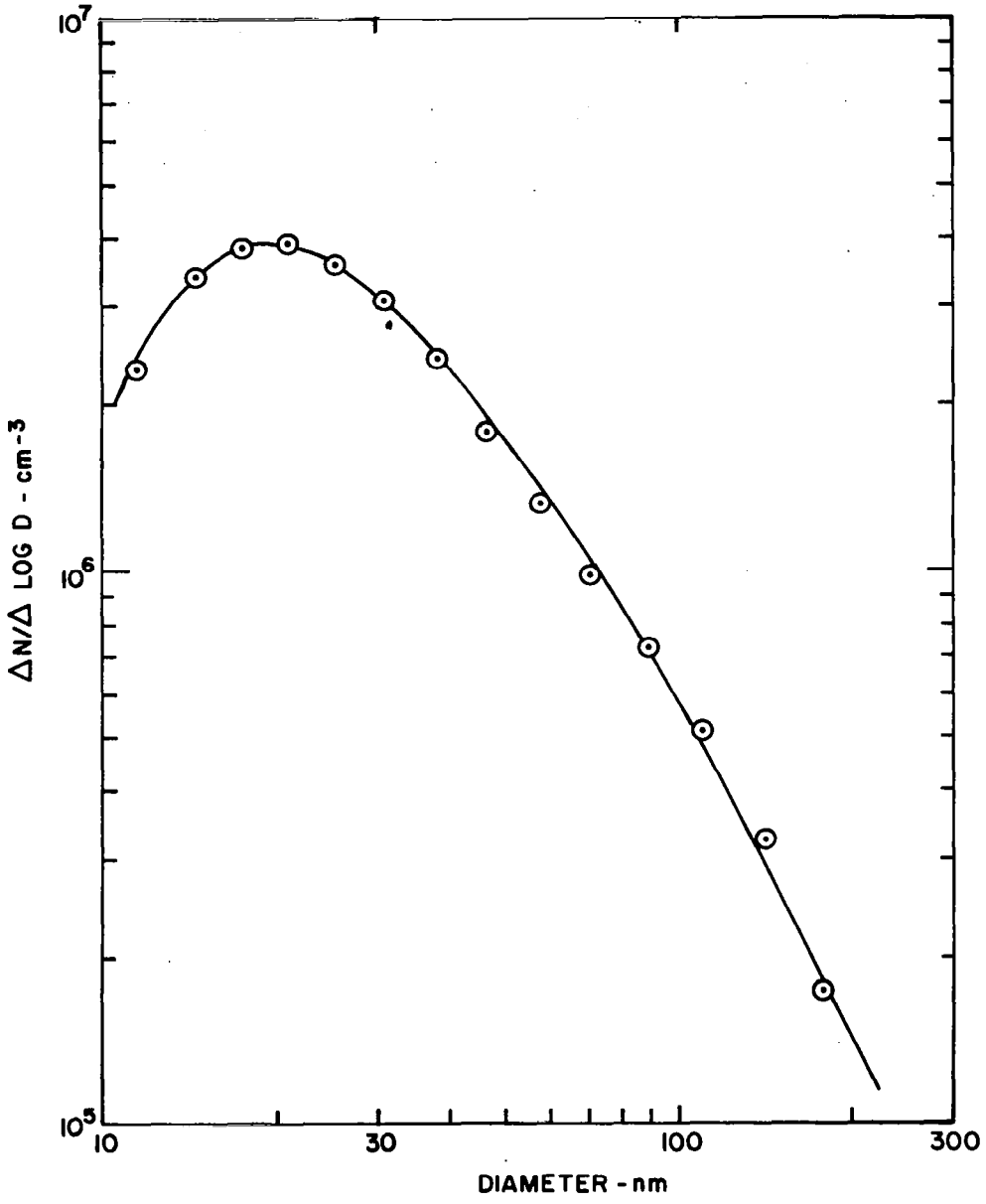

Figure 3-43. NaCl particle size distribution generated by ducted jet VGA with 0.025% solution and 30 psi.

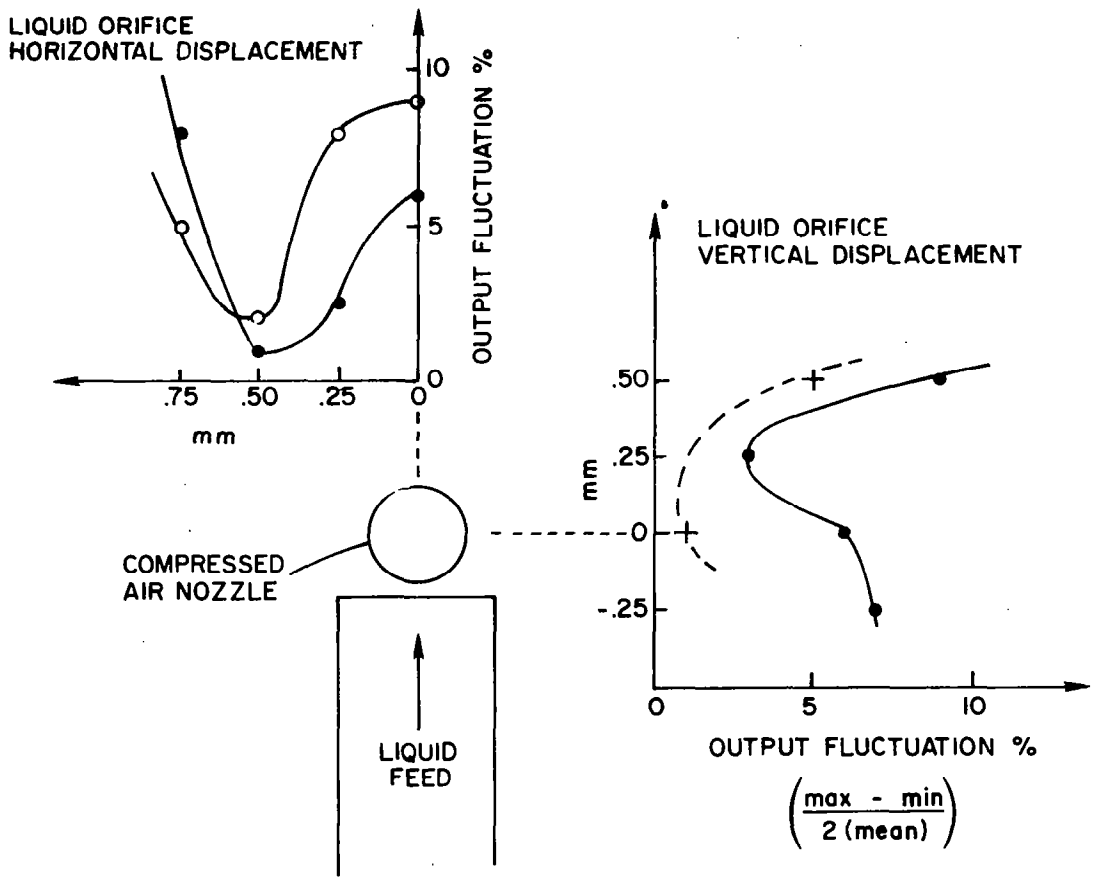

Figure 3-44. Aerosol output fluctuation as a function of liquid feed orifice position relative to jet axis.

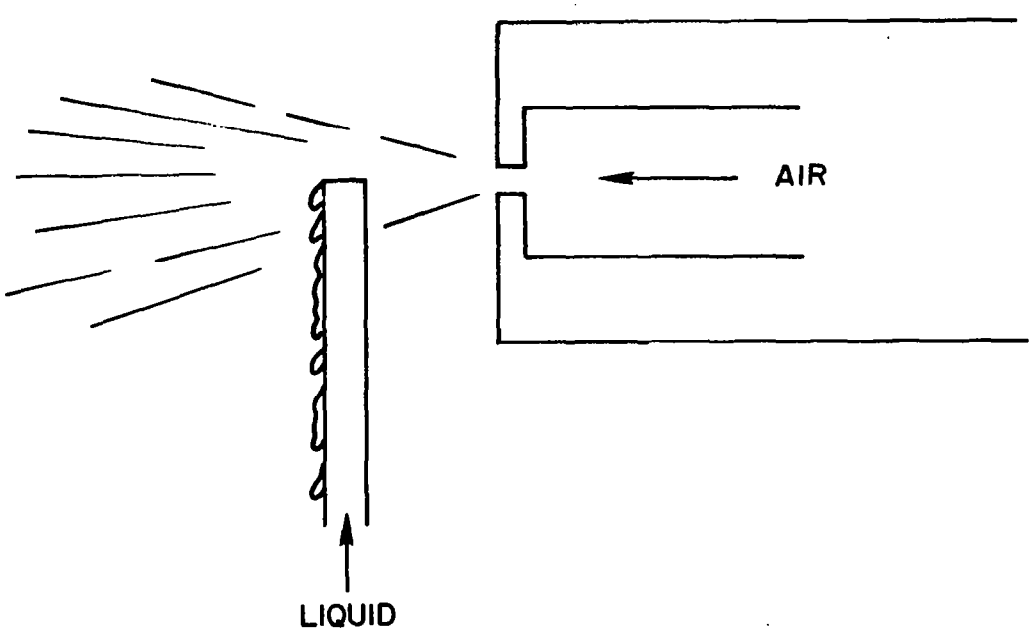

Figure 3-45. Schematic representation of one cause for output fluctuations: fluid accumulating on liquid feed tube entrained into jet once the drops are large enough.

when large enough, were entrained into the jet giving rise to an output increase. In an attempt to correct the problem, the outside of the liquid feed tube was made wettable by sandblasting its surface. As a result, the liquid would run off in a thin layer and was much less frequently entrained into the jet; thus, the output fluctuations were reduced considerably as indicated by the dashed line in Figure 3-44.

An example of how the output size spectra vary with changing vertical position of liquid feed orifice is plotted in Figure 3-46. Essentially, the output decreases monotonically for all particle sizes with increasing distance of the orifice from the jet axis. This is in contrast to the behavior of the TSI-COA (see Section III.B.b) which showed higher output values in the fluctuating mode, indicating that possibly different mechanisms were responsible for the two sets of observations.

As quantitative experiments did not readily point to the causes of output fluctuations, intensified visual and stereomicroscopic observation of the VGA in operation provided essential clues that led to an understanding of the stability problem.

Thus it was possible to discern the formation of salt deposits on the rim of the liquid feed tube where the air jet first encounters the liquid. As the salt gradually accumulated, the amplitude of the output fluctuations continued to increase; conversely, removal of the salt deposit from the top of the liquid feed tube immediately restored the stability of the output. Apparently, the minute salt deposit alters the flow pattern of the jet sufficiently to cause the liquid to be dispersed differently. Since the salt deposits are more likely to form when

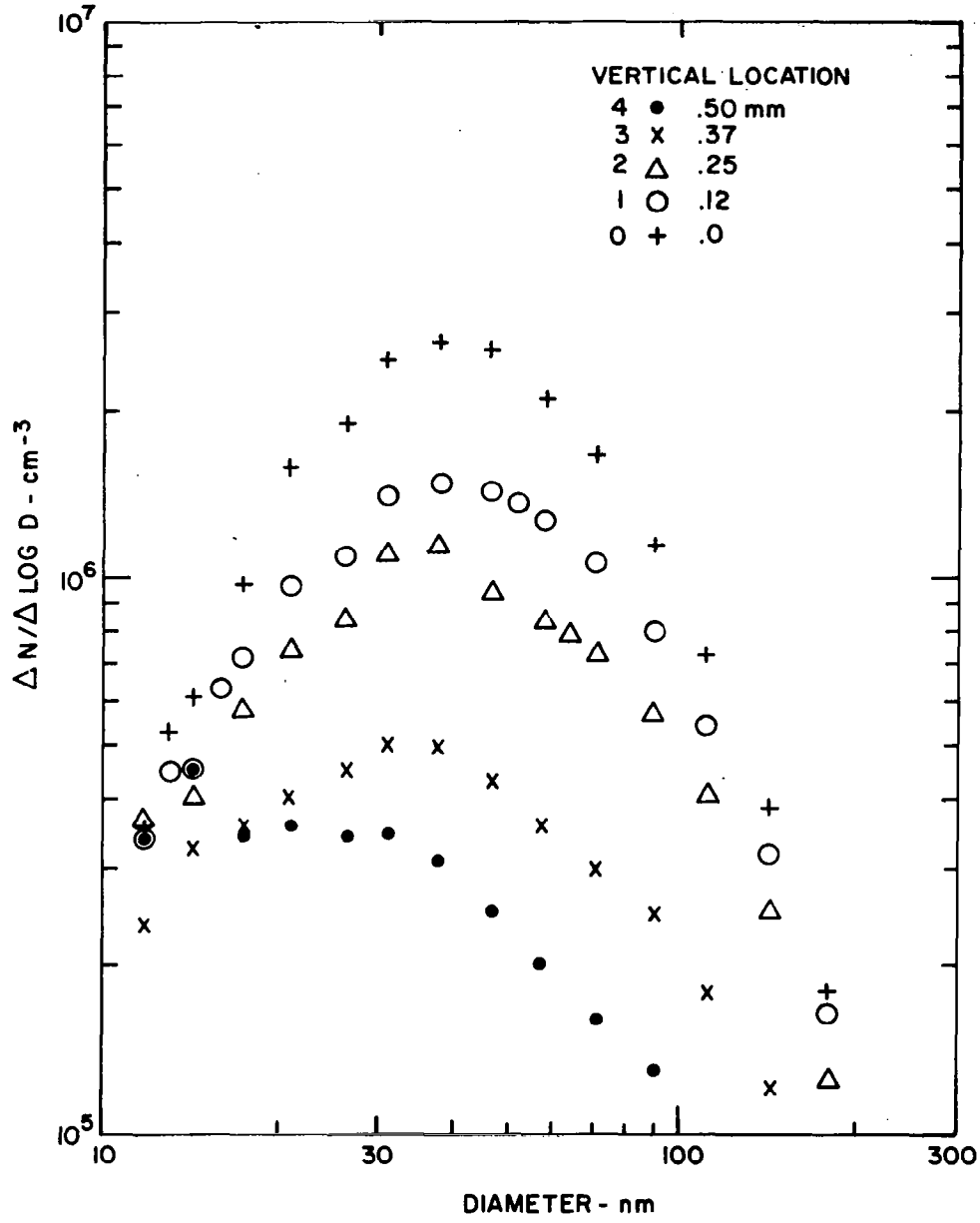

Figure 3-46. Particle size spectra from VGA output as a function of liquid feed tube position (cf. Fig. 3-39).

solutions of high concentration are atomized, it is obvious why concentrated salt solutions were leading more frequently to more severe output fluctuations.

In another experiment, the atomizer performances with two different sizes (1 and 0.5 mm I.D.) of liquid feed tubes were compared. As long as no salt deposits formed, the thinner tube produced a much steadier output than the wider tube on which the liquid surface was oscillating irregularly under the influence of the jet resulting in liquid injection into the jet at irregular intervals.

Further attention was focussed on the previously mentioned case of drops on the outside of the liquid feed tube which caused output fluctuations due to quasi-periodic entrainment of these drops into the jet. It was found that the fluid originated from the liquid orifice except in those instances where spray from a too closely positioned impaction surface deposited on the liquid feed tube (as on most other internal surfaces).

Based on these findings, it seemed that atomizer output fluctuations could be eliminated if a nozzle arrangement could be devised that would prevent formation of salt deposits on the jet-liquid interface, and that would cause all liquid fed to the device to be atomized while preventing any settling or impacting spray from accumulating in such a manner that it re-enters the jet.

(4) Design of Improved Constant Output Atomizer (ICOA)

Initially, in attempting to fulfill the above criteria, a variety of simple modifications of the original liquid feed configuration were tried, such as the ones depicted in Figure 3-47 which were, however,

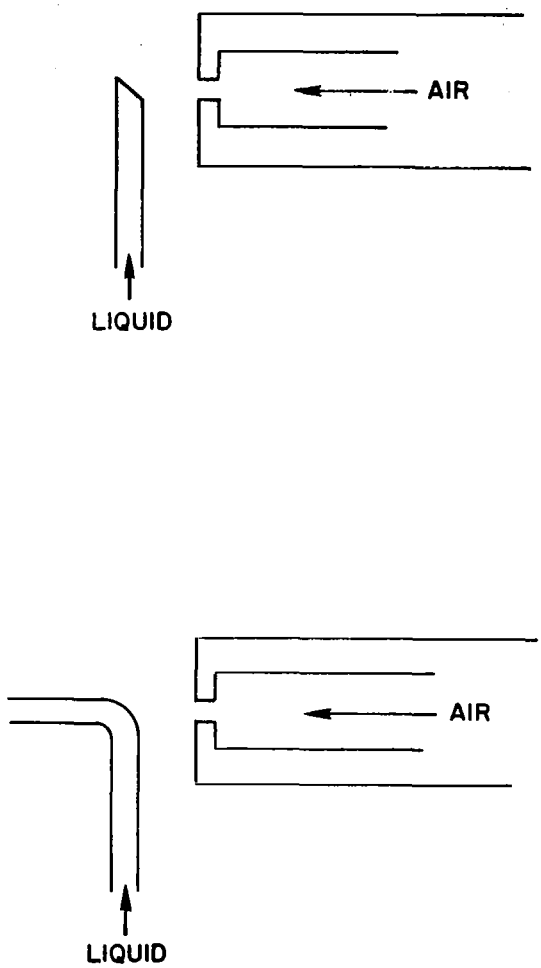

Figure 3-47. Two examples of liquid feed configurations which were tried out.

unsuccessful. In considerable deviation from those more conventional nozzle geometries, experiments were run with an atomizer consisting of the usual VGA air jet nozzle over which a disc of fine wire mesh (~0.1 mm openings) was placed and a liquid feed orifice positioned to contact the wire mesh about 3 mm off the jet axis. In operation, the wire mesh held the liquid pumped from the orifice by capillary action while the jet penetrating the wire mesh atomized the liquid being sucked into its path. In this arrangement where the liquid was flowing radially towards the jet in the center, no salt deposits were formed and no liquid left the main stream to be entrained later. This design provided an output with much fewer fluctuations, but the wire mesh in the path of the jet seemed to have a somewhat detrimental effect on reproducibility. Also from the standpoint of decontamination and maintenance, the wire mesh was impractical.

The next step in the evolution of the ICOA was the version illustrated schematically in Figure 3-48. The wire mesh was substituted by a groove which ducted the fluid (again by capillary action) to the center into the jet and, judging from the performance, the positive features of the wire mesh model were retained while the disadvantages had been eliminated. Output stability proved to be excellent, but the size distributions (Figure 3-49) were too broad to be acceptable for ACPL; also, the total particle output was rather low.

For this reason and to achieve better mechanical stability, a much improved model schematically shown in Figure 3-50 was fabricated; this model represents the final version of the DRI-ICOA built under this contract. The liquid feed tube was changed to enter the groove from inside

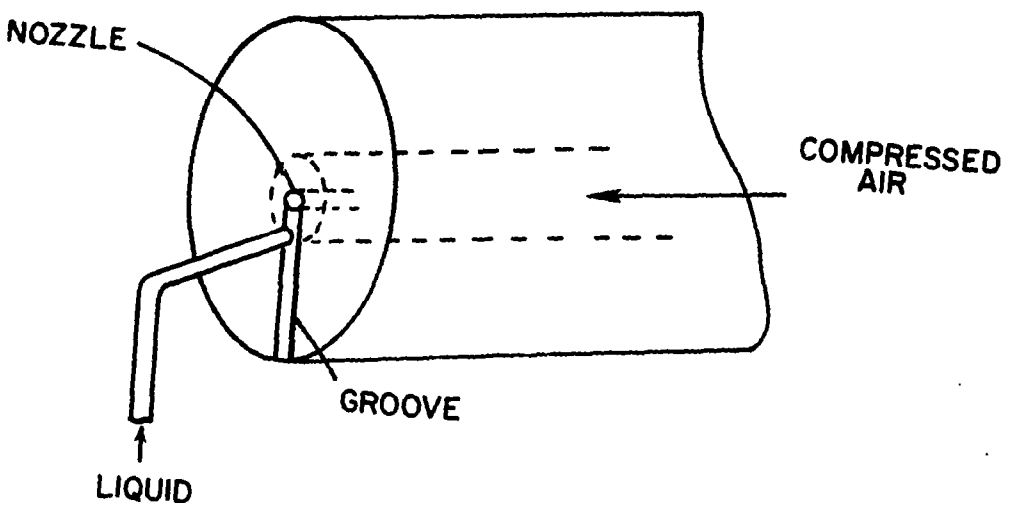

Figure 3-48. Schematic of early version of improved constant output atomizer.

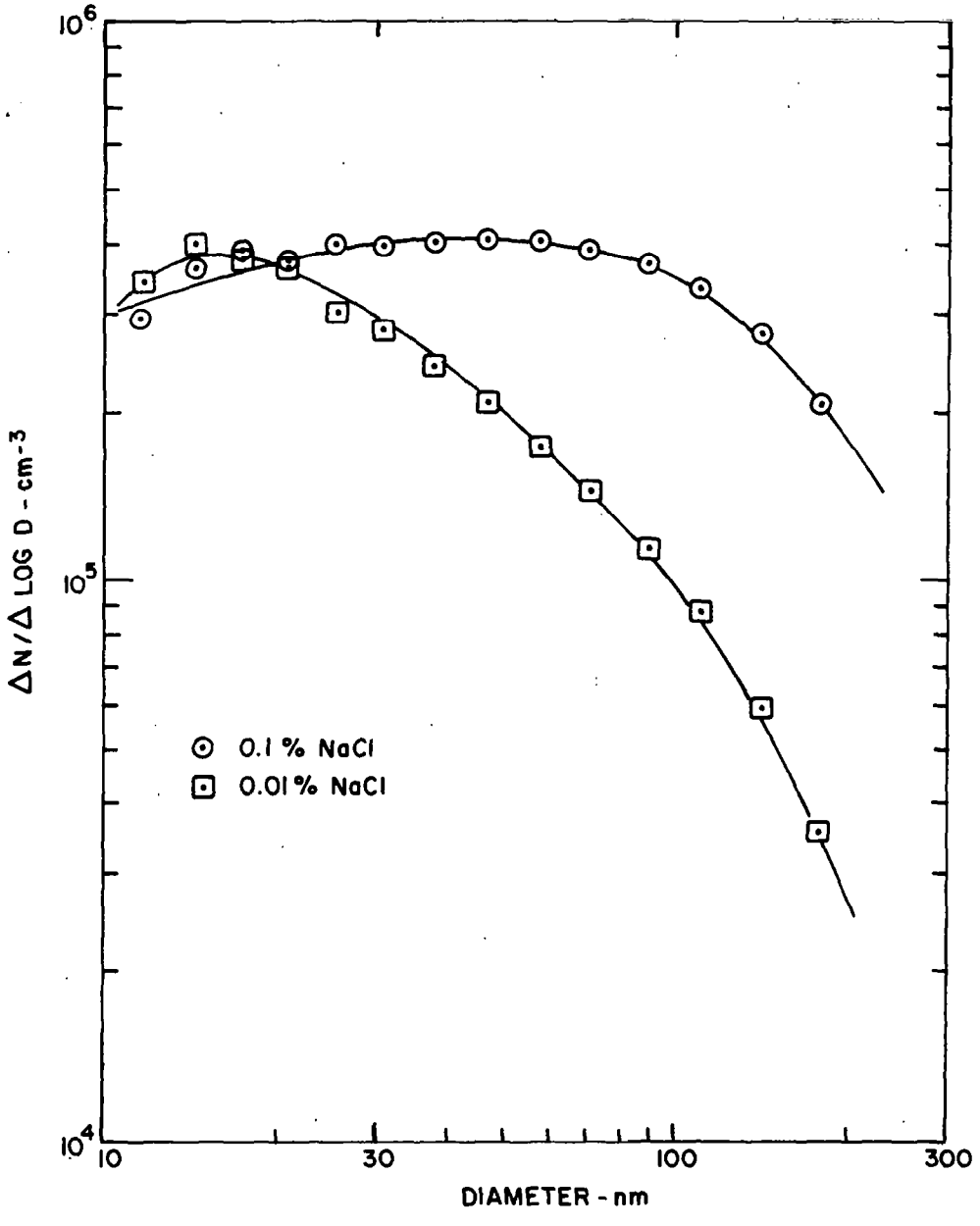

Figure 3-49. NaCl size distributions obtained with nozzle shown in Fig. 3-48 operated at 30 psi.

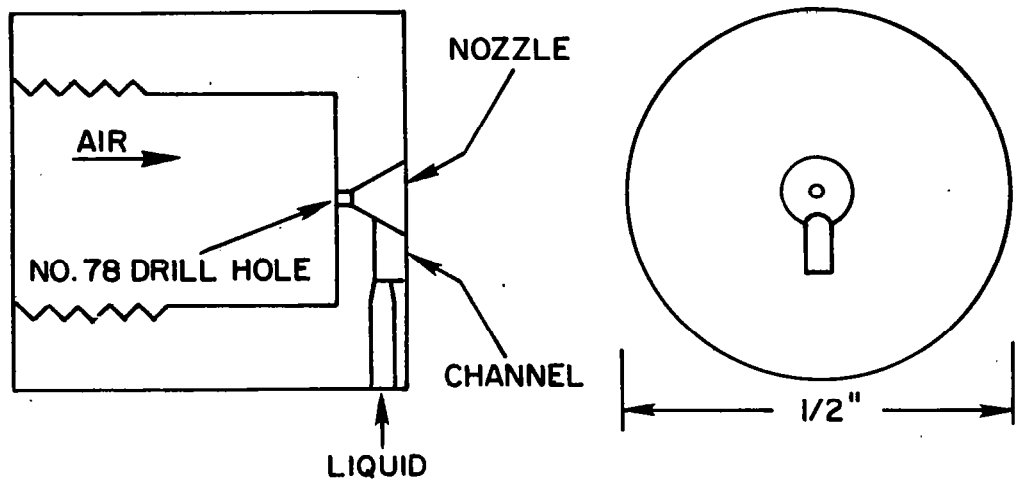

Figure 3-50. Schematic of final version of ICOA, showing the conical exit of the air nozzle and the liquid feed entering the groove from "inside".

and the air nozzle was fitted with an exit cone. Instead of replaceable nozzle plates as used in the TSI-COA, the GE-ACPLA and the VGA, the ICOA nozzle assembly is machined in one piece from brass bar stock. The former VGA housing was subsequently used as an enclosure for the ICOA whereby, in general, the impaction plate was positioned 4 cm from the nozzle.

Examples of the device's performance are presented in Figures 3-49 and 3-51. Size distributions for three different air pressures and 0.025% NaCl concentration shown in Figure 3-51 are a considerable improvement over those of Figure 3-49 with respect to total output and width of the distribution. Indications are that this improvement resulted from the air nozzle exit cone and the reduced distance between liquid feed and air nozzle.

The major accomplishment is demonstrated in Figure 3-52, showing the beginning and end of a 6-hour run which is free of fluctuations larger than $\pm$2% and having drifted only about 2% over that whole period. Equally satisfactory were stop-and-start sequences of which an example is depicted in Figure 3-53.

Use of several copies of the ICOA over a period of half a year confirmed the initial findings that this design surpassed all other atomizers tested at DRI with regard to output stability and reproducibility. Nevertheless, since there is still a possibility that a unit might fail, it is suggested that the ICOA nozzle assembly be slightly modified by incorporating the liquid feed into the same cylinder as the air feed (two parallel bores) resulting in a nozzle assembly that can easily be plugged into the atomizer housing and removed for replacement.

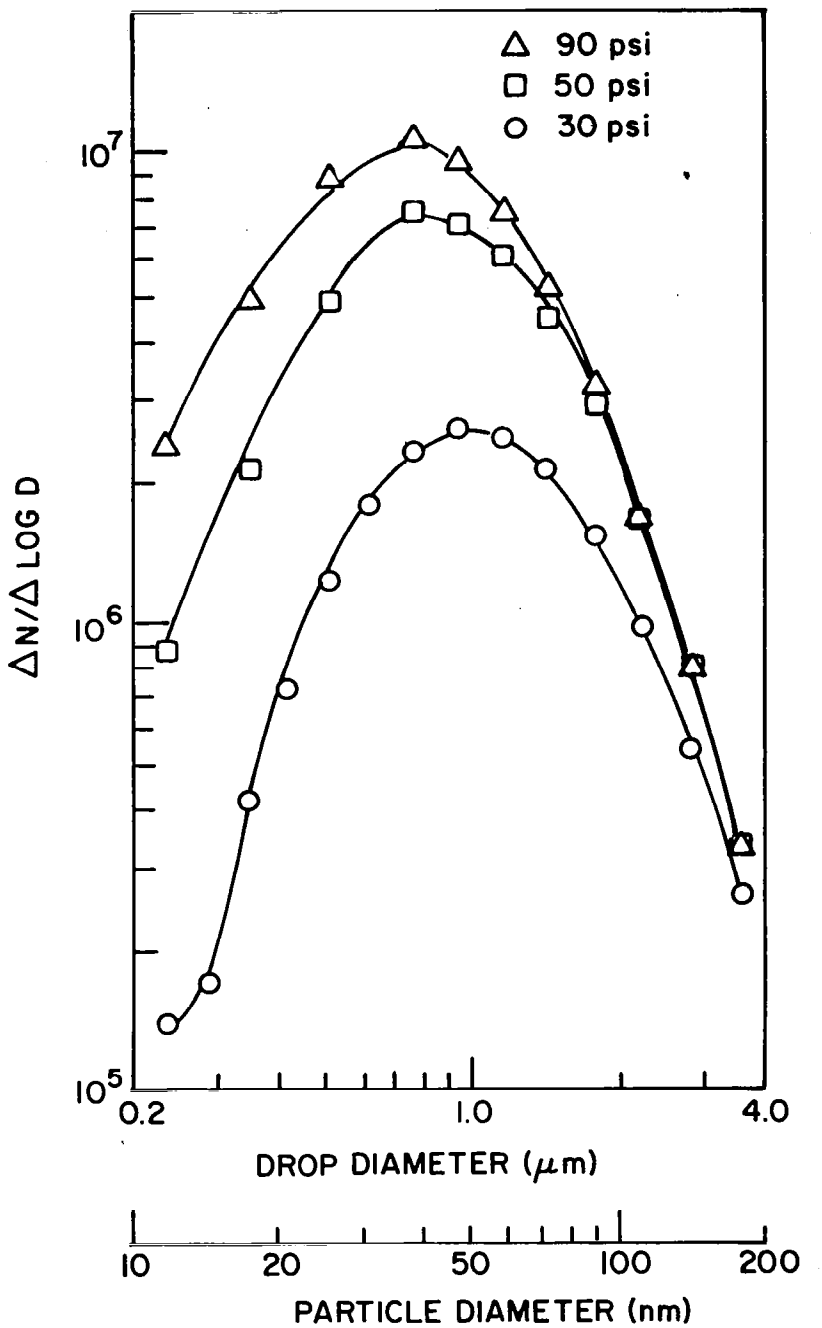

Figure 3-51. NaCl particle size distributions from ICOA at three indicated air pressures. Note the very slight decrease in the mode diameter with increasing pressure (.5 ml/min flow of 0.025% solution).

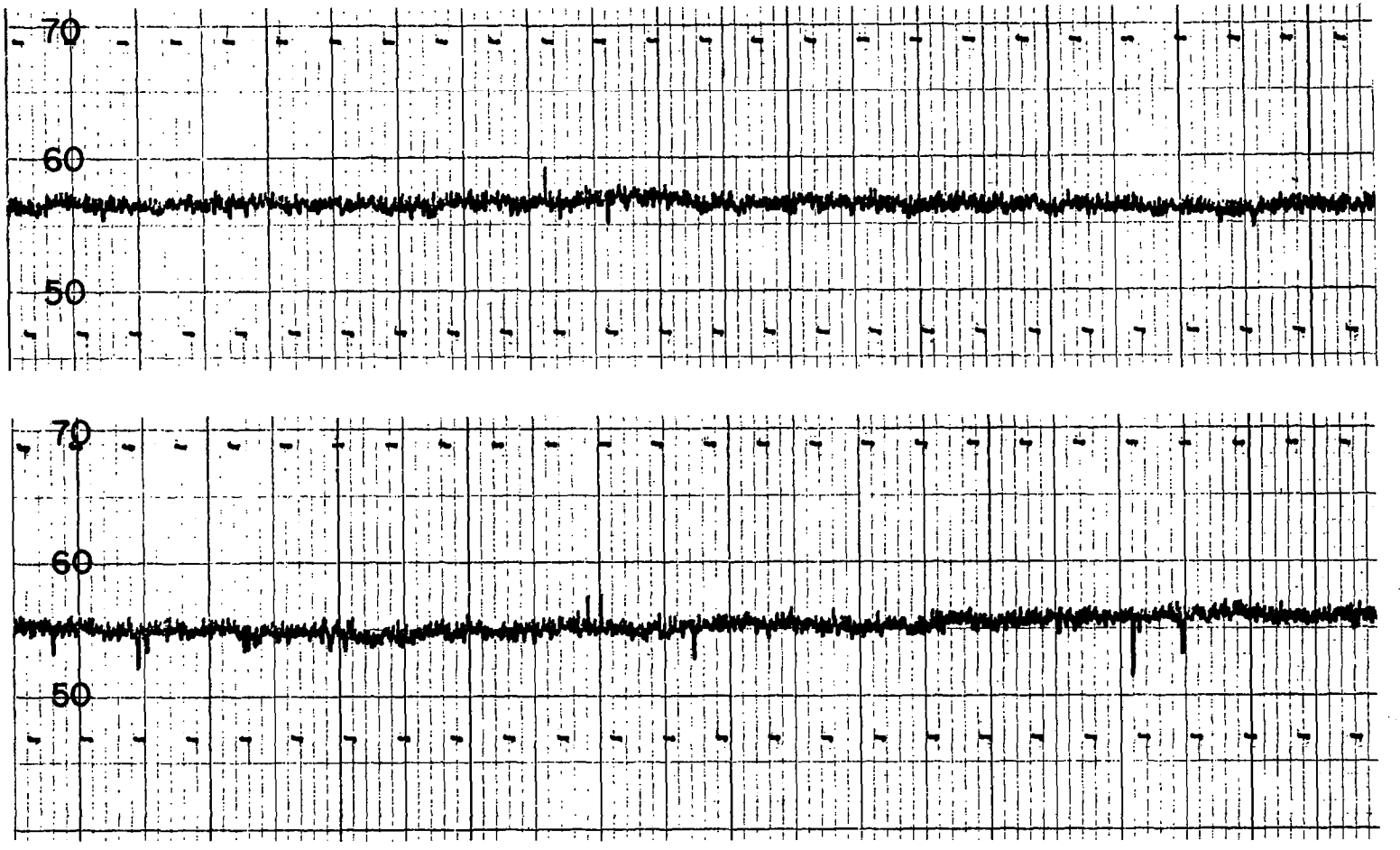

Figure 3-52. Strip chart record of ICOA output as measured by EC-EAD for a six hour run; shown are first and last 20 minutes, demonstrating good constancy over long periods.

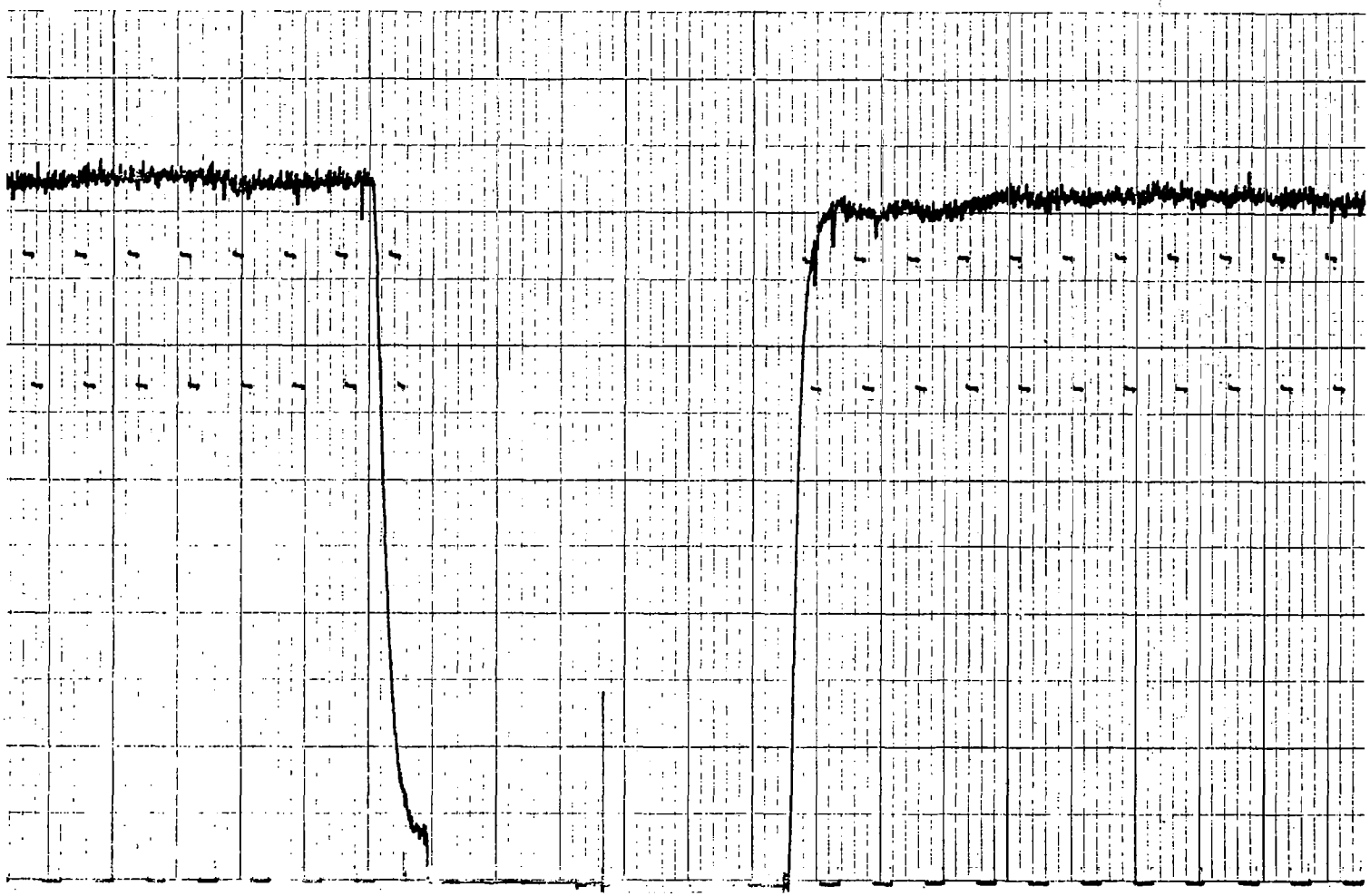

Figure 3-53. Strip chart record of ICOA output during stop-restart event, indicating good repeatability.

Flight hardware would include at least one pretested and precalibrated stainless steel unit per scheduled experiment period.

(5) Evaluation of GE-ACPL Atomizer

The last task of this program was to laboratory test the actual flight model of the GE-ACPL atomizer. In view of the experience with all other atomizers, these tests concentrated on the unit's behavior with respect to output constancy and reproducibility.

Figure 3-54 is an exterior view of the GE atomizer; the front flange incorporates the feed-throughs for inputs of liquid (bottom) and air (top), while the aerosol outlet can be seen on top of the canister. The nozzle and impaction surface geometries are very similar to those of the TSI-COA, except that the GE unit has no drain for the excess liquid but instead utilizes most of the canister volume to retain the liquid by capillarity in packed quartz fibers.

Operation of the unit was carried out according to GE specifications which, among other things, included use of high quality water (such as J.T. Baker HPLC reagent grade), filtration and degassing of the NaCl solution, concentration of which should preferably be 0.1%, solution flow rate of 0.1 to 0.5 ml min^{-1}, and compressed air with relative humidity below 30% and pressure regulated within $\pm$1%. Also, quite plausibly, the airflow had to be on a few minutes before and after the liquid flow in order to protect the air nozzle from salt contamination. The air flows through the EC were recorded as well as the exit temperature of the aerosol on the same stripchart as the output measured by EAD. The important parameter of solution flow was measured with a

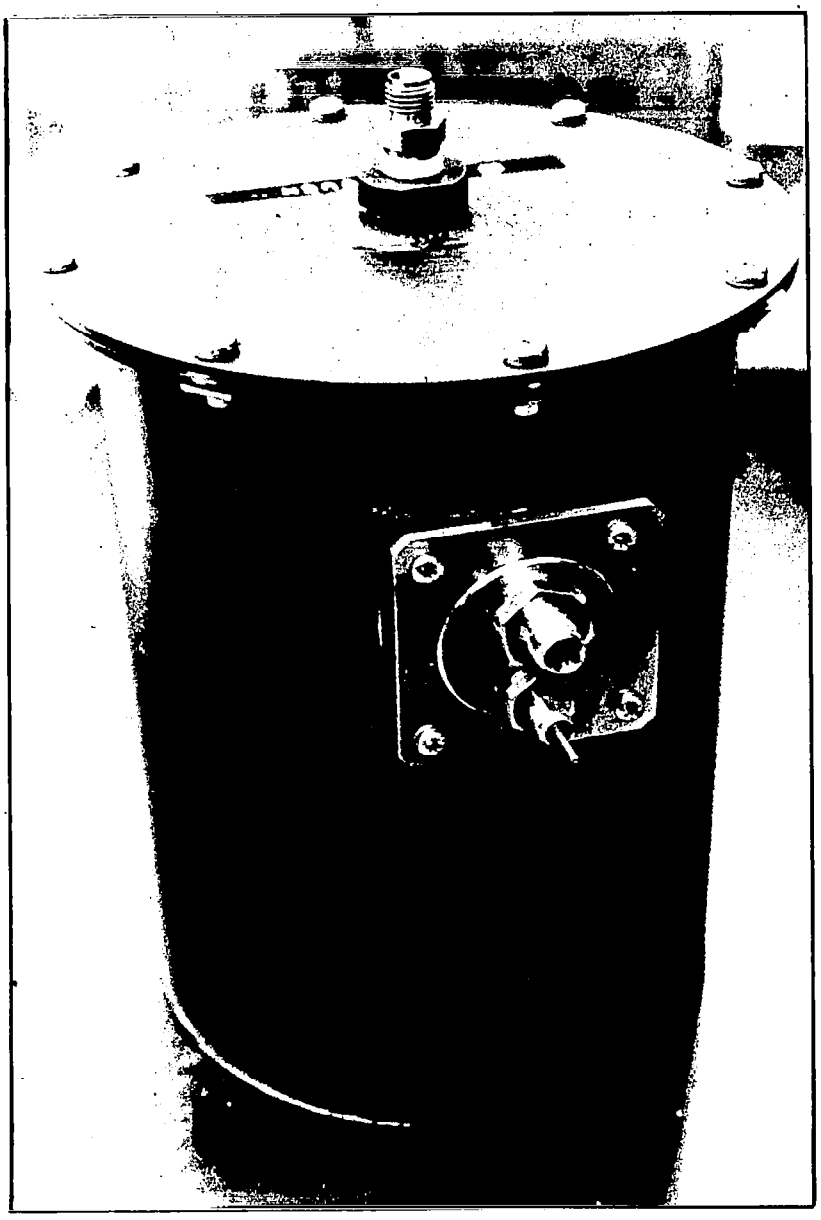

Figure 3-54. Photograph of GE-ACPL Atomizer tested at DRI. Front flange is for liquid (small) and air (large) inlet. Aerosol outlet on top.

rotameter and hand recorded - it never varied more than ±0.5%. The experiments were run at an air pressure of 25 psi.

Figure 3-55 indicates that this atomizer is capable of producing a relatively fine aerosol, but for certain experiments, it may be desirable to obtain higher concentrations for larger particles, i.e., use of more concentrated solutions should be permissible with this device.

During the first six runs of about an hour each for testing output stability, the performance was within specifications except that the output dropped a few percent from run to run. With the seventh run, shown in part on Figure 3-56, output fluctuations exceeded the specifications slightly, while no variations of the other recorded parameters could be noticed.

After several more hours of operation, output variations resembled those of the TSI-COA in its most unstable mode; examples are shown in Figure 3-57. Subsequent atomizing of pure water for two hours nearly restored the original output constancy for a short period as Figure 3-58 attests although at low fluid flow rates, the fluctuations still far exceeded the specified limits. With continued use, the device again deteriorated and had to be run for hours on pure water before it was marginally usable.

Thus, one has to conclude that the GE-ACPL atomizer, due to its lack of output constancy, is not suited for its intended use unless appropriate design changes are put into effect.

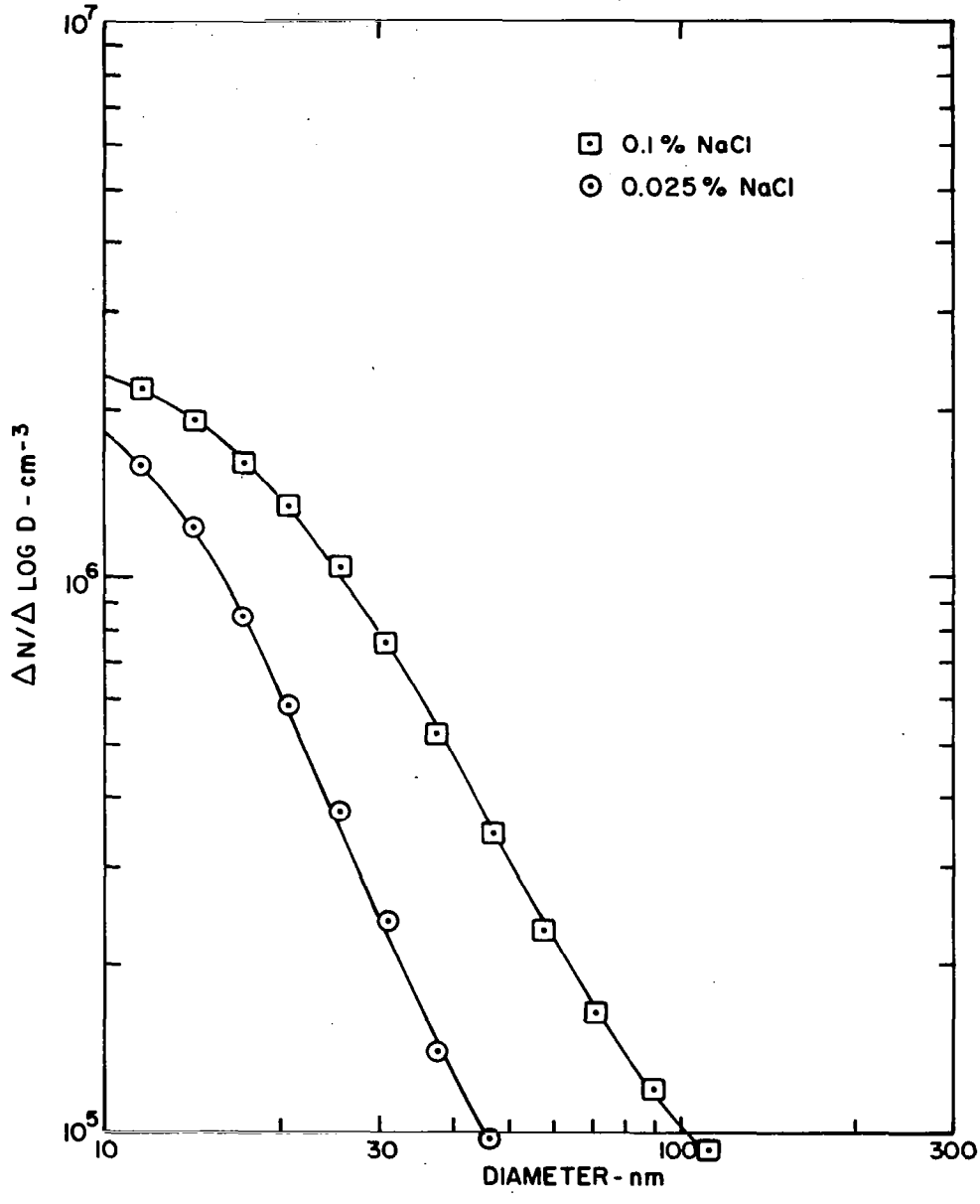

Figure 3-55. Particle size distributions obtained from NaCl solutions with GE Atomizer at indicated concentrations and 25 psi air pressure.

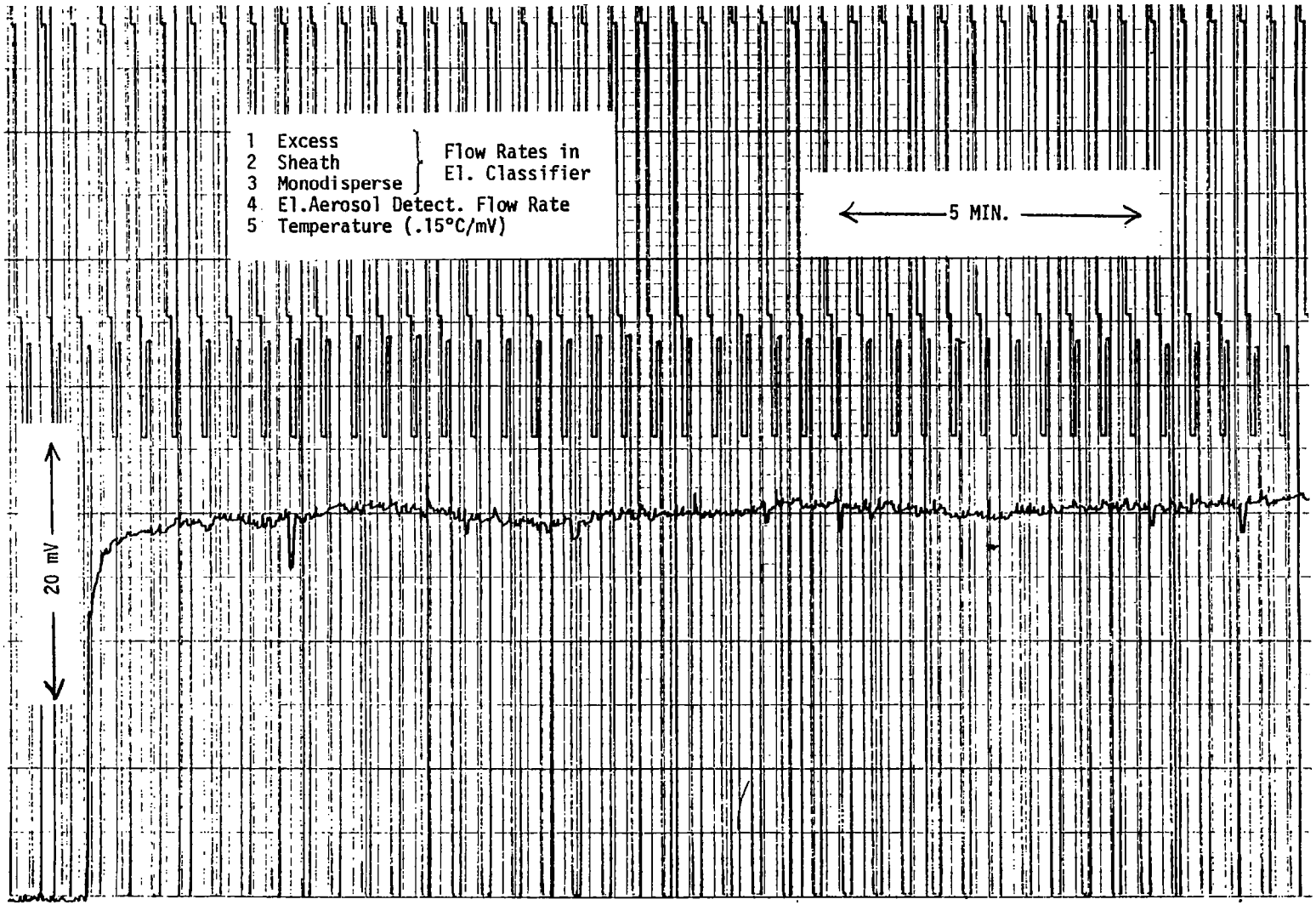

Figure 3-56. Output of GE Atomizer showing initial constancy (25 psi, 0.1% NaCl solution).

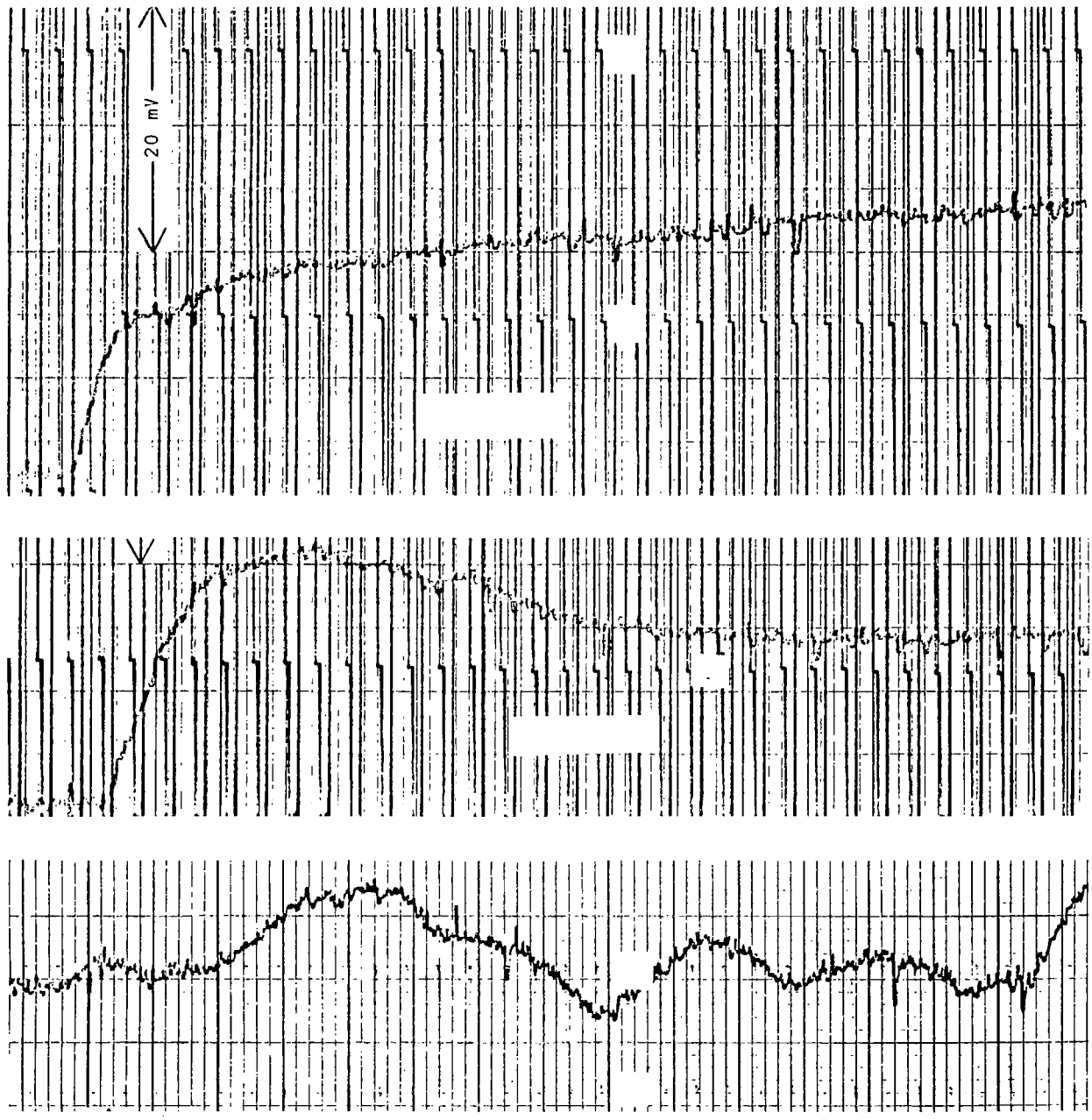

Figure 3-57. Deteriorated output constancy of GE Atomizer after several hours of operation (same time scale as 3-56).

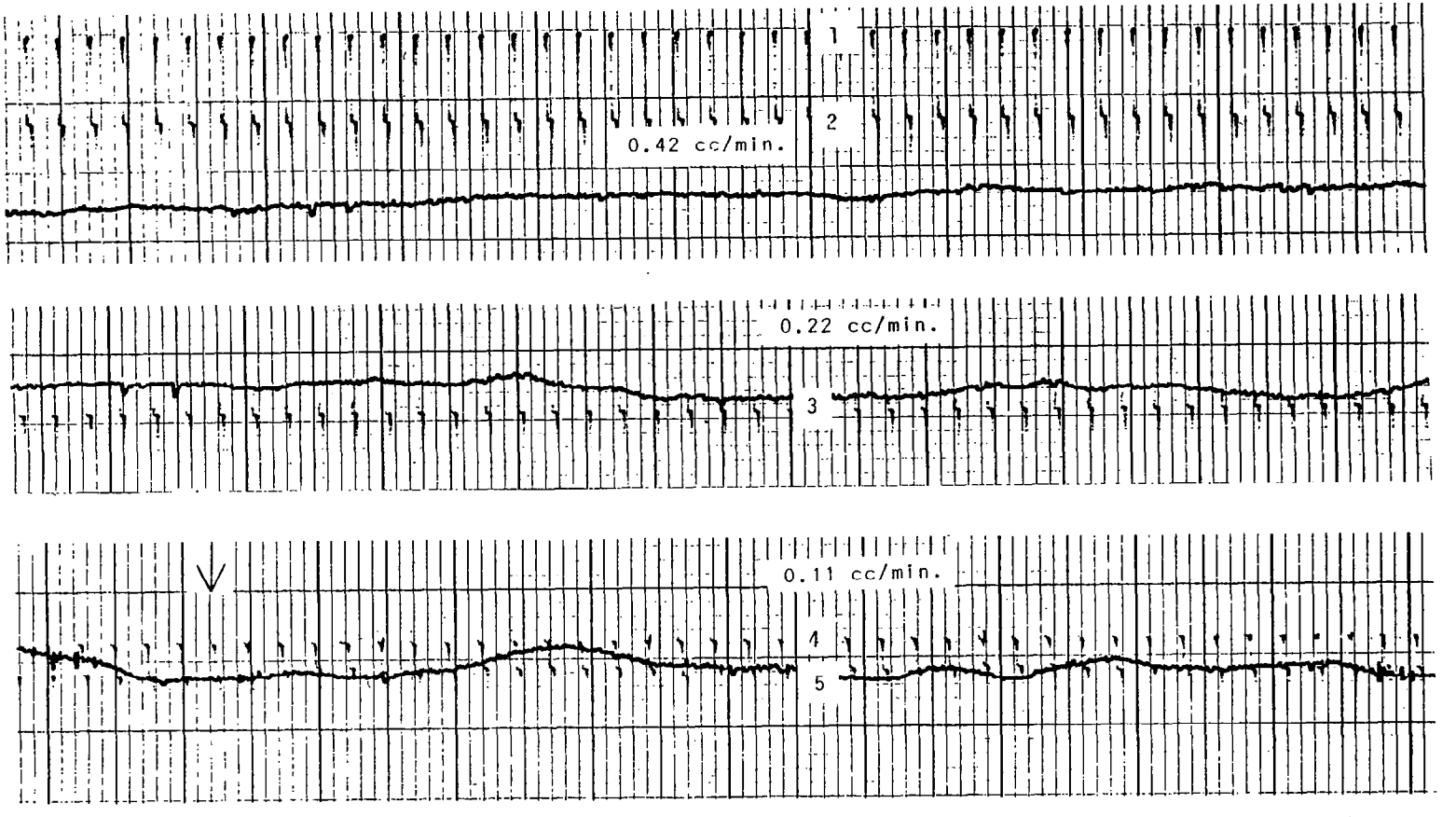

Figure 3-58. Improvement in performance of GE Atomizer through prolonged flushing with distilled water. Note that fluctuations decrease with increasing solution flow.

C. GENERATION OF WATER INSOLUBLE AEROSOLS

Since pneumatic atomization proved to be an excellent method for particle generation from aqueous solutions, one could, of course, extend the atomization technique to non-aqueous solutions with essentially the same success. In terrestrial laboratories, such procedures are, indeed, being applied; however, disposal of solvent vapors which are generally toxic require facilities that would not have been available in the ACPL for reasons of weight and volume and/or complexity.

Among alternate methods, the atomization of hydrosols appears particularly attractive, mainly because of the possibility of using a proven dispersal method for which the equipment would have already been on hand in the ACPL, while the production of the particles (in hydrosol) could be carried out in a suitably equipped terrestrial laboratory. Our efforts pertaining to this approach are described in the following subsection while the very limited experimentation on thermal aerosol generation is discussed in Section 2, Thermal Aerosol Generation, which follows. Based on previous experience of the investigators, dry dispersal of powders for obtaining aerosols in the specified primary size range was given a very low probability of success, and therefore no substantive work was performed.

1. Atomization of Hydrosols

a. General

The performance of atomizers, when working with hydrosols, was generally found to be equal or superior to the case of salt solutions; lesser output fluctuations were attributed to the fact that no salt deposits formed from hydrosols.

One difficulty in working with atomized hydrosols is the much lower number concentration that can be achieved since only a relatively small number of droplets may contain a particle in order to avoid abundance of multiplets. Doublets, for instance, are difficult to eliminate later on even with an EC since doubly charged doublets differ very little in mobility from the singly charged singlets (see Section D, Shaping of the Size Distributions). Depending on the type of experiment planned, one has to find the optimum balance between a high concentration of singlets and interference from multiplets.

A further potential problem may be caused by the presence of the particles consisting of the residue of "empty" droplets. Although these undesired particles are very small, they are present in large numbers and generally are water soluble if not hygroscopic. Thus careful consideration has to be given to their possible influence on the planned experiment. If their removal is deemed necessary, diffusive capture or exclusion in the EC are effective methods to use.

The most serious problem, however, is posed by the residue from the liquid which coats the insoluble particle. If left on the particles, it is likely to influence the particle behavior as CCN, while removal may be a difficult task - mere heating may only drive off the deposit temporarily while subsequent cooling may lead to recondensation on any particles present. Detailed procedures have to be developed separately for each individual case. Methods to clean the particles in the hydrosol stage can be very complex and still leave considerable doubt as to their effectiveness as the vast literature on purification of polymer latices attests (e.g., Wilkinson, et al., 1980).

It is nearly impossible to directly determine whether a residue is left on the particles that would mask their intrinsic surface properties. An indirect procedure (which could not be tried out in the framework of this investigation) is suggested for further study. Thereby, experiments should not only be carried out with the insoluble particles, but also with residue particles of the same size which would be obtained by atomizing a specially concentrated batch of the liquid component of the hydrosol. Identical behavior of the two particle populations would then support the contention that residue was covering the insoluble particles.

Despite the relatively dim outlook on clean-up of aerosols from hydrosols, a limited exploratory effort was undertaken by experimenting with a few specific substances.

b. Experiments with Hydrosols

(1) Commercially Available Particles

Early in this study, hydrosols of monodisperse polystyrene latex particles of various sizes were frequently aerosolized for calibration and test purposes (see, e.g., Figure 2-5). In the context of instrument assessment, there was no reason to be concerned about small amounts of solute (surfactants, minerals, etc.). The only problems in atomizing these hydrosols stemmed from irreversibility of particle agglomeration, which were more severe for smaller sizes. However, due to their complex nature, latex spheres were not considered desirable as CCN test materials. In contrast, Teflon as an extreme in hydrophobicity, and carbon black as a constituent of the atmospheric aerosol were selected as they were also commercially available.

Two batches of Teflon aqueous dispersion* (No. 3416) were procured. Unfortunately, attempts to atomize the dispersions were unsuccessful as the Teflon accumulated on the baffle, clogging the atomizer in just a minute running time. No particles (50-500 nm according to specs) could be found downstream of the atomizer. Since this occurred even before removing the stabilizing components of the liquid, further attempts of transforming this product into an aerosol were terminated.

Similarly, carbon black**, of which several monodisperse batches of different sizes were obtained, resisted incorporation into an aqueous dispersion even when using an ultrasonic agitator and surfactants. Atomization of the suspension showed insufficient de-agglomeration. Thus, no further efforts were expended on this topic.

(2) Laboratory Prepared Hydrosol - AgI, Silica

Another candidate material, AgI, insoluble and hydrophobic in its pure form, was not considered here for the hydrosol-atomization technique since Vali, et al. (1978) were in the process of studying this and other AgI generation methods. For the very reason discussed above, a hydrosol derived AgI aerosol is impure and hygroscopic, and thus not of interest in the context of insoluble CCN.

There is a considerable amount of literature pertaining to the preparation of hydrosols of inorganic compounds. For instance, silica (Stöber, et al., 1968), magnetite (Sugimoto and Matijevic', 1980), ferric oxide (Matijevic' and Scheiner, 1978), alumino silicates and gold (Newton, et al., 1975), and aluminum hydroxide (Tentorio, et al., 1980);

*E.I. DuPont de nemours, Wilmington, Del.

**Particle Information Services, Inc., Grants Pass, OR.

all of these contributions describe formation of monodisperse submicron particles. The work on silica was known to the author and, since silica is a constituent of the atmospheric aerosol, it was decided to evaluate this hydrosol and its applicability to ACPL aerosol generation.

By carefully following the procedures described by Stöber, et al., it was possible to prepare hydrosols of silica in a reproducible fashion. Briefly, preparation involved dropwise addition of tetraethyl silicate to a vigorously stirred aqueous solution of ethanol and ammonium hydroxide. The make-up of the resulting particle populations depends on the concentration ratios used. Figure 3-59 represents the size distributions from aerosolized silica hydrosols obtained with three different ammonium hydroxide concentrations. It is interesting to note the increasing predominance of a small size peak with increasing NH_4OH concentration. At first, it was thought that the real silica particles were only those at the 100 nm peak and that the small particles were "empty" droplet residues. To test this, the aerosol was passed through a tube oven where the volatile water, alcohol and ammonium hydroxide evaporated while the fourth constituent, silicic acid, becomes silica upon dehydration. The size distribution before and after the oven were not significantly different. Both modes, therefore, have to be attributed to silica particles. Since the particle sizes of the two peaks were a factor of five apart, it can be established that the larger particles are not multiplets of the smaller particles.

In view of the intended ACPL application, the question of colloidal stability had to be addressed since in-flight preparation of the hydrosol would be impossible as there is considerable release of heat

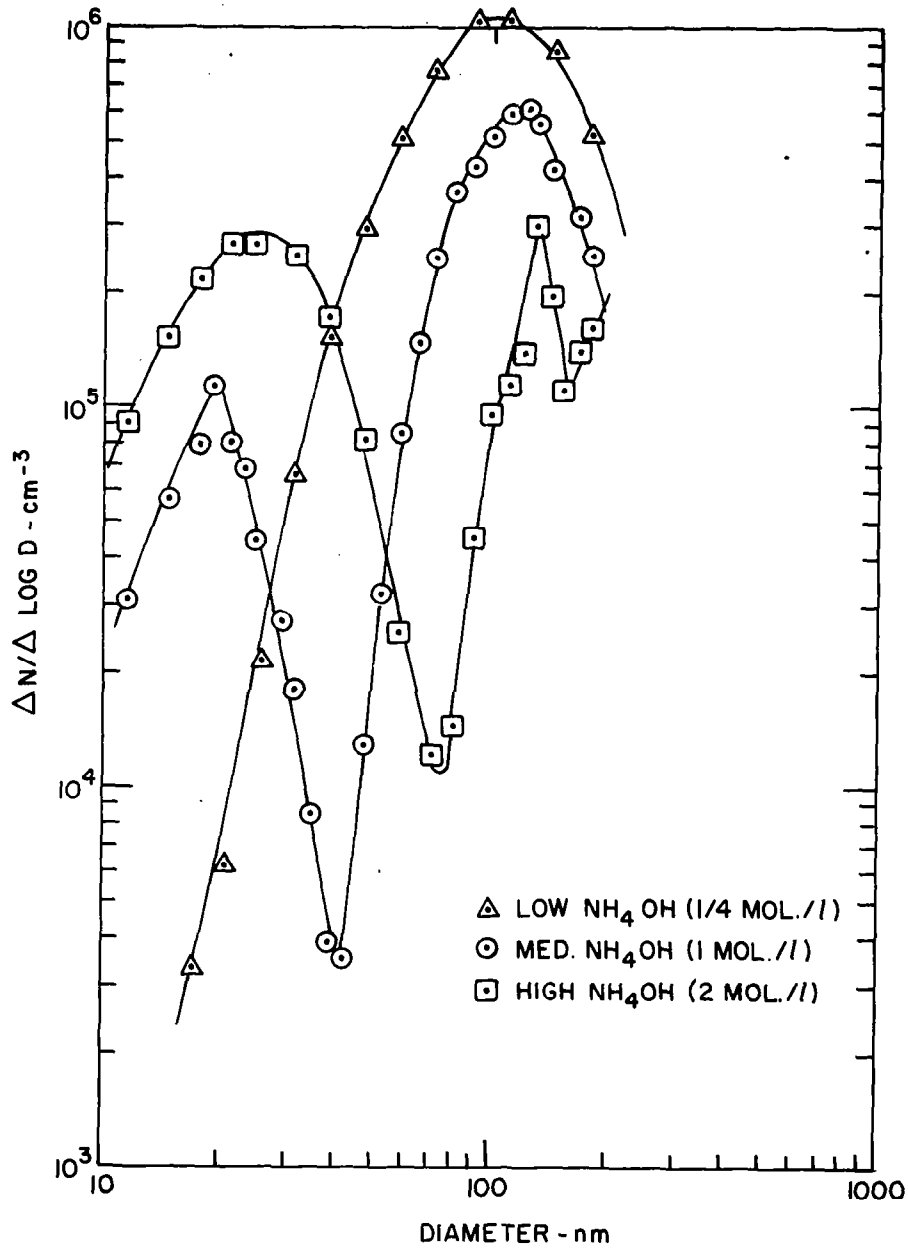

Figure 3-59. Size distributions of silica aerosols prepared from silica hydrosols. The effect of the ammonium hydroxide concentration during the hydrosol preparation is shown.

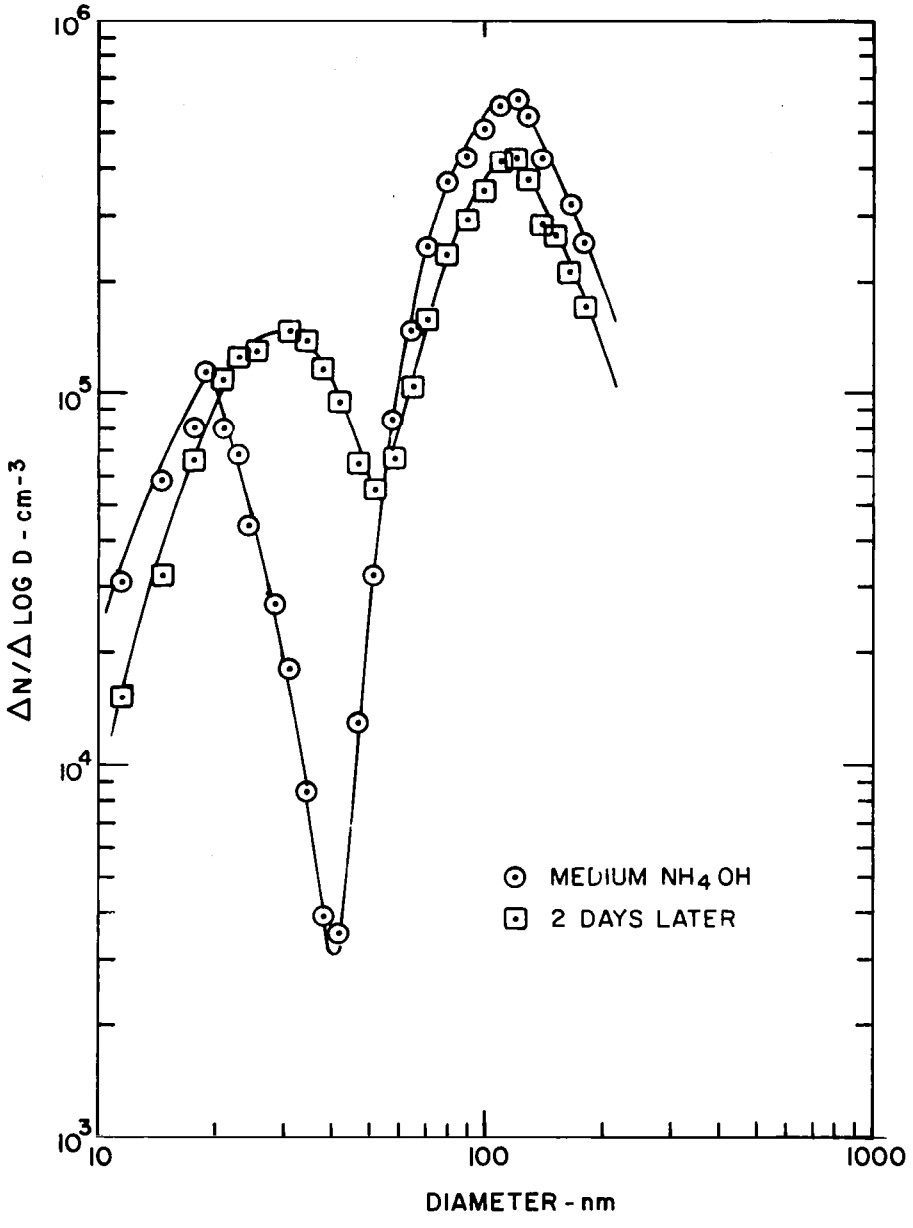

Figure 3-60. Two silica aerosol size distributions showing the effect of aging of the hydrosol.

and vapor during some of the preparatory stages. Figure 3-60 indicates that in the two-day period between the two measurements, some coagulation may have caused a slight shift of the small particle peak towards larger sizes. However, the effect was definitely not large enough to impair the usefulness of this hydrosol for ACPL type of experiments.

The influence of the tetraethylsilicate concentration on the size distribution is shown in Figure 3-61 which indicates that a better separation of the two modes can be achieved if a relatively low concentration of tetraethyl silicate is used. This assumes that interference from larger, doubly charged particles, after passage through one EC (see 3.4), can largely be avoided as long as multiplet formation can also be prevented.

A SEM view of an amply exposed sample of the silica aerosol is presented in Figure 3-62 which confirms that the particles are reasonably spherical.

Although the question of surface contamination by residues from the liquid could not be pursued in depth, there is a reasonable probability that a sufficient clean-up in the hydrosol stage can be achieved to at least minimize the danger from toxic vapors during atomization in the ACPL; therefore, further study of this hydrosol/aerosol is strongly indicated. The above mentioned ferric oxide hydrosol (the literature on which came to our attention too late to allow experimentation with the substance) should also be investigated carefully as it may be even more suitable for the ACPL application.

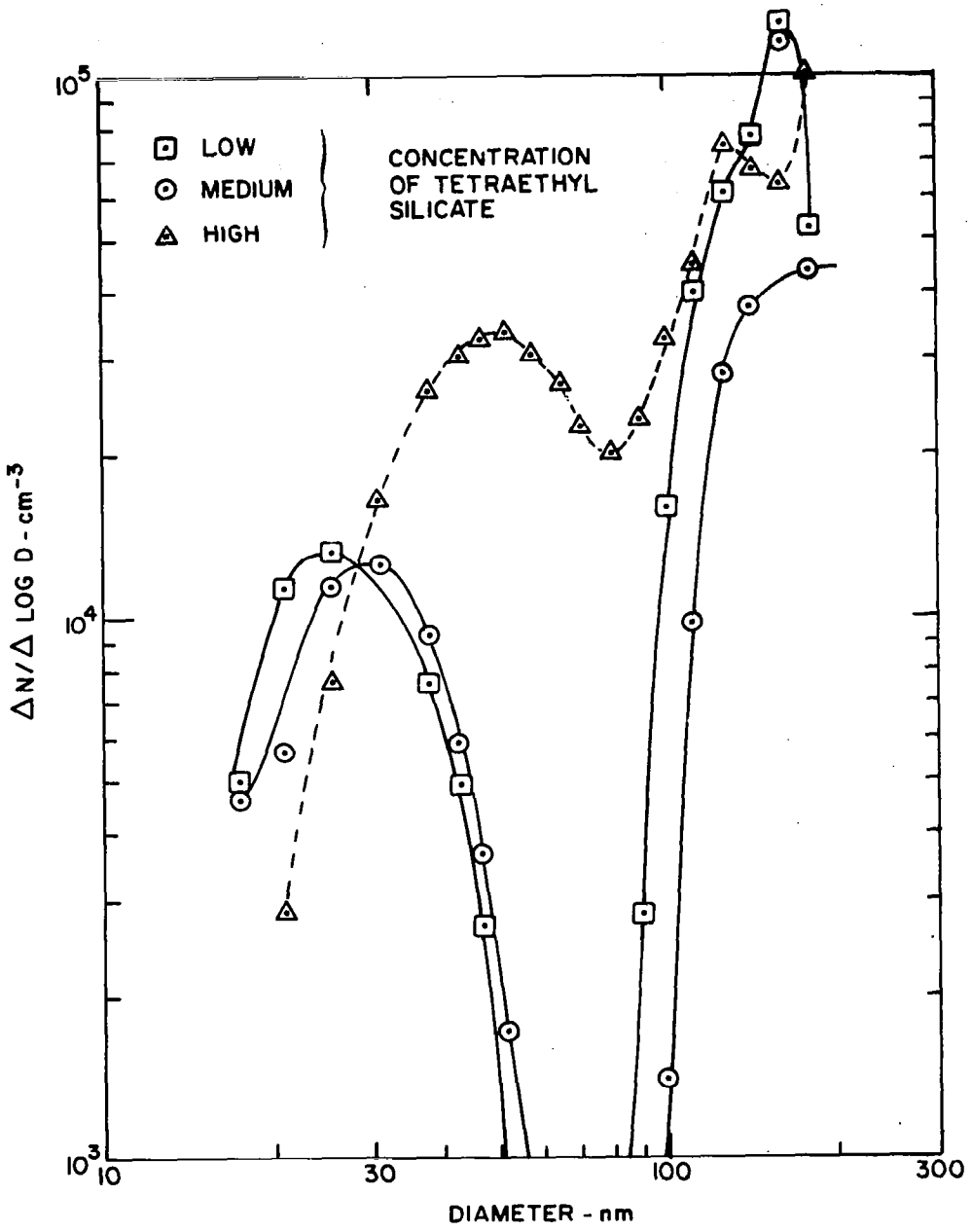

Figure 3-61. Effect of the tetraethylsilicate concentration (in the process of hydrosol preparation) on the size distribution of silica aerosols generated from silica hydrosols.

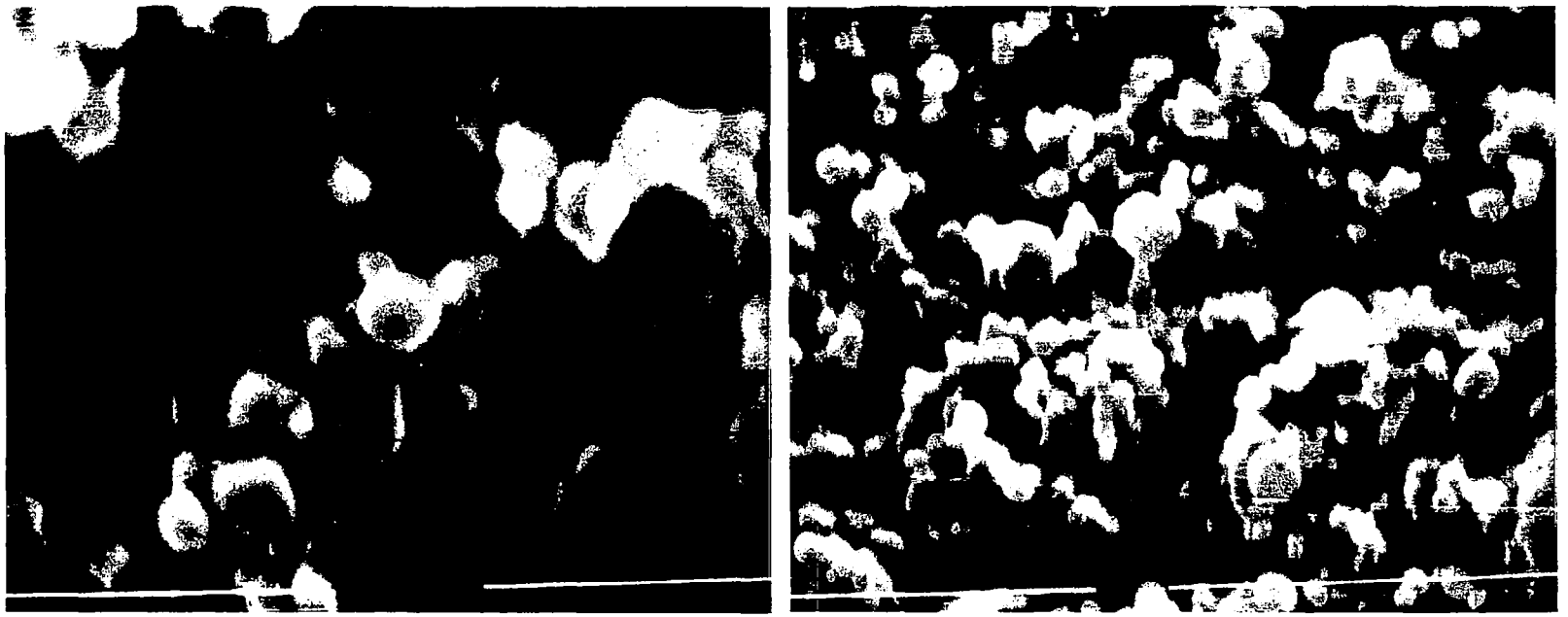

Figure 3-62. Two different SEM views of a sample of electrostatically precipitated silica aerosol (gap in line represents 500 nm).

2. Thermal Aerosol Generation

Aerosol generation by thermal means was only considered for insoluble particles and only briefly explored as a less desirable alternative to the hydrosol technique - less desirable because of additional heating and gas supply requirements which might have been prohibitive for the ACPL while, on the other hand, the atomizer was intended to be a part of the ACPL anyway.

a. AgI

As mentioned previously, Vali, et al. (1978) investigated and compared various methods of AgI aerosol generation. They selected the hydrosol atomization as the most satisfactory generation scheme. Since their aim was to produce ice nuclei, the NH_4I residue remaining on the otherwise fairly pure AgI particles was not considered detrimental; however, as discussed earlier, a purification method would have to be devised before the attractive feature of AgI as a test CCN, namely, its water insolubility would become evident.

Thus, a simple thermal generator was devised, a schematic of which appears in Figure 3-63: a tantalum boat stretched between two copper electrodes served as the low voltage electrical heat source which was mounted inside a Pyrex flask; a stream of nitrogen was directed at the hot AgI in a Ta-boat, presumably quenching the vapor to form the aerosol. The use of N_2 allowed heating up to 650°C without particles being generated from the tantalum. This requirement, however, would probably make this technique unacceptable for ACPL despite the relatively good output constancy that was achieved with this setup. The size distributions obtained at 500°C and 650°C are plotted in Figure 3-64

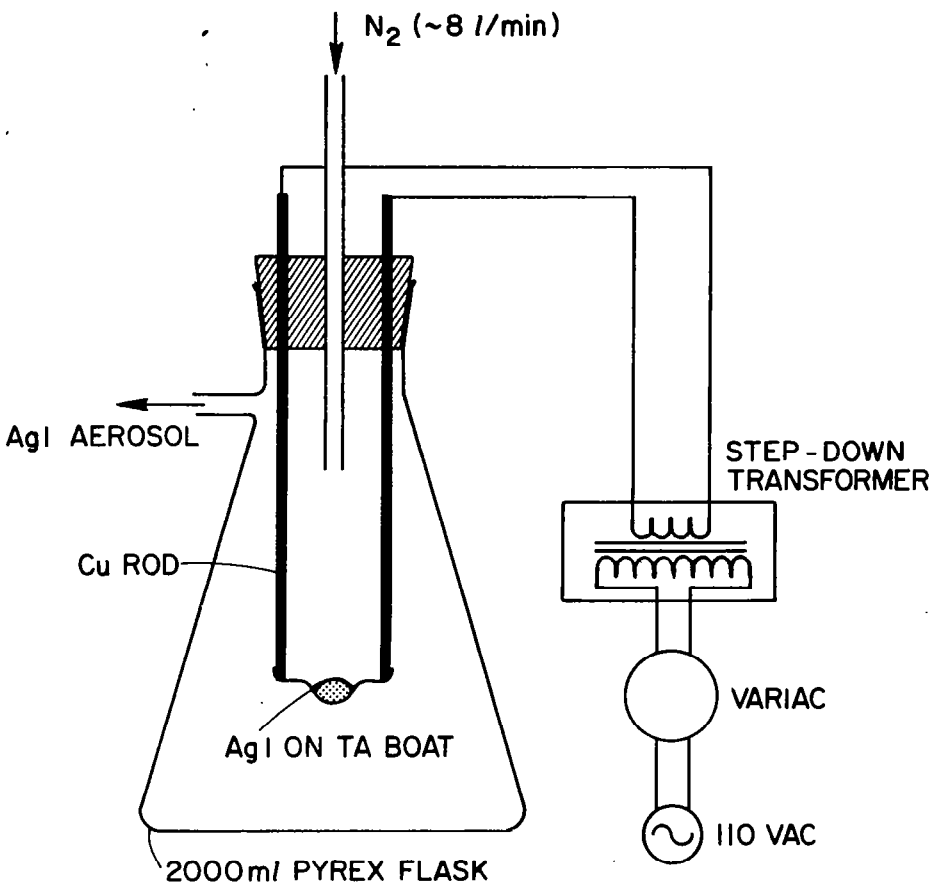

Figure 3-63. Schematic of thermal silver iodide aerosol generator.

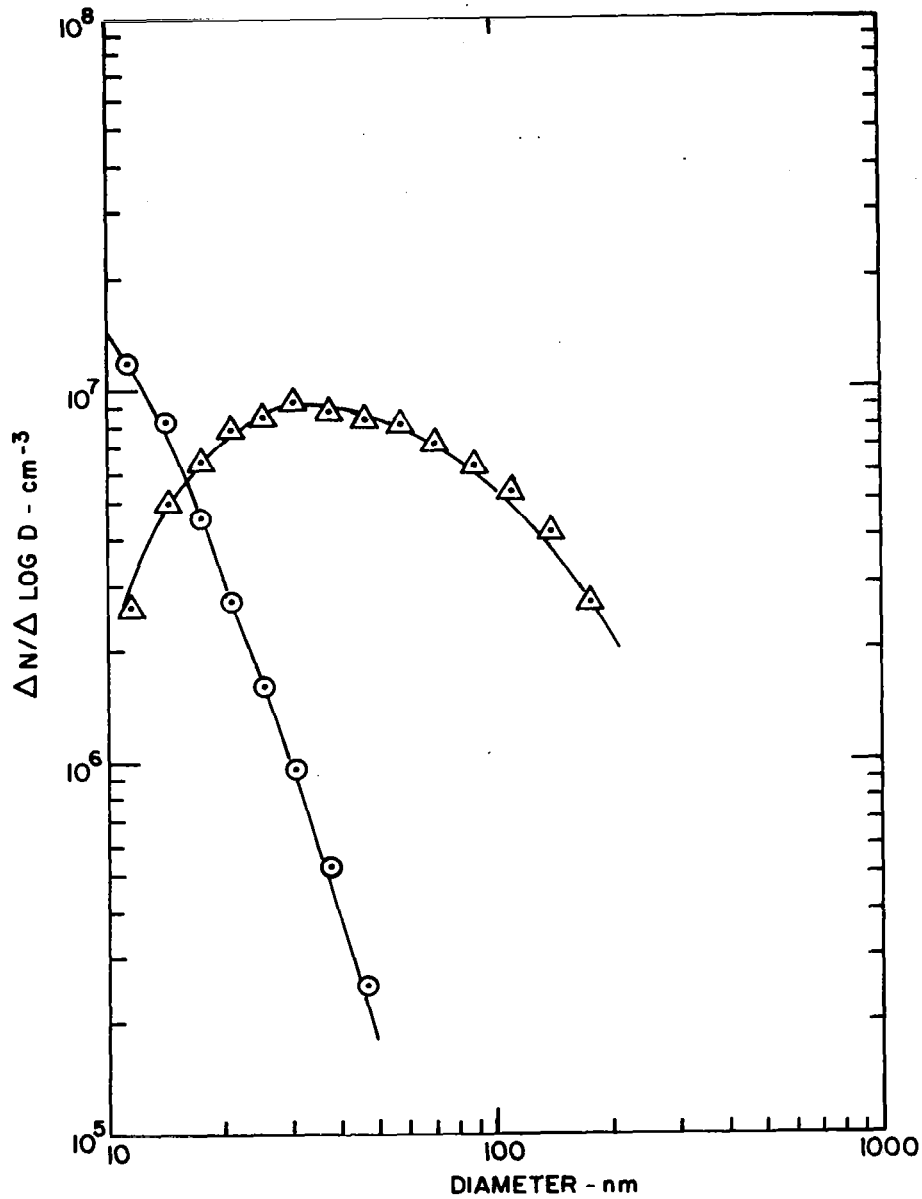

Figure 3-64. Size distributions of AgI aerosol generated with device of Fig. 3-63 at two different temperatures, 500°C (θ) and 650°C (▲).

which indicates a considerable dependency on temperature that provided the desired control over the particle size.

b. Paraffin Wax

Common paraffin wax or the more refined related waxy compounds such as eicosane are water insoluble, hydrophobic, have a relatively low melting point and a high enough vapor pressure over the liquid to generate particles by condensation. Generally, one would utilize a different aerosol (such as NaCl) to nucleate the wax particles from the vapor. In the present case, an attempt was made to produce the wax aerosol homogeneously without the help of an auxiliary aerosol for two reasons: (1) simultaneous operation of two particle generators would add to complexity and (2) the presence of even a small number of particles from the auxiliary aerosol that (for one reason or another) did not participate as CN for the paraffin wax, could jeopardize the experiments.

The very simple apparatus depicted in Figure 3-65 produced paraffin particles mainly in the 80 to 200 nm range (with a long tail of the size distribution reaching into the optical range) at concentrations of 5 to $8 \times 10^{3} cm^{-3}$. Apparently the gas jet emanating from the capillary produced a high enough supersaturation to cause homogeneous nucleation from the paraffin vapor. No tests with air in place of N_2 were carried out, nor were attempts made at optimizing the system to obtain outputs that could be treated with the EC. The constancy of the output was encouraging ($\pm$5%) but could probably be improved.

ACPL adaptation would most likely have required a considerable effort since a liquid is involved that needs to be contained. Also, the

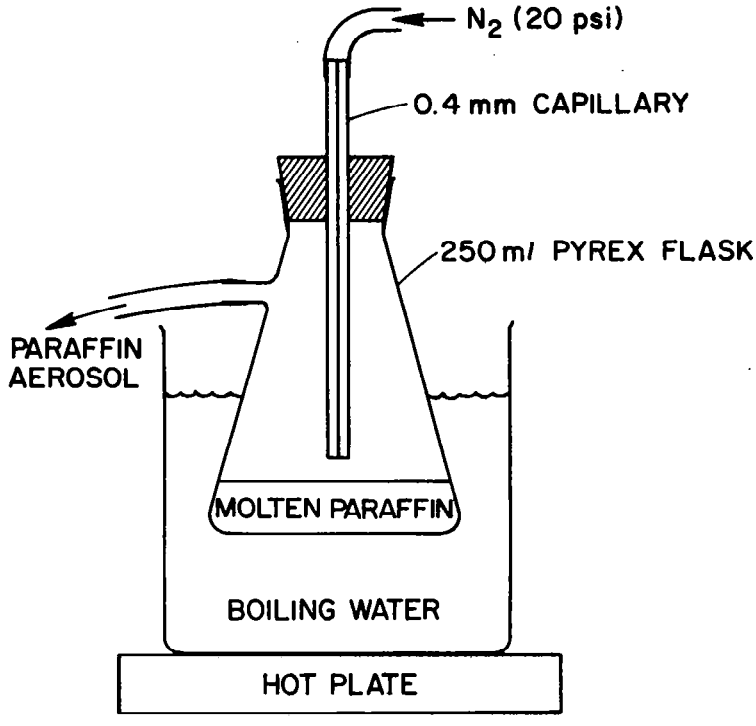

Figure 3-65. Schematic of set-up to thermally generate paraffin wax aerosol.

large particles (>500 nm) would have to be eliminated, mainly to avoid clogging of critical passage ways in the flow system.

It is planned to use and improve this generator in conjunction with the "complex aerosol" study.

D. SHAPING OF SIZE DISTRIBUTIONS

In the context of CCN experimentation, the purpose of manipulating the shape of aerosol size distributions is mainly to control the slope of the resulting CCN supersaturation spectra in order to be able to either simulate naturally occurring types of CCN populations, or to test instrumentation or theoretical models.

Some control over the shape of particle size distributions can, to some extent, already be exercized at the source of the aerosol as has become evident so far: the type of atomizer, the solution concentration, the temperature in thermal aerosol generators, or the size distribution of hydrosol particles are just some of the available means. However, there are limitations to these techniques in general and, in particular, with respect to intended ACPL applications, only one atomizer type was on hand. Thus, a few methods for shaping an already existing size distribution are discussed below.

1. Impaction

Since the efficiency with which aerosol particles can be removed from their suspended state by aerodynamic capture strongly increases with increasing particle size, this technique mainly serves to reduce the number of large particles in a given population. However, even impacting the large particles in our size range of interest is relatively inefficient and, therefore, this method is best applied in conjunc-

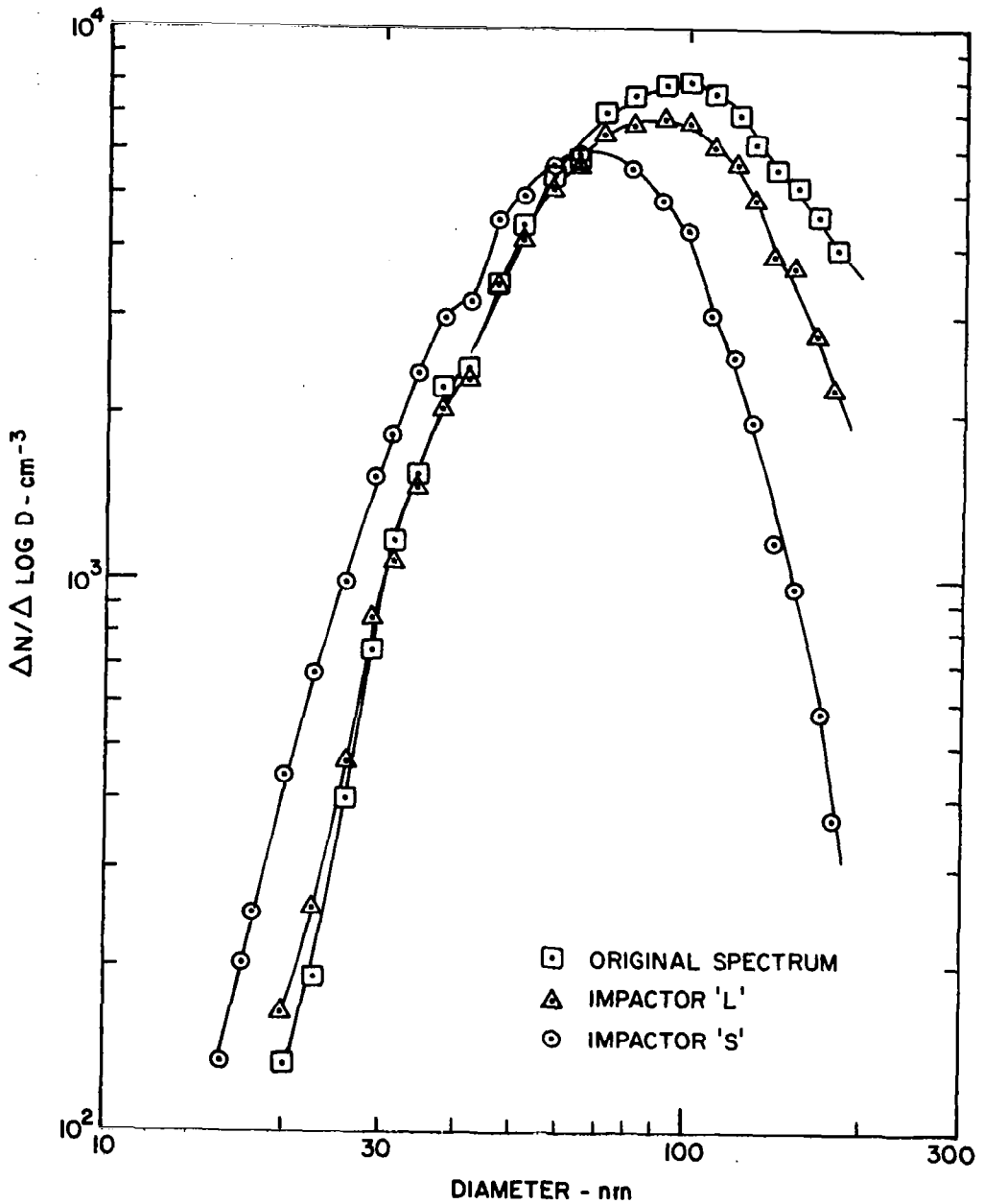

Figure 3-66. Size distributions of NaCl aerosols from VGA; ⊡ designates the original spectrum, while the other curves demonstrate the effect of impactors for precipitating larger droplets at the atomizer exit.

tion with atomizers where the removal procedure can be applied to solution droplets prior to evaporation, i.e., about an order of magnitude larger in size. Although most atomizers are already equipped to impact the large droplets, further removal of large particles is still possible as Figure 3-66 demonstrates. The original size spectrum obtained with a DRI-VGA had a modal diameter of 100 nm; by forcing the atomizer output through simple jet impactors with round nozzles of 1 mm (S) and 1.5 mm (L), the size spectra were made to peak at 65 nm and 88 nm, respectively, in addition to slightly steeper slopes (it is not clear why the smaller impactor caused an increase in small particles).

Since jet impactors would probably have been unsuitable for ACPL due to the considerable pressure their operation requires, a filtration method was explored. The effect of passing the atomizer output through a series of wire screens (mesh openings $\sim$40 μm) is seen in Figure 3-67 which indicates that large particles were removed at about the same rate as in the jet impactor, while the screens retained approximately half the particles smaller than the mode diameter. Reducing the mesh size of the screens only slightly accentuated the effect illustrated in Figure 3-67.

Although the size distributions were narrowed by only about 20% (in terms of geometric standard deviation) with the array of screens in these experiments, the system could be further optimized, especially by adding a set of screens after the dryer to remove a substantial portion of the smallest particles by diffusive capture. In view of the simplicity of this technique its application in the ACPL should be considered; however, since these devices tend to clog up during use, the

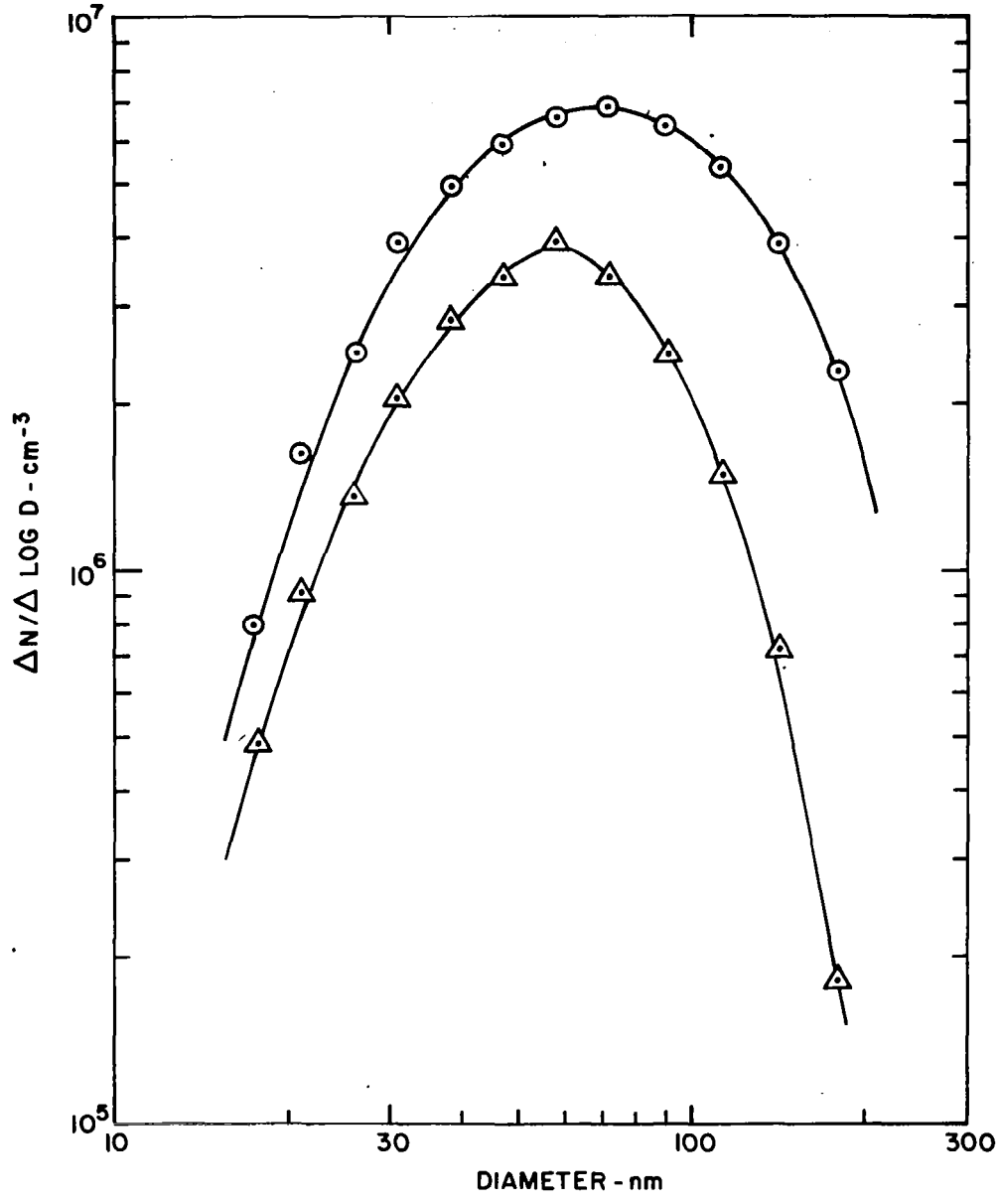

Figure 3-67. Effect of wire screens at atomizer exit on the size distribution of the VGA aerosol output (⊙ original, ▲ passed by screens).

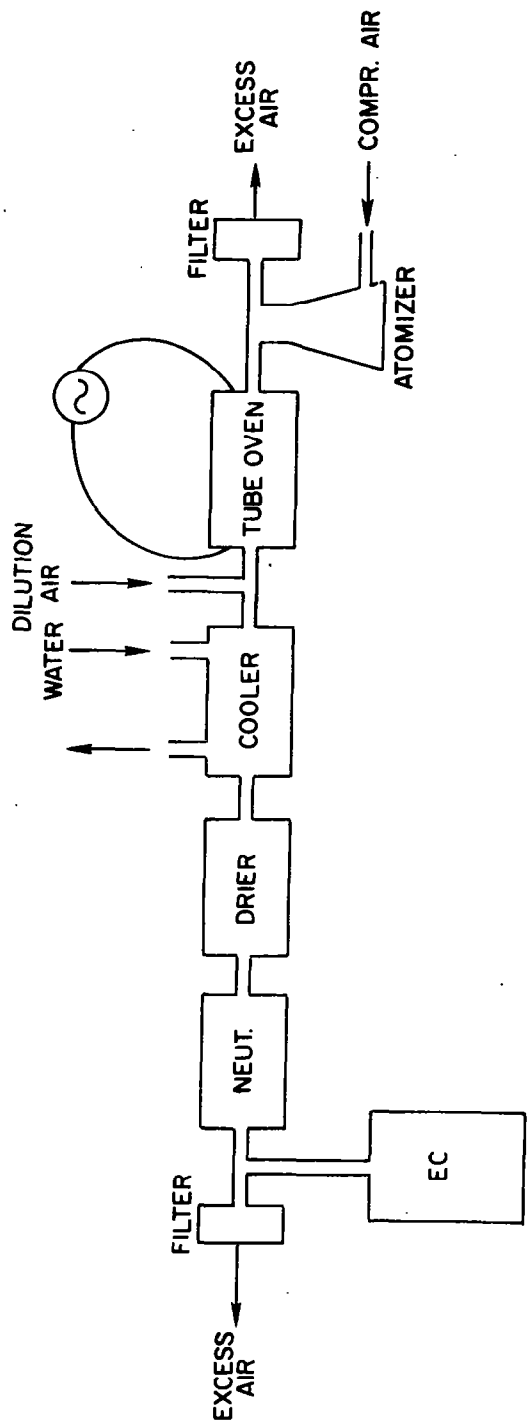

Figure 3-68. Schematic of laboratory set-up for experimenting with the recondensation scheme as narrowing method for particle size distributions.

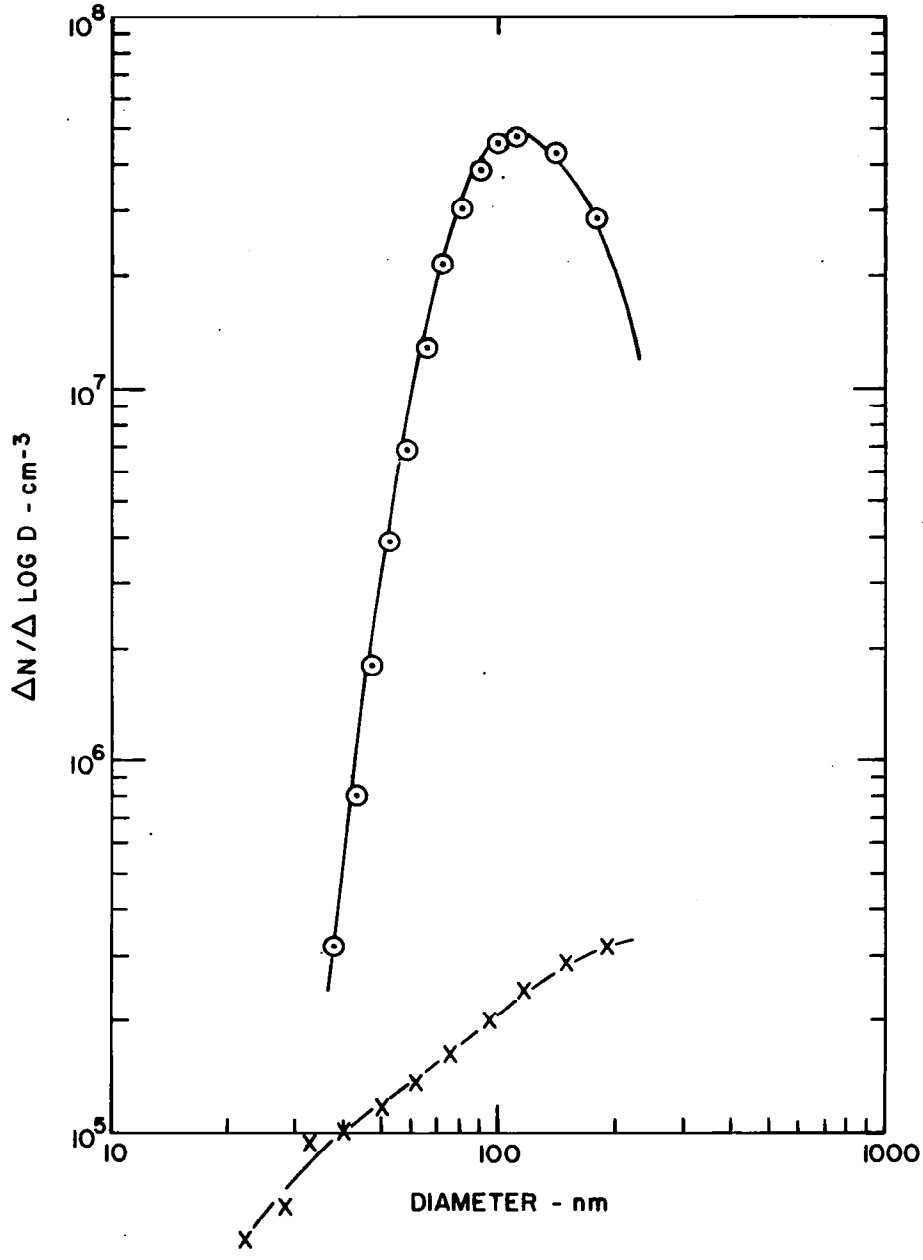

Figure 3-69. Two Dioctyl Phthalate aerosol size distributions as an example showing the effect of the recondensation technique. DOP aerosol from atomizer (X), and after recondensation (θ).

design should provide that spare units in cartridge form can easily be flipped into the flow path.

2. Thermal Modification of Size Distributions

This relatively well known technique is based on the fact that evaporation of a particle generally leaves a residue of contaminants which will act as condensation nucleus in subsequent rapid cooling and recondensation. Applied to a polydisperse population of particles, this means rapid condensation on polydisperse nuclei which yields nearly monodisperse condensate particles.

A laboratory-built oven and cooler combination, schematically shown in Figure 3-68 was used to experiment with this concept. Since the maximum oven temperature was insufficient to evaporate NaCl particles, tests were performed with dioctyl phthalate (DOP) for which the thermal treatment is routinely applied (TSI produces an oven-recondensation unit designed for this). Figure 3-69 illustrates the DOP droplet size spectrum obtained directly with the Nano-Mist atomizer (bottom curve, mode diameter larger than upper EC range limit), and the much narrowed distribution evolving from the heat treatment. The geometric standard deviation of about 1.5 is an excellent improvement over the extremely broad original distribution, but in the case of the much less viscous salt solutions, the original distribution may have a σ_g in the vicinity of 2.10 compared to which the recondensed aerosol would not constitute a significant enough improvement to warrant the additional complication of an oven and cooler unit with the necessary controls.

3. "Monodisperse" Aerosols from the Electrostatic Classifier

The ability to produce extremely narrow ("monodisperse") size distributions is most important since this will improve the quality and decisiveness of information obtained from experiments involving size dependent properties.

In the previous discussion on the EC (in Section II.B.a.) it was shown how well this instrument can extract particles of a very narrow mobility range. The fact that this translates into a multitude of size peaks due to the unavoidable presence of multiply charged particles causes a complication in using the EC as a sizing tool which can, however, be dealt with mathematically. In contrast, if the output of an EC should serve as a monodisperse aerosol the problem of addititional though smaller modes in the size distribution (as shown in Figure 3-70, an example where the EC was set for the size of 58 nm) is much more difficult to solve. One successful approach, taken by Gerber, et al. (1977), was to use an aerosol centrifuge as a filter by operating it such that any particle larger than the desired size was precipitated thus completely suppressing the modes originating from multiply charged particles. While this solution is acceptable for a terrestrial laboratory, it would have added too much complication to the ACPL and is, therefore, not recommended.

Having two EC's at our disposal, we explored the suitability of their use in series to improve upon monodispersity. In order to better visualize the partitioning the aerosol undergoes, one is referred to Figure 3-71. On top, the aerosol treatment is represented in terms of EC voltage (which is inversely proportional to the mobility), while the

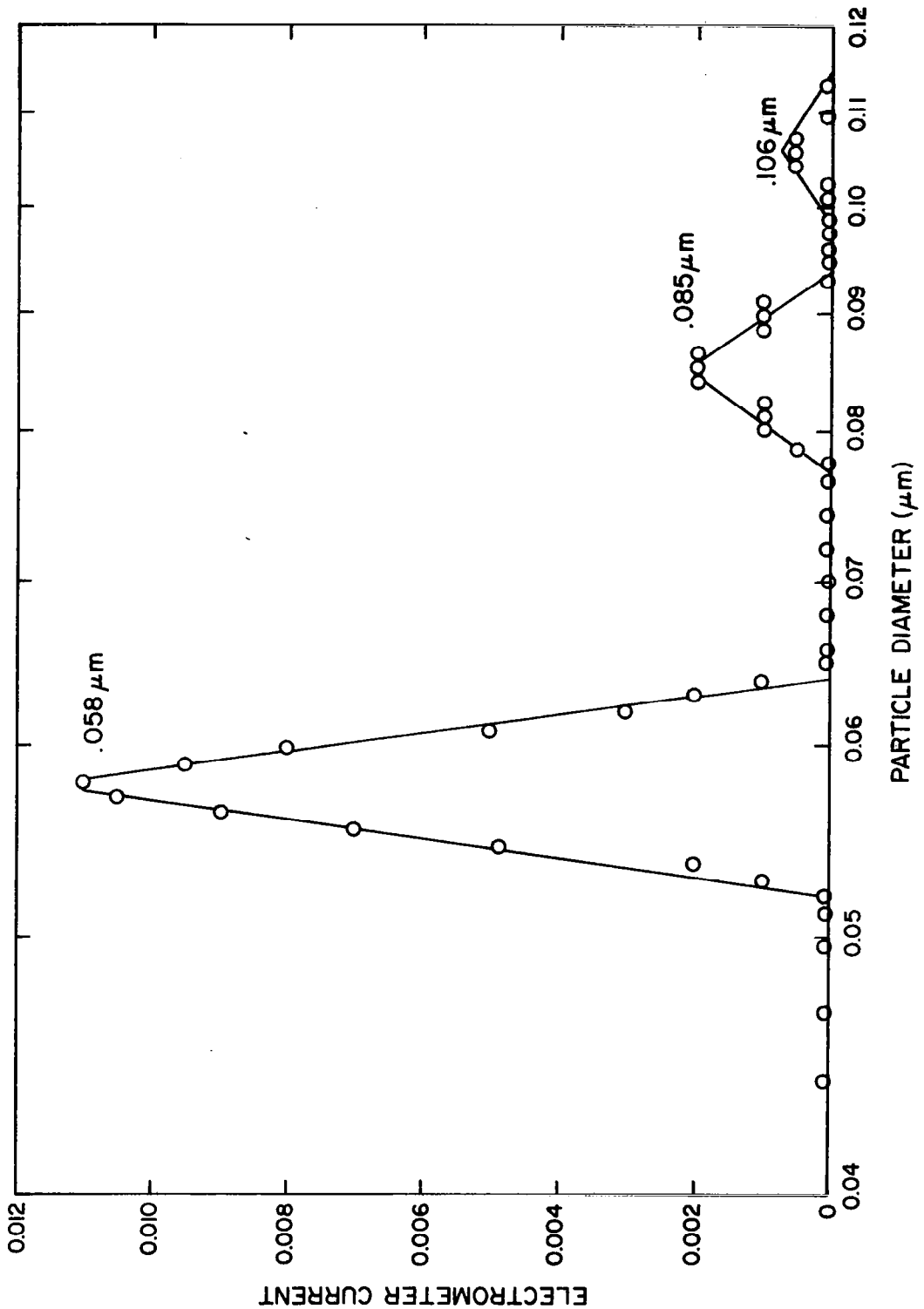

Figure 3-70. Trimodal output of one EC as diagnosed with second EC (.058 μm, singly charged; .085 μm, doubly charged; 0.106 μm, triply charged).

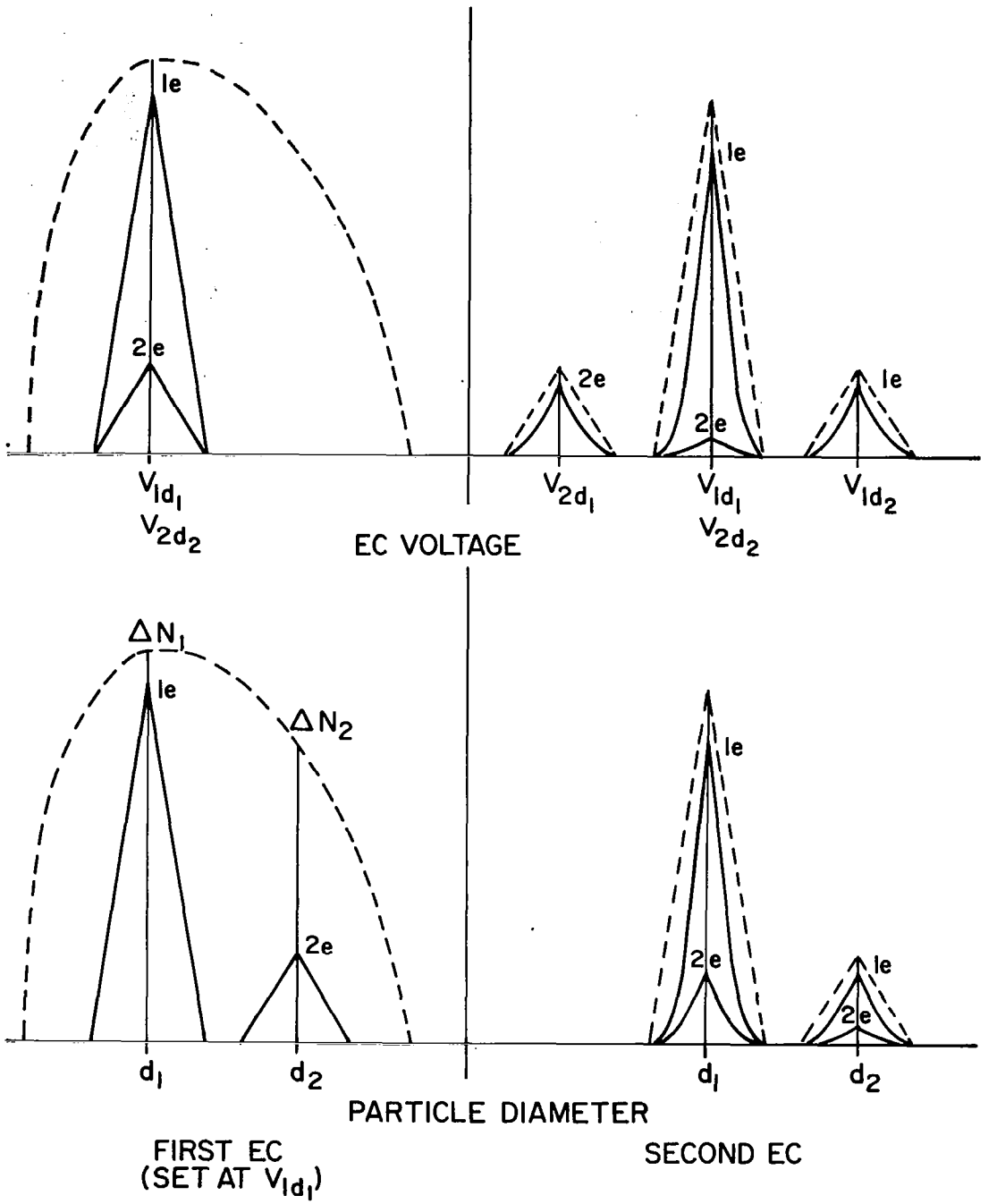

Figure 3-71. Schematic representation of the utility to use two EC's for narrowing size distributions and reducing multiply charged particle interference. (--- input; ——— output; for details, see text).

bottom part shows the same procedure in terms of particle size. On the left, the dashed line indicates a typical input into the first EC which is set at a fixed voltage V_{1d_1} which corresponds to particles with size d_1 and one elementary charge. One recalls (cf. Fig. 2-2, Section II.B.(c), Multiple Charge Compensation) that $V_{1d_1} = V_{2d_2}$, meaning that a certain d_2 exists for which doubly charged particles have the same mobility. Since Figure 2-3 indicates that triply charged particles are very infrequent in our size range, we limit the present argument to singly and doubly charged particles. The size distribution of the output from the first EC (at bottom left) shows the two modes at d_1 and d_2. At this point one has to determine the number ratio of the two populations $n_{d_2}/n_{d_1} = \Delta N_2 \cdot f_{2d_2}/\Delta N_1 \cdot f_{1d_1}$ where ΔN_i represents the total number of particles in the output in the EC size range centered on d_i, and f_{jd_i} the fraction of particles with diameter d_i carrying j charges (plotted in Figure 2-3). Depending on the type of experiment, the shape of the input size distribution, and d_1 the ratio n_{d_2}/n_{d_1} may be satisfactorily small. If not, passage through a second EC can provide the improvements shown on the right of Figure 3-71. One must remember that the two different charge and size populations emerging from the first EC are again neutralized prior to entering the second EC; thus, there are now four different populations that concern us (the vast majority of particles having become uncharged is lost for our purposes). Depicted at the bottom right (solid lines) are the singly and double charged d_1 particles and the singly and doubly charged d_2 particles whereby their number ratios are determined according to the data of Figure 2-3. While the singly charged d_1 and the doubly charged d_2

particles are again having the mobility associated with V_{1d_1} ($=V_{2d_2}$) as indicated at top right, the doubly charged d_1 particles have twice the mobility, i.e., they are extracted at $V_{2d_1} = V_{1d_1}/2$, and, similarly, the singly charged d_2 particles can be found at $V_{1d_2} = 2\ V_{1d_1}$. Thus, there are three choices of monodisperse outputs, and the selection has to depend on the total number of particles available in each category, and on the question whether the new ratio of doubly to singly charged particles at V_{1d_1} is acceptable, or whether one needs total lack of contamination as featured by the two other peaks. A partial answer can be obtained by considering the general expression for the available particle numbers: $\Delta N_1 \cdot f_{1d_1}^2$ for the main peak, and its contaminant, $\Delta N_2 \cdot f_{2d_2}^2$ which show that the percentage of contamination with two EC's is f_{2d_2}/f_{1d_1} times the value for one EC. The peak at V_{2d_1} provides $\Delta N_1 \cdot f_{1d_1} \cdot f_{2d_1}$ particles, whereas the number of singly charged d_2 particle amounts to $\Delta N_2 f_{2d_2} \cdot f_{1d_2}$. Since $1 > f_{1d_1} >> f_{2d_1}$, one notices immediately that the main peak at V_{1d_1} contains much higher particle concentrations than the two uncontaminated side modes - except when the original size spectrum is such that $\Delta N_1 << \Delta N_2$ and $d_1 > 100$ nm, a condition not very probable in the context of ACPL experiments.

An example showing how two EC's reduce the percentage of contaminating doubly charged particles can be found in Figure 3-72 in which the assumptions for the original size spectrum were log-normality with mode at 80 nm and $\sigma_g = 2$. Evidently it is mainly for small particles below about 70 nm where the 2 EC method using the main peak is of great advantage, whereas above 100 nm the doubly charged d_1 particles become numerous enough to be useful (20% at 100 nm; 40% at 200 nm).

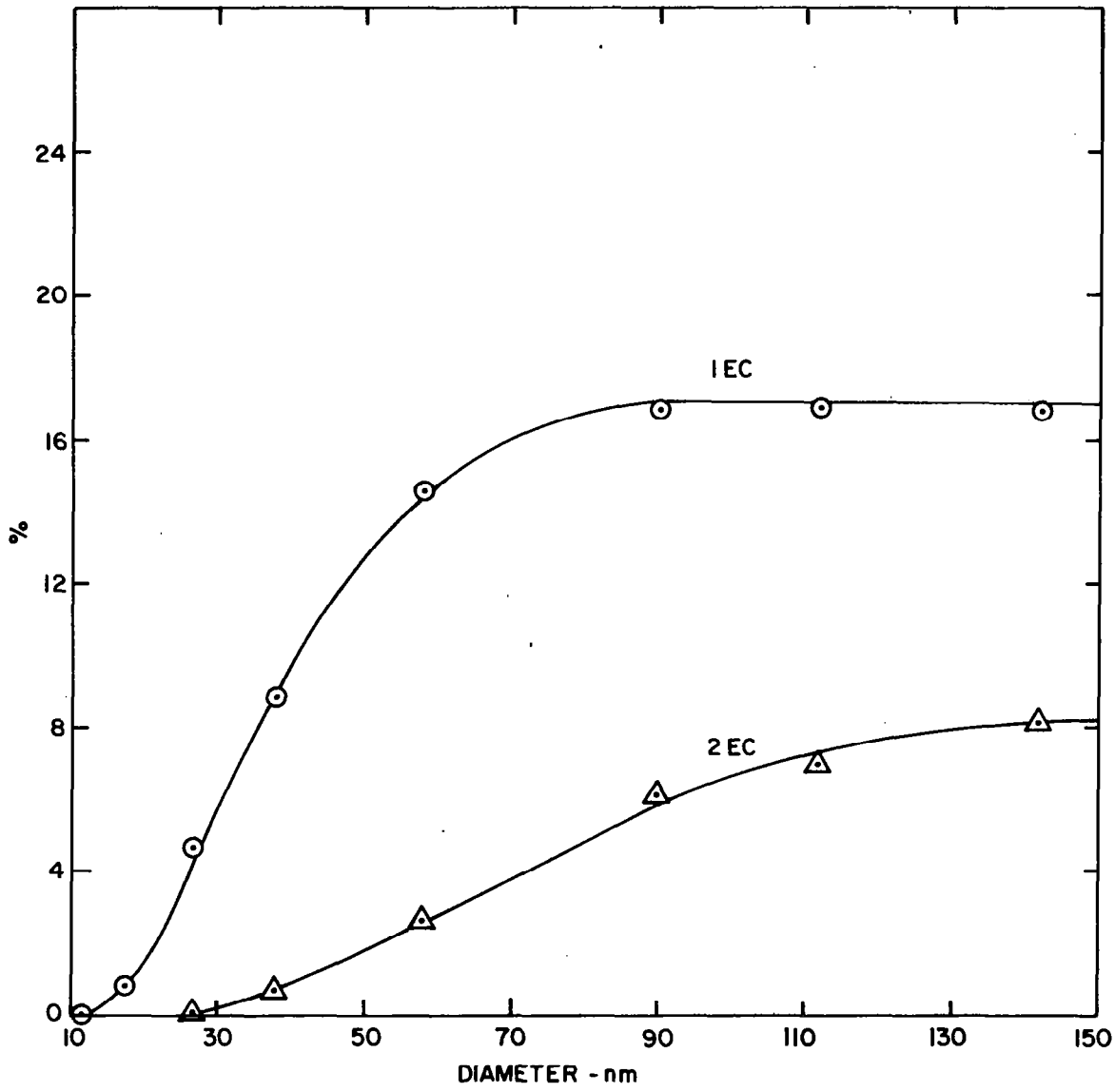

Figure 3-72. Percentage of doubly charged particle interference with one EC and two EC's for the example of a log-normal distribution centered at 80 nm with $\sigma g = 2$.

The 2 EC method not only provides less contaminated monodisperse aerosols, but also a more monodisperse one than with single EC. This fact is also illustrated in Figure 3-71 where the input into the second EC is represented by the dashed triangular peaks which are reduced to the narrower peaks (solid lines) delineated by segments of parabolas.

Based on the above considerations, it appears that a second EC would have been very valuable for the ACPL program where experiments with particularly well defined monodisperse aerosols were called for.

IV. CONCLUSIONS AND RECOMMENDATIONS

A. AEROSOL CHARACTERIZATION

The task of characterizing an aerosol in low-g consists of establishing the size distribution and should be provided in two forms. The first involves obtaining real time information on the aerosol for the experimenter and for electronic processing/storage which would then allow computerized post-flight evaluation. The second form consists of acquiring representative collections of actual aerosol particles ("hard copy") for post-flight examination, mainly by electron microscopy which offers the best possible size calibration as well as morphological insight.

Application of an electrical mobility method is currently the only proven way for real time measurement of size distributions in the 10 to 100 nm size range. The two possible modes that were examined in the form of commercial instruments were the TSI Electrical Aerosol Analyzer (EAA) using unipolar charging and the TSI Electrostatic Classifier (EC) working with aerosol in bipolar charge equilibrium. Despite its higher particle number sensitivity, the EAA should not be used for a precision size distribution analysis because of its insufficient resolution. However, the EAA would be beneficial by providing a time history of the operation of the aerosol generators.

An accurate aerosol size distribution measurement can be obtained with the EC due to its excellent size resolution. A problem lies in the choice of the particle detector. The Electric Aerosol Detector (EAD) that is generally used requires rather high number concentrations, and a

switch to a different particle counter is recommended. The new TSI-CNC would be nearly ideal if adapted to zero-g, and if the vapors of its working fluid (butyl alcohol) can be contained in a manner compatible with low-g operation; also, the device's detection limit of 20 nm has to be kept in mind. One has to be aware that, even with improved particle counting capabilities, the EC would have to sample at a point in the system before final dilution of the aerosol.

If a monodisperse aerosol is generated by means of one or two EC's, it is, of course, not necessary to re-analyze it with an additional EC - only a particle count is needed.

Acquisition of a hard copy sample, regardless of method used, is accompanied by the difficulty of obtaining a sufficiently high particle density on the substrate in the allotted time, especially since the sample should be taken at the stage of final dilution near the point of entry into the experiment area. This latter condition is very important because this sample should be most representative, and thus not contain elements which may be lost further downstream (during dilution and transport).

After reviewing the various sampling procedures, it is concluded that collection on membrane filters would provide the highest yield and most contamination safe in-flight handling; but this would also require that the best procedure of post-flight sample transfer onto electron microscope specimen grids be further studied experimentally. It is also recommended that a back-up sample be taken at a point where particle concentration is high such that direct deposition on grids by electrostatic precipitation can be accomplished. A special miniature sampler

would have to be designed according to guidelines found in the literature.

The collection and preservation of liquid aerosol samples (such as H_2SO_4) is considerably more difficult and was not explored as a part of this study. It is suggested that encapsulation schemes described in the literature be the subject of a further experimental study; even if general feasibility can be demonstrated, the necessary volatile chemicals may be excluded from an ACPL type of environment and other methods would have to be isolated.

B. AEROSOL GENERATION

The problem most common to all particle generation techniques investigated on this project was temporal instability of the output. Only in the case of the pneumatic atomizer was it possible to achieve a satisfactory solution.

The photolytic aerosol generator, despite its apparent simplicity could not be made to behave predictably enough for an ACPL type of task. In the meantime, through work performed under other sponsorship, it has become clear that the photochemical processes are too complicated to be fully described at this time. More basic research rather than engineering is recommended to further elucidate the phenomena involved in the particle formation mechanism - a necessary first step towards the goal of closely controlling the output of the aerosol generator.

Close examination of pneumatic atomizer performance showed that the only fault of this type of aerosol production was a tendency to flip unpredictably from a stable to an unstable output mode. Close scrutiny of the atomizing process during operation of specially designed variable

geometry atomizers allowed us to identify the following causes for the unstable behavior:

(1) Fluid accumulation of various amounts are periodically entrained into the air jet causing sudden increase in output. These accumulations partly originate from relatively large droplets being whirled around between nozzle and baffle, eventually impacting somewhere - a situation that is aggravated when higher salt concentrations cause foam formation. Depending on the liquid feed tube configuration, some fluid may also migrate directly from the orifice to some other location before being entrained by the jet.

(2) Salt deposits may gradually form on the rim of the liquid orifice altering the air jet flow pattern sufficiently to cause different atomization characteristics. The probability of growing salt deposits increases with solution strength.

Based on these findings, an improved constant output atomizer (ICOA) was designed which avoids the above cited problems. Extensive tests and routine use proved the validity of the design. For a flight version a minor modification is recommended whereby both air and liquid are fed through parallel bores within the same nozzle cylinder. This would enable the experimenter to quickly exchange atomizer heads and thus, by having spares along, it would be possible to start .each experiment with a clean, though pretested, atomizer head.

Most aerosol generation techniques produce rather broad size distributions ($\sigma_g > 2$) with the possible exception of atomized hydrosols. In order to obtain narrower distributions as required for many low-g experiments, three shaping methods were evaluated:

(1) Simple round jet impactors were able to reduce the large tail end of the distribution (>200 nm) by an order of magnitude. This could make many otherwise unacceptable polydisperse aerosols suitable for low-g experiments.

(2) One or two EC's are able to narrow down size distributions better than other candidate methods. While one EC provides essentially a bi- or tri-modal distribution with sharp individual peaks ($\sigma_g \sim 1.05$ for each), a second EC can reduce or totally suppress the secondary peaks and further narrow the primary one. Unfortunately, this is accomplished at the expense of particle number concentration.

(3) The recondensation method was briefly examined with the aid of DOP aerosols and found to be of moderate effectiveness.

It is recommended that methods (1) and (2) be utilized in low-g while (3) should only be considered if ovens and coolers are part of the flight facility.

Since pneumatic atomizers can easily be used to generate aerosols of water insoluble particles by dispersing hydrosols or colloidal suspensions, efforts were undertaken to produce, as an example, silica hydrosols following published procedures. The result was successful with regard to the physical characteristics of the ensuing aerosol; however, to what extent the non-aqueous components of the liquid can be driven off, is a question that is very difficult to answer. In many cases as in the present example, passage through a tube oven evaporates the liquids, but disposal of the vapors remains a problem in a flight situation where heating energy and weight and volume for activated charcoal are at a premium - not to mention the toxicology of the vapors.

Furthermore, it is extremely difficult to ascertain that no residue contaminates the particle surfaces.

It is suggested that future efforts in this area include the search for procedures to clean the hydrosol prior to flight such that only modest in-flight vapor treatment is necessary. Also, methods for testing the purity of particle surfaces should be established.

Brief experimentation with thermal generation of aerosols of the hydrophobic substances AgI and paraffin wax proved moderately succcessful, but even prior to designing low gravity adaptations these systems require further study to optimize their performance in the terrestrial configuration.

V. REFERENCES

Anderson, R.J., 1977: A literature review for aerosol generation and characterization techniques suitable for use aboard the Atmospheric Cloud Physics Laboratory. Calspan Report No. CK-6033-M-1, Calspan Corp., Buffalo, NY.

Binek, B., 1965: Sampling finely dispersed aerosols for electron microscopic particle analysis. Staub, 25, 13-19.

Chatfield, E.J., R.W. Glass and M.J. Dillon, 1978: Preparation of water samples for asbestos fiber counting by electron microscopy. U.S. EPA Report No. EPA-600/4-78-011, pp. 118.

Collins, G.F., 1975: Measurement of variation in output rate from aerosol generators. J. Aerosol Sci., 6, 169-172.

Cooper, G. and G. Langer, 1978: Limitations of commercial condensation nucleus counters as absolute aerosol counters. J. Aerosol Sci., 9, 65-75.

Frank, E.R., K.R. Spurny, D.C. Sheesley and J.P. Lodge, Jr., 1970: The use of Nuclepore filters in light and electron microscopy of aerosols. J. Microscopie, 9, 735-740.

Fuchs, N.A., 1964: The Mechanics of Aerosols, Pergamon Press, New York, NY, pp. 408.

Gerber, H.E., W.A. Hoppel, and T.A. Wojciechowski, 1977: Experimental verification of the theoretical relationship between size and supersaturation of salt nuclei. J. Atmos. Sci., 34, 1836-1841.

Ho, A.T., K.A. Bell, R.F. Phalen and A.F. Wilson, 1979: Fixation and microscopic sizing of aqueous sodium chloride aerosols. J. Colloid Interface Sci., 72, 351-357.

Hoppel, W.A., 1978: Determination of the aerosol size distribution from the mobility distribution of the charged fraction of aerosols. J. Aerosol Sci., 9, 41-54.

Kalmus, E.H., 1954: Preparation of aerosols for electron microscopy. J. Appl. Phys., 25, 87-89.

Knutson, E.O. and K.T. Whitby, 1975a: Aerosol classification by electric mobility: apparatus, theory and applications. J. Aerosol Sci., 6, 443-451.

Knutson, E.O. and K.T. Whitby, 1975b: Accurate measurement of aerosol electric mobility moments. J. Aerosol Sci., 6, 453-460.

Knutson, E.O., 1975: Extended electric mobility method for measuring aerosol particle size and concentration. Proceedings of a Symposium on Fine Particles, Minneapolis, Minn., Oct 1975, B.Y.H. Liu, Ed., Oct. 1975, 739-762, NTIS PB-249514.

Kremer, C.P., Jr. and M.O. Powers, 1978: Mist Generator, U.S. Pat. No. 4,116,387.

Lamb, D. 1978: A laboratory investigation of the roles played by oxides of sulfur and nitrogen in the formation of secondary particulates. Desert Research Insitute, 1977 Annual Report for Southern California Edison Company, Rosemead, CA.

Lamb, D., 1979: A laboratory investigation of the roles played by oxides of sulfur and nitrogen in the formation of secondary particulates. Desert Research Institute, 1978 Annual Report to Southern California Edison Company, Rosemead, CA.

Liu, B.Y.H., K.T. Whitby, and H.Y.S. Yu, 1967: Electrostatic aerosol sampler for light and electron microscopy. Rev. Sci. Instr., 38, 100-102.

Liu, B.Y.H. and D.Y.H. Pui, 1974: A submicron aerosol standard and the primary, absolute calibration of the condensation nuclei counter. J. Colloid Interface, 47, 155-171.

Liu, B.Y.H., K.T. Whitby, and D.Y.H. Pui, 1974: A portable electrical analyzer for size distribution measurement of submicron aerosols. J. Air Poll. Contr. Assoc., 24, 1067-1072.

Liu, B.Y.H. and K.W. Lee, 1975: An aerosol generator of high stability. Am. Ind. Hyg. Assn. J., 36, 861-865.

Liu, B.Y.H. and D.Y.H. Pui, 1975: On the performance of the electrical aerosol analyzer. J. Aerosol Sci., 6, 249-264.

May, K.R., 1973: The Collison nebulizer: description, performance and application. J. Aerosol Sci., 4, 235-243.

Mercer, T.T., R.F. Goddard and R.L. Flores, 1968: Operating characteristics of some compressed air nebulizers. Amer. Ind. Hyg. Assoc. J., 29, 66-78.

Morrow, P.E., and T.T. Mercer, 1964: A point-to-plane electrostatic precipitator for particle size sampling. Amer. Ind. Hyg. Assoc. J., 25, 8-14.

Newton, G.J., O.G. Raabe, R.L. Yarwood and G.M. Kanapilly, 1975: Generation of monodisperse aerosols of ^{67}Ga-labeled aluminosilicate and ^{148}Au-labeled gold spheres. Proceedings of a Symposium on Fine Particles, Minneapolis, Minn., May 1975. B.Y.H. Liu, Ed., Oct. 1975, 129-143, NTIS PB-249514.

Novak, J.W., Jr. and R.F. Browner, 1980: Characterization of droplet sprays produced by pneumatic nebulizers. Anal. Chem., 52, 792-796.

Phalen, R.F., W.C. Cannon, and D. Espanza, 1975: Comparison of impaction, centrifugal separation and electron microscopy for sizing cigarette smoke. Proceedings of a Symposium on Fine Particles, Minneapolis, Minn., May, 1975. B.Y.H. Liu, Ed., Oct. 1975, 731-737., NTIS PB-249514.

Pui, D.Y.H. and B.Y.H. Liu, 1979: Electrical Aerosol Analyzer: Calibration and Performance. Aerosol Measurement, D.A. Lundgren, et al., Ed., U. Florida Press, Gainesville, FL, 384-399.

Raabe, O.G., 1975: The generation of aerosols of fine particles. Proceedings of a Symposium on Fine Particles, Minneapolis, Minn., May, 1975. B.Y.H. Liu, Ed., Oct. 1975, pp. 57-108, NTIS PB-249514.

Remiarz, R.J., G.J. Sem, J.K. Agarwal, and C.E. McManus, 1980: An Automated Diffusion Battery Condensation Nucleus Counter System for Sizing Submicron Aerosols. TSI Quarterly, 6, 5-12, a publication of TSI Incorporated, St. Paul, MN.

Sinclair, D., D.A. Christy, and K. Snyder, 1977: Calculation of Aerosol Size Distribution from Diffusion Battery Measurement - A Computer Program for the Graphical "Stripping" Method. Aerosol Measurement, D.A. Lundgren, et al., Eds., U. Florida Press, Gainesville, FL., 615-631

Sinclair, D., R.J. Countess, B.Y.H. Liu, and D.Y.H. Pui, 1979: Automatic Analysis of Submicron Aerosols. Aerosol Measurement, D.A. Lundgren, et al., Eds., U. Florida Press, Gainesville, FL, 544-563.

Spurny, K.R., J.P. Lodge, Jr., E.R. Frank, and D.C. Sheesley, 1969a: Aerosol filtration by means of Nuclepore filters, structural and filtration properties. Environ. Sci. Technol., 3, 453-464.

Spurny, K.R., J.P. Lodge, Jr., E.R. Frank, and D.C. Sheesley, 1969b: Aerosol filtration by means of Nuclepore filters, aerosol sampling and measurement. Environ. Sci. Technol., 3, 464-468.

Stöber, W., A. Fink and E. Bohn, 1968: Controlled growth of monodisperse silica spheres in the micron size range. J. Colloid Inter. Sci., 26, 62-69.

Tillery, M.I., 1979: Aerosol Centrifuges. Aerosol Measurement, D.A. Lundgren, et al., Ed. U. Florida Press, Gainesville, FL, 3-23.

Twomey, S., 1975: Comparison of constrained linear inversion and an iterative nonlinear algorithm applied to the indirect estimation of particle size distributions. J. Computational Phys., 13, 188-200.

Vali, G., D. Rogers, G. Gordon, C.P.R. Saunders, M. Reischel, and R. Black, 1978: Aerosol and nucleation research in support of NASA cloud physics experiments in space. University of Wyoming, Final Report to NASA, Contract No. NAS8-32067.

Wilkinson, M.C., C. Pope, J. Hearn, and A.R. Goodall, 1980: Comments on the purification of polymer latices by the dialysis technique. J. Colloid Interface Sci., 77, 566-570.

*U.S. GOVERNMENT PRINTING OFFICE: 1981 539-007/29 1-3

TECHNICAL REPORT STANDARD TITLE PAGE

1. REPORT NO.	2. GOVERNMENT ACCESSION NO.	3. RECIPIENT'S CATALOG NO.
NASA CR-3486		

4. TITLE AND SUBTITLE	5. REPORT DATE
STUDY TO PERFORM PRELIMINARY EXPERIMENTS TO EVALUATE PARTICLE GENERATION AND CHARACTERIZATION TECHNIQUES FOR ZERO-GRAVITY CLOUD PHYSICS EXPERIMENTS	January 1982
	6. PERFORMING ORGANIZATION CODE

7. AUTHOR(S)	8. PERFORMING ORGANIZATION REPORT #
Ulrich Katz	

9. PERFORMING ORGANIZATION NAME AND ADDRESS	10. WORK UNIT NO.
Desert Research Institute University of Nevada System Reno, Nevada	M-368
	11. CONTRACT OR GRANT NO. NAS8-32313
	13. TYPE OF REPORT & PERIOD COVERED
12. SPONSORING AGENCY NAME AND ADDRESS	Contractor Report
National Aeronautics and Space Administration Washington, D.C. 20546	14. SPONSORING AGENCY CODE

15. SUPPLEMENTARY NOTES

Marshall Technical Monitor: Robert E. Smith
Final Report

16. ABSTRACT

This report presents the results of an investigation of methods of particle generation and characterization with regard to their applicability for experiments requiring cloud condensation nuclei (CCN) of specified properties which were planned for a zero-gravity Atmospheric Cloud Physics Laboratory (ACPL) originally considered for flight aboard the Space Shuttle. The results of the study would be applicable to other low-g flights.

Since aerosol characterization is a prerequisite to assessing performance of particle generation equipment, one section of the report is devoted to the evaluation of techniques for characterizing aerosol particles. Another section contains a discussion of aerosol generation; the studies of atomizer and photolytic generators represent the major portion, including subsections on preparation of hydrosols (used with atomizers) and on the evaluation of a flight version of a GE atomizer. Conclusions and recommendations are summarized in the final section.

17. KEY WORDS	18. DISTRIBUTION STATEMENT
Particle generation Particle characterization Aerosols	Unclassified - Unlimited Subject Category 47

19. SECURITY CLASSIF. (of this report)	20. SECURITY CLASSIF. (of this page)	21. NO. OF PAGES	22. PRICE
Unclassified	Unclassified	195	A09